SOIL STRESS FIELD AROUND DRIVEN PILES

Thesis by

Marie-Agnès Allard

In Partial Fulfillment of the Requirements

for the Degree of

Doctor of Philosophy

California Institute of Technology

Pasadena, California

1990

(Submitted October 2nd 1989)

ACKNOWLEDGMENTS

My sincere gratitude goes to the many whose guidance, encouragement, friendship and support sustained me throughout these years of graduate studies. I am also indebted to the U.S. National Science Foundation, Chevron Oil Field Research, Inc., Exxon, Unocal, Earth Technology, and the Earthquake Research Affiliates of the California Institute of Technology for their support of this research.

Thank you Professor R.F. Scott for your teaching and education during these years, for sharing your vast and rich experience and interests with me, for your trust and support in my work and for your friendship.

Thank you professors of Civil Engineering, Geology and Seismology for your enthusiasm and generosity in sharing with the students your insight and experience.

Thank you Robert for your invaluable help as a dedicated system manager of the Earthquake Engineering Research Laboratory computer, for developing this powerful data processing and analysis software package, SIG, that you always tailored with much kindness to my ever changing needs, for sustaining a constant interest, enthusiasm and source of advice through many challenging discussions, and for offering your friendship.

Thank you John and Brian for advising on or building centrifuge mechanical, electrical and electronic equipment and hardware parts.

Thank you Elmer and Marty for teaching me the ins and outs of the machine shop and for helping in the construction of many parts.

Thank you Sharon, Crista, Carmen and the whole staff of Thomas for your kind help towards a student ever lost in the CIT and TEX mazes.

Thank you to the GSC members, to the graduate office staff for working together to alleviate the hardships of Caltech student life.

Thank you to Eric, Sylvie, Maria-Luce and the many friends from Caltech and outside for your support in my work and life, for creating a warm-hearted, enriching and lively environment.

Thank you to my family, for giving me the possibility and encouraging me to pursue studies.

Thank you, Francois, for your love, strength and patience, for believing in something greater, for giving me freedom.

ABSTRACT

The description, equipment, and results of a series of pile-driving experiments conducted in a centrifuge using a model pile driven in dry sand are presented.

The work was conceived on the basis of the modelling of a soil-structure system under an artificially generated gravitational field, and motivated by the need for experimental data for a better understanding of the complex phenomena involved in the pile-soil interaction during driving. The behavior of the pile itself has been the focus of more attention in the past, but few full-scale or model experimental results have been obtained to the present concerning the soil stress field during pile driving. These are necessary for comparison with analytical and theoretical work. The work presented here appears to be the first attempt to obtain dynamic response of the soil during driving. The objective was to obtain a good understanding of the physical phenomena occurring in the soil and pile during driving.

In order to achieve these objectives both dynamic (transient) and static responses of the soil and pile were measured by means of transducers: accelerometers and strain gages for the pile, pressure transducers for the soil. In particular, the relations between static and dynamic data were explored, which resulted in the modelling of the soil-transducer interaction with a non-linear, history-dependent, model.

Results were obtained regarding pile dynamics, soil dynamics, and soil stress field (radial and vertical distribution, stress contours). Both linear and soil-cell model assumptions were used, which enabled a comparison between the two, leading to an estimate that each constitutes a bound of the real stress field, with the linear giving the higher, and the non-linear the lower bound, and the true stress being closer to the lower bound.

The soil response during driving is obtained, filling the gap in the study of the pile-soil system, where only the pile response was known. Recommendations for further work and better experimental procedures are given.

TABLE OF CONTENTS

LIST OF TABLES

LIST OF FIGURES

Chapter 1

INTRODUCTION

The use of piles is the oldest method of overcoming the difficulties of providing a support on soft soils; it dates back to the prehistorical lake villages. Nowadays, piles are frequently required as the primary foundation support in poor soil for a wide variety of buildings, bridges, towers, dams and other massive structures. Piles can be divided into two groups: displacement piles and bored piles, according to their method of placement into the ground. Displacement piles are placed in the ground by operations such as driving, jacking or vibration, while for bored piles a hole is excavated into the soil prior to their installation. Pile driving is a dynamic procedure in which the pile is forced into the soil by means of impacts of a mass on the pile head. If the energy transmitted by the falling mass to the pile is sufficient to overcome the dynamic resistance of the pile, then, at each blow, the soil surrounding the pile is displaced to allow for the penetration of the pile, and the pile experiences a permanent downward displacement. The diversity of pile types, driving equipment, and of designs in all sorts of soils, including layered soils, presents the designing engineer with great difficulty in establishing a safe but economical installation.

1.1 PILE DRIVING DATA AND ANALYSIS

Pile design is guided by the axial capacity that needs to be achieved. Because of the costs involved in performing axial static tests, only a small percentage of piles is actually tested. For small projects, the testing expense can exceed the installation expense. In some cases, such as offshore installations, the large loads and physical restrictions practically prohibit this approach. Therefore, an installation criterion often must be established by other methods.

One of the tools in the analysis of pile driving has been the use of dynamic formulae based on an idealization of the action of the hammer on the fully embedded pile, and

obtained from energy considerations. A review of some of these formulae are found in Sorensen and Hansen [146], Poulos and Davis [111], Holeyman [65]. These formulae reduce the design of pile foundation to a very simple procedure, but present obvious deficiencies and unreliability because pile driving cannot be accurately analyzed by rigid-body mechanics.

D.V. Isaacs (1931) and E.A.L. Smith (1960) first developed an analysis using wave theory that takes into account the fact that the impact of the hammer on the pile produces a stress wave that propagates down and up the pile, or in other words, the entire length of the pile is not stressed simultaneously as assumed in the dynamic formulas. The finite difference scheme, for the one-dimensional wave equation introduced by E.A.L. Smith [141], where the pile is discretized into lumped masses connected by springs and the soil response is represented by a series of rheological model (Figure 1.1), is a major step in the analysis of pile driving. The Smith soil model consists of a spring and frictional element, which gives an elastic-perfectly plastic response, in parallel with a dashpot for viscous damping, Figure 1.2. The driving equipment is also discretized.

The development of numerical models for the analyses of pile driving based on the one-dimensional wave equation, which evolved from this work, aims at offering a tool to the engineer to estimate the ultimate load capacity of a pile from the pile's dynamic response during driving, and to choose the best suited driving equipment. From this point of view, Holloway *et al.* [67] present and compare various models. Goble *et al.* [59] give a review of the development of the various measurement techniques and the analysis methods for the interpretation of the pile dynamic response during driving, in order to assess pile bearing capacity, integrity, driveability, and driving equipment performance. In these models, the pile is treated as an elastic rod and only one-dimensional stress wave propagation is considered. The soil response is represented by spring, dashpot, and friction elements distributed at discrete points along the pile length. Dynamic measurements of the force and acceleration of the top of the pile are done during the actual driving (*e.g.*, [9], [26], [33], [44], [45], [56], [85], [90], [116]). A set of soil parameters is selected, and the measured acceleration is used as input to the model (boundary value). Then using the model, the soil response is computed as well as pile element displacement and forces. The soil parameters are interactively changed to obtain good agreement between the measured and calculated pile top force. When good agreement is reached, the soil parameters are considered best

estimate values, and are then used for the prediction of the pile static load curve. Limitations of the method arise because of shortcomings in the soil model and the non-uniqueness of the solution. It is crucial to adequately model the dynamic pile-soil interaction so as to estimate, from the predictions of the pile performances during driving, soil parameters that really represent the characteristic of the soil. Thus, in turn, a reliable distribution of the soil resistance along the pile and at the toe can be obtained.

The modelling of the pile in the one-dimensional model is straightforward; the difficulty in the modeling of pile driving lies in the representation of the soil behavior. Since the work of E.A.L. Smith, a very large number of publications have dealt with the improvement (*e.g.*, [6], [17], [48], [57], [58], [59], [72], [91], [98], [115], [121], [122], [123], [140], [141], [152], [153]), or implementation of new soil models (*e.g.*, [15], [27], [29], [34], [39], [60], [66], [79], [82], [84], [88], [114], [160]). In the last decade the need for soil models using parameters that have some analytical or physical basis, rather than simply empirical correlation, has been recognized (Holeyman [65], Simons and Randolph (1985), Corte and Lepert [34]). The finite element method (*e.g.*, [70], [164]) has been applied to solve the dynamics of the pile-soil system under one impact. The use of finite element models (Smith and Chow [143], Levacher [83], [84], Couthino *et al.* [35], [36], Ebecken *et al.* [47]) offers the possibility of a three-dimensional analysis of the pile driving problem, and allows the modeling of the full soil continuum. This improvement over the simplified one-dimensional approach provides more understanding of the dynamic soil-pile interaction, and shows the importance of inertial effects neglected in previous one-dimensional models. Although finite element analysis of pile driving can help in the development of improved simpler models (Randolph [113]), it is still limited because of the difficulty in handling wave propagation into two very different materials, the large deformations involved, the separation soil-pile, the limitations in soil constitutive models, and the very high computational requirements.

1.2 WHAT IS NEEDED

Some 450 pile driving formulae exist, and are now less and less used. As mentioned above, pile driving analysis by the wave equation analysis has been developed over the last decades. Since the beginning, the various investigators have shown good agreement between the prediction from the different models and experimental data (*e.g.*, [17], [73]), and no agreement (*e.g.*, [22], [63]). New programs have been and are being created, and

improvements added to existing ones with a trend which seems far from converging. Several international conferences specializing on the application of the stress-wave theory on piles have been held. This only demonstrates that engineers are still uncomfortable with the analytical and numerical techniques available and with their ability to predict field performance of a pile.

Analysis methods are still inadequate and a better understanding of the physics of pile driving and axial loading is required. A way to gain a better understanding of the complex phenomena that control pile driving is through experiments that give real data. Experimental data provide a basis for the development and calibration of numerical models that otherwise can be cut from physical reality. The need for experimental data as expressed by Smith [142] is still very present.

The insertion of the pile provokes a perturbation in the surrounding soil, which is translated into a change of the stress in the soil. This change in the stress field evolves as the pile penetrates deeper into the soil. As a consequence of driving, the disturbed soil surrounding the pile, in a new state of stresses, exhibits new strength characteristics. The ultimate capacity of the driven pile depends on the final properties of the soil that surround it. Pile driving analysis, using the one-dimensional wave equation, attempts to predict the static capacity of the pile from dynamic measurements of the pile response to the final hammer impacts. Although the pile response reflects the interaction between the pile and the surrounding soil, a proper understanding and modeling of this dynamic interaction is lacking; furthermore, the correlation of the dynamic and static interaction is not established. A study of the regularities of the change of stresses both at the pile-soil interface and in the soil around the piles during driving and at rest is a necessary condition for developing analytical and numerical methods.

The soil stress field around piles driven in clays and saturated soils has been the subject of some experimental studies (*e.g.*, [8], [86]). The analysis of the expansion of a cylindrical cavity has been applied to the understanding of the state of stress around driven piles in clays (*e.g.*, [23], [24], [40], [42], [106], [157], [163]). In Davis *et al.* [42] the theoretical pore pressure increase obtained from the analytical solution for a rapid undrained expansion of a long cylindrical cavity is compared with the various field test data. With the large scatter

of experimental results it is difficult to confirm the validity of any theoretical development. Obviously more experimental information is required.

In the analysis of pile driving, much attention has been given to the dynamic response of the pile. As mentioned above, the improvement of the current pile-soil models rests on the study of the pile response to the hammer impact. Knowing that the major difficulty in the characterization of the pile-soil model lies in the modeling of the soil response and the pile-soil interaction, it is proposed here not to restrict the analysis to the response of the pile, but to also study the response of the soil during driving. This gives, then, the complete actual representation of the response of the pile-soil system from both the pile and soil point of view. This information on the soil response is essential in the development of numerical models for pile driving, in order to improve soil modeling and obtain better characterization of the soil properties following driving.

1.3 PILE DRIVING EXPERIMENTS

The ideal situation would be to measure and monitor the stress field around a prototype (full scale) pile both during and after driving. This is not practical even if one has the required financial means. Because the effects of pile installation decay quite rapidly with distance from the pile, measurements have to be made quite close to the pile. The difficulty with full scale experiments lies in the placement of the instrumentation in the soil, the changes of the soil conditions that result, and the precision in the estimation of the gage location. Also, the non-uniformity and often unknown characteristics of the prototype soil increase the level of complexity of the analysis. All these difficulties make the validity and utilization of the results obtained (for other piles and soil conditions) at the very least questionable. Also, in some cases, as for offshore foundations, this is simply not possible. In the development of analytical and numerical analysis methods, the first stage is to evaluate the fundamental concepts, and confirm the predictions with experimental data. The following stages then involve the expansion of the theory to study more complex cases.

Model experiments offer an alternative to obtain data under controlled conditions, in particular uniform soil properties, as a basis for theoretical comparisons. The control over the parameters is an essential tool in the study of fundamental phenomena governing a complex problem. The results of a model experiment are valid when in the model, the true

conditions, which exist in the real prototype problem, are modeled correctly. Because of the dependence of soil behavior on ambient stress conditions, centrifuge modelling is a powerful technique in geotechnical investigations. The centrifugal acceleration field recreates the same stresses and strain at homologous points in the model and prototype. Analytically, the approach has been the subject of a number of studies and justifications, see Appendix A. Experimentally the use of the centrifuge in geotechnics has proven useful in many areas, in particular in the study of pile behavior (*e.g.*, [75], [134], [129], [130], [136]) and also soil dynamics (*e.g.*, [21], [71]). Model pile experiments in the centrifuge were first conducted with the pile installed in a soil container at $1g$ prior to testing at a higher g-level. A review of installation procedures for model piles tested in a centrifuge is given by Craig [38], and some errors in prediction under various loadings, due to the effect of lack of similarity in installation between model and prototype, have been singled out. It was recognized that to maintain the correctly-scaled stress field around the pile and pile-soil interaction it is necessary that the model pile be driven and tested in flight; a mechanism capable of driving the model in flight on the centrifuge was built and tested, Allard [2].

In-flight pile driving experiments have been conducted in the Caltech centrifuge to evaluate the driveability of piles, Allard *et al.*[4]. Other investigations of driving and static loading of piles in a centrifuge have followed (*e.g.*, Nunez [101]). Another experimental technique for geotechnical investigations, the hydraulic gradient method, has been used to study the driving and subsequent axial loading of piles in saturated sand, (Zelikson [165]). Measurements of pile dynamic response have been obtained as well as some information on the pore pressure and total stress field around the pile. The need for stress measurements in the soil around the pile for the resolution of the pile driving problem has been addressed, and the lack of adequate instrumentation and soil stress information has been recognized.

1.4 THESIS OUTLINE

The work presented in the following chapters consists of experiments on piles driven in flight in the centrifuge in a uniform dry sand. The objective of the investigation is to study both the dynamic and static stress field in the soil around the pile during driving, to gain a better understanding of the dynamic pile-soil interaction.

Experimental data can be obtained by conducting model pile-driving experiments in a centrifuge. This involves the design, building and procurement of special equipment and instumentation. The size and characteristics of the Caltech centrifuge guided the choice of the many parameters in the experiments. It is possible to study the behavior of the pile-soil system by monitoring the response of the soil and the pile during driving using various transducers and data acquisition systems. The equipment and instrumentation are presented in Chapter 2. Test procedures and data acquisition and reduction methods are discussed in Chapters 3 and 4. Because of the particular interaction between the soil and the pressure transducers, the interpretation of the cell measurements requires a careful understanding of the phenomena occurring at the local level of the cells. A non-linear soil-cell model for the evaluation of stresses in the soil from gage readings is developed in Chapter 5. Experimental results are presented and discussed in Chapter 6. The stress field data is reduced and interpreted according to a linear approximation as well as to a non-linear model, and the results compared, permitting the conclusions and recommendations proposed in Chapter 7.

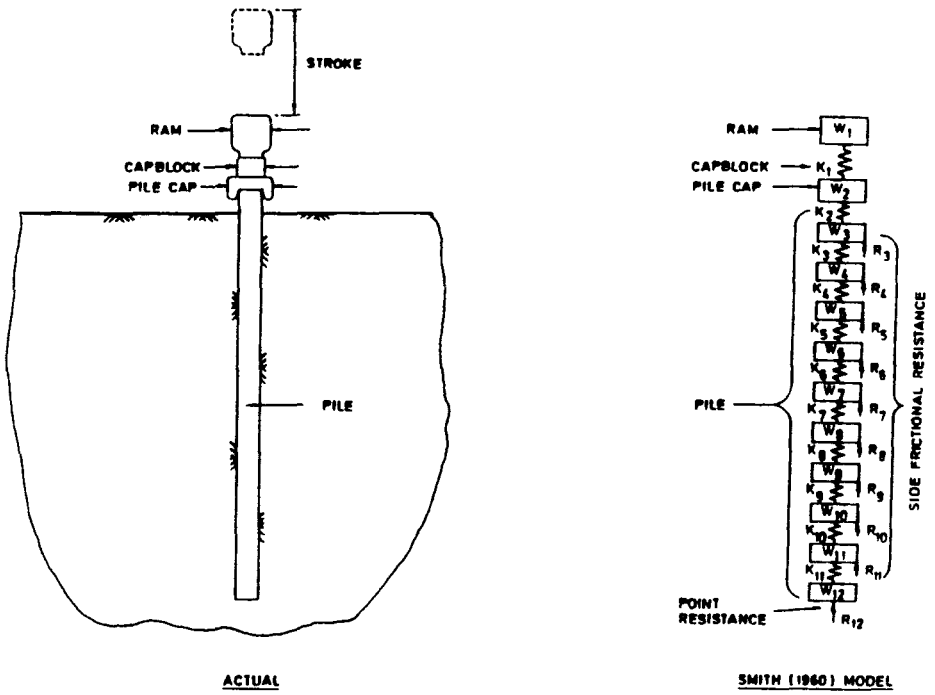

Figure 1.1 Pile driving one-dimensional wave equation: discrete element model

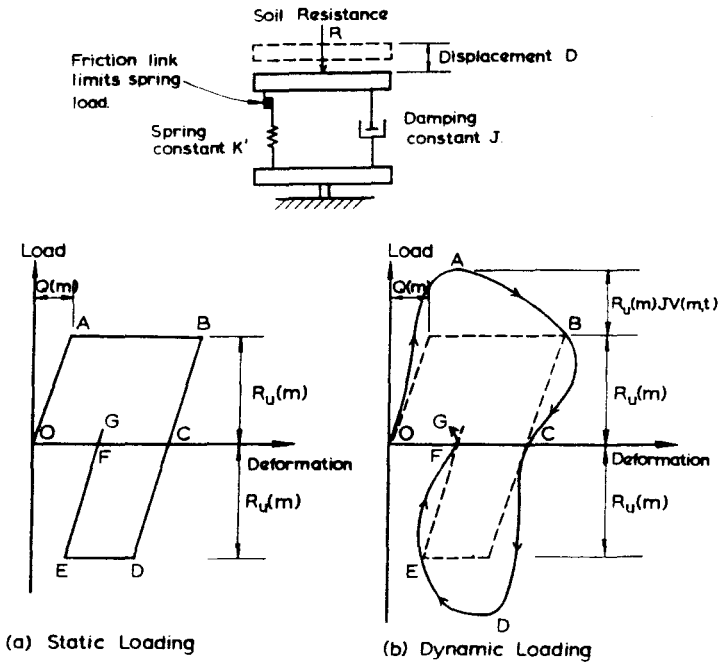

Figure 1.2 Rheological model of soil resistance at pile-soil interface, Smith (1960)
(a) and (b) Soil model load deformation behavior

Chapter 2

DESCRIPTION OF EXPERIMENTAL FACILITIES

2.1 CENTRIFUGE EQUIPMENT

2.1.1 Caltech Centrifuge

The centrifuge used for the pile driving experiments is shown in Figure 2.1. The centrifuge rotates in the horizontal plane and is rated at 10,000 g-pounds payload capacity. At each end of the symmetric arm is located an 18 x 22 inch magnesium pivoting mounting frame. The distance from the centrifuge axis to the mounting frame pivot is 36 inches. The acceleration range, at a 40-inch radius, is 1 to 175 g. Electrical power and signals to and from the rotating arm or frame are conducted through 44 sliprings of various capacities from 10 to 30 amps. Two rotating unions can offer 4 hydraulic sliprings for compressed air or hydraulic fluid. More details about the technical aspects of the centrifuge are given in several publications (*e.g.*, [3], [71], [104], [132]).

2.1.2 Test Containers

As can been seen from the previous description, the Caltech centrifuge is of a limited size both in geometry and load capacity. To conduct a pile-driving experiment in the centrifuge, a vertical clearance at the experimental platform of at least two-and-a-half times the pile model length (L) is needed. Before driving, the pile sits vertically on top of the soil, so that its height above the surface is L, and the pile will be driven in soil of a depth of at least 1.5 L to limit the boundary effects. Thus a general-purpose soil container was not suitable. In order to make as much use as possible of the weight available for the experimental platform, the pile driving tests were performed using, in the first phase of the experiment, a special bucket constructed by Chevron Oil Field Company in La Habra, California. This bucket is both mounting frame and soil container. A photograph of the bucket, a cylindrical vessel 22 inches long and 6 inches diameter, mounted directly on the

centrifuge arm, is shown in Figure 2.2. The apparatus for driving and testing the pile in flight was designed for this container; it is described in the section 2.1.2.

The first series of experiments (referred to as SA hereafter) conducted in the Chevron bucket led us to the conclusion that the radial boundary conditions were affecting the driving process. Soil stresses on the container wall generated by the pile-driving were not as small as previous studies had shown (*e.g.,* [5], [86]), and could not be neglected. There were two ways to solve this problem: either reduce the model pile diameter, or increase the size of the container. The first solution was abandoned because the new size requirements for the stainless steel tubing, out of which the model pile is made, were out of range for the commercially available stock. Also the strain gage instrumentation of a smaller diameter tube would be very difficult; and acceleration measurements would be impossible. Therefore a larger container and its mounting frame were designed and constructed for the second series of experiments (referred to as SB hereafter).

The second bucket is shown in Figure 2.3. The soil container can be separated from the mounting frame; it consists of a cylindrical stainless steel vessel 2 feet tall and 10.75 inches in diameter. An exterior ring at about 1/3-height is used as a connection with the frame, which consists of a platform with a circular hole in which the container fits, see Figure 2.4. The design of the new bucket was carried out following centrifuge requirements, simplicity, and cost considerations.

The Chevron bucket offers a very strong and efficient structure, especially considering the centrifuge constraint on weight. However, its construction is delicate and requires advanced professional fabrication equipment and experience. One of the major difficulties in building a test platform for the centrifuge lies in the necessity of getting a perfect alignment of the bearings of the mounting frame so that the bucket would get to the proper operating position during flight. For this reason it was decided to use the bearing plates of one of the existing magnesium mounting frames, abandoning the idea of a combined frame-container structure. The magnesium platform or plate is replaced by a light frame composite aluminum platform with a center hole where the new cylindrical soil container fits. A mandatory requirement was to stay within the load capacity of the centrifuge. The total weight for the mounting frame plus container, soil, driving, and testing equipment was therefore limited. The diameter of the container was chosen as a function of construction

material availability and soil volume considerations. The mounting frame structure is based on a light-weight design concept with two plates linked together by stiffeners. For reasons of simplicity and time the same operational concepts were used as for the Chevron bucket, retaining the pile driving and bearing capacity mechanisms with as few modifications as possible.

The design of the platform was performed on a first approximation using beam analysis theory, and complying with the requirements for size, weight, assemblage, and welding. It was further improved using a simple finite element analysis executed with a program supplied by Prof. John F. Hall. A finite element mesh is shown in Figure 2.5; it makes use of the two symmetries of the platform. The Young's modulus, Poisson's ratio, unit weight, and height of each plate element of the mesh were calculated to provide the characteristics of the composite platform. After completion, the platform was instrumented with strain gauges, see Figure 2.4, on the outer sides of the top and bottom plate near the center hole, to check the maximum compressive and tensile stresses experienced by the platform under full load during flight. Calibration of the platform, under various loading configurations, was done in the centrifuge. Predictions of stresses in the platform for the different loadings were obtained with the finite element analysis. The experimental results and the numerical model gave good agreement. Figure 2.6 shows the comparison of the maximum compressive and tensile stresses obtained during calibration and with the finite element analysis for 2 loading cases:

a. load applied along the center axis for maximum bending.

b. load applied along the circumference of the center hole: soil bucket in place.

2.1.3 The Pile Driving Mechanism

The pile driving mechanism designed by John Lee and Prof. Ronald Scott fits in the upper part of the pile test container, see Figure 2.7. It is made of a rigid structure connected to the container and fixed during driving, and of a moving part on which the model pile driver is attached. The model driver will drive the pile, situated just underneath it, into the soil, in flight.

The first part, the *frame*, consists of two one foot tall columns held together by two circular plates of diameter slightly less than six inches. One plate of aluminum is at the

base of the columns, which were forced into it to ensure rigidity. The other plate of lucite is near the top (its height is adjustable). Each column has two diametrically opposite rows of notches equally spaced (1/8 in.), over the total driving length of 8 in.. The second part, the *carriage*, consists of a horizontal beam that slides up and and down the columns. Ratchets are placed on the carriage so that when they are in position they fit into the notches of the columns and prevent upward motion of the carriage relative to the frame. A small pneumatic piston ("Tiny Tim") is attached to the top of the carriage to act as the model pile driver.

The frame, during driving, is at a fixed position inside the container. The mechanism is suspended by its columns to two sets of horizontal rods connected together above the container. Three teflon screws on the edge of the bottom plate allow for the positioning of the frame inside the Chevron bucket. Four aluminum extension legs, attached to the bottom plate, allow for the positioning in the large container. Figure 2.8 shows the actual mechanism.

The pile is placed underneath the carriage and is forced into the soil by the action of the model pile driver. The impact cycle is shown in the illustrations on Figure 2.9:

- 1st sketch: the stroke of the piston is near its minimum, the pile is resting on the soil and supports the carriage.
- 2nd sketch: the stroke is at its maximum, the pile is hit by the hammer, and by the energy transferred to it, the pile is forced down into the soil.
- 3rd sketch: due to the effect of gravity (centrifugal acceleration) the carriage slides down until it rests on the pile again. A cycle of the pneumatic piston is completed, and we return to sketch 1 configuration with the pile deeper in the soil. Because of the ratchets, upward movement of the carriage (and therefore of the pile) relative to the frame or to the container is prevented. Thus only downward motion of the pile is permitted. These sequences are repeated and the pile is driven into the soil.

The model pile driver, consisting of the pneumatic piston simply connected to the air source, originally did not perform very well. Because of the length of the air tubing and the frequency of driving, a few Hertz, it is assessed that a cushion of air forms in the chambers of the piston. As a consequence the power delivered by the piston is substantially reduced.

The flow of air through the piston has been improved by the addition of two solenoid valves. These valves, Figure 2.18, installed on the centrifuge arm and activated by the computer through relays, control the flow of air in and out of the chambers of the piston. The driving frequency is easily adjustable in the software. For mechanical reasons a frequency in the order of 1Hz is employed. The implications of this restriction are discussed in the section on scaling. A second reason for a low initial efficiency of driving was that the ram of the piston moved before air pressure fully built up. A simple mechanism with a groove in the ram's shaft and an O-ring in the piston body holding the ram in its upper position has been added. Thus the ram moves down only when the pressure reaches the level needed to release the O-ring from the groove; the impact is then much stronger, the energy delivered to the pile higher, and consequently the driveability is improved.

One of the crucial aspects of driving is in the alignment of the pile. If the pile penetrates into the soil at a small angle off of the vertical then the destabilizing action of the soil will increase this angle as the pile gets deeper and this will lead eventually to the buckling of the pile, see Figure 2.10. The pile is guided at the top using the pile cap and through the bottom plate of the mechanism, see Figure 2.11. The pile cap is attached to a teflon cylindrical sleeve that slides along the guide built into the lower part of the carriage, see Figure 2.9, sketch 2. Therefore, a connection between the top of the pile and the carriage is always preserved. A piece of teflon with a hole whose diameter is a few thousands of an inch greater than the pile outside diameter is placed at the center of the aluminum bottom plate of the mechanism. With these two guides we ensure a perfect positioning of the pile before penetration, and maintain the pile alignment during driving, since the pile, mechanism and container axes coincide. With the large container, alignment is a problem because perfect circularity of the container is lost during construction. In the small bucket, the general positioning of the pile driving mechanism frame inside the large container was carried out at the top using the horizontal suspension bars. Extension legs were attached to the bottom aluminum plate of the frame, to provide contact with the container wall now farther away from the plate edge. Two of the legs have a spring-loaded ball bearing at the end to provide adjustable length and contact force, see Figure 2.12. Because of the small thickness of the wall (0.134"), the cylindrical part of the container deformed during the careless welding of the closing head, the mid-height heavy ring and the top angle ring. No reference was left with which to find the central vertical axis of the bucket. Consequently

the adjustment of the legs was done on a trial-and-error basis. The two guides and holding system for the pile in the driving mechanism are the same as before. In Figure 2.12 we can see the flexible tubings connected to the 2 chambers of the piston, which allow for the motion of the driver during driving. The flexible PVC tubing is reinforced by a spring to preserve flexibility and prevent squashing of the tubing in flight.

As explained in the functioning of the mechanism, the carriage holding the model hammer rests on top of the pile. In other words, at all times the pile has to support this driving structure: carriage plus driver. At the very beginning of the test when the centrifuge is spun to the experiment acceleration level, there is a critical stage where the pile, resting only on top of the soil, cannot offer enough bearing resistance to support the driving structure. The pile then penetrates into the soil until enough bearing capacity is reached. This is undesirable, and thus, to prevent penetration prior to the actual driving, the pile is held at its initial position with the mechanism shown in Figure 2.11. The idea is to use an aluminum sheet whose thickness is such that it provides just enough strength to support the weight of the driving structure. The first impact of the driver on the pile causes the pile to punch through the aluminum foil and start the penetration into the soil.

2.1.4 The Pile Static Loading Mechanism

The ultimate object of pile driving analysis is to estimate the bearing capacity of the driven pile. At the experimental level this means that after the pile is driven, it is necessary to perform an axial loading test on it. In our setup, the driving mechanism takes the pile to the depth of interest, where the pile static loading mechanism is activated, and the bearing capacity of the driven pile is obtained. This loading mechanism is an extension to the driving mechanism. From Figure 2.7 we see that the frame is suspended by its two columns from the horizontal rods that hinge from a fulcrum bolted to the lip of the container. The outer hydraulic piston is inactive during driving, and constitutes the second support of the rods. When activated it can push or pull on the two rods. It thus transmits an up or down translation to the frame with respect to the container. As mentioned before, the carriage will undergo only downward movement relative to the frame. Therefore, by activating the hydraulic piston, penetration of the pile into the soil is induced under rate-controlled loading. Figure 2.13 shows the sequences involved in a bearing capacity test.

- 1st sketch: reference configuration; the hydraulic piston is in the lower position.
- 2nd sketch: the piston is going up, pushing the frame up. It can be seen that only the frame undergoes an upward movement. The carriage subjected to the centrifuge acceleration does not move and allows the columns of the frame to slide up; the ratchets will then occupy a new position further down the columns.
- 3rd sketch: upper position of the piston; the pile is still at the same level in the soil.
- 4th sketch: the piston is going down, pulling the frame down. Because the ratchets prevent upward motion of the carriage relative to the frame, the whole mechanism is experiencing a downward motion. Hence the pile, attached beneath the carriage, is forced into the soil.
- 5th sketch: final configuration after one complete cycle of the piston.

One cycle of the hydraulic piston performs an axial loading test on the pile. The penetration of the pile for a cycle is controlled by regulating the stroke of the piston. Apart from bearing capacity testing it can be noted that by repeating these sequences the pile can be statically pushed into the soil by steps, each step corresponding to a cycle.

The pressurized hydraulic fluid coming from a hydraulic pump is delivered to the two chambers of the piston through a valve and a rotating union. The Haskell Engineering and Supply Co. Model DEN.PR51 pump, located next to the centrifuge enclosure, is driven by a 10 HP motor and has a line capacity of 3000 psi at a maximum rate of 5 gallons per minute. The pressure and return lines of the pump are connected to a valve located in the control room. From the valve two other lines go to the rotating union (Deublin 1895-100) mounted on top of the centrifuge enclosure at the center axis. This rotating union offers two hydraulic sliprings: one is connected to the top chamber of the piston, the other to the bottom chamber, see Figure 2.14. The valve has three positions:

1. at rest the hydraulic fluid goes from the pump through the valve back to the pump
2. the fluid goes from the pump to line 1 of the valve in turn connected to the top chamber of the piston through the rotating union, and the bottom chamber, linked to line 2 of the valve, is connected to the return line of the pump so that the fluid can circulate. In this position we can perform a loading test on the pile.

3. the fluid goes from the pump to line 2 of the valve and therefore to the bottom chamber of the piston. The top chamber, linked to line 1 of the valve, is in turn connected to the return line of the pump. In this position the pile driving frame is pulled back up to prepare for an axial loading test.

2.2 CENTRIFUGE INSTRUMENTATION

As mentioned before, the experiments were conducted to investigate several aspects of pile driving:

a. the evaluation of the stress field around the pile during driving,

b. the analysis of the dynamic response of the pile and the soil to the hammer impact throughout the driving;

c. the ultimate capacity of the pile subsequent to driving.

A wide range of instruments is used to monitor the different parameters of interest during an experiment. A displacement transducer, which follows the pile top, allows us to know the position of the pile during driving. The stress field in the soil is captured by pressure transducers located at various positions in the soil. As we have seen in chapter 1, current analyses of pile driving are based on the one-dimensional wave equation whose solution, in the elastic domain, for a semi-infinite pile subjected to an impact at one end, tells us that the strain and the particle velocity at the impact end are proportional. Thus, in order to monitor the response of the pile to the hammer impact during driving, both the acceleration, to obtain the velocity, and the stress wave in the pile are measured. For this we use piles instrumented with shock accelerometers and strain gauges. For the dynamic response of the soil following the hammer impact on the pile, we capture the transient pressure waves in the soil using pressure cells and bender elements. The pile penetration and pile capacity after driving are measured using a displacement transducer attached to the pile driving mechanism frame, and a load cell situated at the top of the pile.

2.2.1 Accelerometers

For our model pile, miniature accelerometers with very high acceleration range and frequency response are needed to obtain the acceleration in the pile due to the hammer impact. During driving, acceleration in a prototype pile can reach $500g$, where g is the

Earth's gravitational acceleration. For a model with a scaling ratio of 100, the maximum acceleration would then be 50,000g, (see Appendix A for scaling relations in the centrifuge). The accelerometer has to be attached to the pile and therefore must be of light weight and very small dimension. Miniature piezoelectric shock accelerometers (Endevco 2255A- 005), with built-in microelectronic converter modules, were used. This model utilizes a shear design where a hollow cylinder of ceramic material is bonded to a center post. A concentric hollow cylindrical mass is then bonded to the crystal. When the unit is subjected to an acceleration along the axis of the post, the entire cylinder of crystal is subject to a shear stress. The polycrystalline ceramic is made to exhibit piezoelectricity by a process of artificial polarization. Thus the transducer element produces an electrical output proportional to the acceleration applied to the mass. These piezoelectric accelerometers have an acceleration range of 100,000g, a nominal sensitivity of .05 mV/g, a frequency response of 50 KHz and a resonant frequency of 270 KHz. They are .305 inches (7.75 mm) high, with a mounting head of .312 inches (7.92 mm) Hex, and weigh 1.6 grams. One accelerometer is fixed inside the top of the pile in the pile cap, the other is fixed in the bottom of the pile in a plug, see Figure 2.15.

For measurements of acceleration in the soil around the pile generated by the dynamic effect of the hammer impact on the pile, we use Entran Devices Model EGA(X) -125(F)-500(D) miniature accelerometers. The accelerometers are a single degree of freedom oscillating systems using a viscous fluid medium for damping. They employ a fully active Wheatstone bridge, (Appendix B configuration 5), consisting of semiconductor strain gages. The strain gages are bonded to a simple cantilever beam that is end-loaded with a mass. The effect of acceleration on the mass generates a force at the end of the cantilever, which in turn creates a bending moment on the beam. The strains resulting from the loading of the beam will cause a bridge unbalance. With an applied voltage, this unbalance produces a millivolt deviation at the bridge output, which is proportional to the acceleration. The accelerometer has a range of 500g, a nominal sensitivity of .50 mV/g, a useful frequency range of 1KHz, a resonant frequency of 3KHz, and has 0.7 of critical damping. The unit is .27 inches (6.86 mm) long and a .140 x .140 inches (3.56 x 3.56 mm) section can be mounted on a flange .04 inches (1 mm) thick, and weighs .50 grams.

2.2.2 Bender elements

We used Piezo Electric Products R205-S series connected bender elements, made with G-1195 piezoceramic material. The element consists of two thin piezoceramic plates that are rigidly bonded together with conducting surfaces between them and on the outside in a sandwich-type arrangement. The polarization of the ceramic material is oriented in opposite directions for each plate, and the electrical leads are attached to each of the outer electrode surfaces. When the element is forced to bend, one layer goes into compression and the other into tension, which results in an electrical signal.

2.2.3 Displacement transducers

We want to know, at all times throughout driving, the position of the pile in the soil. For this we use the output of a rotary potentiometer, 10 KΩ - 10 turns, which is fixed to the upper lucite plate of the driving mechanism frame and connected to the carriage by a string and pulley system, see Figure 2.8. Before the test the pile, held by the aluminum foil, is at a known position. During driving the frame is fixed relative to the container, and only the carriage following the top of the pile moves. The position of the pile tip in the soil will, from now on, be referred to as the depth of the pile .

The penetration of the pile during an axial loading is caused by the downward translation of the pile-driving mechanism frame induced by the motion of the hydraulic piston. It is calculated using the output of a linear potentiometer, 15 KΩ - 3 in travelling length, connected between the mechanism frame and the top of the container, see Figure 2.16.

2.2.4 Load cell

During an axial loading test the load is applied to the top of the pile through the carriage's beam. The ratchets preventing upward motion of the carriage create a simple support condition at each end of the beam, and the load, reaction at the pile head, is applied at the center. The beam deforms in bending. It is instrumented with strain gages to form a fully active Wheatstone bridge, (Appendix B configuration 5). This constitutes a load cell, linear to at least 1000 lbs, that allows measurement of the pile load. The gages used are: CEA-03-062UW-350 from Micro-Measurements.

2.2.5 Pressure transducers

For the determination of total normal stresses in the soil, miniature pressure cells were used. Many investigations concerning pressure cells for soil have been conducted, (see section 5.1), and the results tell us that, for best measurement, the cells should be flat with wires to the side. Also the size of the cell-sensitive area must be such that the number of grains in contact with it is large enough so that the multiple point force loading can be considered a uniform loading. In the case of a circular sensitive area this condition is fulfilled when the ratio of the diaphragm diameter to the grain size is greater than 20. We have several different diaphragm-type pressure cells. For all of them, the cell sensitive area consists of a thin circular diaphragm a few thousands of an inch thick and 0.11 to .2 inches (2.7 to 4 mm) diameter, instrumented with strain gages in a Wheatstone bridge configuration, and supported on its circumference by a circular ring. A pressure applied on the cell corresponds to a uniform loading of the diaphragm, which provokes its deformation in bending, and the resulting strains create a bridge unbalance proportional to the pressure acting on the diaphragm.

Our five types of soil pressure cells are described as follows:

1: EPF-200-50 (now called EPL-200-50). It is a flatline pressure transducer from Entran Devices, which consists of a fully active semi-conductor gage bridge, (see Appendix B configuration 4). It has a 50 psi range with a nominal sensitivity of 2.5 mV/psi for a 6 VDC input voltage, a resonant frequency of 50 KHz, and a 0 to 10 KHz useful frequency range. It is a light weight and small size transducer: .400 inches (10.2 mm) long, .200 in (5.08 mm) wide and .040 inches (1.02 mm) thick.

2: PM-156-500. A Precision Measurement pressure transducer with one active foil gage, (see Appendix B configuration 1). It has a 500 psi pressure range, and a nominal sensitivity of 1.5μV/V/psi. The sensing face is a .140 inches (3.5 mm) diameter diaphragm, and the unit is .312 inches (9.5 mm) long, .156 inches (3.96 mm) wide and .062inches (1.55 mm) thick. It is furnished with teflon coated three conductor wire and can be immersed inches liquids.

3: PM-105S-500. A miniature stainless steel cell from Precision Measurement. It has a one active foil gage arm bridge with a range of 500 psi. The nominal sensitivity is 1.5μV/V/psi. It is our smallest cell: .105 inches (2.6 mm) in diameter and a thickness of

.013 inches (.33 mm). A spherical shell acts as support for the diaphragm and as casing for the transducer.

4: PM-105S-500-1/2 bridge. It is a prototype transducer built by Precision Measurement for us, following the design of the 105S model, but with a thicker diaphragm and 2 semi-conductor gages to increase the output sensitivity of the cell. The nominal sensitivity is .107 mV/V/psi.

5: ED-EPF-200-500. A flatline pressure transducer from Entran Devices similar to # 1, but with a 500 psi range, a resonant frequency of 120 KHz and a 0 to 24 KHz useful frequency range. The unit is the same size as # 1, but differs in the thickness of the diaphragm, so that it is stiffer than # 1. The nominal sensitivity is .25 mV/psi for a 10 VDC input voltage.

1, 2 and 3 cells were used in the first series of experiments (SA), and cell types # 4 and 5 in the second series (SB).

2.2.6 Strain-gaged piles

For the measurement of the stress wave propagating in the pile following the hammer impact we use strain gages bonded to the pile wall. In the first series of experiments (SA), the model piles are made out of stainless steel tube 9 in. long, 3/8 in. diameter and a wall thickness of 6/1000 in. One of the pile tubes is instrumented with five strain gages along its length for the evaluation of the axial load along the pile, see Figure 2.15. Each gage constitutes an active arm of a Wheatstone bridge, (see Appendix B configuration 1). In the second series (SB), the model pile is now 10 in. long, to allow full length driving of the totally instrumented piles, 3/8 in. diameter and 10/1000 in. wall thickness, the latter because the 6/1000 in. thick tubes were no longer available. Some piles have two pairs of gages near the top and the bottom of the tube respectively. One pile has five pairs of gages installed on the inside of the tube, and the top pair on the outer side. The two gages of a pair are diametrically placed on the side of the tube, and occupy two opposite arms of a Wheatstone bridge to eliminate bending, (see Appendix B configuration 3). The gages used are: CEA-09-062UW-350 from Micro-Measurements.

2.3 DATA ACQUISITION SYSTEM

2.3.1 What is needed

As can be seen in the previous section we are using a wide range of instruments. The signals that we obtain have different characteristics and will require different treatments. We can classify the signals in two categories for requirement of speed of data acquisition. On the one hand we have the "static" signals; in this category we group together the output of:

- displacement transducers for the position of the pile during driving or the penetration of the pile during an axial loading,
- the load cell during an axial static loading of the pile,
- pressure transducers for the evaluation of the changes in the stress field in the soil during driving. In this case only one point per transducer is taken at the end of each blow.

In this group, the signals we are looking at contain low frequencies, so we use a general purpose analog-to-digital converter, the treatment procedure will allow up to a few tens of KHz range.

On the other hand we have the dynamic signals, generated by the impact of the hammer on the pile. This category consists of the output of:

- the shock accelerometers that measure the acceleration in the pile,
- the strain gage bridges of the instrumented pile that pick up the stress wave propagating in the pile,
- the pressure cells and bender elements that capture the transient pressure waves in the soil,
- the accelerometers in the soil around the pile.

We want to analyze the stress waves, generated by the hammer impact, travelling up and down the pile and in the soil around the pile. For the model pile, the travel time to the tip and back to the top is about 100 μs, and the time for a P-wave to propagate radially from under the pile tip to the container vertical boundary and back is of the order of 200 μs in the first bucket (SA) and 400 μs in the larger one (SB). For the pile response monitoring,

we are dealing with data acquisition rate in the hundreds of KHz range, in order to be able to capture the stress wave. Hence, a very high speed data acquisition system is required to capture the dynamic transient signals.

Because of the location of the centrifuge, connection to a main-frame computer for high speed data acquisition presented some difficulties. The data would need to travel through very long cables, and this would create problems for the reliability of data acquisition when we deal with sampling frequencies up to 1 MHz. Our solution was then to use data acquisition systems controlled by personal computers. We had two types of recording systems. The first one consisted of a 16 channel general purpose digital acquisition system connected to a Zenith Z120 personal computer with 768 Kbytes memory, and was used for the static signals. The second one, used for the dynamic signals, consisted in the first series of experiments (SA) of a signal memory recorder SMR2 connected to the Z120, and for the second series of experiments (SB), of a high speed data acquisition card that plugs into an IBM PC XT compatible computer.

2.3.2 General purpose digital acquisition systems

We used different general purpose 16 channel analog-to-digital converters linked to the Z120 through an interface card, (see Appendix C.1). The circuit diagram of one converter can be seen in Appendix C.2. Because the data acquisition was always done at a frequency less than 10 KHz the data was directly stored onto the computer memory RAMs, and then, at the end of an experiment, transferred to diskettes.

2.3.3 High speed digital acquisition systems

The Signal Memory Recorder, SMR2, from Soltec, is a 12 bit resolution analog-to-digital converter capable of acquiring data at the rate of 500,000 samples per second, or 2 μs between samples. We had one module of 4 channels, each with 128 Kbytes of memory, or 64 K of 16 bit words, which could be recorded simultaneously at 1/2 MHz. The memory for each channel could be partitioned in blocks that could be filled sequentially. This feature was used to record 64 blocks of 1K points, each block corresponding to an impact on the pile. Internal and external triggers are available and it is possible to save pre-trigger events.

The RC Electronic high speed data acquisition card uses a 12 bit resolution analog to digital converter with 16 channels multiplexed and a maximum sampling rate of 1 million

points per second, or a sampling frequency of 1 MHz. Because of the multiplexing, if data is acquired on 4 channels, the maximum sampling frequency is 250 KHz (1 MHz/4), and there is always a 1μs delay between channels. The RCE has a 64 Kbyte memory buffer. With the card is provided software that allows, for data acquisition, the setting of the number of channels to be saved, the sampling rate, the size of the record (up to 64 Kbyte), the trigger mode, and the pre-trigger option. After each record, the data is transferred from the card memory buffer in files onto the hard disk of the computer.

2.4 SIGNAL CONDITIONING

In our setup, we have at one end the transducers in the centrifuge, and at the other end the data acquisition systems located in the control room, adjacent to the centrifuge room. The analog signals of the different instruments will then be conditioned according to the signal, transducer, acquisition system and environment characteristics, so that the final digital signal represents as best as possible the original signal. The location of the centrifuge on the roof of Thomas Laboratory at CIT in close proximity to air conditioning units and elevator drive motors makes for a very noisy electrical environment. Also the analog signals have to run through the sliprings and long cables. The conditioning of the signals may be done in several steps. If the signal at the output of the transducer is not big enough (in the Volt range), it is amplified directly on the centrifuge arm before transfer through the sliprings to the data acquisition systems. Certain transducers, especially pressure transducers, require large amplification. This is obtained in a two-stage amplification. The first stage is done in the centrifuge before the sliprings and the second stage in the control room in front of the data acquisition system.

2.4.1 Amplification and offset adjustment

A 16-channel amplifier, built for the centrifuge, is used for the static signals or for the pressure transducers, see Figure 2.18. It uses Burr Brown 2962 instrument amplifiers with a frequency response of 100 KHz at a gain of 1. Refer to Appendix C.3 for the circuit diagram. A set of switchable resistors allows for the selection of the gain between a value of 5 and 1000. Increase of the gain acts as a filter: the frequency cutoff (-3db response) drops from 25 KHz at a gain of 5, to 15 KHz at a gain of 100, and to 3 KHZ at a gain of 1000. Built-in with the amplifier is a digital offset adjustment to utilize, in the best way possible,

the data acquisition system range. As the offset comes after amplification we have to make sure that the amplified signal will not saturate the amplifier (±15 V.).

Some of the transducer' signals, such as the strain gage bridge output of the instrumented piles, are high frequency signals, and also need a high gain. A special amplifier, see Figure 2.18, that can be mounted on the centrifuge arm, and offers a high frequency response, was built using AD254 Analog Devices precision instrument amplifiers with a frequency response of 1 MHz at a gain of 1, 400 KHz at a gain of 10, 150 KHz at a gain of 100, and 25 KHz at a gain of 1000. The instrument amplifier is in a series with an operational amplifier LF 356 that offers a frequency response in the MHz range. The gain on the op-amp and on the inst-amp is set to 10 to provide the highest frequency response for a gain of 100.

For the second stage amplification in the control room, we use the 16-channel signal conditioner that gives a choice of 1, 10, and 100 for the amplification gain, through a PGA102 precision instrument amplifier. Appendix C.4 shows the complete circuit diagram of the signal conditioner designed and built by John Lee. It offers the options of AC or DC coupling, offset input, amplification and filtering of the signal.

2.4.2 Filtering

To reduce the noise in the signal before acquisition, and especially to eliminate very high frequency noise, we can use filters in the last stage of conditioning. The 16-channel signal conditioner offers selectable Bessel low-pass filters. The filters are 4 pole Bessel filters, with each operational amplifier stage contributing 2 poles. A set of six resistors chosen with a computer program can be placed in the circuitry to provide the desired cutoff frequency profile. To change the filter cutoff frequency another set of resistors can be placed in the circuitry. A typical frequency response of the Bessel filters shows for a cutoff frequency of 1 KHz an amplitude ratio of the output signal to the input signal of .7, corresponding to -3db.

2.5 RPM COUNTER

The evaluation of the g-level during an experiment is obtained from the count of the number of rotations of the centrifuge arm per minute. For this a magnetic transducer,

placed at the base of the centrifuge, records the passage of the teeth on a 600-tooth gear wheel (Figure 2.1) located on the main drive shaft. Each revolution of the centrifuge produces 600 sinusoid cycles as output of the magnetic pickup. This signal is read by an electronic counter and converted to RPMs accurate to 0.1 RPM. The RPM value is presented on a LED display. The signal is also fed to a RPM detector front end that converts a variable amplitude sinusoidal input to a constant 5V pulse waveform of the same frequency, see Appendix C.5. This generated TTL signal is in turn the input to the digital counter circuitry located on the S100 plug-in-board of the Z120 computer, see Appendix C.6. As the tooth gear wheel produces 600 pulses per revolution, 1 pulse is expected in a 100 ms period for each RPM. Through the use of oscillators and counters the number of pulses occurring in 100 ms is counted, this number corresponds to the RPM value. At the end of each 100 ms period the RPM value is latched and the counters reset. The RPM is effectively updated 10 times a second and can be read directly by the computer using a simple BASIC INP statement with the appropriate address.

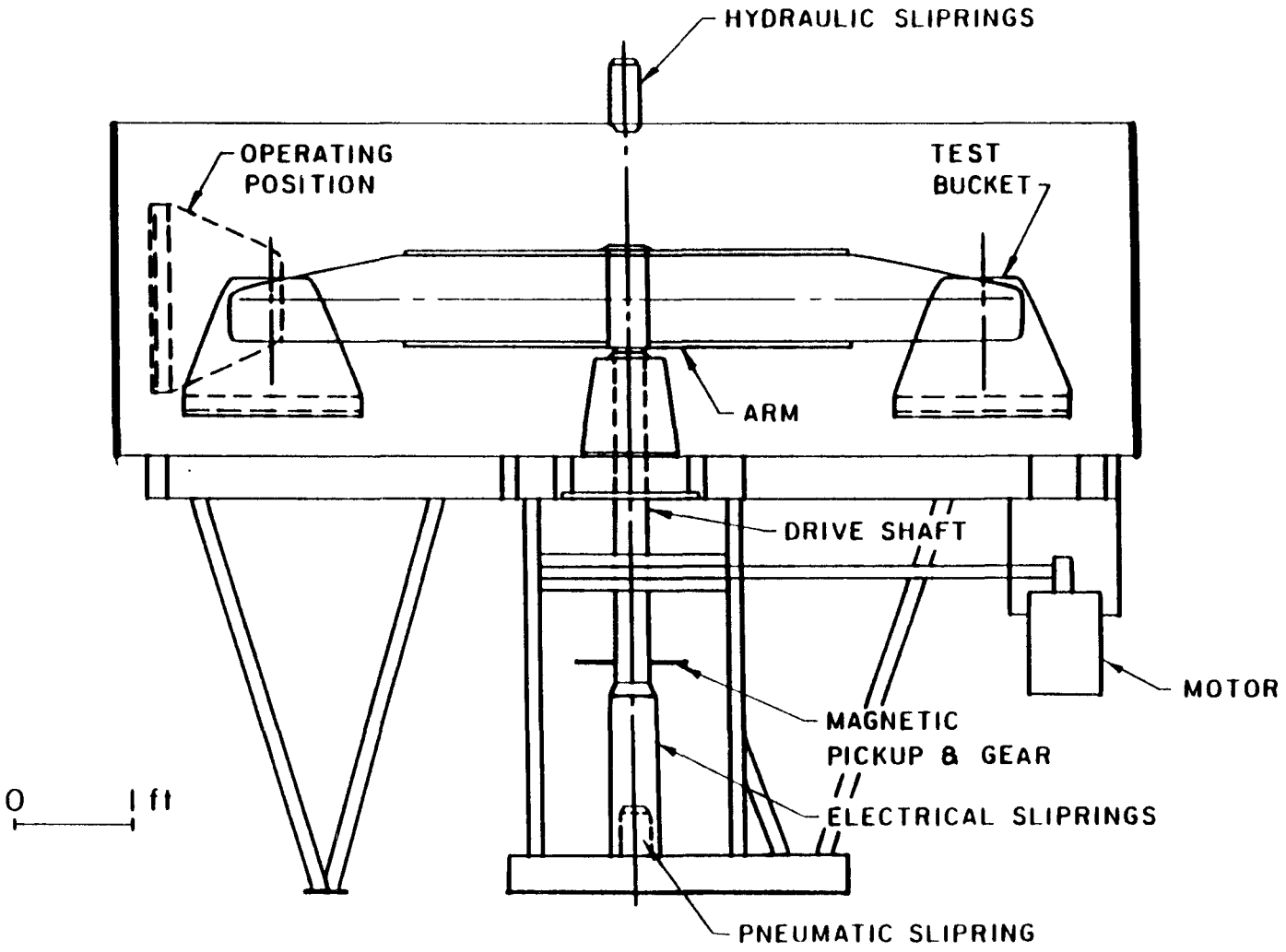

Figure 2.1 Caltech centrifuge

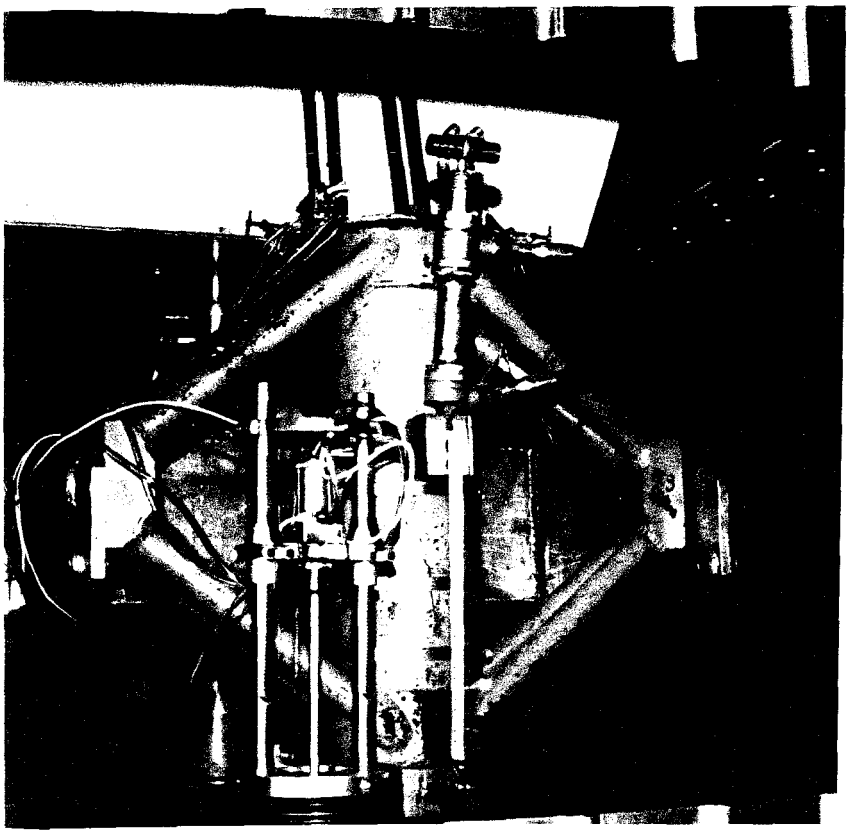

Figure 2.2 Chevron pile bucket mounted on the centrifuge arm

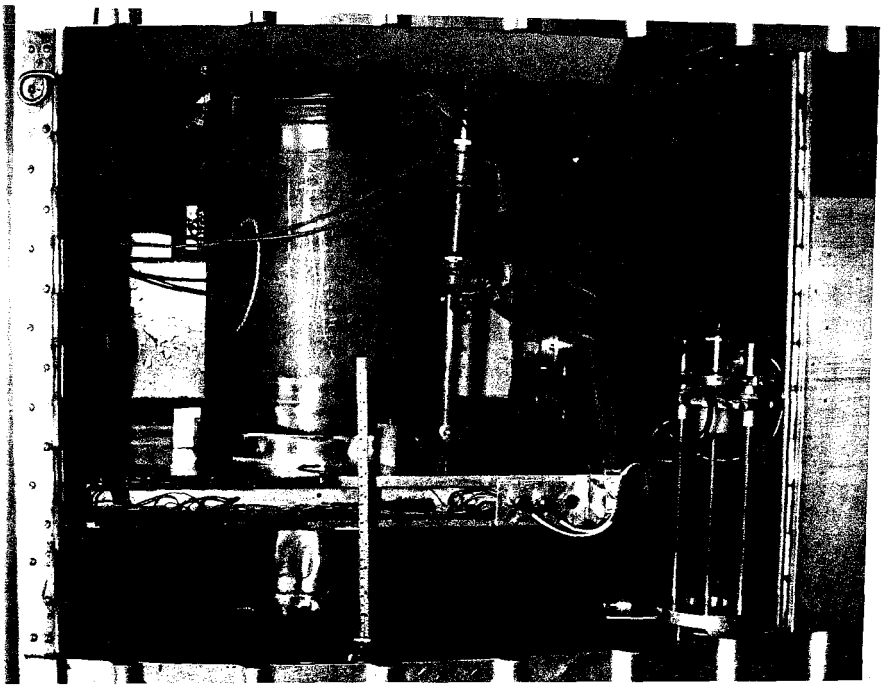

Figure 2.3 New bucket for pile driving experiments

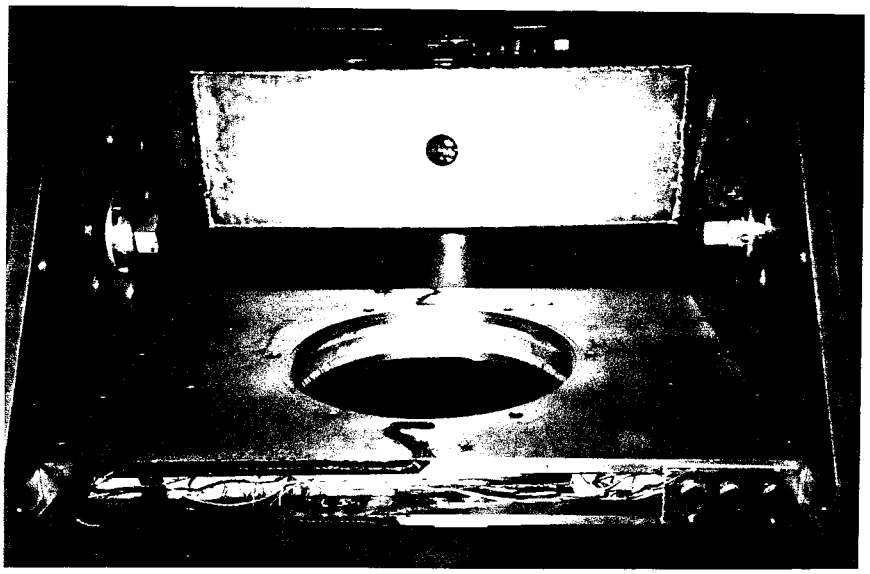

Figure 2.4 The centrifuge platform for the large pile container

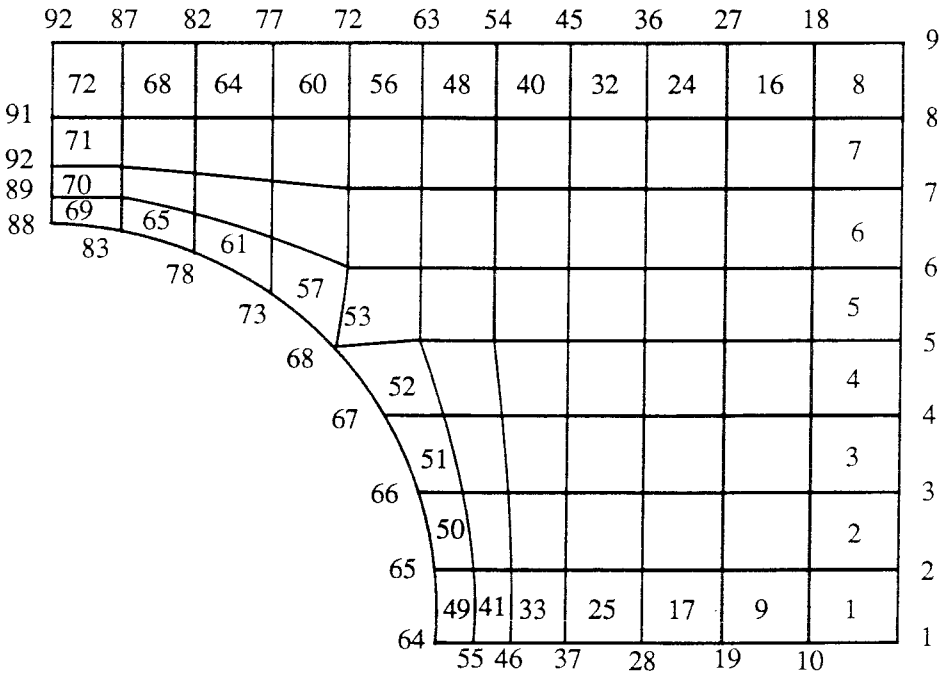

Figure 2.5 Finite element mesh for the analysis of the platform

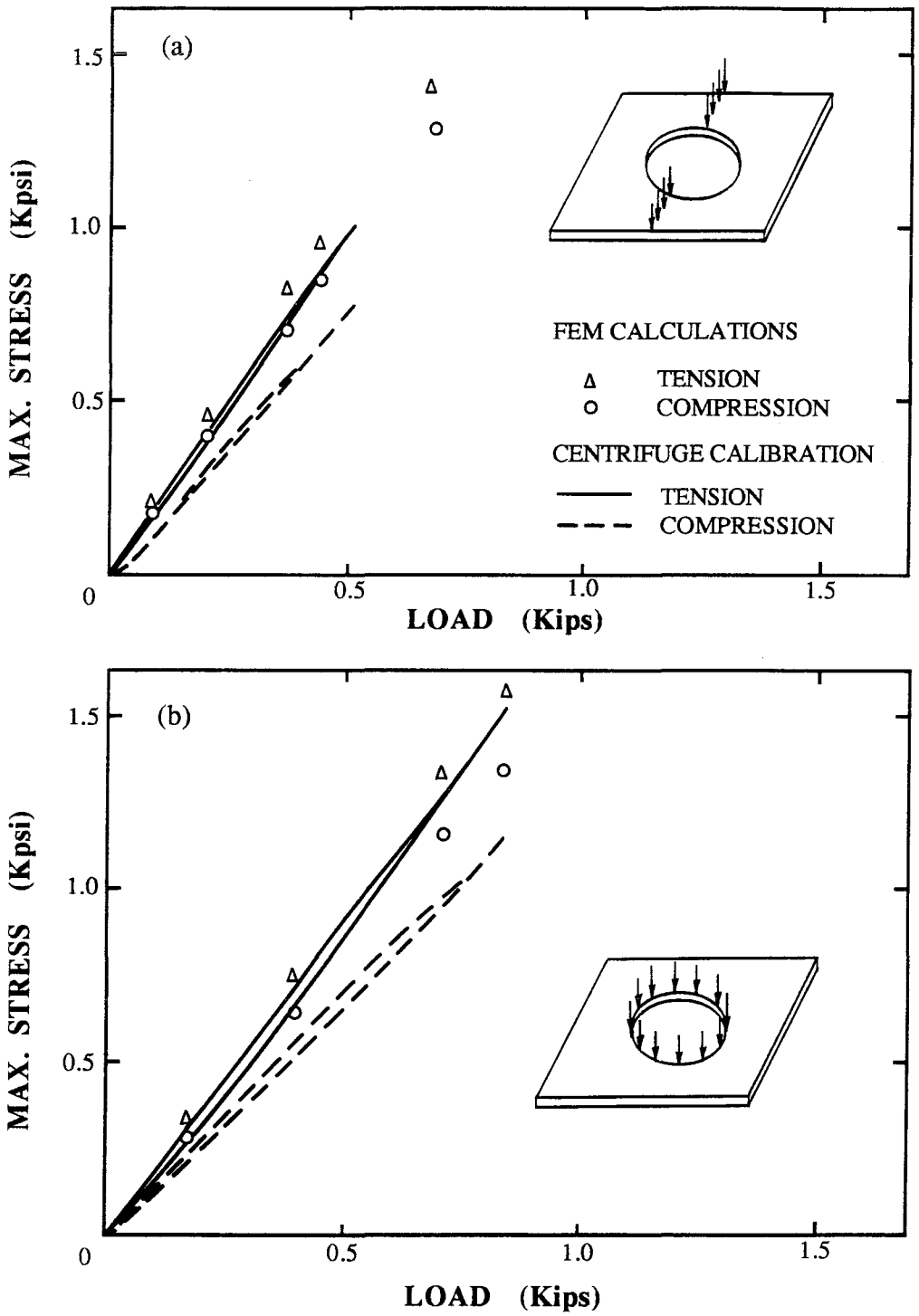

Figure 2.6 Comparison between the experimental calibration and the finite element analysis of the platform
(a) Load applied along the center axis for maximum bending
(b) Load applied along the circumference of the center hole: soil container in place

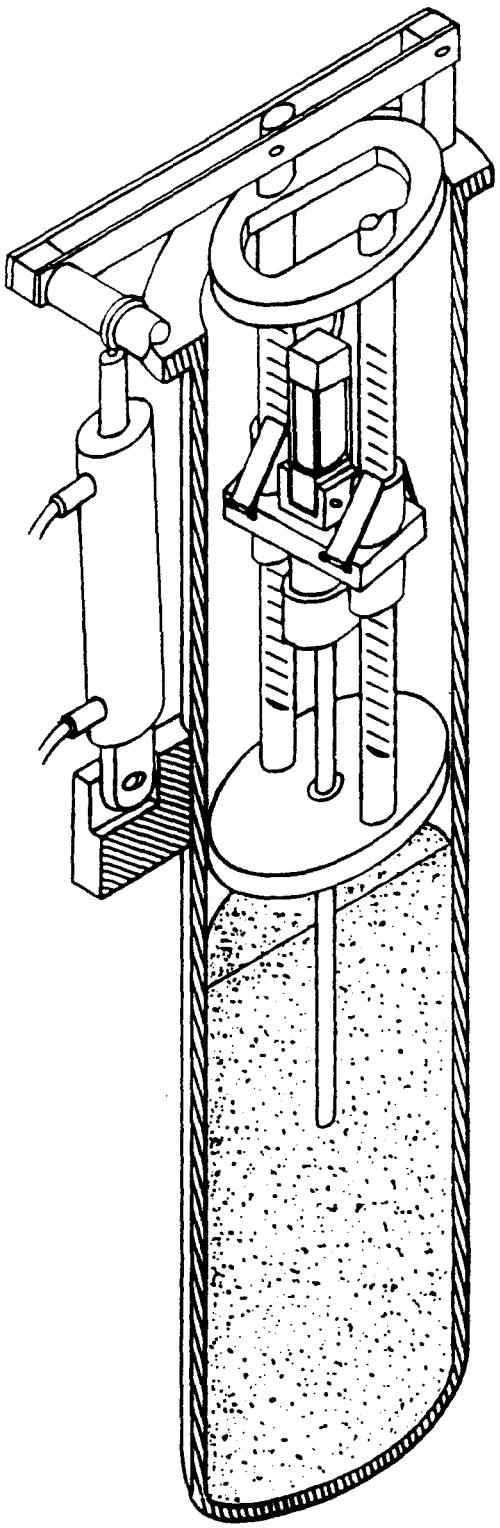

Figure 2.7 Apparatus for pile driving and axial loading

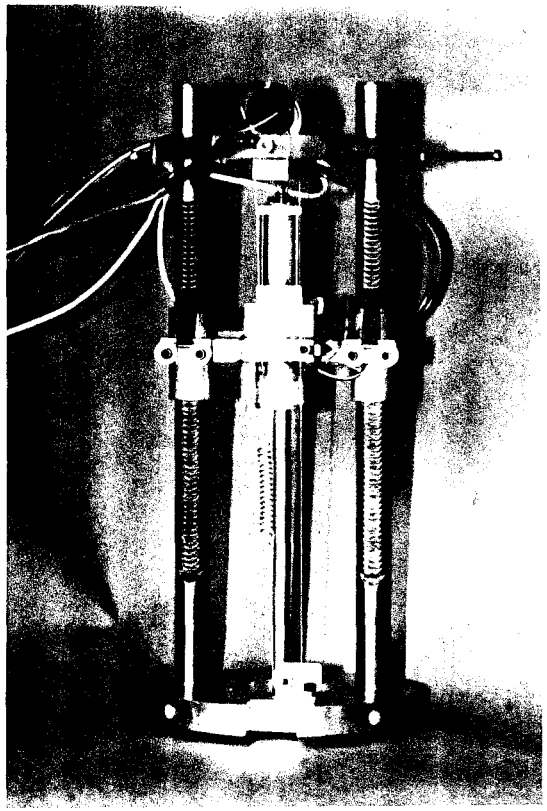

Figure 2.8 The pile driving mechanism

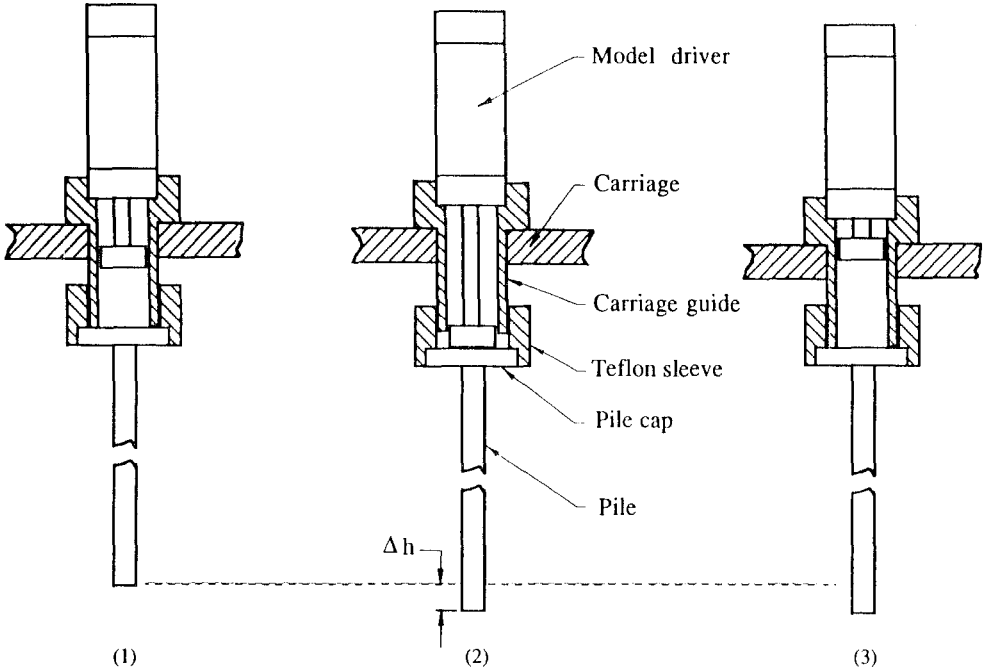

Figure 2.9 Driving cycle

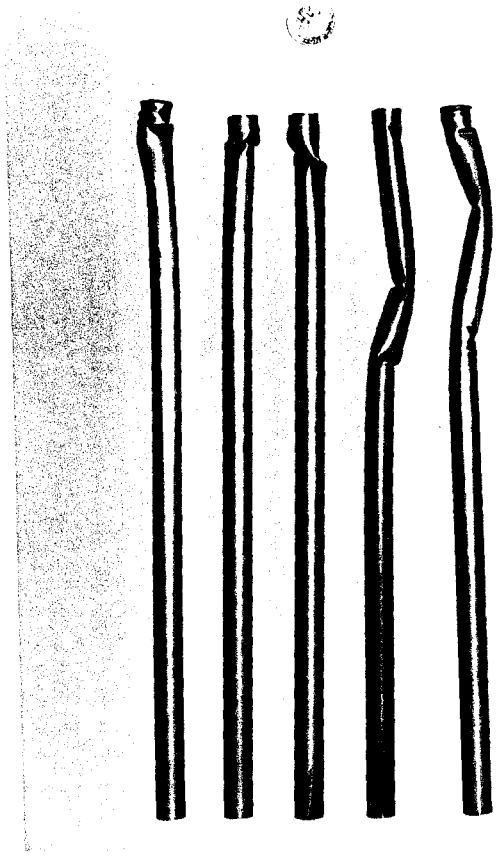

Figure 2.10 Buckled piles

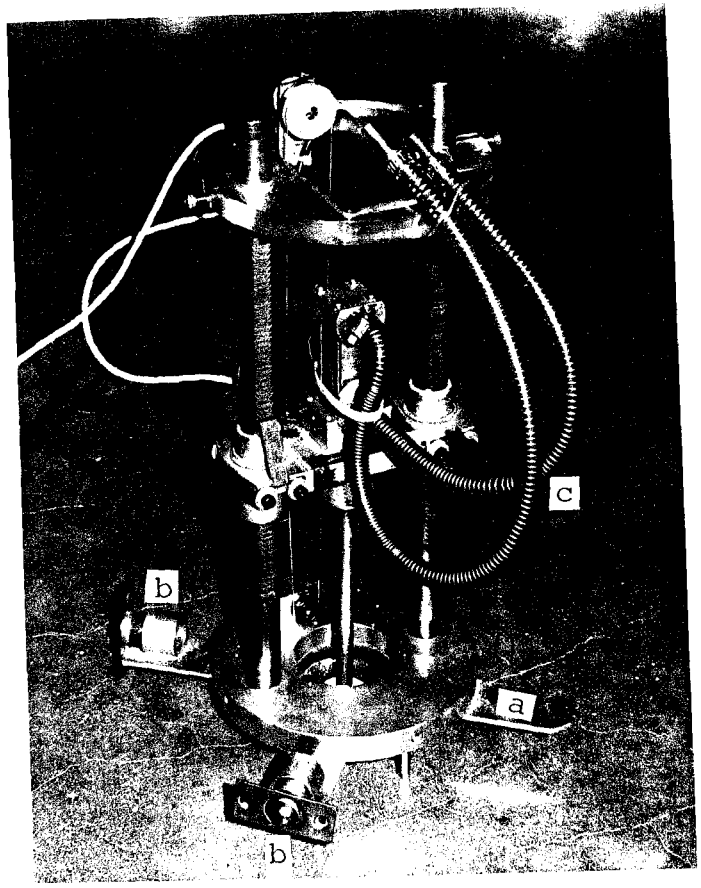

Figure 2.12 Pile driving mechanism
a = extension leg
b = spring loaded ball bearing
c = reinforced flexible tubing

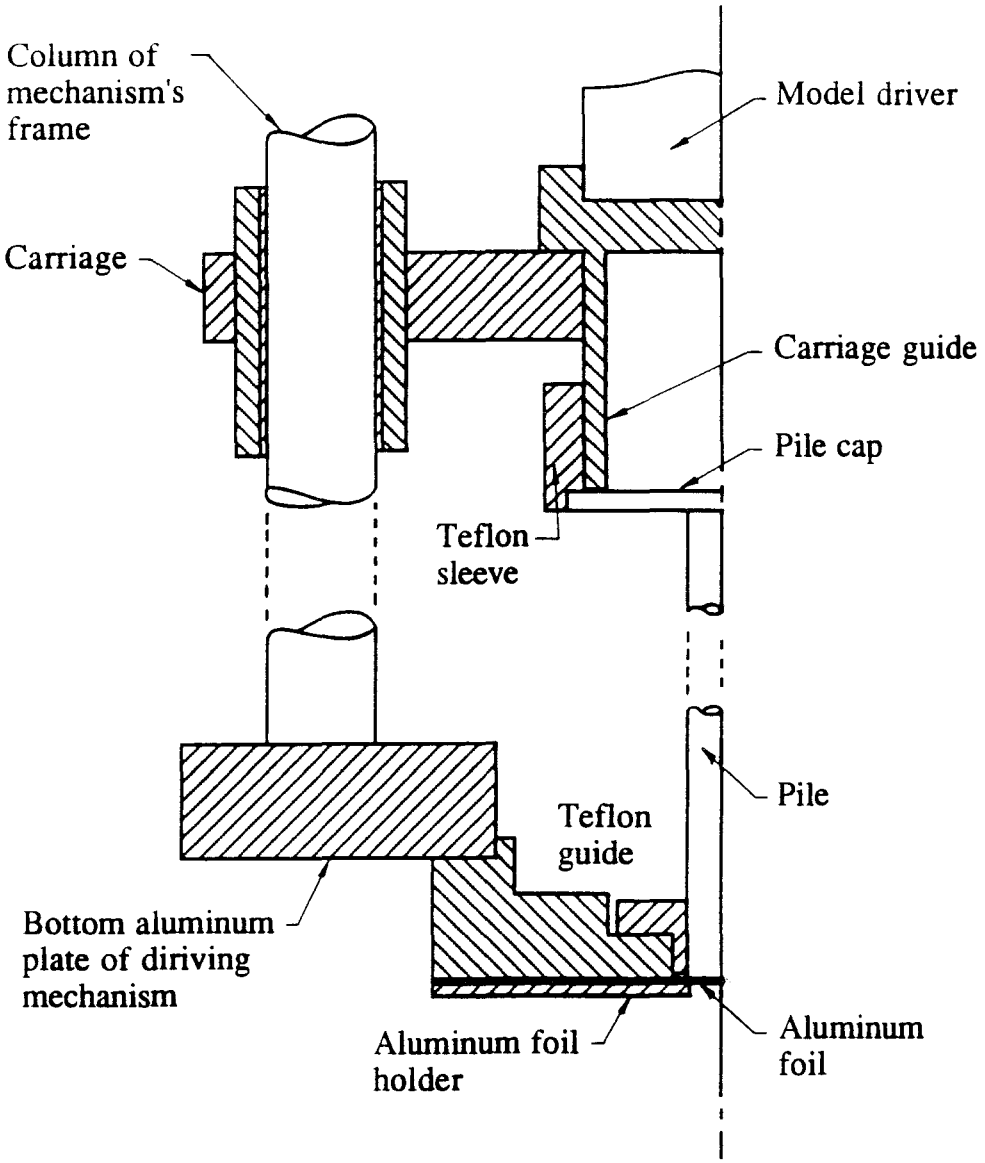

Figure 2.11 Guiding and holding of the pile in the pile driving mechanism

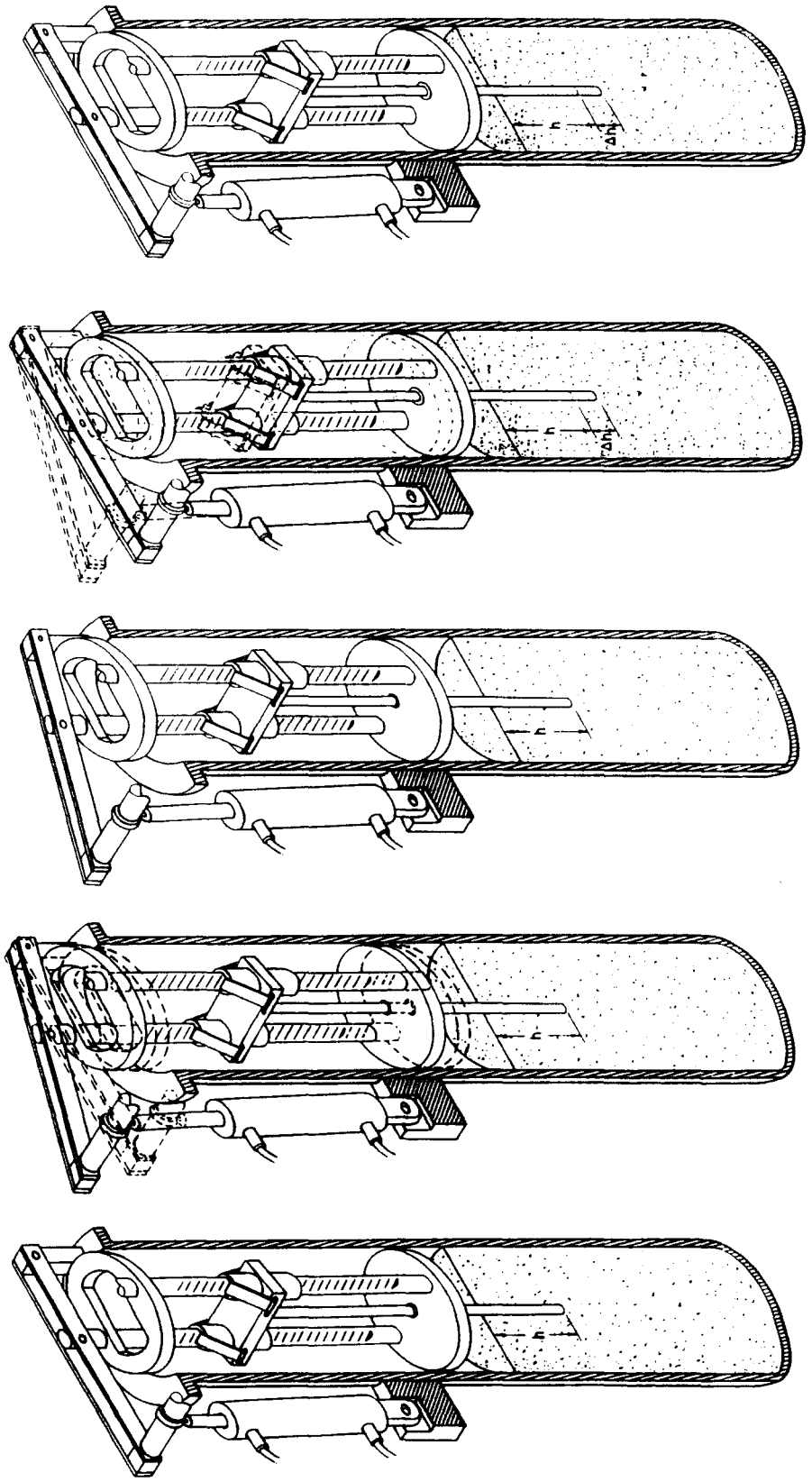

Figure 2.13 Pile axial loading sequences

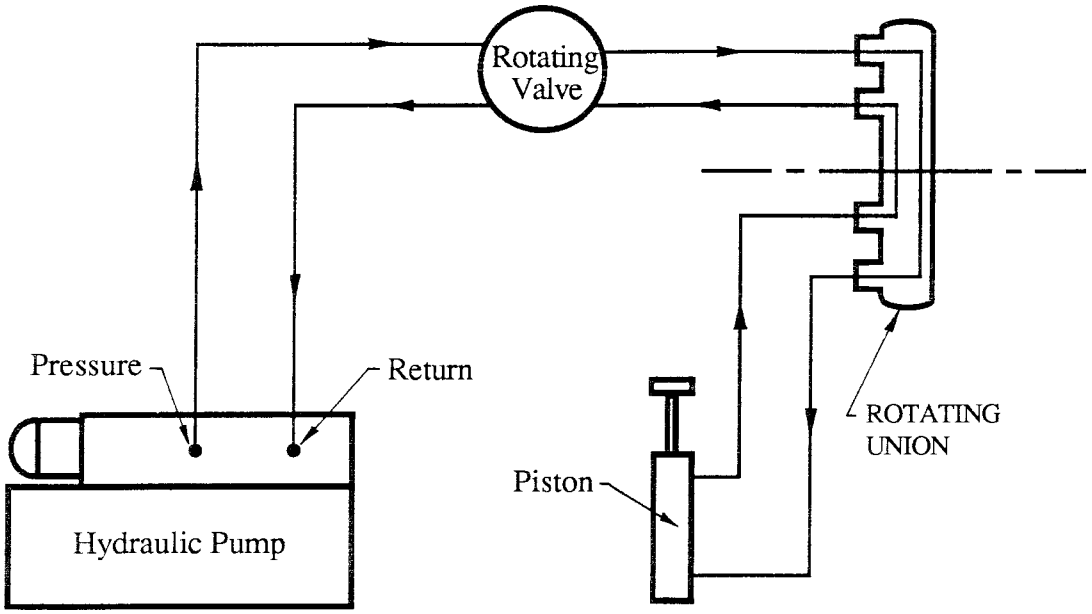

Figure 2.14 Hydraulic circuit for the static axial loading mechanism

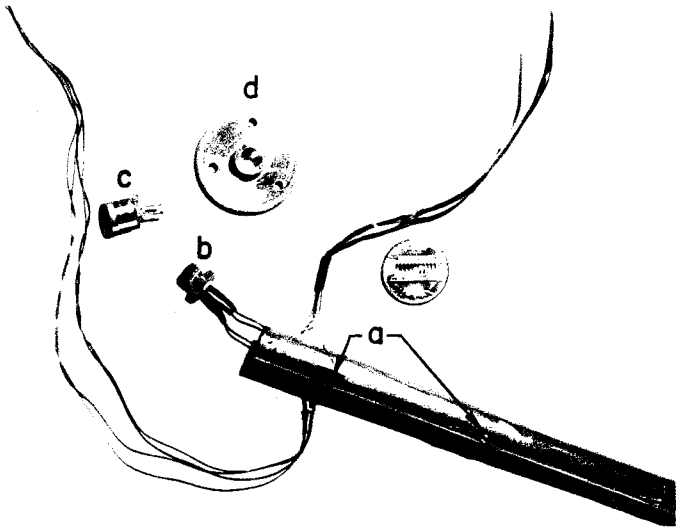

Figure 2.15 Instrumented model pile
a = strain gage
b = shock accelerometer
c = shock accelerometer in pile plug
d = pile cap

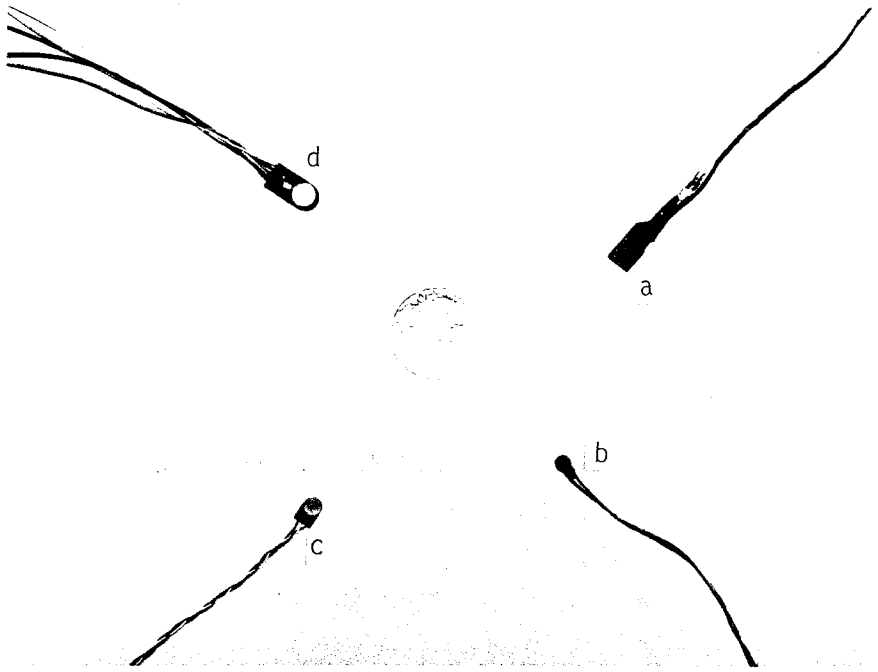

Figure 2.16 Miniature pressure transducers
a = Precision Measurement 156, type #2
b = Precision Measurement 105-S, type #3
c = Precision Measurement 105-S (1/2brige), type#4
d = Entran Devices EPL-200, type #1 and #5

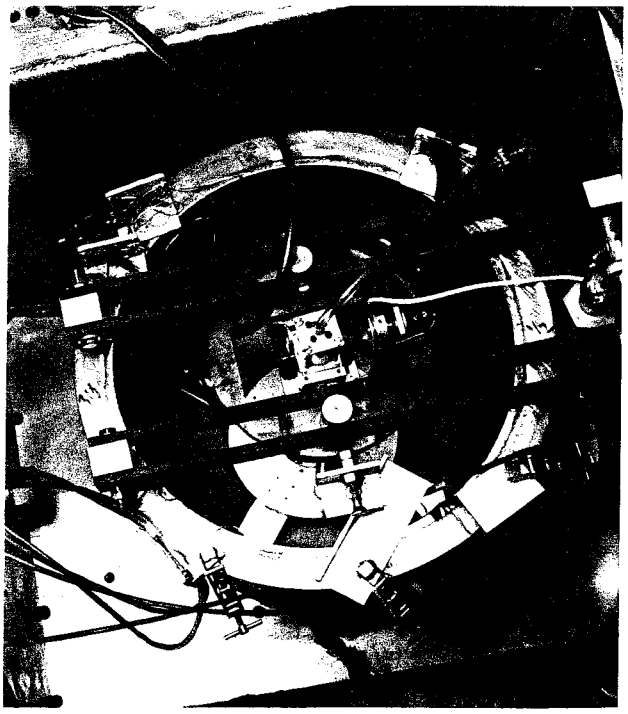

Figure 2.17 Top view of pile driving mechanism in soil container

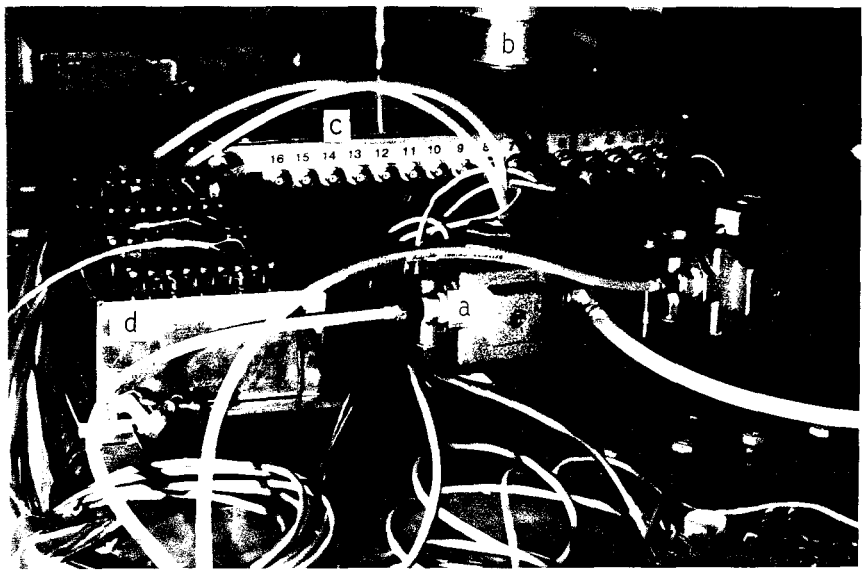

Figure 2.18 View of some of the signal conditioning and mechanical equipment mounted on the centrifuge arm
d = solenoid valve for the pile driver air supply
b = rotating union
c = 16-channel amplifier
d = 8-channel high speed amplifier

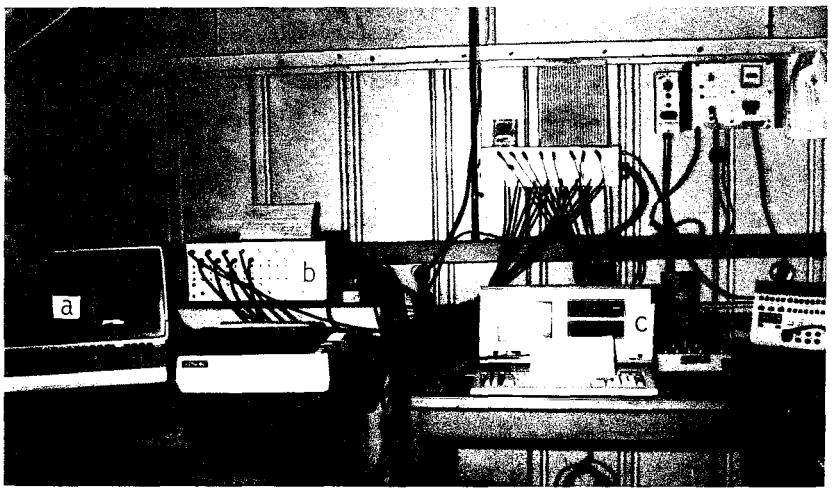

Figure 2.19 Data acquisition
a = Zenith 120 Personal Computer
b = Signal Conditioner and data acquisition system
c = Zenith-148 Personal Computer with RC Electronic high speed data acquisition card

Chapter 3

TEST PROCEDURE

3.1 EXPERIMENTAL SETUP

The experimental platform at the end of the centrifuge arm rotates into position during the wind up of the centrifuge to the test acceleration. This allows preparation of the soil model at 1 g in the soil container directly in place on the centrifuge arm.

Part of the electronic support for the different transducers is placed directly on the centrifuge arm. This consists of the power supplies, and everything that corresponds to first stage signal conditioning as mentioned in section 2.4. Also the solenoid valves, the air reservoir for the pile driver, etc., are located on the arm. Because of the acceleration level generated in the centrifuge, all the equipment and instrumentation must be fixed tightly to the centrifuge arm, and placed as close as possible to the center axis where the acceleration level is the lowest, see Figure 2.18.

3.1.1 Description of soil

The soil was a Nevada 120 silica sand, referred to as Nevada fine sand. This sand is uniform and fine-grained (mean grain size is 0.1 mm); a grain size distribution is shown in Figure 3.1. The sand density ranges from 88 pcf, in its loosest condition, to 108 pcf, in its densest state. The minimum and maximum void ratios are 0.53 and 0.82 respectively. In all the tests the soil was dry and prepared in a medium state with a density of about 99 pcf, equivalent to a relative density of 57.5% and a void ratio of 0.65. The friction angle for the medium density sand is about 35°. Laboratory experiments such as resonant column tests and ultrasonic pulse tests were conducted on the Nevada fine sand by Hushmand [73] to determine the dynamic properties of the soil. A Poisson's ratio of 0.3 was measured, and the shear modulus of the soil increased with the 0.47 power of the confining pressure, which is in close agreement with the average value of 0.50 derived for

other dry sands. For the sand at a void ratio of 0.7, the shear modulus G varied from about 4.6 x 10^3 psi at a confining pressure of 2 psi, to 21.1 x 10^3 psi at 50 psi.

3.1.2 Preparation of soil model

The sand was dried overnight in the oven in the laboratory at about 100^o C. Some soil samples were taken before placing the soil in the container, and after the experiment was completed, to check the water content. For the soil sample a uniform density distribution was desired. The sand raining techniques as discussed by Bieganousky and Marcuson [14] were not adequate for our soil. Our sand is a uniform fine sand with typical particle size is 0.1 mm., as shown by the sieve analysis in section 3.2.1. Some raining experiments done in the laboratory with a single hose showed that, by increasing the height of drop from 1 inch to 2 feet, the density of the soil would only increase from 88 to 91 lb/ft^3. Therefore in order to cover a wider range of densities the soil had to be first rained and then compacted in the container by layers. For the experiments the soil was placed in the container in layers of constant thickness (1 or 2 inches). Compaction was performed by giving a determined number of blows on a circular plastic plate placed over the soil and fitting just inside the container, to obtain level layers. For the determination of the stress field or the accelerations in the soil around the pile during driving, we used transducers placed in different locations in the soil. For each transducer in the soil, there are three parameters to define its position: depth, radial distance from the pile, and orientation. We chose in the model increments of 1 inch for the different depths, radial distances of 0.5, 1.0, 1.5, 3.0, 4.5 inches, and two different orientations: one for radial and one for vertical stress. At a desired depth, with the soil level, the pressure cells were placed using a cardboard cross with indentations to give the different positions. Special care was given to the positioning of the wires to limit their interference. For example, for a pressure transducer placed to read radial stress around the pile, the wires first describe an arc of radius equal to the radial distance of the cell, then cross the soil container to reach the wall where they are attached with electrical tape. When all the transducers for a given depth are in place the sand is rained and then compacted for the subsequent layers, until the next transducer level is reached. The soil density is then calculated according to the weight of soil put into the container and the volume attained.

3.1.3 Equipment and instrument setup

When both the soil and all the instrumentation are in place, the pile and the driving and axial loading mechanisms have to be set up.

A rotating union placed at the very base of the centrifuge axis brings two air tubing lines inside the centrifuge. One of them is connected to a small air reservoir installed in the arm next to the solenoid valves. The air runs from the air source of the building or a compressed air bottle to the reservoir through the rotating union. The reservoir feeds the two solenoid valves. Each valve is connected to one of the chambers of the model pile driver through heavy wall flexible hoses. Because of the downward motion of the driver the last part of the tubing must be flexible enough to bend inside the container and the driving mechanism without provoking resistance to driving. At the same time the tubing must maintain a certain rigidity to limit the interaction with the air flow. To achieve this we used flexible PVC tubing with an outside spring reinforcement as seen in Figure 2.12. The solenoid valves that control the flow of air in and out of each chamber of the model driver are operated by the computer in the control room, which sends signals to two electronic relays that in turn switch on and off two solid-state relays placed next to the valves that activate them. The air-flow through the driver and therefore the rate of driving is then software-controlled throughout an experiment. The air pressure in the line is set by a pressure regulator. The functioning of the model driver is checked at 1 g before each test.

The pile with all its instrumentation is then set in place in the pile driving mechanism. The carriage is at its highest position, the top guide is moved into position, and the bottom guide and the pile holding mechanism are then installed. The driving mechanism, with the pile in place, is now introduced in the upper part of the container and attached to the horizontal rods by the columns of the frame. The linear potentiometer that measures the pile driving mechanism's frame position relative to the bucket is connected. The different signal conditioning electronic packages (strain gage completion bridges, temperature compensation modules,etc.) are clamped to the bucket top flange. The horizontal rods of the pile driving mechanism are attached to the hydraulic piston of the axial loading mechanism and the link between air hoses and tubing is secured. All of the equipment is then in place for the experiment.

We now take care of the connections to the different centrifuge signal conditioning devices. Figure 3.2 gives an overall view of the signal processing arrangement. Here we deal with all that is required to bring the output of each transducer to a slipring. First, we make sure that each instrument gets its required input voltage. The different power supplies are attached inside the centrifuge arm. We chose to have 110 VAC run through 2 or 4 sliprings from the main power supply to the inside of the centrifuge, and make the transformation to the different voltage requirements there: 3, 5, 10, ±15, 28 VDC; 24 VAC, etc.; this permits the use of sliprings for signal output and controls. For the transducers placed in the soil, the very thin teflon coated wires of the cells run all the way to the top of the container to an aluminum angle where the connections to the completion bridge or temperature compensation module are made. From there larger wires run to the power supplies for input and amplifiers for output. This is also true for the instrumented pile whose strain gage completion bridge box is fixed on the container top flange. We do this in order to have the shortest length of wires for the bridges, as we look for bridge unbalances caused by very small changes of resistance of the strain gages. After the completion of the bridge the wires' impedance is not critical any more. The output of the transducers is connected to the amplifiers and signal conditioners for first stage signal processing; these are fixed on top of the arm. After conditioning, the output is connected to the sliprings for transfer to the control room and data acquisition systems. Some transducers do not require first stage conditioning, and their output is then directly plugged into banana sockets, which are connected to sliprings.

To avoid a "ground loop," which generates 60 Hz noise, all the instruments are connected to the same ground. The reference ground is the centrifuge structure.

All the wires running between the different instruments are firmly attached to the arm of the centrifuge with hose clamps and tape. The slack and attachment of all the wires is checked.

3.1.4 Signal processing implementation

The output of each transducer is treated according to the requirements of the experiment. The overall view of the signal processing arrangement is sketched in Figure 3.2. The first stage offsets and amplifications are set, taking into account the expected output during the experiment, the characteristics of the instrumentation, and making sure

that the signals are as strong as possible before getting through the sliprings, for we know that more noise will be introduced at that stage. In the second stage, where the signal may be offset and amplified again, and also filtered before getting to the acquisition systems, we aim at using the data acquisition range as fully as possible.

The potentiometers have a large input voltage, so that their output is up to several volts. Their signals are then fed directly through the sliprings to the second stage signal conditioner for filtering of high frequency noise before acquisition. The beam load cell output is amplified and offset in the centrifuge, and only filtered in the second stage. The shock accelerometer signals have a special conditioning. The piezoelectric transducer is effectively a capacitor that produces a charge across its plates, proportional to the force applied to the crystal. Our transducers have their own integrated electronics that provide a voltage output, which is then sent directly to the acquisition system. For the bender elements we use the high speed amplifier of the centrifuge at a gain of 10, with a shunt resistor of 2KΩ. There is, of course, a choice of the combination of gain factor and resistor value. The voltage signal obtained at the output of the amplifier is not further treated. The soil accelerometers and pile strain gage bridge ouputs are amplified in the centrifuge through the high speed amplifier, and have no other conditioning before acquisition. The pressure transducer signals are first amplified and offset in the centrifuge, and then amplified again and filtered in the signal conditioner before being fed to the acquisition systems. Two stages are used to get the best output, taking into consideration the level of the gain, the problems of offset, and frequency response. The RPM signal is fed directly to the computer at a different address from the one of the acquisition system.

3.1.5 Progress of an experiment

The preparation, setup, and development of an experiment requires a large number of steps. A check list that covers geotechnical, mechanical, electronic and computer checks has to be followed. We will mention here some of the important points that need to be checked before starting an experiment:

* the preparation of the soil sample and all the different instruments
* the balance of the centrifuge arm
* the functioning of the model driver and of the axial loading mechanism

* the connections and attachment of every part inside the centrifuge enclosure, to make sure that nothing will get loose during flight
* the signal conditioning: input voltages, output-settings, offsets, gains, filters, noise level, ground-loop, cabling continuity and coherence
* the control of the relays for the model driver, and of the different steps of the experiment
* the data acquisition: the software is run and the files are checked. For each new test we have a new setup of transducers and data acquisition files are prepared accordingly.

The experiment then proceeds in several stages:

1. the winding up of the centrifuge to the test acceleration level. At different RPM levels data is taken. We record the RPM as a reference for the calculation of the acceleration; the output of the soil transducers to follow their behavior and check calibration values; the potentiometer output from which the position of the pile tip is calculated, (we want to make sure that the pile is held in place before starting driving); for an instrumented pile, the output of strain gage bridges to check calibration, and for the experimental platform we monitor the level of stresses with the output of the strain gage bridges.
2. the driving phase: the centrifuge is at the test acceleration. The air source is open, and air pressure regulated; data acquisition is checked for the different systems. The pile driving proceeds: the Z120 computer sends the signals to the relays to control the model driver, and, after each blow, acquires data from the potentiometers, the load cell, and the pressure transducers, and gives the signal for the trigger of the high speed acquisition system. We record dynamic data only every nth blow, where n is chosen at the beginning of the experiment. High speed data acquisition then automatically triggers on the signal from one of the transducers (pile top accelerometer in general), and the data are saved on file in the hard disk after each trigger. The dynamic signals can be seen on the computer screen. The pile tip depth is displayed on the Z120 screen at each blow, as well as the current output of the transducers. This allows us to monitor the test and possibly make decisions to change the setup or stop the test.
3. the axial loading test. We know that the pile has reached the depth of interest, so the model driver is stopped, the hydraulic pump started, and the hydraulic piston

connected to the pile driving mechanism is activated to perform a loading test. Data from the potentiometer, the load cell, and the pressure transducers is saved on file.

4. the axial loading test can be repeated as many times as desired. After the last loading, pile driving can be resumed. The cycle driving plus axial loading can be repeated as needed.

5. winding down of the centrifuge. Driving and axial loading are over, so we now bring down the centrifuge to a stop. In the same way as for winding up, the different transducer output are recorded.

3.2 CALIBRATION OF TRANSDUCERS

Calibration tests are performed on all the instruments. Tests are sometimes done first in the laboratory because these are, in practice, easier to perform, and allow us to cover the calibration ranges of interest for the different transducers. But a calibration test is also run in the centrifuge in order to use the equipment in its test configuration and to use the entire experimental signal processing setup so that the specific experimental calibration values can be determined.

3.2.1 Accelerometers

The calibration of the shock accelerometers requires special laboratory equipment that is not available to us. Thus we rely on the manufacturer's calibration provided with the instrument.

The soil accelerometers are calibrated in the centrifuge. They are placed on the platform of the container's mounting frame, so that we know their exact distance from the center axis of the centrifuge. By winding up and down the centrifuge they will undergo different g levels. By recording their output as a function of the RPM, we easily obtain a calibration curve. We find a very good match between our calibration and the manufacturer's one.

3.2.2 Bender elements

The transducers are built in our laboratory out of a piece of piezoceramic material. We do not have adequate equipment to perform a quantitative calibration to relate their output to a stress level. However, for example, we can rely on the time domain

response of the transducers and obtain information on the velocities of waves in the soil. Some soil column experiments, using bender elements along with pressure transducers, have been performed in the laboratory, see section 3.2.5.

3.2.3 Displacement transducers

Our transducers use potentiometers, which are calibrated using a special structure with a fixed frame and a moving part whose motion is controlled by a micrometer. Then the calibrations are checked in the centrifuge with the instruments in their final position, with all the signal conditioning used during a test. The output are measured for given displacements covering the full range of the experimental setup.

3.2.4 Load cell

We calibrate the carriage load cell in an arrangement where the load is applied to the cell the same way as during an axial loading experiment following driving in the centrifuge.

In the laboratory, the carriage is in place in the pile driving frame, the whole frame is upside down, and the motion of the carriage is restrained by the ratchets. First we apply dead weights by increments and record the output signal, conditioned the same way as in the centrifuge. This method allows a calibration up to 100 lbs. Then, to increase the calibration range, we connect the mechanism to a compression cell, and apply a load up to 600 lbs.

In the centrifuge we have the pile driving frame in place in the container and the carriage inserted upside down so that it rests on the ratchets on the bottom aluminum plate of the frame. The centrifuge is spun up and down, which provides different g levels. Some dead weights are placed on the carriage where the pile exerts the force, and therefore a calibration check is obtained.

3.2.5 Pressure transducers

Each pressure transducer comes with a calibration performed by the manufacturer under hydrostatic pressure conditions. We know that under this condition these diaphragm-type cells will behave linearly. This is not true anymore when the cell is inserted into a granulated material. The presence of such a device in the material alters the stress

state that would otherwise exist. Measurement of a stress field in a soil medium requires an understanding of the interaction between the pressure gage and the surrounding media. Many factors affect the response of the embedded cell: the more important ones for our application are: the shape of the transducer (with its aspect ratio, its diaphragm deflection, its stress distribution characteristics, and the effects of the electrical connections) and its relative stiffness (material stiffness over cell stiffness). With all the problems inherent with the soil pressure-cell interaction it is not possible to find the perfect cell in the market, especially for centrifuge applications where the requirement on size is very strong. The actual construction of a prototype cell is not feasible for it requires very sophisticated fabrication methods. Therefore an extensive calibration is performed in the centrifuge with the different pressure cells that we use, in order to describe their specific behavior and arrive at subsequent stress predictions.

At first the cells are installed in a horizontal position on the bottom of a container, and the effect of gravity is checked by spinning the centrifuge up and down and monitoring the cells' output. As given by the manufacturer, the gravity sensitivity of the bare cell is negligible. Then a thin wall plastic bag is placed over them and filled with several inches of water. The cyclic winding up and down of the centrifuge allows us to check the values and linearity of the hydrostatic calibration; we obtained good agreement with the manufacturer's values. For the soil calibration, different configurations are tested: the cell can be placed on the bottom of the container and covered with soil, the cell can be placed in a special metal mount so that its sensitive face is flush with the soil interface, or the cell is simply embedded in the soil at different levels. Different soil densities are used. On a simple loading-unloading cycle, each cell embedded in soil exhibits an hysteretic behavior; it is therefore important to perform various repeated cyclic loadings to characterize this behavior. This is easily done in the centrifuge by increasing and decreasing the g-level, which in turn varies the stress applied to the cell. A typical cell response to a cyclic loading is shown in Figure 3.3. This static cyclic calibration of a soil pressure gage shows that the behavior cannot be reduced to a linear assumption, but can be represented by a model as described in Chapter 5.

The pressure cells are also calibrated qualitatively for their dynamic response. For this we use a soil column experimental apparatus. A 1 foot long and 1 inch diameter soil column enclosed in a thin rubber membrane tubing is connected at both ends to a 1

inch diameter steel rod, arranged so that a vacuum can be applied to the soil. The entire steel-soil-steel column is suspended horizontally, by means of hangers, to a rigid frame (see Figure 3.4). A hard steel ball that rolls down an inclined aluminum tube impacts the free end of one of the steel rods connected to the soil column. A bender element is placed at the interface soil-rod. After impact of the ball a wave will propagate in the steel rod. If the impact is not too long and the rod is long enough, the wave can be approximated as plane. On reaching the boundary with the soil the wave will propagate into the soil with a new velocity, depending on the characteristics of the soil, and will also reflect back into the rod. The wave in the steel rod will bounce back and forth many times and decay according to the steel properties. Similarly the wave in the soil will bounce back and forth and decay. The transducer placed at the interface between the soil and the rod will be able to pick up the waves in the rod and in the soil. The typical output is a superposition of 2 decaying sine waves, one of higher frequency corresponding to the wave propagation in the steel rod, on top of a lower frequency wave that corresponds to the propagation in the soil. Figure 3.5.a and b shows the signal from three transducers, the first one (top signal) is at the soil-impact bar interface, the second one is embedded in the soil column, 2 inches away from the impact rod, and the third one is at the end of the 1 foot long soil column. Figure 3.5.b is an enlargement of first portion of Figure 3.5.a. The impact is propagated through the steel rod and gets to the soil column when the top signal starts. The wave propagating in the soil is picked up by the other transducers, and the wave velocities in the soil can then be determined from the output signal of the transducers. The high frequency vibrations in the top signal correspond to the wave reflecting back and forth in the steel rod. From it the wave velocity in the steel can be calculated. By using several transducers and subjecting the soil column to different vacuum levels, the wave propagation speed and the Young's and shear modulus of the soil under various confining pressures can be determined. Also by shortening the length of the impacted rod we increase the frequency of the wave propagating in the rod, and can then test the frequency response of our transducers. We want to understand the response of the transducers to dynamic loading and see if their dynamic response can be assumed to be linear or if their behavior and interaction with the soil under dynamic loading has to be represented by a model too. This is important for us in our application to pile driving for we know that at each blow the soil is subjected to dynamic loading. Therefore, in our estimation of the overall "static" stress field changes

during driving we have to keep in mind that dynamic loading occurs at each blow. Refer to Chapters 5 and 6 for more detailed discussion.

3.2.6 Strain gaged piles

A theoretical calibration of the strain gage bridge is easily obtained using the output equation of the Wheatstone bridge (see Appendix B). This gives us a good estimate of the sensitivity of our strain gage bridge, but we perform experimental calibrations to obtain our final values.

The instrumented pile can be calibrated in tension and in compression in the laboratory. To apply load in tension on the pile we use a special setup that utilizes two sets of plugs and clamps that fit the pile tightly. The first one, attached at the top of the pile, is connected to a plate that will allow us to fix the complete mechanism to a bench (see Figure 3.6). The second one, attached at the bottom of the pile, has connected to it a rod with a loading platform. Weights are placed on the platform, the pile is then subjected to axial tensile force. Calibrating under tension induced by dead weights, we have the advantage of knowing exactly what the force applied is, and we avoid pile bending. But, for practical reasons, this method limits the range of calibration. To check the calibration value on a larger range of force we use a compression cell. This time the pile is submitted to an axial compressive force. In order to eliminate bending, the pile is placed in the pile driving mechanism, and the use of the guiding mechanism ensures a proper positioning of the pile in the compression cell.

The pile is calibrated in the centrifuge using the pile axial loading mechanism. With the pile in place in the mechanism, we replace the aluminum foil of the holding mechanism by a plate that prevents any displacement of the pile. A calibration with dead weights resting on top of the carriage is then performed using centrifugal force. Otherwise, with the centrifuge at rest, calibration can be done with the loading mechanism; this time the plate that prevents pile motion is placed on top of the soil. The motion of the frame due to the pulling down with the hydraulic piston is transmitted through the carriage to the pile. Because of the plate on the soil the pile cannot move down and therefore undergoes compression. We rely then on the beam load cell calibration. We may note that, during the winding-up stage of an experiment, the pile is held in place, at its base, by the aluminum

foil, and is under compression due to the added weights of the carriage and the model driver, directly applied at its top.

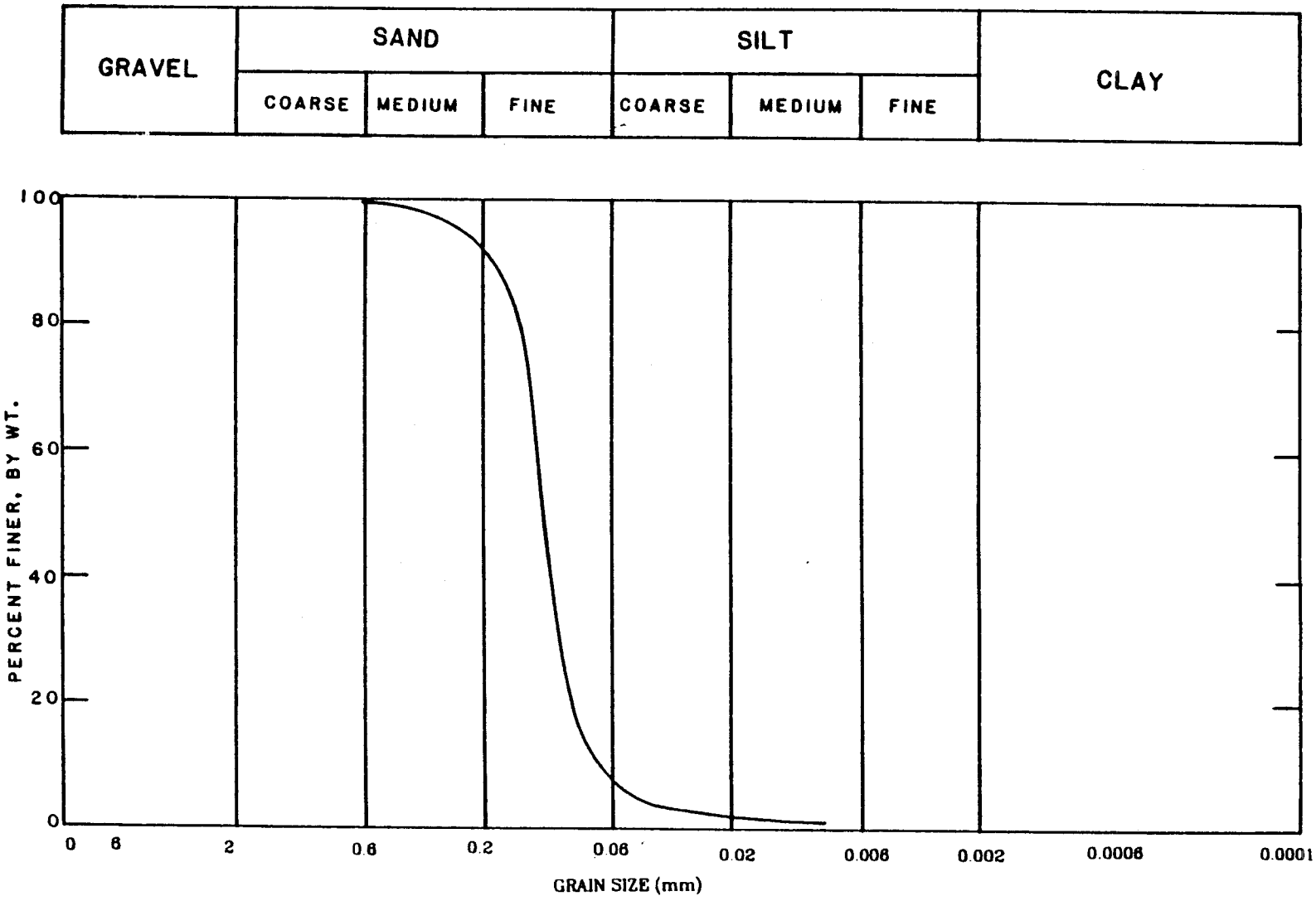

Figure 3.1 Grain size distribution of the Nevada silica 120 sand

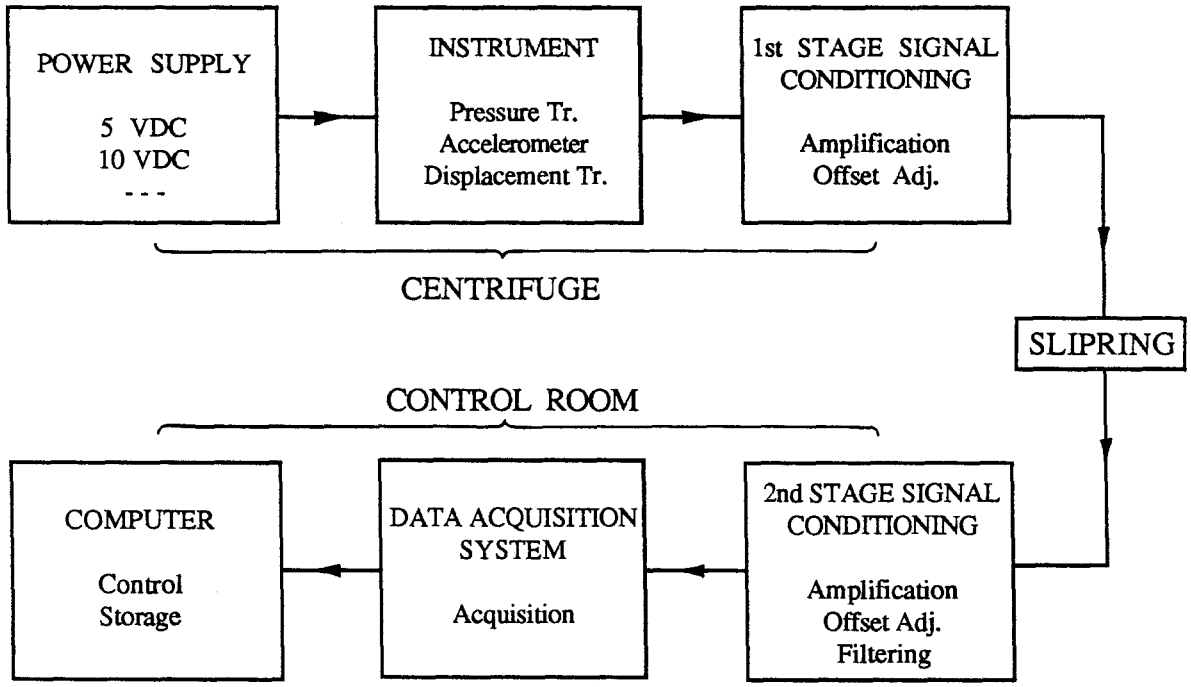

Figure 3.2 Signal processing implementation

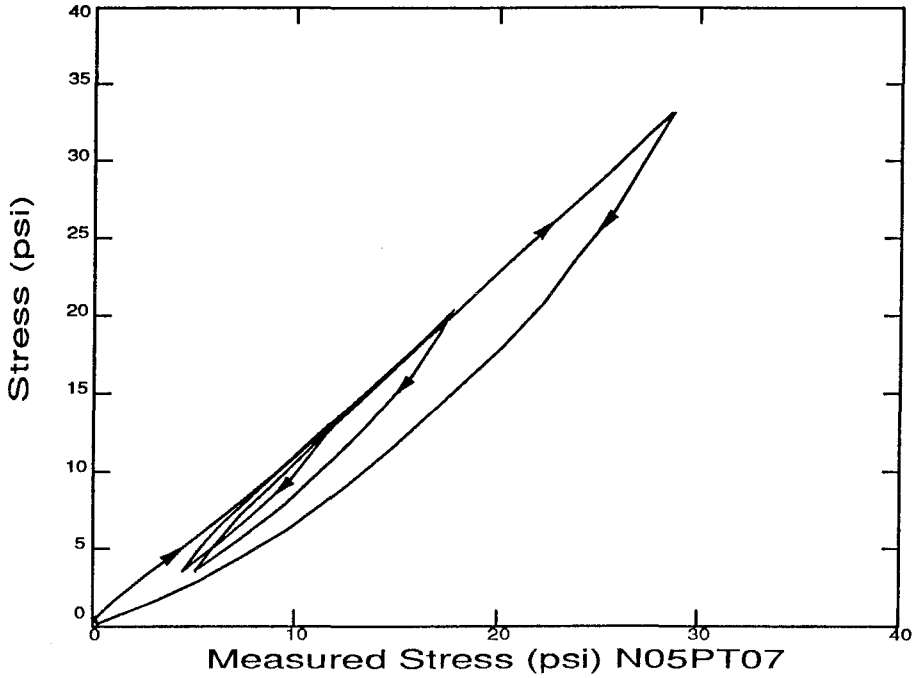

Figure 3.3 Pressure cell response to static cyclic loading

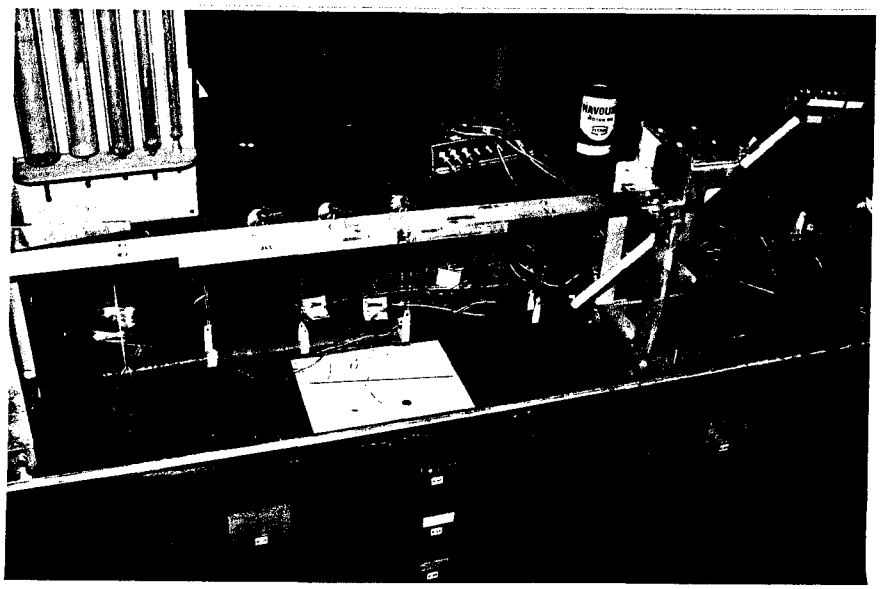

Figure 3.4 Soil column experiment set-up

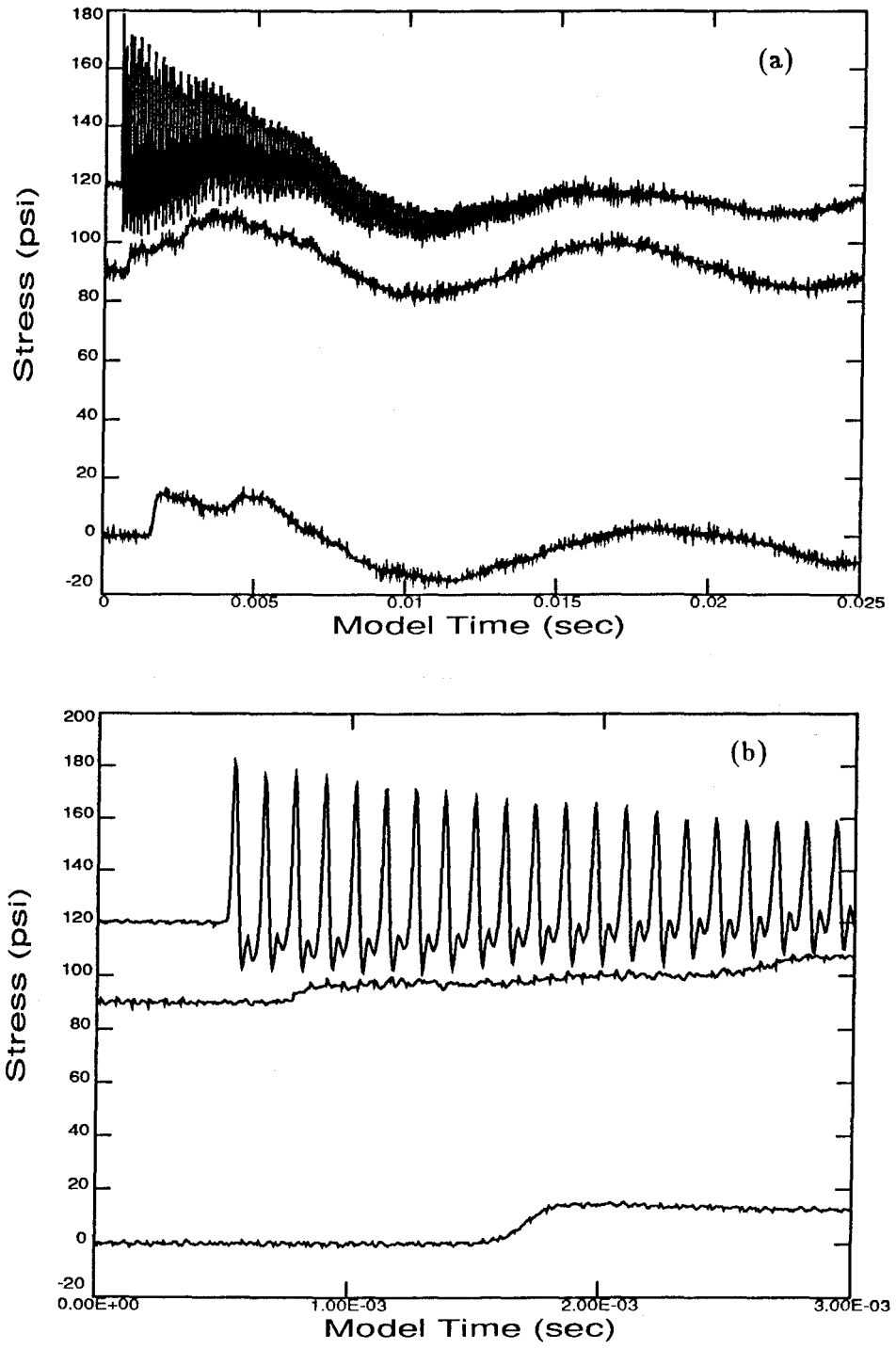

Figure 3.5 Soil column experiment
(a)Pressure cell responses to waves propagating in rod and soil
(b)Wave velocitites in rod and soil

Chapter 4

SELECTION AND REDUCTION OF DATA

4.1 SELECTION OF DATA

Pile driving is a complex process governed by a great number of parameters resulting from the soil properties, pile, and pile driving equipment characteristics. Experimental work on pile driving, and more specifically model testing performed in a centrifuge, is further complicated by the availability and requirements of the instrumentation, and mechanical limitations. To alleviate some of these problems, we have chosen and fixed most of the parameters throughout the tests that were conducted using the same soil, same pile, and same driving equipment. This has enabled us to focus on and study in depth the physical phenomena occurring during pile driving.

Taking into consideration the various constraints in equipment and instrumentation, led to the following choices. The experiments were conducted at an average gravitational acceleration of 50 *g*s. The model pile of 10 inches length, 3/8 inch diameter and 0.01 inch wall thickness corresponded to a prototype pile of 41.7 feet length, 18.75 inches diameter and 0.5 inch wall thickness. This is a full scale pile of comparable dimensions to actual prototype piles, with a somewhat large wall thickness (the .006 inch wall thickness tube available in the first series of experiments gave a 0.3 inch prototype wall). The soil used was a fine Nevada sand whose average grain size is 0.1 mm. Because of the small grain size, the modeling considerations allowed for the use of the same soil in the model experiments as in the equivalent full scale prototype. The soil is placed uniformly in a medium density and dry condition. It was mentioned in Chapter 1 that one of the difficulties of full scale experiments lies in the uncertainty associated with soil characteristics. The uniformity of the model soil, and the choice of a dry condition reduces the level of complexity for the analysis of the pile-soil system during driving. The study of driving in a saturated soil would bring about a lot of pertinent information, but this implies a different system with a

more complicated analysis, that goes beyond the scope of the present work, which aims at understanding some of the fundamental physical phenomena governing pile-soil interaction during driving.

The selection of data is defined not only by the set of parameters that should be measured to give a proper account of the physical phenomena, but also by the availability of the instrumentation required. In each of the following paragraphs we have identified for each physical parameter, the measures taken or the reasons preventing their attainment.

4.1.1 Pile dynamics

In the past decades analysis and experimental techniques for the study of the dynamic response of a prototype pile during driving have evolved and become more sophisticated. The data available to us at the experimental level consist of measurements of strains and accelerations in the pile. Because of the practical difficulties and the high costs involved in the instrumentation of a prototype pile, a minimal instrumentation for the monitoring and analysis of the dynamic response of a real pile during driving usually consists of a strain gage bridge and an accelerometer at the top of the pile.

In our model experiments, strains and accelerations in the pile are measured, and sometimes this is done at different locations along the pile. Despite its small size, it is possible to instrument the model pile with pairs of strain gages along its length. The pairs of gages allow for the measurement of the axial strain (bending cancellation takes place in the Wheatstone completion bridge), from which we get the force in the pile at different locations. The first and last pairs of gages in our model are at 0.5 inches from the top or the tip of the pile. For the acceleration measurements, there are some limitations in what can be done at the model scale. Because of the scaling relations characteristic to centrifuge testing, we know that the acceleration amplitudes and the frequencies of the record will be N_g times larger in the model pile than in the prototype, where N_g is the experimental g-level, (see Appendix A). We also know that the acceleration at the top of the prototype pile due to the hammer impact reaches a level of several hundreds gs (g being the Earth's gravitational acceleration) (Goble *et al.* [56]); in our model this acceleration will then be in the order of several tens of thousands of gs. An available accelerometer that is small enough to be fixed to the pile, but yet fulfills these requirements, is the Endevco 2255-A-005 piezoelectric accelerometer, with an acceleration range of 100,000 gs.

As described in section 2.2.1, this transducer is about 0.3 in. in diameter and 0.3 in. long. Because of its size, it is not possible to attach it to the pile next to the strain gages as is done for prototype instrumentation. Instead, the transducer is fixed inside the top of the pile in the pile cap. The acceleration measured by the transducer is the acceleration of the pile transmitted to the pile cap, which is tightly connected to the pile. The measure corresponds to the acceleration of the top end section of the pile. Similarly, accelerations at the tip section of the pile are measured by a transducer fixed in a plug inside the pile bottom. This implies that when measurements of the tip acceleration are made, the pile is necessarily a closed-ended pile. Because of the connection of the pile cap and pile plug we have a pile with added masses at the top and the tip, which give dynamic response and driving characteristics different from those of a simple tubular pile.

Data from the accelerometers and gages are taken using the high speed acquisition system described in Chapter 2, at a minimum acquisition frequency of 250 KHz. The top accelerometer located on the pile serves as the trigger for the high speed acquisition system. Records of the pile response are saved on disk every tenth blow. Duration of data acquisition is in the order of 100 times L/c (where L is the pile length and c the wave speed in the pile, and L/c = 50 μsec. in the model). The pile dynamic response to the hammer impact will be over within a time in the order of a few times L/c, the data acquisition recording time is longer so that the soil dynamic data, which will cover a longer time history, can be recorded simultaneously.

4.1.2 Soil stress field during driving

To study the soil-pile interaction that occurs during driving and to estimate its influence on dynamic and static penetration, the evolution of the stress field around the pile is monitored throughout driving.

A representation of this stress field is obtained by measuring, using pressure transducers, the total stresses at given points in the soil as a function of the pile depth. The driving of a cylindrical pile in a semi-infinite soil mass, or a cylindrical bucket, is an axisymmetrical problem, so that the position of each transducer is defined by its depth and its radial distance, that is the distance from the center axis of the pile to the cell. On a horizontal plane, the orientation of the cell is such that either radial or vertical stress is measured.

In the model scale, increments of 1 inch were chosen for the different depths, which correspond to a non-dimensionalized depth increment, defined as depth over pile radius, of 5.33, and radial distances of 0.5, 1.0, 1.5, 3.0, and 4.5 inches that correspond to dimensionless distances (radial distance over pile radius) of 2.7, 5.3, 8, 16 and 24 respectively. In the first series of experiments (SA) the maximal dimensionless distance was 16, which corresponded to the bucket wall boundary. From previous work (*e.g.,* [8], [86]) we expected to find a very small excess stress generated at this distance due to driving. This hypothesis turned out not to be valid under our experimental configuration for pile driving in medium dense dry sand. The results that will be presented hereafter are the ones obtained with the large container, whose wall boundary is at a non-dimensional distance of 28.

The output of the transducers are recorded and stored at the end of each blow. Similarly the pile position is recorded at each blow, so that it is then possible to present the stress change due to driving as a function of the pile depth.

Soil pressure cells as described in section 2.2.5 are the only instrumentation currently used and available to measure stresses in a soil. The interpretation of the output signal of a pressure transducer embedded in soil, and its conversion to soil stresses requires a lot of caution. Chapter 5 deals with the understanding of the complex cell behavior due to the interaction with the soil, presents a numerical model used to describe the nonlinear cell behavior, and describes the various problems and limitations encountered in the interpretation of the transducer output.

4.1.3 Soil dynamics

Pile driving is a dynamic process. Different types of stress waves emanating from the pile-soil boundary will propagate into the soil. The overall stress field change that we measure as mentioned in section 4.1.2, is a result of the dynamic and static loading of the soil after each hammer impact on the pile. It is clear from all the existing methods of analysis of pile driving that the behavior of the soil during driving is still not well understood. The purpose of these model experiments is to look at what happens in the soil and how the stress change occurs in the soil surrounding the pile at the dynamic level. Therefore, to understand better the dynamic interaction of the pile and the soil under the impact of the pile driver, we monitor at the same time the dynamic stresses in the pile and the dynamic stresses in the soil around the pile.

The pressure transducers have a frequency response high enough to be able to record transient loading of the soil, *i.e.,* the waves propagating in the soil. The transducers measure the pressure normal to their sensitive area and their cross sensitivity is negligible. Therefore the transducer will respond to pressure wave (P) loading, but not to shear wave (S) loading. Because of the boundary condition due to the presence of the bucket wall we have reflection of the waves inside the container. The dynamic data from the pressure transducers is recorded using the high speed acquisition system, and stored on disk. For a blow, the record duration is equivalent to 10 times the travel time of a P-wave from the pile to the bucket wall, which allows us to see the decay of the dynamic stresses in the soil. The pile-soil-container system also has its dynamic vibration modes. Therefore the pile-soil dynamic interaction is specific to the experiment conditions and is somewhat different from the simpler case of a pile in an infinite medium. However, before the reflected front comes back from the wall, the vibration condition of contained and unbounded soil is identical. During the time it takes the fastest soil wave to reach the container, the compression wave passes in the order of 7 times down and up the pile.

4.1.4 Pile axial loading

The purpose of any pile driving monitoring and analysis is to be able to estimate, from the experimental data describing the driving conditions, the final bearing capacity of the pile in place in the soil. The correlation between the dynamic response of the pile during the driving and the final static response of the pile is still unclear due to a lack of understanding of the various physical phenomena involved.

The model experiments described here are aimed at obtaining both dynamic and static data for the uniform soil and pile system at different stages during penetration. When the pile reaches a depth of interest the driving is stopped and an axial loading test is performed; driving is then resumed, so that various cycles of driving and axial loading can be performed. The strain gages on the pile give the load distribution in the pile, and the pressure transducers monitor the stress field changes around the pile during the axial loading. The data is recorded using both the regular and the high speed data acquisition systems.

4.2 DATA REDUCTION

4.2.1 Overview

During data acquisition, some quantities, such as the depth of the pile, are computed and displayed on the screen for the monitoring of the progress of the experiment; the digital values of the different transducers are also displayed for control of the signal processing. The high speed data acquisition card comes with software that allows for the display of the recorded signals. Therefore, during an experiment, the raw data is monitored visually, and the data stored in computer memory or hard disk. At the end of an experiment the data are retrieved from memory to disk and then transferred to diskettes for storage, and to a main frame computer for storage and data manipulation. Because of the dynamic data records, the number of files and size of the data bank for one experiment are very large (*i.e.*, average of 8 MBytes of binary data, when dynamic data are saved every tenth blow only). We also have special parameter files for each experiment which will contain all the necessary information about the experiment: pile driving equipment, pile and soil characteristics; transducer types and parameters describing their characteristics, their signal conditioning, their positioning in the soil or on the pile, and their location in the data files. Data processing is performed using different routines and programs such as SCM (*e.g.*, Soil-Cell Model, the numerical model described in section 5.3, for non-linear soil-cell interaction), and SIG, a signal analysis program written by Caltech graduate Robert T. Beck. SIG allows for the analysis and processing of different signals in the time or frequency domain. It offers a wide range of operations and manipulations of the signals: elementary mathematical operations, integration and differentiation, basic statistics, approximation, transform techniques, correlation and convolution, filtering, generation of simple and special functions and display and plotting facilities. The structure of the program is such that one can perform a step-by-step interactive treatment of the signal, monitoring the different changes by displays on the screen, and also use command files to perform a given sequence of signal manipulations to be applied to a large number of records. The raw output from transducers are therefore converted into specific quantities of interest such as time, length, force, stress, or non-dimensional quantities.

In the following, each data reduction method adopted for the different data types will be described.

4.2.2 Pile Dynamics

4.2.2.1 Measurement and reduction of acceleration data

The measured pile accelerations are used to calculate the forces acting on the pile with the one-dimensional wave equation analysis approximation (see Chapters 1 and 3). The raw data consists of 2 sets of 12-bit words coming from the top and bottom accelerometers. The data has a sampling rate of 500 KHz (only two accelerometers) or 250 KHz (two accelerometers and two strain gage bridges) and a record length of 2 KBytes of data per blow per channel, which corresponds to 48 to 60 KBytes per test (24 to 30 recorded blows) of data for accelerometer. The level of noise is small in comparison to the high level of the signal coming from the piezoelectric transducers at impact. A variation of one bit in the record corresponds to 125 g; impact accelerations are in the order of 10,000 g. Therefore in the integration (Simpson or trapezoidal rule) of the signal to obtain velocities, ramps due to bit jumps are frequently encountered. It is then necessary to apply some form of correction. The detection of bending modes of the pile during a blow, which are expected, can be made by Fourier analysis. If bending mode frequencies are encountered, the signal will be processed to subtract the bending mode frequencies from the original signal. However, this treatment was avoided. The data is presented, in section 6.2, as plots of calculated force versus time in the model scale for a given blow.

4.2.2.2 Measurement and reduction of axial strain data

Strain measurements on the pile are also used to calculate the forces acting on the pile. The raw data consists of two sets of 12-bit words for the signals coming from the top and bottom pairs of strain gages. The data has a sampling rate of 250 KHz (two accelerometers and two strain gage bridges) and a record length of 2 KBytes of data per blow per channel, which corresponds to 48 to 60 KBytes per test (24 to 30 recorded blows) of data for each strain gage pair. Due to the necessary amplification of the signal before acquisition, the signal being very weak as is usual with strain gages, there is a presence of high frequency noise. A variation of one bit in the record corresponds to 4 lbs in the model scale while peak forces of 400 lbs is seen. The complete range of encoding was not used because it is difficult to obtain very high gain amplifications with high frequency response (*i.e.,* imposed here by the sampling rate used). The data is presented, without

any signal processing, as plots of measured force versus time in the model scale, see Figures 6.2.1 and 6.2.2.

4.2.3 Soil Stress Field

4.2.3.1 Static Stress Data

The data for the static soil stress field, which corresponds to the output of the pressure transducers at the end of each blow, is recorded through the general purpose 12-bit ATD. One bit corresponds to 0.1 or 0.04 psi according to the amplification used to capture the level of the measured stresses, which can reach up to several hundred psi. Filtering of the high frequency noise (25 KHz and above) is done in the signal conditioner. The final results, see Chapter 6, are obtained using the following formats:

1. radial and vertical stress history versus non-dimensional pile depth for the various transducer locations: when the radial distance is variable for a given depth, and vice versa;
2. vertical and radial stress history comparison;
3. stress contours;
4. peak stresses versus radial distance;

4.2.3.2 Soil Dynamics Data

The signal from the pressure transducers is also recorded in the high speed ATD, in order to get the transient soil stresses after a blow. The raw data consists of 12-bit words recorded from each of the transducers. The data is sampled at a rate of 250 KHz or 125 KHz; the top accelerometer is used as trigger and reference. The record length is 2 to 4 KBytes of data per blow per channel, which corresponds to 48 to 120 KBytes of data per test (24 to 30 recorded blows) for each pressure cell. The signal is conditioned as for the general purpose ATD and so one bit corresponds to 0.1 or 0.04 psi depending on the amplification used, because the measured level of stress may reach up to several hundred psi. The 25 KHz frequency level used in the filtering corresponds to the characteristic frequency response of the transducers. The records show frequency content within 10 KHz. The high sampling rate is explained by the fact that the top accelerometer is used as trigger, so that it is possible to synchronize the two separate high speed ATDs

that record the pile and the soil dynamic responses. The data are presented in Chapter 6 without any raw signal conditioning and show:

1. the typical transient stress history after a blow (stress versus time);
2. the evidence of p-wave propagation by plotting transient stress versus time for various transducers located at the same depth but different at radial distances and vice-versa;
3. the dynamic stress decay with distance (as in 2.);
4. the estimation of the static stress field from the dynamic records (stress versus blow number);
5. the comparison of the dynamic records for a complete driving history, between the linear and non-linear soil-cell model assumptions;
6. the results of the soil-cell model assumption, (see Chapter 6) are presented using the format of the previous section. When the non-linear soil-cell model (SCM) assumption is mentioned, it implies running the complete dynamic history of each transducer through the SCM. Details of the data reduction implications of the use of the SCM are given in section 6.3.3.1.

Chapter 5

MEASUREMENT OF SOIL STRESSES USING PRESSURE TRANSDUCERS

5.1 INTRODUCTION

The evaluation of soil stress implies the use of a stress cell to measure stresses at discrete points in a given soil. The use of a measuring device for soil stresses involves many considerations that are not often fully appreciated. The insertion of an instrument into the soil to measure the actual stress field alters the stress state that would otherwise exist (the "free-field soil stress" state). Ideally a stress cell, to be "transparent," should have exactly the same constitutive properties as the soil it replaces; but this is virtually impossible to achieve. Therefore an understanding of the interaction between the cell and the soil is needed to interpret the response of a cell in terms of soil stresses. Many investigations of the various factors characterizing the soil-cell system have been conducted (*e.g.*, [1], [6], [32], [46], [62], [69], [77], [97], [102], [137], [138], [149], [150], [154], [155], [156], [161]) and the principal conclusions will be presented here.

Because of the soil-cell interaction, the stress registered by the cell does not correspond to the free-field soil stress. This means that a correction factor has to be applied to obtain actual soil stresses from measured stresses. The *registration ratio* R is commonly used in the literature to refer to this correction factor; it is defined according to the following procedure:

First a calibration of the cell is performed in a fluid medium (air, water, or oil), because of the linear and reversible behavior of the fluid-cell system. A calibration factor c_f relating the actual applied stress to the cell electrical output is obtained:

$$\sigma_f = \frac{V_1}{c_f} \tag{5.1}$$

where

σ_f = applied fluid stress

V_1 = cell electrical output

c_f = fluid calibration factor

Then the cell is placed in the soil in a mass of soil with dimensions many times larger than those of the cell, the soil is stressed with a stress σ one-dimensionally, and various calibration tests are performed. The output of the cell V_2 is now expressed in terms of "measured stress" θ:

$$\theta = \frac{V_2}{c_f} \tag{5.2}$$

and the registration ratio R is defined as:

$$R = \frac{\theta}{\sigma} \tag{5.3}$$

The ideal gage would have a constant registration ratio of 1, but as mentioned earlier, this is not achievable. This ratio varies for different cell types and shapes, and is not a unique value for a given cell. Many factors, including the cell and the soil properties, influence the value of R, and lead in some cases to a non-constant R on a simple load-unload-reload cycle. Weiler and Kulhawy [161] discussed many of the factors affecting the stress cell measurements and summarized them in a table given here as Table 5.1. These factors play an important role and can be grouped into three categories: (1) Stress cell properties and geometries, (2) Soil properties, (3) Experimental conditions, which are related for interactions between the cell and the soil under various environments. From the various studies we can obtain some understanding of the soil-cell system and also some guidelines in the use of such devices.

(1) Stress cell properties and geometries:

Of the two categories of cell type, flexible diaphragm cell and stiff cylinder cell, the second kind will not be considered here because the bulkiness of the cell and the discontinuity in displacement between the cell and its case cause excessive errors in the free-field stress measurement. The flexible diaphragm cell, as used in the experiments, consists of a thin, circular diaphragm attached to a stiff case; the diaphragm will deflect under normal pressure applied to it. The presence of an inactive, stiff annular rim around the cell diaphragm reduces the stress concentration at the cell boundaries. Monfore [97], and then Peatty and

Sparrow [154] recommended that the sensitive area of the cell be less than 45 % and 25 % respectively, of the total cell area to reduce the effects of these stress concentrations; ($d^2/D^2 = 0.45$, or 0.25 , where d = diameter of the sensitive area, and D = diameter of the cell). Figure 5.1 gives a sketch of the stress redistribution over and around the cell embeded into the soil.

Following some experimental studies and theoretical investigations, Collins *et al.* [32], Monfore [97], Taylor [149, 150], Tory and Sparrow [154], it is shown that to minimize the error in the stress field due to the disruption produced by the thickness of the cell, a cell with a low *aspect ratio* (defined as the cell thickness to cell diameter ratio) should be used. An aspect ratio less than 0.2 is recommended. The magnitude of the stress redistribution around and over a cell depends a great deal on the aspect ratio of the cell. The effect of the aspect ratio can be seen in Figures 5.1 to 5.3.

Also the presence of wires and protuberances existing at the back of the transducer contribute to the disturbance of the stress field. It is important to select a thin cell with wires coming out in the plane parallel to the sensing area.

The *soil-cell stiffness ratio* S defined as:

$$S = \frac{E_{soil}}{E_{cell}} \frac{d^3}{t^3} \tag{5.4}$$

where

E_{soil} = Young's modulus of the soil

E_{cell} = Young's modulus of the cell material

d = cell diaphragm diameter

t = cell diaphragm thickness

plays a very important role in the variation of the registration ratio. In the early investigations on soil pressure it was recognized that a stress cell stiffer than the soil will over-register, and a cell softer than the soil will under-register, see Figure 5.1. Tory and Sparrow presented the result of the analysis of an embedded cell with a rigid guard ring surrounding a flexible diaphragm, for the case of one-dimensional compression. Variations of the registration ratio are plotted as a function of the soil-cell stiffness ratio for different cell aspect ratios, see Figure 5.2. These results show that, for monotonic loading:

1. for a stiff cell (S smaller than 0.3) the registration ratio remains almost constant,

2. the registration ratio decreases rapidly as the cell becomes soft compared to the soil (S greater than 10),
3. important variations of the registration ratio can be observed for a cell with a stiffness comparable to the soil stiffness.

Because soil stiffness varies with so many parameters, a soil-cell stiffness ratio less than 0.5 is recommended for consistency in the measurement of stresses.

These guidelines have been followed to choose the cells used during the present experiments. The geometrical characteristics of the cells fit the recommendations, because the aspect ratio of the gages is about 0.2. According to the manufacturer's information the type # 5 gage (see section 2.5.2), with a range of 500 psi, used in the later experiments has a soil-cell stiffness ratio of 1.5, for a soil's Young's modulus of 10 Kpsi, which tells us that the cell is not stiff enough and therefore variations of the registration ratio are to be expected. It was observed that the cell displays large variations of the registration ratio (see section 5.4.3).

If we want to estimate the deflection of the cell's diaphragm we know that the maximum deflection will occur in the center and will be bounded by the two values obtained for a circular plate simply supported (upper bound) and perfectly clamped (lower bound). We obtain from Roark [117] the following formulas for the maximum deflection, y_m, at the center of the plate,

circular plate simply supported, uniform loading:

$$y_m = \frac{3(5+\nu)(1-\nu^2)qa^4}{16(1+\nu)Et^3} \tag{5.5}$$

circular plate clamped, uniform loading:

$$y_m = \frac{3(1-\nu^2)qa^4}{16Et^3} \tag{5.6}$$

where

ν = Poisson's ratio of the plate

E = Young's modulus of the plate

a = radius of the plate

t = thickness of the plate

q = applied uniform load

We obtain for the present cell under a 100 psi uniform pressure:

$$2.5410^{-5}\text{inches} < y < 1.0410^{-4}\text{inches}$$

From the soil properties mentioned in Chapter 3, we expect the Young's modulus of the sand to vary from about 12 Kpsi at a confining pressure of 2 psi, to 55 Kpsi at a confining pressure of 50 psi. If we consider a layer of soil of the same thickness as the cell under a uniform pressure of 100 psi then for a Young's modulus of 12 Kpsi and 55 Kpsi we obtain a deflection of 3.3310^{-4}inches and 7.2710^{-5}inches respectively.

Therefore, considering the cell in its stiffest configuration (diapragm perfectly clamped), the cell is approximately thirteen times stiffer than the soil at low confining pressure and less than three times stiffer than the soil at a higher confining pressure. In other words, the cell is not stiff enough for the effects on the soil-cell system of the variations in soil stiffness to be negligible. For these values of soil Young's modulus, the soil-cell stiffness ratio S, defined in Eqn. (5.4), varies from 1.8 to 8.2, which confirms that the cell is not stiff enough. However, because of limitations in the choice and availability of miniature pressure cells and because of the fact that the electrical output of the cell becomes small as the stiffness increases, these gages were used. A careful study of their interaction with the soil was made, as presented in the following sections, to take this limitation into account in the interpretation of their readings.

(2) Soil properties:

In a multi-axial stress field, the disruption due to the presence of the cell will cause a portion of the lateral stress to be felt in a direction normal to the cell, the phenomenon studied by Askegaard [6], Collins *et al.* [32], and referred to as the cell *lateral stress rotation.* Though a thinner cell reduces this effect, the lateral stress rotation effect also depends heavily on the value of Poisson's ratio of the surrounding material, and can be significant for the lower range of Poisson's ratio (see Figure 5.3). Another influence of the lateral stress on the cell is the presence of nonuniform in plane (lateral) compression on the cell diaphragm. This effect, called the *cross sensitivity*, can be removed by suitable arrangement of the strain gages attached to the diaphragm so that the Wheatstone bridge does not measure in-plane stresses.

The soil grain size must be sufficiently small relative to the cell diameter to avoid "point load" effect in the loading of the diaphragm. Weiler and Kulhawy found that for an active cell-diameter-to-soil-grain size ratio (d/D_{50}, with D_{50} being the grain diameter at which 50 % of the soil is finer) greater than 10, the multiple point loads yield the same results as a uniform load.

The deformation of the cell diaphragm may cause arching in sand. Recommendations suggest a cell diaphragm diameter-to-deflection ratio of up to 5000 be used in dense sand to minimize the arching problem with diaphragm-type cells. This considerably reduces the cell sensitivity.

The sand used in the experiment has a Poisson's ratio of 0.3, which makes the lateral stress effect for our gages reasonably low. It is a very fine uniform sand with $D_{50} = 0.15mm$, so it provides a uniform loading of the cell diaphragm. The deflection of the diaphragm will be in the order of 10^{-4}, which gives a deflection ratio of about 1000, so that arching may occur.

(3) Experimental conditions:

Variation in the placement of the cell in the soil can greatly influence the registration of the gage. Hadala [62] reports variations in the registration ratio as large as 40 % for laboratory soil stress measurements. He also found that the simplest placement techniques, being the more reproducible, will cause less scatter; and with sand he suggested gently placing the gage on top of the last lift placed and continuing backfilling as if the cell was not present. Also Reiff and Langler provide some guidelines for the influence of proximity of structures and other cells. A clearance of four cell diameters in any direction generally satisfies their recommendations. These guidelines have been followed for our experiments.

For dynamic soil-stress measurements, matching the bulk weight of the gage to that of the soil is desirable to avoid inertial effects, and is particularly important in saturated soil. The cell should have a high natural frequency and consequently a short rise time response to record the rate of stress change and the peak of the stress pulse. A resonant frequency of the cell of at least three times the maximum frequency of the loading is recommended. A safe rise time to which our transducer will respond linearly within 5% can be expressed

as a function of the period T up to which the cell has a flat frequency response:

$$T = \frac{1}{0.2 f_n} \tag{5.7}$$

$$t_r = \frac{T}{4} \tag{5.8}$$

where

f_n = natural frequency in Hz

t_r = cell safe rise-time response in sec.

For our cell $t_r = 10\mu sec$. In these experiments, the actual rise time of the transducer is much faster than the safe rise time.

The soil-cell stiffness ratio is very important. It is reported in the literature that for high strain rate associated with shock-type loadings, the soil Young's modulus can increase over a large range, which implies a consequent decrease in the cell registration ratio. Durelli and Riley [46] performed some static and dynamic calibration experiments on gages embedded in cylinders of urethane rubber. The response of the embedded gage to static loadings on the rubber was found to be approximately 40 % higher than its response to static air pressure; for dynamic loadings on the rubber the response was 80 % higher. Though the response in soil is expected to be different, the phenomenon mentioned above relates to an increase of the registration ratio of the cell, as the soil appears stiffer under dynamic loading. The estimation of the registration ratio for dynamic loading in soil was not achieved with our facilities.

Many factors come into play in the performance of a soil-cell system. The complexity in the interaction and behavior of such systems implies the need of doing a thorough calibration specific to each particular configuration of the soil-cell system. The calibration used in the present experiments is described next.

5.2 EXPERIMENTAL CALIBRATION OF PRESSURE TRANSDUCER BEHAVIOR IN DRY SAND

5.2.1 Static calibration

The purpose of the static calibration of the pressure cells in the centrifuge is to get the necessary data in order to represent their behavior by a model for the specific

centrifuge experimental conditions. The model must describe the transducer behavior under any kind of loading configuration, so that the electrical output of the cells during an experiment can be interpreted in terms of soil stresses.

At first the linearity of the diaphragm-type cells under hydrostatic pressure is checked in the centrifuge environment. For this, as described in section 3.2.5, the gages are placed at the bottom of a container under a plastic membrane that covers the container walls. Several inches of water are poured inside the membrane. The calibration then consists of monitoring the output of the cells as the centrifuge is spun up and down. A linear behavior is observed, see Figure 5.4, and good agreement with the manufacturer's calibration is obtained.

With this understanding of the pressure cell mechanical system under hydrostatic pressure, we proceed with calibration of the transducers embedded in the soil. It is a new system in which the cell, the soil and the soil-cell interaction all play an important role. In the introduction section we saw that the registration ratio of a cell is not a unique property of the gage but varies with the physical properties of the soil in which it is embedded and the stress field. Consequently the pressure cells have to be calibrated for each specific application. Therefore the calibration tests were conducted in the centrifuge in the container and with the soil used for the pile driving experiments. As mentioned in section 3.2.5, various configurations of the cell soil system were tested. The gages were embedded in dry fine Nevada sand at a medium density, which corresponds to the soil conditions of the pile driving experiments. The transducers are placed in the sand to read vertical stresses. By spinning the centrifuge up and down, we increase or decrease the stresses in the soil. In particular we know that the overburden stress at a point in the soil will follow the acceleration variation of the centrifuge, as this stress is linearly proportional to the g-level. Because we deal only with vertical stresses, in a dry sand for which the settlement due to loading is negligible, so that the height of soil above a cell is constant, it is worth noting that we actually know with confidence and quantitatively the stresses acting on the gages during calibration.

On a simple loading-unloading cycle the cell exhibits an hysteretic behavior during unloading (see Figure 5.5.a). The arrows indicate the loading path, and we see that "virgin" loading gives a linear response and unloading a non-linear one. In Figures 5.5 to 5.9, and

Figure 5.12, the top plot (a) shows the soil stress during the centrifuge calibration versus the measured stress obtained from the pressure cell output; and the bottom plot (b), which will be referred to later, shows the comparison between the centrifuge calibration and the prediction from the soil-cell model described in section 5.3.

Let us consider a layer of soil of a given initial thickness. During loading the layer will decrease in thickness; on unloading, if the material was purely elastic, the layer would get back to its original configuration. Now we know that sand exhibits a non-linear behavior, so for large loading, the layer of soil will deform inelastically and therefore will not go back to its original configuration but to a new configuration described by a thickness smaller than the initial thickness. If we look at the pressure cell by itself we know that under the range of utilization it is linear (refer to the calibration under hydrostatic condition). Now consider the layer of soil whose thickness is equal to the thickness of the pressure cell. After a first loading the soil layer ends up with a smaller thickness, and during unloading it exhibits non-linearity. In turn, the cell embedded in that soil layer wants to go back to its initial configuration during unloading, but can not because the surrounding soil prevents it. Therefore the cell will read some residual stress. The stress in the gage is higher on unloading than the nominal stress in the soil: this explains the non-linear curve describing unloading. This can be expressed also in terms of lateral stress buildup in the soil during loading. As the vertical stress increases, the lateral stress follows the K_0 line, and is therefore proportional to the axial stress. Upon unloading, the lateral stress decreases at a much slower rate; this results in an increase in the ratio of lateral to axial stress. As mentioned in the introductory section, this relative increase in lateral stress will cause over-registration of the cell.

During reloading and repeated cyclic loading (see Figure 5.6.a to 5.9.a), this hysteretic behavior will come into play.

The aim is to model the different aspects of the non-linear behavior of the cell embedded in the soil, in terms of the soil stress, with as few parameters as possible. For this purpose different cyclic loading configurations are used to get an understanding of the governing rules of the non-linear behavior observed. Some of these calibration curves are presented here, and, of course, apply only to the soil and gage tested. All the pressure transducers used in the experiments are diaphragm gages and do present similar behavior governed by

the same rules. Now each gage type (refer to section 2.2.5) will have a particular set of parameters to describe its behavior. Figures 5.5 to 5.8, and Figure 5.12 correspond to a type # 4 gage that shows a larger hysteresis (which makes it easier to follow the loading path on the plots presented) than the type # 5 gage, whose behavior is shown in Figure 5.9.

Let us call the initial stress state of a gage the zero state: ($\sigma = 0, \theta = 0$), and a "simple cycle" a loading from σ_0 to a maximum stress state σ_{max} and back down to σ_0.

Some of the cyclic loading configurations are:

1. repeated simple cycles of increasing (Figure 5.6.a), constant, or decreasing σ_{max}, to investigate cyclic loading effects on the linear and hysteresis behavior.
2. cycles with partial unloading and increasing σ_{max}, (Figure 5.7.a), to see whether or not the linear behavior will always prevail during "virgin" loading.
3. cycles with partial loading and unloading during unloading (Figure 5.8.a), to look at the evolution of the behavior in the purely non-linear domain.
4. repeated unloading cycles with constant maximum stress but increasing cycling range (Figure 5.12.a) , for the evidence of residual stress explained by the change of the characteristics of the soil-cell system.

5.2.2 Dynamic calibration

During pile driving experiments the pressure transducers embedded in the soil will be submitted to dynamic loading by the soil stress wave following each impact of the hammer on the pile. It is therefore important in the interpretation of the stress history during driving to know the behavior of the cells under dynamic loading. The question to answer is the following: can the transient behavior of the soil-cell system under dynamic loading be assumed linear as a first approximation, or, if not linear, then equal to the static loading behavior, or is it something different? Engineering judgment guides one to assess that the cell under dynamic hydrostatic loading shows the same linear behavior as the one observed under static loading. Similarly the sand is expected to display approximately the same behavior under static and dynamic loading. What can be said for the soil-cell interaction under the two different loadings? We mentioned in the previous section that it is important for the calibration of the system, to know with confidence the qualitative

and quantitative values of the stresses seen by the cells. We do not have any equipment in our laboratory that can allow us to do a quantitative calibration of the transducers under dynamic loading, nor is it easy to see how this could be achieved. We can only perform a qualitative calibration, to assess the rules that govern the behavior of the soil-cell system under dynamic loading.

Soil column test experiments were performed as described in section 3.2.5. A check of the transducer responses was done by changing the length of the impacted rod. The cell at the interface rod-soil sees the stresses generated by the wave bouncing back and forth in the rod. The frequency of the rod stress pulse is inversely proportional to the length of the rod. The records from the transducer give an accurate representation of the wave propagation.

5.3 NUMERICAL MODELING OF PRESSURE TRANSDUCER RESPONSE IN DRY SAND

The extensive set of calibration tests performed brought about an understanding of the mechanisms that govern the soil-cell static behavior under various loading configurations. The model that we present here is based on the expression of these mechanisms in terms of rules.

The first rule that can be extracted from the various calibration plots obtained is that regardless of the previous loading history, the virgin loading is linear (see Figures 5.6 and 5.7).

The linear equation is simply:

$$\sigma = R\theta \tag{5.9}$$

where

σ = actual soil stress

θ = measured stress (obtained from the cell voltage and the linear calibration factor c_f, Eqn. (5.2)

R = linear calibration factor of virgin loading line (see Figure 5.10.a)

The second rule is that the unloading follows a logarithmic decay from the local maximum stress to the zero stress state, independently of the past loading history (see Figures

5.5 to 5.9). The corresponding equation is used for different unloading during cyclic loading cycles, regardless of the level at which unloading starts.

The logarithmic decay equation is as follows:

$$\sigma = \sigma_{\max}\left[1 - \frac{\log(1+\theta_{\max}-\theta)}{\log(1+\theta_{\max})}\right] \tag{5.10}$$

where

$\sigma_{\max}$ = local maximum soil stress (see Figure 5.10.b)

$\theta_{\max}$ = local maximum measured stress

As mentioned in section 5.2, the pressure gage type # 4 exhibits a larger hysteresis than the gage type # 5. To take this difference between gage type into account, we introduce a second parameter N that will characterize the specific shape of the unloading curve for a gage type. We see that the hysteresis curve of the type # 4 gage displays some asymptotic behavior as the stress decreases, whereas the simple logarithmic decay equation represents the hysteresis of gage type # 5.

So we define unloading as follows:

$$\sigma = \left(\frac{\theta}{\theta_{\max}}\right)^{N} \sigma_{\max}\left[1 - \frac{\log(1+\theta_{\max}-\theta)}{\log(1+\theta_{\max})}\right] \tag{5.11}$$

where

N = gage parameter

By setting N equal to zero in Eqn. (5.11) we get back to Eqn. (5.10), that corresponds to the # 5 gages.

The third rule is that the reloading follows a logarithmic-asymptotic curve from the local minimum to the absolute maximum, the linear curve of Eqn. (5.9) being the asymptote (see Figures 5.7 to 5.9).

The equation is:

$$\sigma = R\theta - \Delta\sigma \tag{5.12}$$

to interpret the data from a pressure cell embedded in the soil in terms of soil stresses. In the case of a known purely static loading history, by using the soil-cell model described in section 5.3, we know that we can interpret with good confidence the output of the cells in terms of stresses.

Now for pile driving experiments the loading history is a dynamic loading history, each blow being a dynamic event. Therefore to interpret the data from the pressure cells embedded in the soil surrounding the pile in terms of overall stress field change during driving (which corresponds to a data point (final static stress) for each transducer following each hammer blow on the pile), we need to take into account the dynamic loading history at each blow. The axial loading of the pile at the end of driving is a static loading, and the model can then be applied to interpret the pressure cell readings. But we have to keep in mind that the past loading history that corresponds to the driving of the pile is needed because it defines the starting point for the model as well as the values of $\sigma_M, \sigma_{\min}$ and $\theta_{\min}$, or $\sigma_{\max}$ and $\theta_{\min}$.

5.4.2 Dynamic loading

From section 5.2.2 we know that we do not have enough data to describe the dynamic behavior with the same confidence as for the static loading case. Therefore we have to make some assumptions.

The first possible simplifying assumption is to consider the soil-cell system to be linear under dynamic loading. Then for the case of pile driving where the stresses in the soil are the results of the dynamic loading of the soil, this means that the stresses measured by the gages are directly proportional to the soil stresses throughout driving. We expect this not to be true: engineering judgment leads us to think that during dynamic loading the soil-cell mechanical system will exhibit similar non-linear characteristics as for static loading.

A second assumption is to consider the behavior of the soil-cell system to be the same (non-linear) under static or dynamic loading. Then we can use the model described above for any loading static or dynamic. The parameters for the model are assumed to be the same in both cases, and are obtained from the static calibration. Then the soil-cell model is fully determined by the static calibration curves. The interpretation of the data is obtained

by the application of the model to the complete loading history. This means in the case of pile driving that we need the dynamic loading history of the transducers at each blow.

Now if the soil-cell model parameters for static and dynamic loading are different, or if the soil-cell system is governed by different rules for dynamic loading, then we are not able to interpret the data from the pressure cells for soil dynamic experiments such as pile driving.

5.4.3 Obtaining the soil-cell model parameters for a pile driving experiment

At this stage, a choice was needed and it was assumed in the rest of the work that the second hypothesis holds: the behavior of the soil-cell system is described by the model of section 5.3 with the same parameters for static or dynamic loading.

The model that is used requires first the evaluation of the calibration factor for the linear virgin loading line. With the many calibration experiments conducted it has been observed that the cells and the soil stiffness are of the same order. This implies as discussed in the introduction section that any change in the stiffness ratio: cell stiffness/soil stiffness will cause variation in the stress ratio: measured stress/soil stress. Therefore the virgin line calibration factor is not just a cell parameter but depends on the soil and the soil-cell system characteristics. For a given cell and a given soil at a fixed density this factor will change with the position of the cell: as the cell gets deeper into the soil the soil stiffness increases, so the stiffness ratio decreases; therefore the stress ratio, or the calibration factor decreases (see Figure 5.11).

The knowledge of the loading history from the zero state is also needed. For a centrifuge experiment, the initial stress state at the beginning of an experiment is to be determined as well as the past history: from the zero state to the initial state. When we prepare an experiment, the cells are placed in the soil at different locations and at different orientations. We can estimate from the soil parameters and the cells' positions the stress acting on the cell at this reference value of the cell output. When the centrifuge is spun up to the test acceleration the output of the cells is continuously monitored. Therefore, before starting an experiment we have a record of the loading history of the cells. It consists of a simple monotonic loading, so that the measured stress and soil stress relation follows the virgin loading line, and the maximum past stress is the initial stress value. So the only value

needed for the use of the model is the initial stress acting on the cells just prior to pile driving. Also the spinning-up of the centrifuge corresponds to a calibration loading, which allows us to check the calibration factor of the virgin loading line obtained by previous static loading calibration tests, against the value calculated during the spinning up of the centrifuge for the very experiment.

5.4.4 Discussion

We know that we have been able to develop a model that accurately represents the soil-cell behavior under static loading. But we have to keep in mind that there are some limitations in the use of the model. We will enumerate some of these points:

1. Limited confidence in the estimate of calibration factor of the virgin loading line, and in its remaining constant during an experiment.
2. Limited confidence in the estimate of initial stress state.
3. Assumption of uniformity of the soil at the beginning of an experiment.
4. The effect of the placement of transducer in the soil is neglected.
5. Same behavior and same calibration parameters are assumed for measurement of vertical, radial, or other orientation of stress.
6. The effect of the stress field on the properties and characteristics of the soil-cell system is neglected.

Because during an experiment there will be changes in the stress field, in the soil distribution, in the position of the cells (translation or rotation), etc., we know that there will then be changes in the properties of the soil-cell system. Therefore the soil-cell stiffness ratio will vary giving rise to new values of the calibration factor of the virgin loading line for example, or the parameter that describes the shape of the unloading curve, which is certainly soil-cell interaction dependent, will change, or important residual stress effect can come into play. Figure 5.10a shows the evidence of residual stress due to cyclic loading. As mentioned earlier in section 5.2.1, during loading the soil deforms inelastically, but the gage deforms elastically. When unloading the cell cannot return to its original configuration because of the inelastic deformation that occurred in the soil. Therefore the cell sees some residual stress. By repeating the cyclic loading, the residual stress will at first increase and

then converge for a large number of cycles. This residual stress effect is not included in this simple model (see Figure 5.10b), as it requires keeping track of the complete previous loading history as loading proceeds.

Now pile-driving experiments involve also dynamic loading and various complex phenomena such as plastic flow or creep, which imply even more limitations as to the use of the pressure transducer model. These are:

a. Large changes in the soil conditions during the experiment, leading to variations in the parameters and eventually in the soil-cell system behavior.

b. Important movement of the transducer during the experiment, with displacement and rotation.

c. Rotation of the axes of principal stresses.

d. Plastic deformation and creep.

So not only the parameters characterizing the transducer-soil behavior are different for each soil condition for each cell, but as the experiment proceeds and the stress field changes, these parameters are changing.

Although pressure transducers are the only technology available to measure soil stresses today, it can be said that we are actually measuring stresses with an instrument whose calibration is dependent on the stress that it is measuring, but in a way that is not fully understood. Therefore, the straightforward interpretation of pressure cells output in terms of stresses is not possible. Thus, the hypothesis concerning the definition and the use of the soil-cell model (Eqn. (5.9), (5.11) and (5.12)) constitutes one of the first attempts to confront this problem and contribute to its solution. Many efforts, however, in the understanding of the physical phenomena in the soil-cell interaction and in the improvement of the technology of stress cells are still required.

Factor (1)	Description of error (2)	Correction method (3)
Aspect ratio (cell thickness to diameter ratio)	Cell thickness alters stress field around cell	Use relatively thin cells ($T/D < 1/5$)
Soil-cell stiffness ratio, S	Changing soil stiffness may cause a nonlinear calibration	Design cell for high stiffness ($S < 0.5$) and use correction factors
Diaphragm deflection (arching)	Excessive deflection changes stress distribution over cell	Design cell for low deflection ($d/\Delta >$ 2,000–5,000)
Cylinder or piston cell deflection	Much lower allowable deflection than for diaphragm cells	Design cell for low deflection ($d/\Delta >$ 20,000)
Stress concentrations at cell corners	Causes cell to over-register by increasing stress over active cell face	Use inactive outer rims to reduce sensitive area ($d^2/D^2 < 0.25$–0.45)
Eccentric, nonuniform and point loads	Soil grain size too large for cell size used	Increase stress cell active diameter (diaphragm, $d/D_{50} \geq 10$ cylinder, $d/D_{50} \geq 50$)
Lateral stress rotation	Presence of cell in soil causes lateral stresses to act normal to cell	Use correction factors (Eq. 3)
Cross-sensitivity	Nonuniform direct lateral compression of cell causes error in measurement	Change strain gauge arrangement or add outer rings
Stress-strain behavior of soil	Cell measurements influenced by confining conditions	Calibrate cell under near-usage conditions
Placement effects	Physical placing of cell causes disturbance of soil	Random error; use duplicate measurements
Proximity of structures and other stress cells	Interaction of stress fields of cell and structure causes errors	Use adequate spacing; see text for criteria
Dynamic stress measurements	Response time, natural frequency and inertia of cell causes errors	Use dynamic calibration
Corrosion and moisture	May cause cell "failure" by attacking cell materials	Use extra water-proofing precautions
Placement stresses	Overstressing during soil compaction may permanently damage cell	Check cell design for yield strength
Temperature	Changes "zero reference" of cells; does not change slope of calibration	Calibrate or use balance resistors

Table 5.1 Factors affecting stress cell measurement (from Weiler and Kulhawy)

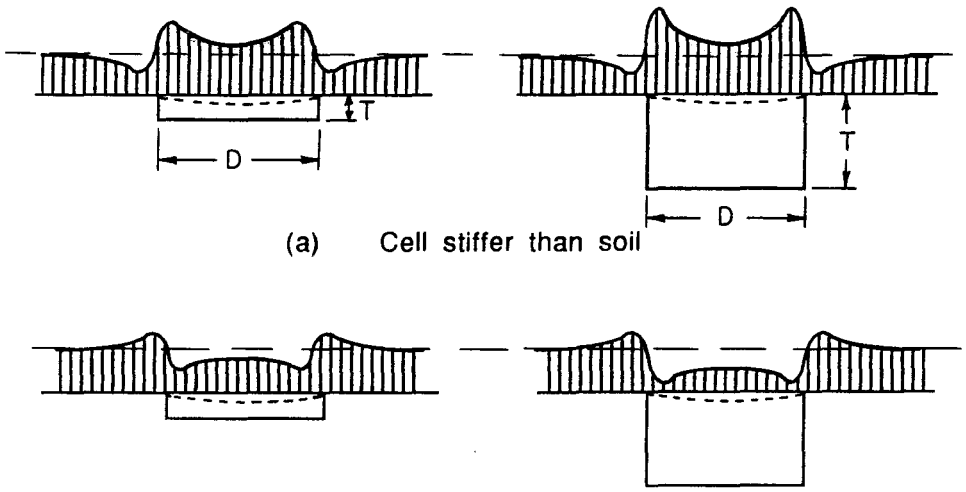

Figure 5.1 Stress redistribution around and over cells of small (left) and large (right) aspect ratio T/D

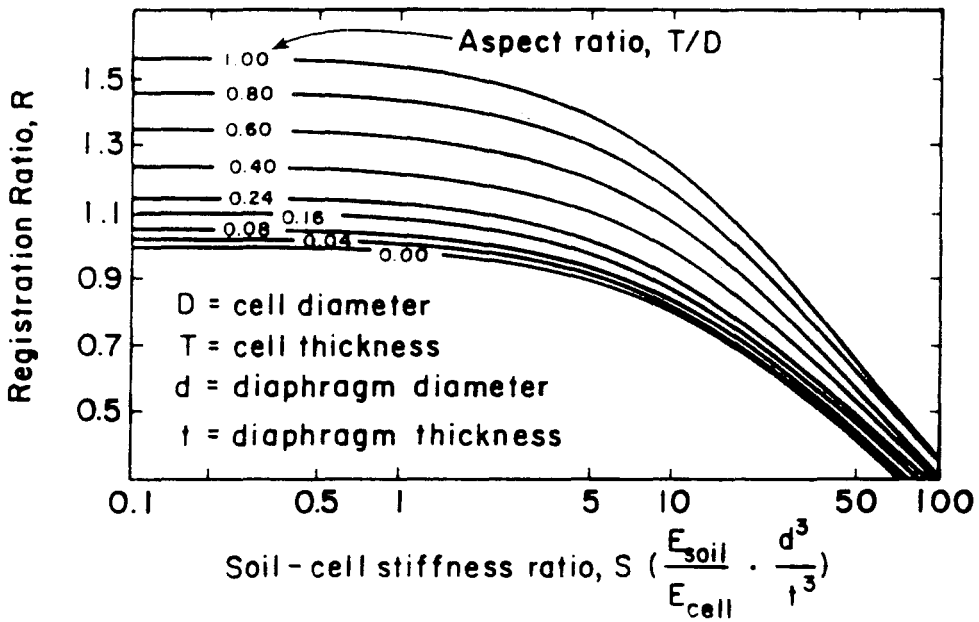

Figure 5.2 Theoritical effects of soil-cell stiffness and aspect ratio for diaphragm type cells in uniaxial stress field (from Tory and Sparrow)

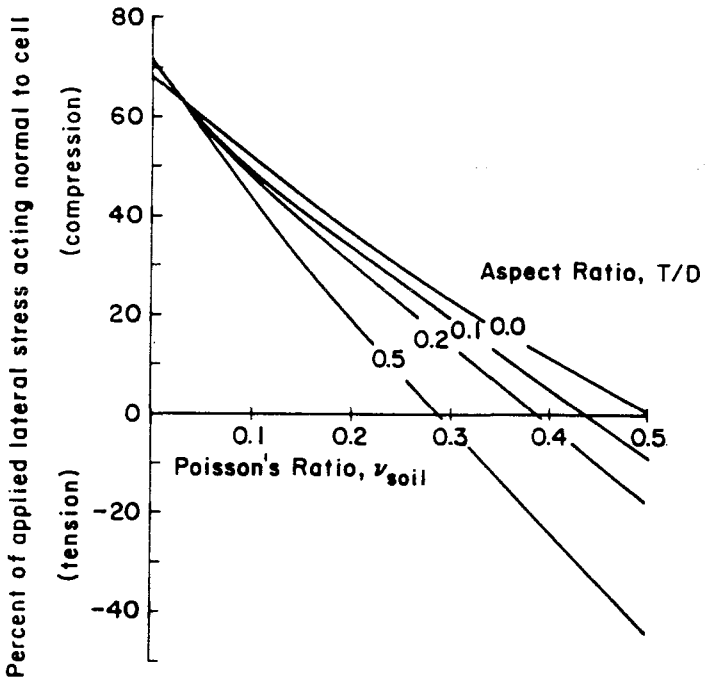

Figure 5.3 Theoretical lateral stress rotation for ellipsoidal inclusion (from Askegaard and Collins et al.)

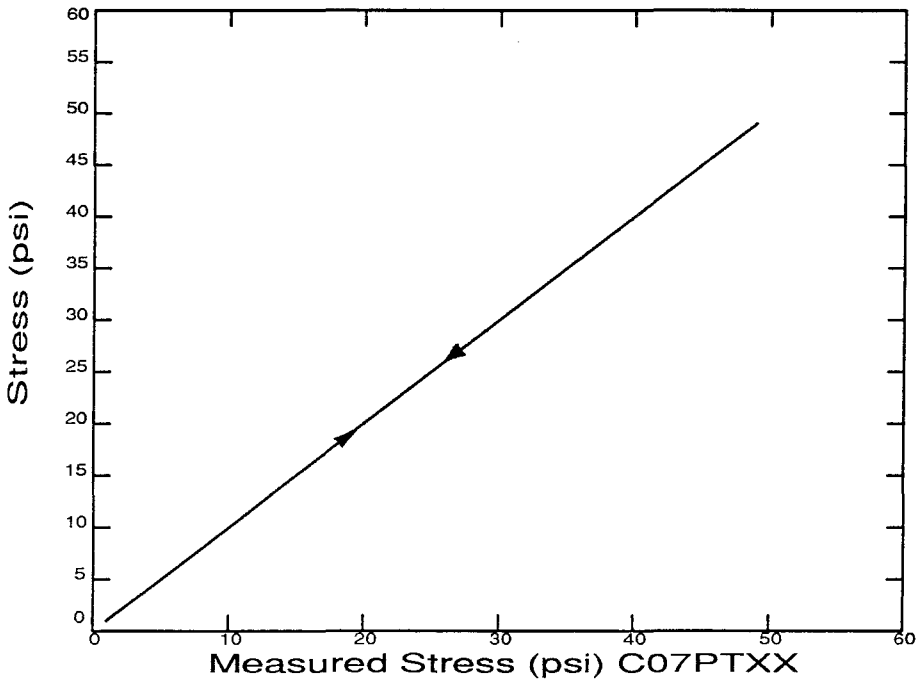

Figure 5.4 Pressure cell hydrostatic calibration

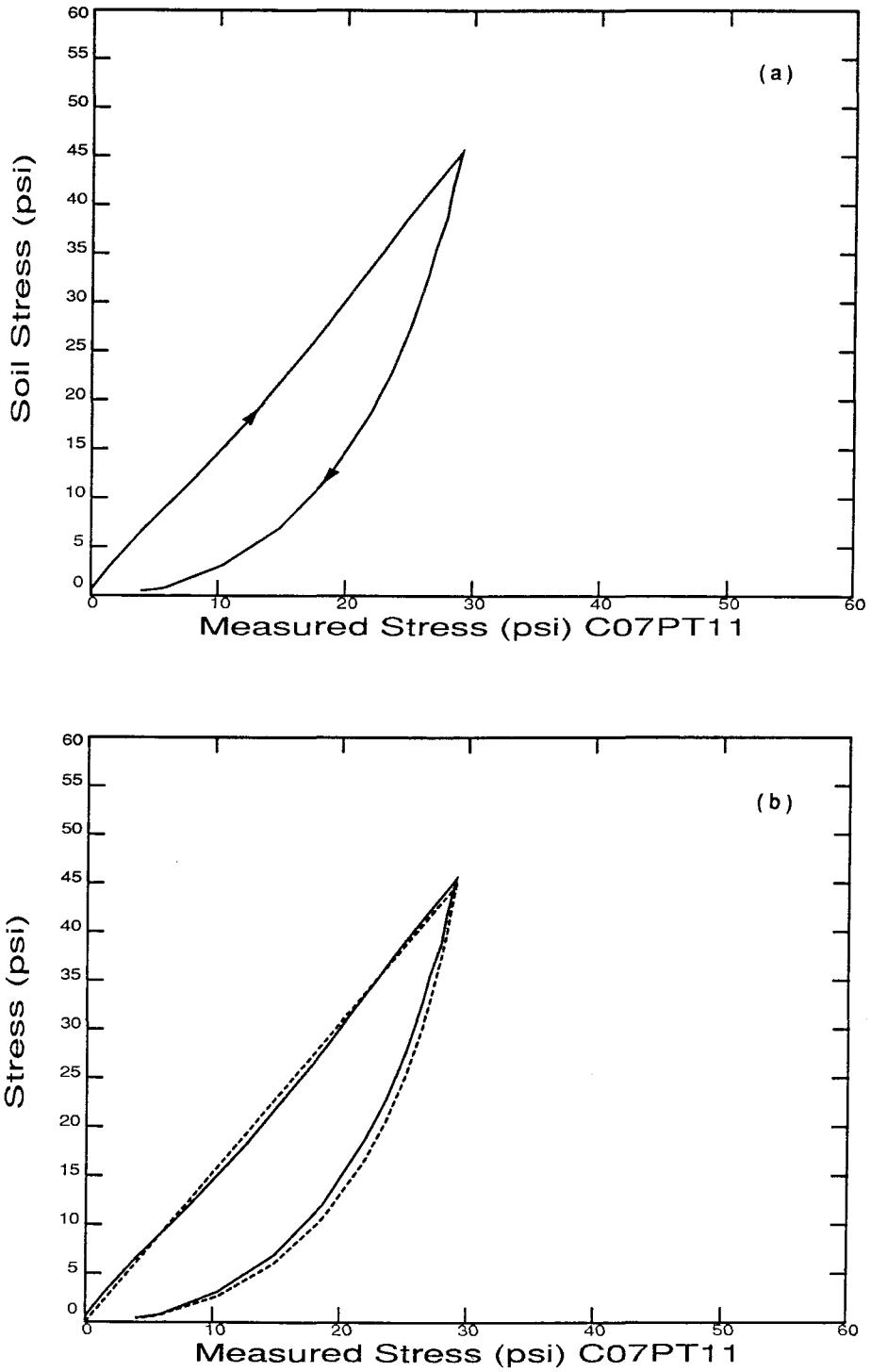

Figure 5.5 Pressure cell response to simple loading cycle
(a) centrifuge calibration
(b) comparison between centrifuge calibration (___ soil stress) and SCM prediction (. . . calculated stress)

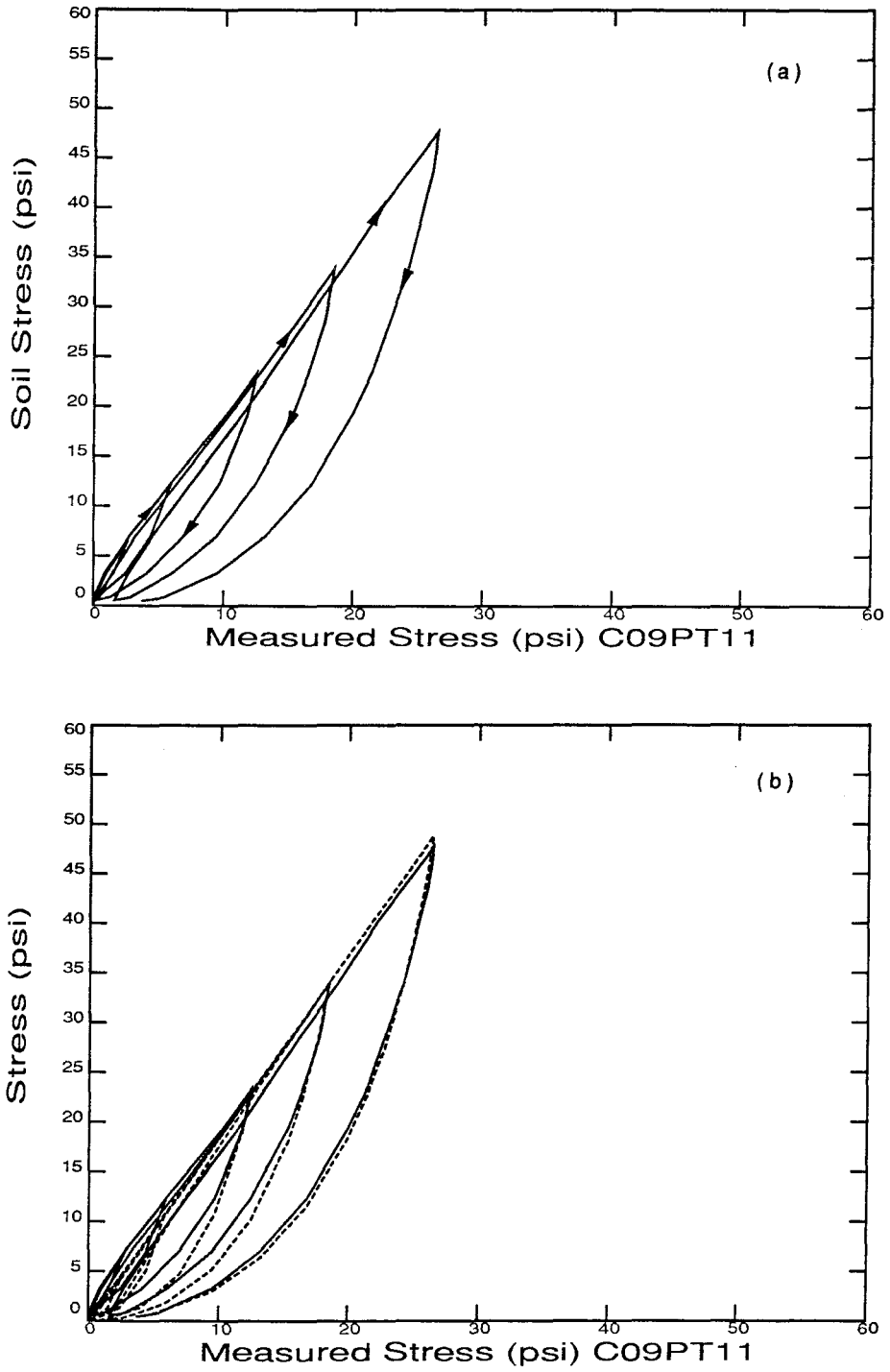

Figure 5.6 Pressure cell response to repeated cycles of increasing σ_{max}
(a) centrifuge calibration
(b) comparison between centrifuge calibration (___ soil stress) and SCM prediction (. . . calculated stress)

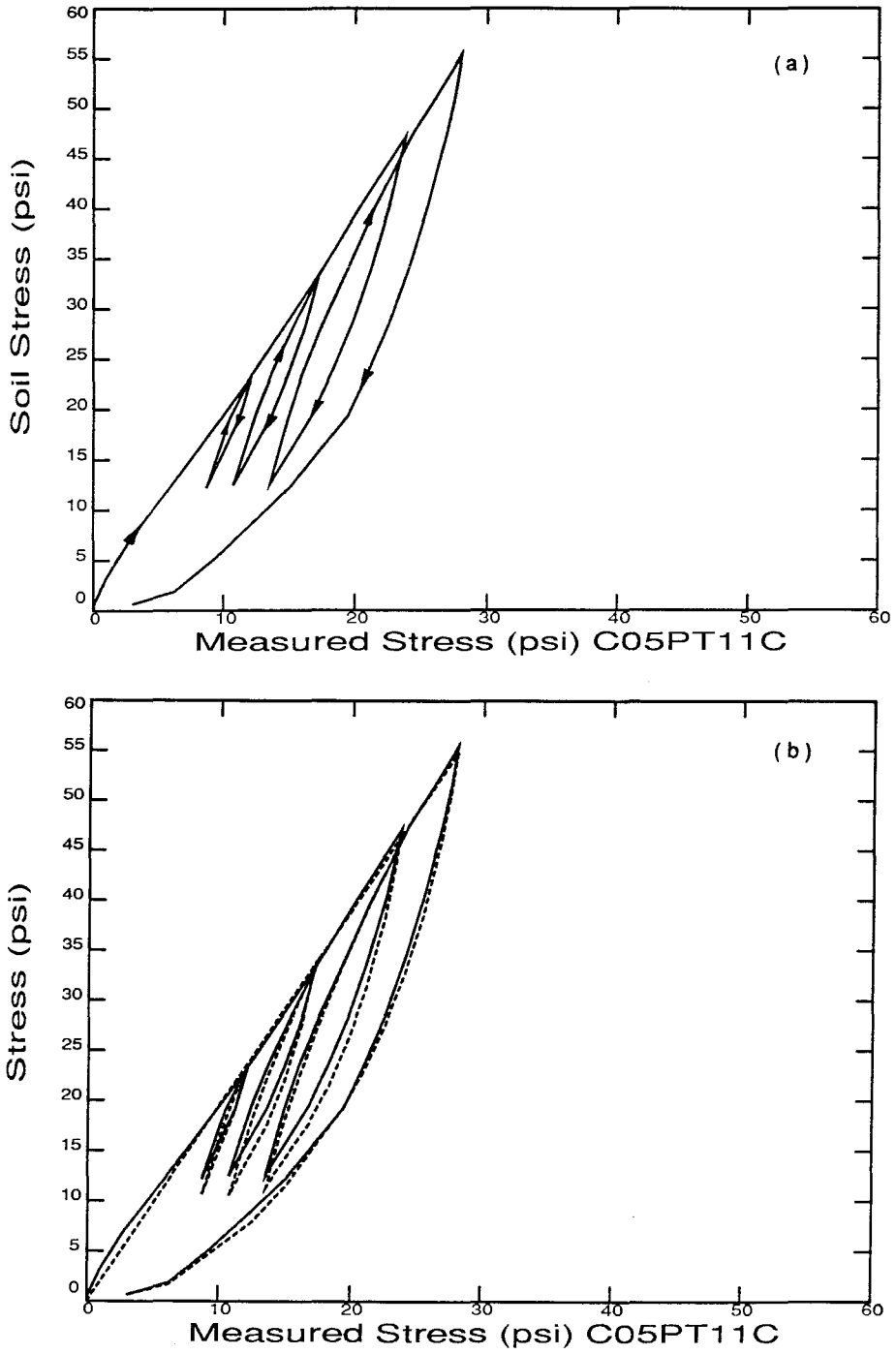

Figure 5.7 Pressure soil cell response to cycles of increasing σ_{max} and partial unloading
(a) centrifuge calibration
(b) comparison between centrifuge calibration (___ soil stress) and SCM prediction (. . . calculated stress)

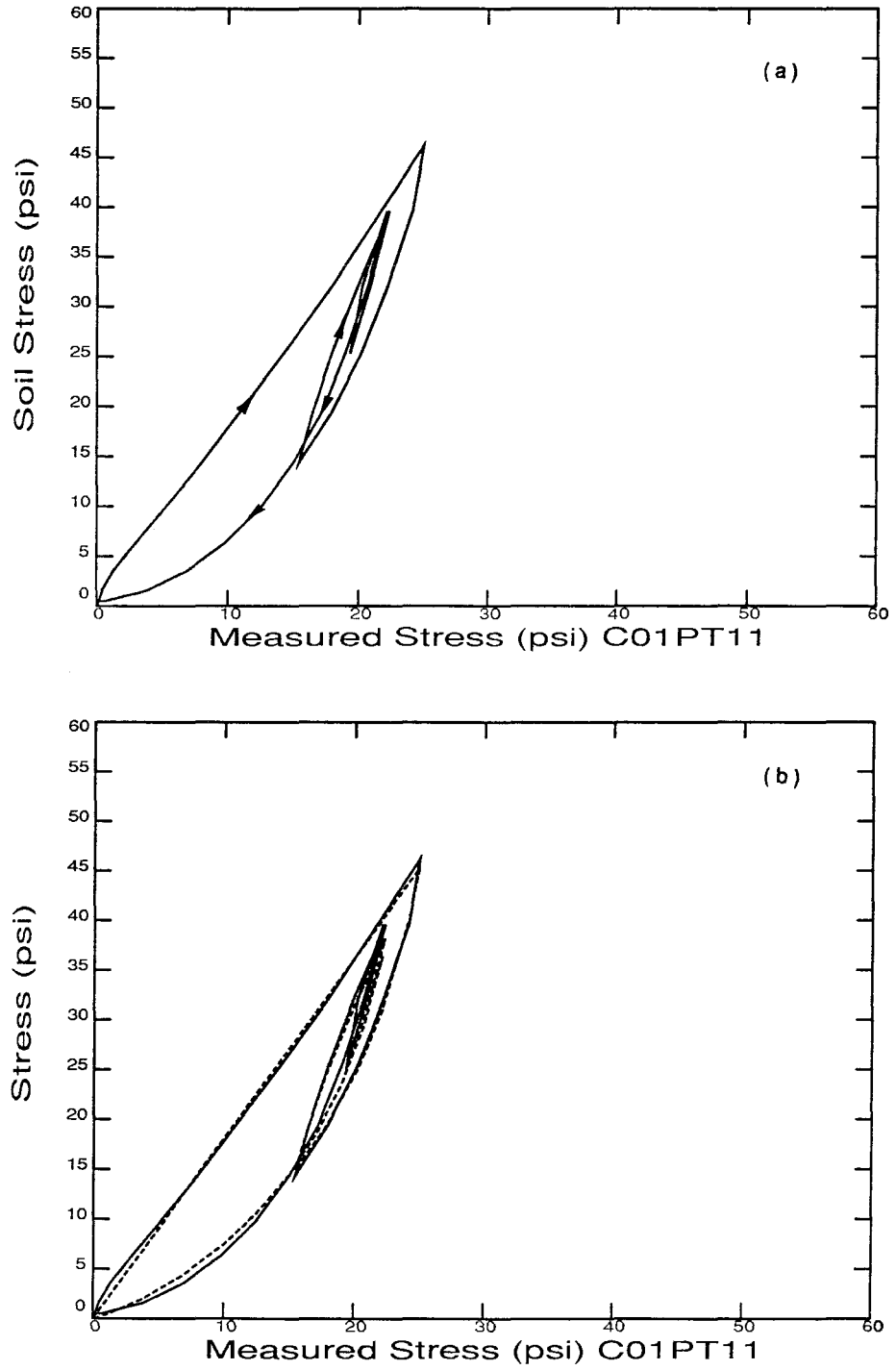

Figure 5.8 Pressure cell response to cyclic reloading during unloading
(a) centrifuge calibration
(b) comparison between centrifuge calibration (___ soil stress) and SCM prediction (. . . calculated stress)

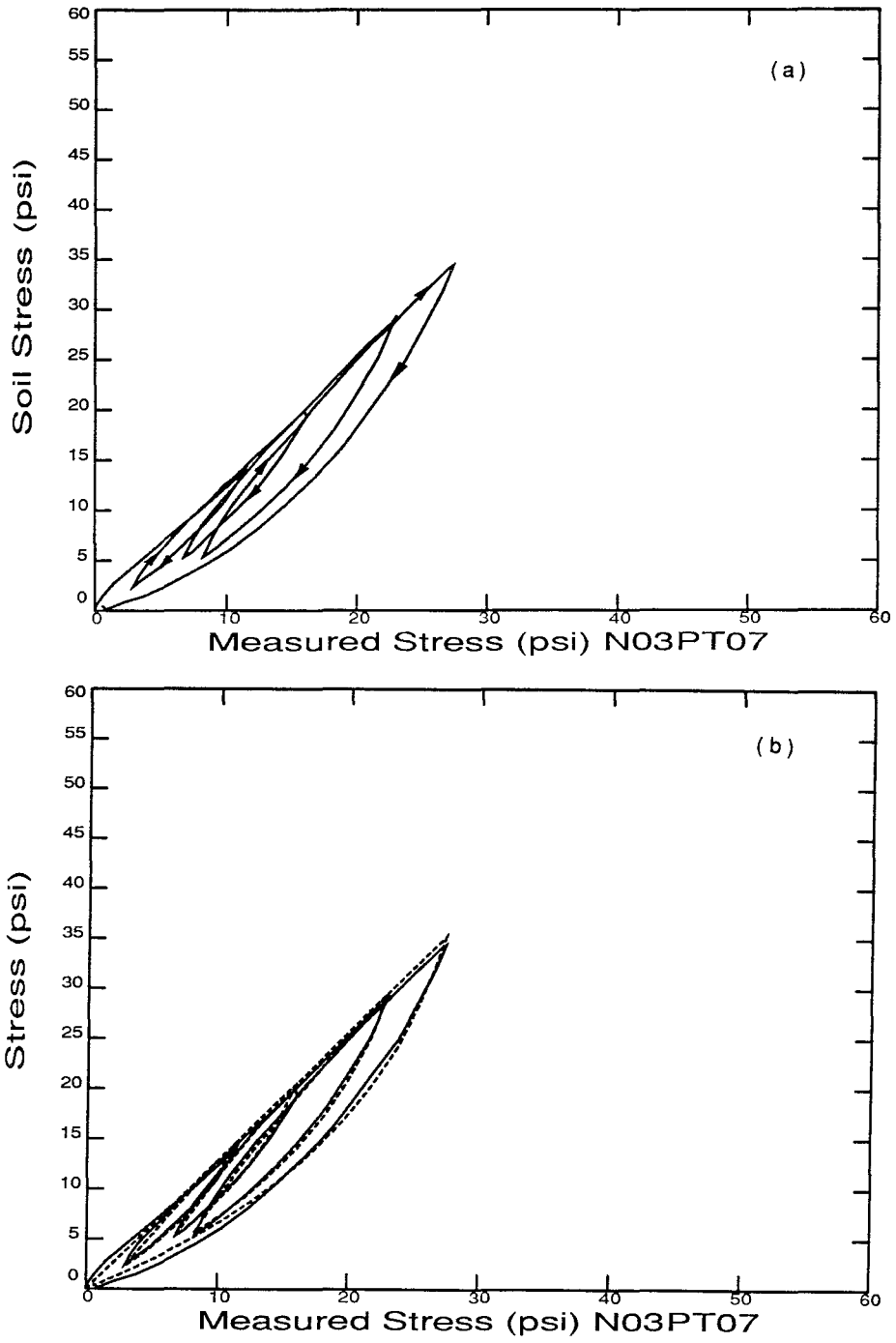

Figure 5.9 Type #4 pressure cell response to cycles of increasing σ_{max} and partial unloading
(a) centrifuge calibration
(b) comparison between centrifuge calibration (___ soil stress) and SCM prediction (. . . calculated stress)

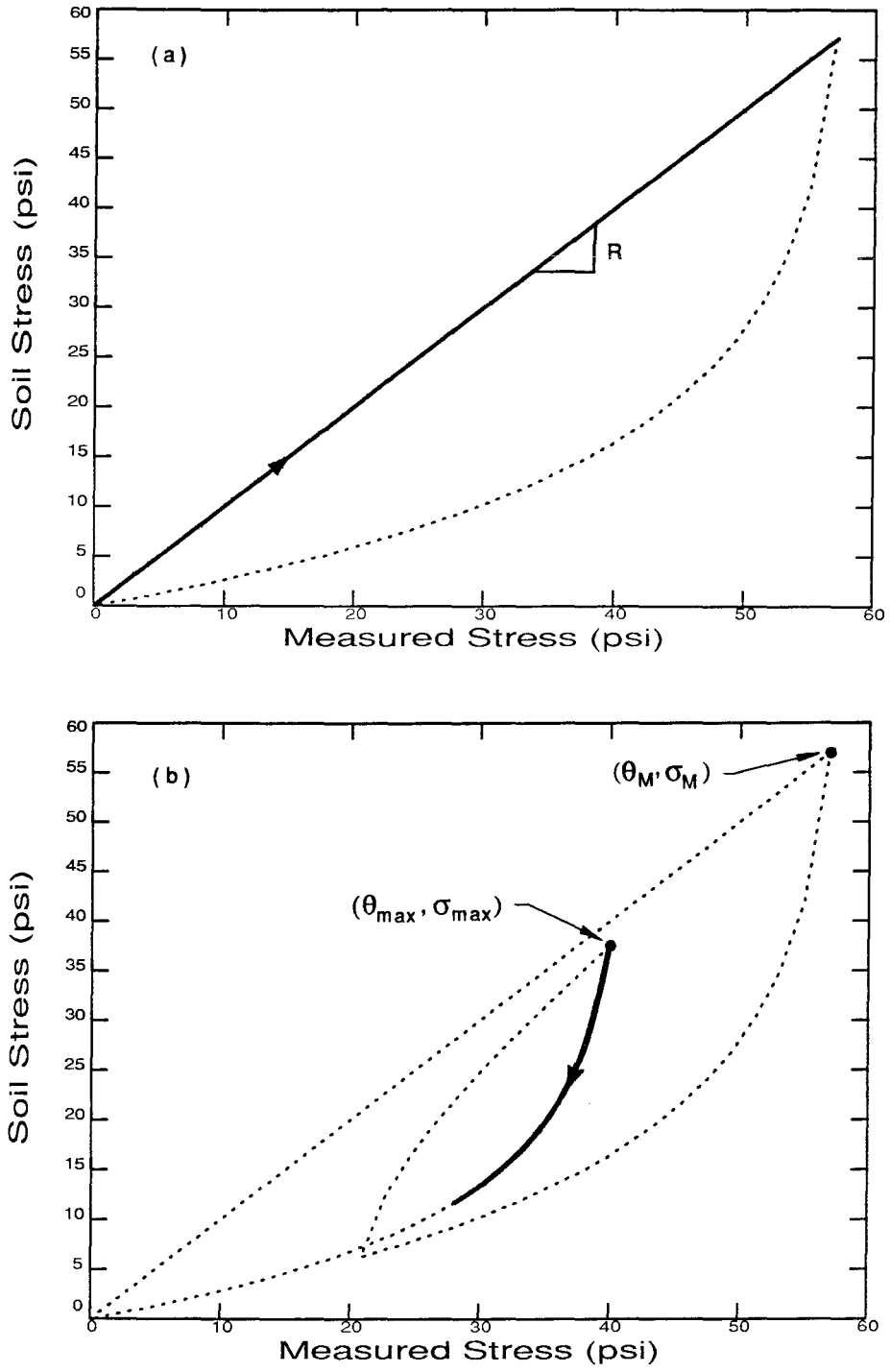

Figure 5.10 Soil-Cell Model
(a) "Virgin line" slope R (cell registration ratio)
(b) Logarithmic unloading from $(\theta_{max}, \sigma_{max})$

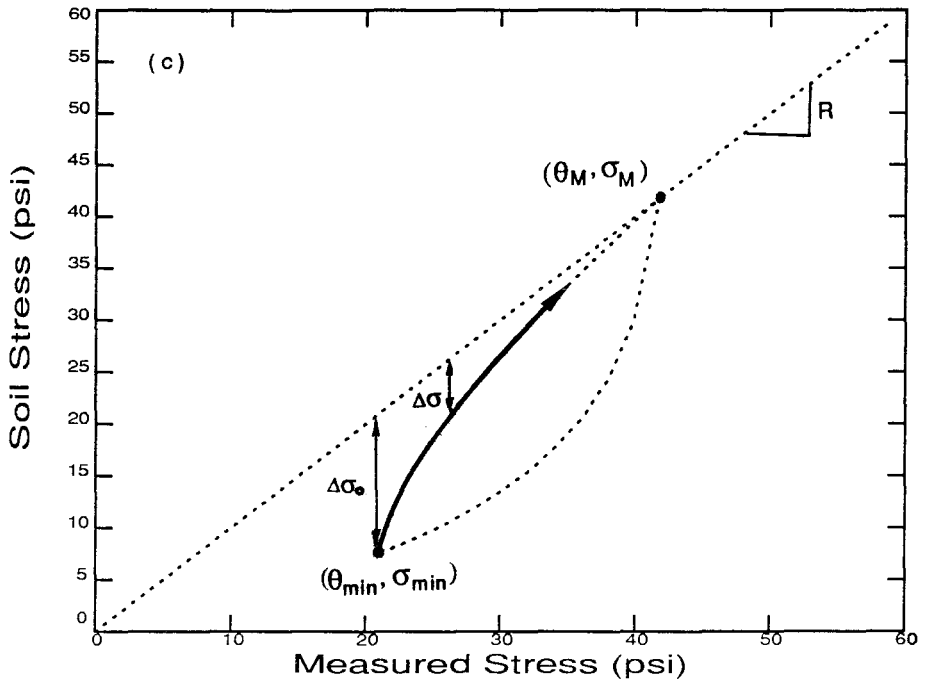

Figure 5.10 Soil-Cell Model
(c) Asymptotic reloading from $(\theta_{min}, \sigma_{min})$

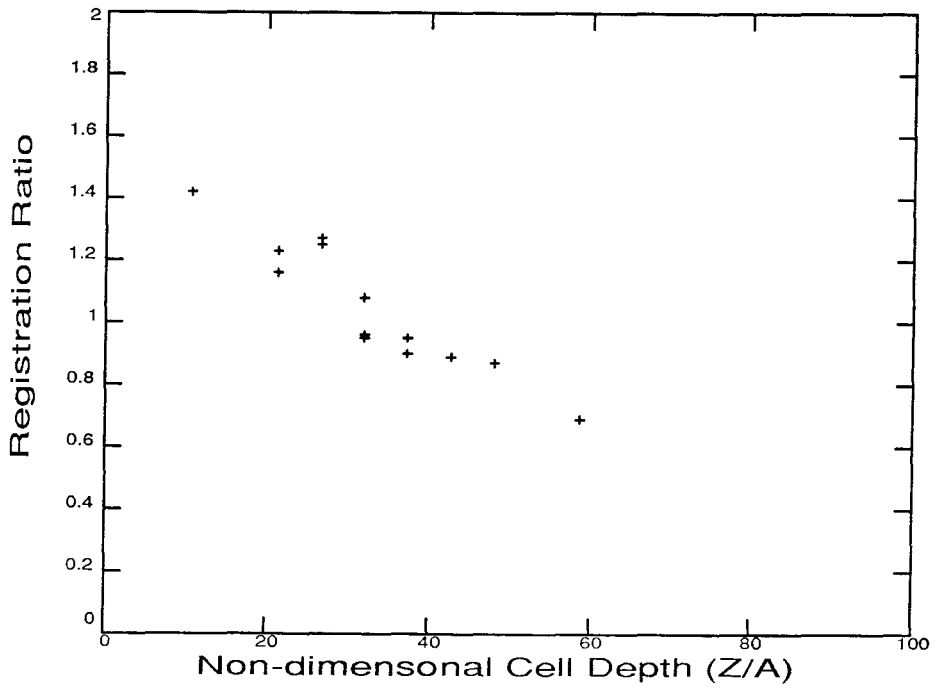

Figure 5.11 Experimental registration ratio variation with cell position

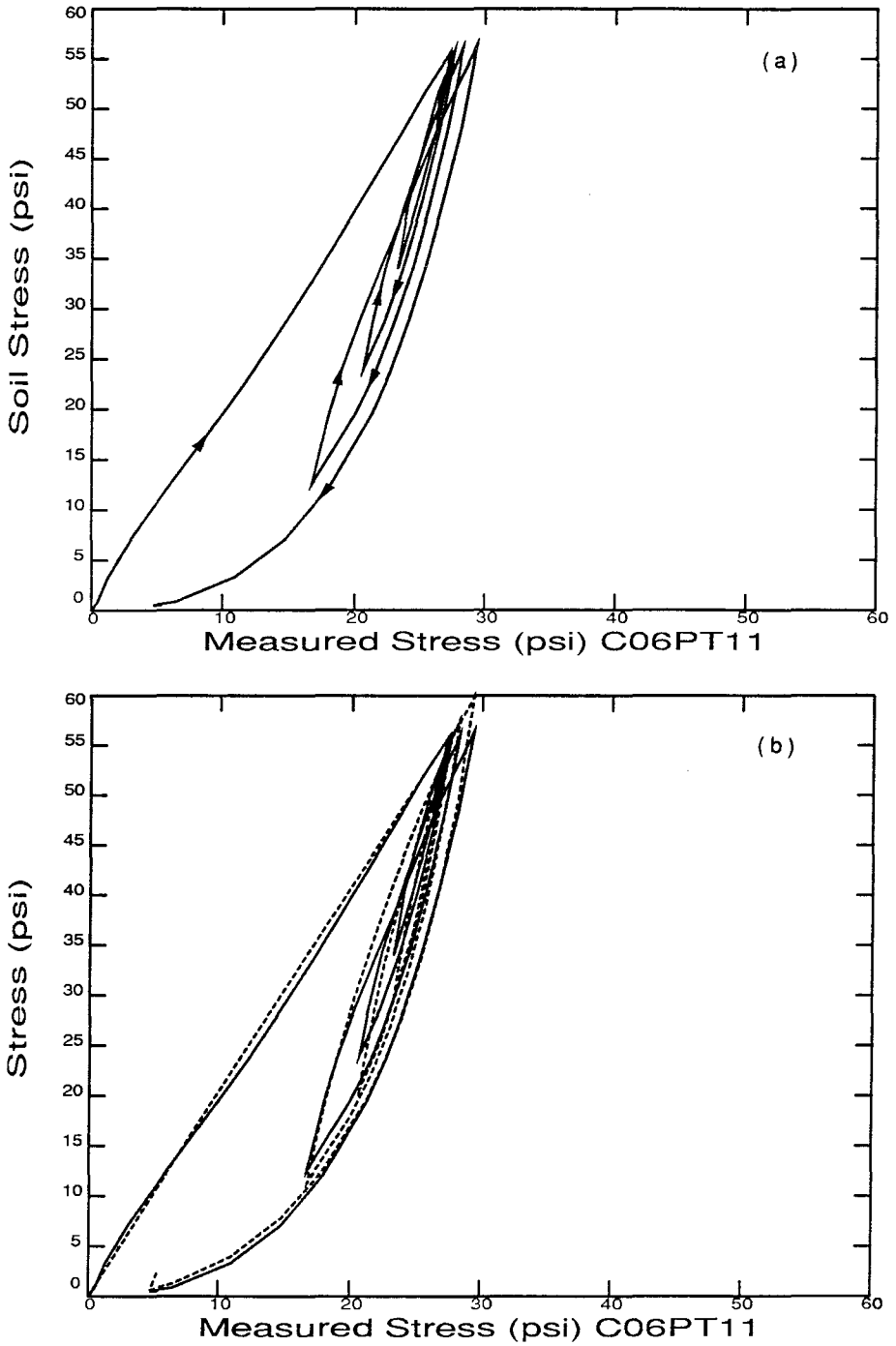

Figure 5.12 Pressure cell response to cycles of constant σ_{max} and partial unloading
(a) centrifuge calibration
(b) comparison between centrifuge calibration (___ soil stress) and SCM prediction (. . . calculated stress)

Chapter 6

EXPERIMENTAL RESULTS

6.1 CENTRIFUGE SCALING CONSIDERATIONS

The model experiments are run following the centrifuge scaling laws as described in Appendix A. The overall g-level for the experiments was 50 times the earth gravitational acceleration (50 g). The Caltech centrifuge is small in size, with a radius at the experimental bucket bearings of 36 inches. For experiments such as pile driving where there is a large motion, over 8 inches, of the model pile, the g-level gradient between the beginning to the end of the experiment becomes important. The g-level for the Caltech centrifuge is calculated from the following equation:

$$N_g = 2.8416e^{-5}\omega^2 R_g \tag{6.1}$$

where

N_g = g-level

ω = the number of rotations per minute of the centrifuge

R_g = the radial distance, in inches, from the center axis of the centrifuge to the point at which the g-level is calculated

The ratio of g-levels for the fully embedded pile from the top to the tip of the pile is:

$$\frac{g_{piletop}}{g_{piletip}} = .75$$

There are up to 25% variations in the g-level from top-to-tip of the pile or from beginning-to-end of an experiment. This g-gradient is very high, and cannot be neglected. It implies that, as the model pile is driven into the soil, the equivalent prototype pile gets longer and larger. Therefore it is not possible to simply choose one single value of the g-level to represent the scaling, from model to prototype, of all the quantities that describe the

experiment and are measured throughout driving. An estimate of the prototype quantities can be obtained using an overall scaling factor of 50, but it is to be kept in mind that this represents an average value, and that the g-level gradient plays a role in the representation of the prototype test.

Several possibilities to present the data are available: to choose the model scale for all the quantities throughout the test, to choose non-dimensional groups to cancel the dependence on the g-level, or to choose the prototype scale at a given point during the driving or axial loading for which a g-level is explicitly defined. It is important in the presentation of the experimental data to select quantities that retain their meaning in the scale chosen. Non-dimensional groups are sometimes difficult to interpret or associate with physical quantities. Consequently we limit the use of non-dimensional quantities for the lengths (*e.g.,* pile length (L), pile depth(D), pile penetration during axial loading (P), position of transducers in the soil: depth (Z), radial distance (R), see Figure 6.1) where the length is non-dimensionalized by the radius of the pile (A); or for stresses where the measured or calculated radial or vertical soil stress is non-dimensionalized by the initial overburden stress (σ_V) at the point of interest. This is what we are going to do:

For the pile; lengths (*e.g.,* pile length, pile depth, pile penetration, gage position) are non-dimensionalized by the pile radius (A) (*e.g.,* non-dimensional pile depth = pile depth/ pile radius (D/A)). Acceleration, force, stress, and time are represented in the prototype dimensions. For a given blow, the pile depth, corresponding to the embedded length of the pile, is known: D (Figure 6.1). The g-level is then calculated for the pile mid-depth (D/2), and applied to the various quantities relating to the pile characteristics, positions and response. R_g, the radial distance from the center axis of the centrifuge to the point at which the g-level is calculated for a given position of the pile is shown in Figure 6.1.

For the soil; the transducers located in the soil, being at a given position during the whole experiment, are not subjected to a g-level gradient, therefore the g-level for each transducer is calculated for its particular position. All the measured quantities can then be presented in the prototype scale or in non-dimensional form.

6.2 PILE DYNAMICS

As explained in Chapter 4, the pile response to the hammer impact is monitored throughout driving using a high speed data acquisition system to capture the transient records from the accelerometers and the strain gages placed on the pile. The experiments were conducted on closed-end piles, the modeling of the plug behavior of open-ended piles driven in sand in the centrifuge being unknown. The model pile driver directly hits the pile cap in which the top accelerometer is fixed, and a second accelerometer is located at the bottom of the pile in the plug. Strain gages are placed at various positions along the pile shaft.

Figure 6.2.1 shows the response of the pile to the hammer impact in terms of force records obtained from four strain gages located at different positions along the pile. Compression is shown downward. The model pile is 9 inches long (L/A = 48); the gages are at 2.67A, 13.33A, 34.67A, and 45.33A from the pile top, and the pile depth is D/A = 16.0 (the pile is 1/3 embedded). The compressive wave from the hammer impact can be followed down the pile. The delays observed in the signals correspond to the propagation time of the wave travelling in the pile. During the early stage of driving, the resistance offered by the soil at the base is limited. Therefore, at the pile tip a free end boundary conditions will dominate, and the compressive wave reflects into a tensile wave. The impact of the hammer on the pile cap does not give rise to a sharp pulse but rather to a long pulse due to prolonged contact between the pile and the driving mechanism. The cancellation of the downward propagating compression wave of the impact by the reflected tensile wave is observed. On reaching the top of the pile the tensile wave will reflect as a compression, which can be seen propagating down the pile. The wave can be seen to propagate down and up the pile, reflecting at the top and a second time at the tip. Because of the soil resistance at the pile tip and along the pile, energy is dissipated into the soil and the wave propagating in the pile is attenuated. This behavior is observed in prototype piles (*e.g.*, [9], [26], [33], [44], [56], [85], [116]). In some prototype experiments on very long piles the duration of impact is in the order of L/2c and therefore a compression pulse followed by an actual tensile pulse can be seen near the pile tip, and the tensile pulse reflected into a compression pulse is also observed near the top of the pile, (*e.g.*, Tagaya [147], Meunier and Gaulois [90]).

Wave propagation in the pile, treated as a semi-infinite elastic rod where only one-dimensional (axial) motion is assumed, is governed by the following differential equation (*e.g.*, Love [87]):

$$\frac{\partial^2 w}{\partial t^2} = c^2 \frac{\partial^2 w}{\partial z^2} \tag{6.2}$$

where

w = axial displacement

t = time

c = wave speed in the rod

z = axial position

with:

$$c = \sqrt{\frac{E}{\rho}} \tag{6.3}$$

where

E = Young's modulus of pile material

ρ = pile material density

The solution of Eqn. (6.2) by the method of characteristics is of the form:

$$w = f(z - ct) + g(z + ct) \tag{6.4}$$

where f and g are functions that represent the downward and upward travelling wave. With the convention of positive downward displacement and compressive strain and stress, Eqn. (6.4) leads to:

$$\epsilon_z = -\frac{\partial w}{\partial z} = -(f' + g') \tag{6.5}$$

$$\sigma_z = E\epsilon_z = -E(f' + g') \tag{6.6}$$

$$F = A\sigma_z = -EA(f' + g') \tag{6.7}$$

where

ϵ_z = axial strain

σ_z = axial stress

F = force in the pile

A = pile sectional area

and the prime denotes the derivative of the function with respect to its argument. The particle velocity, v, is given by:

$$v = \frac{\partial w}{\partial t} = -c(f' + g') \tag{6.8}$$

By decomposing the force and velocity in two terms (F_d and F_u, and v_d and v_u) corresponding to the downward and upward travelling wave respectively we obtain:

$$v = -cf' + cg' = v_d + v_u \tag{6.9}$$

$$F = -EAf' + EAg' = F_d + F_u \tag{6.10}$$

Eqn. (6.9) and (6.10) lead to:

$$F_d = v_d * EA/c \tag{6.11}$$

$$F_u = v_u * EA/c \tag{6.12}$$

which give the proportionality of the force in the pile to the particle velocity for each travelling wave in the one-dimensional wave analysis. The parameter EA/c is commonly referred to as the pile impedance.

Figure 6.2.2 (a) and (b) show the comparison of the force at the top of the pile obtained from the strain gage record (measured force) and the integration of the acceleration record ($v * EA/c$) for two pile depths. We obtain good agreement at short times: $L/c < 2$ (before the arrival of the reflected wave, as we are dealing with a finite length pile) between the measured force (strain gage) and the calculated force (from accelerometer). The assumption of one-dimensional wave propagation for the impact stress wave in the pile gives a reasonable fit for the calculated force in the pile for our model experiments, as predicted by the theory. The delay or time differences in the plots, between the measured and the calculated forces correspond to the difference in position of the measuring devices, and to the limited validity of the application of the one-dimensional analysis for the three-dimensional problem of pile driving. The acceleration is measured in the pile cap and the force is measured directly on the pile, by the strain gages at 2.67 pile radii from the top.

The pile dynamic response to the hammer impact is well observed, and the results show that simulation of pile driving is obtained in these centrifuge experiments. A more detailed analysis of the pile dynamic data is not addressed here. As mentioned in Chapter

1, the dynamic response of the pile has been the subject of many investigations, both experimental and numerical, since the introduction of the Smith's pile driving model in 1960. The present work aims at obtaining a better understanding of the pile-soil interaction from the soil dynamics point of view, a subject which has not been looked at because of the difficulties involved in obtaining experimental data, as described in Chapter 1. The experimental method being established, we now present the results obtained on the soil response during pile driving.

6.3 SOIL STRESS FIELD

As mentioned in section 3.3.2, the soil stress field is monitored during driving by means of pressure cells located in the soil on a grid to represent radial vertical sections of the soil for this axisymmetrical problem.

The insertion of the pile into the soil provokes perturbations in the soil mass. During pile driving, substantial soil remolding occurs below the tip and also along the pile shaft. Currently it is considered that pile driving in cohesionless soils can cause soil densification, which will be most pronounced in the immediate vicinity of the pile shaft and extends with decreasing intensity over a cylindrical region of several pile radii around the pile (see Figure 6.3.0.1). The driving process is also accompanied by changes in the horizontal and vertical soil stresses in the vicinity of the pile. In dense sand, expansion and loosening may take place as well as grain crunching and densification. Also, in the case of hard driving conditions, large residual stresses can exist both in the soil and in the pile. According to model and full-scale experiments it is observed that there exists a highly compressed conical wedge under the pile tip, as shown in Figure 6.3.0.2 As the pile penetrates deeper, the soil wedge (I) pushes the radial-shear zone (II) sideways into the plastic zone (III). The advancement of the pile is made possible by lateral expansion of the soil along the circular ring BD, as well as by compression that can take place within zones (II) and (III), Vesic [158].

Pile driving consists of a succession of impacts of the hammer on the pile. What happens at each hammer blow can be briefly described as follows:

1. The pile is at a given depth in the soil; the stress gages are at one position in the soil, measuring static stresses.

2. The hammer strikes the pile, stress waves propagate down and up the pile at the rod velocity, for the stainless steel pile: $\approx 17000 ft/sec.$

3. Shear and pressure waves are propagated into the soil by the motion of the side and the tip of the pile. The travelling speeds of P and S waves, for the fine Nevada sand, are about 15 and 40 times smaller, respectively, than the travelling speed in the pile, at an average depth.

4. The pile moves down a few hundredths of an inch.

5. The soil stress waves are recorded by electrical signals from the pressure transducers (dynamic data obtained from the high speed analog-to-digital converter (ATD)). Waves are reflected by the side and base of the container. Then, all the transient stresses dissipate, and the soil reaches a new state of stress, referred to as "static stress field," captured by the general purpose ATD.

6. The same sequence is repeated for the next blow. It is to be noted that the complete dynamic response of the pile and the soil is over before the next impact on the pile.

The data consist of:

a. dynamic data: time histories of transient stresses at given locations in the soil for given blows (given positions of the pile);

b. static data: stress histories at given locations in the soil as the pile is driven into the soil.

We present the total static stress history, at the points of interest in the soil surrounding the pile, as a function of the depth of the pile tip.

Both vertical and horizontal stresses are measured. For pressure cells oriented such that they read radial stress (horizontal stress), we make the assumption that the initial horizontal stress, before driving, is on the at-rest pressure, or K_0, line, represented by the following expression suggested by Jaky:

$$\sigma_H = K_0 \sigma_V$$

with

$$K_0 = 1 - sin\phi$$

where

σ_H = initial horizontal stress

σ_V = initial vertical overburden stress, which results from the density of the soil, the acceleration field, and the depth from the surface to the point in question

K_0 = coefficient of lateral stress

ϕ = soil friction angle

It was mentioned in Chapter 5 that the measurement of stresses in the soil by means of pressure cells requires special consideration, and the interpretation depends on the treatment of the data. It was shown that the non-linear soil-cell interaction could be represented by a model described in section 5.3. In most investigations on soil stresses, nothing is said about soil-cell interaction, and this leads us to think that the approximation of a linear interaction and gage response is generally assumed. Therefore, to correspond with previous interpretations based on the linear assumption, the data from the pile driving experiments are first interpreted and presented on the basis of the linear assumption. Then later "real" soil stresses will be discussed. Although the word "stress" will be used in the following description, the real hysteretic behavior of the soil-stress cells on loading-unloading (Chapter 5) means that the actual stresses will be much different from those of the figures and discussions.

6.3.1 Measured static stress field: linear assumption

In the case of the linear assumption, the value of the output of the cell at the end of the blow and the manufacturer's calibration factor are sufficient to calculate the stress; the stress obtained in this case is simply what we referred to as the measured stress $\theta = \frac{V}{c_f}$, Eqn. (5.2).

6.3.1.1 Radial distribution of the radial measured stress

Figures 6.3.1.1.a to 6.3.1.1.c present the evolution of stress in the soil, as a function of the depth of the pile tip, as the pile is driven down, for transducers located at the same given depth (Z/A= 16.00 (Fig. a), 26.67 (Fig. b), 37.33 (Fig.c)), but at different radial distances from the center axis of the pile (R/A= 2.67, 5.33, 8.00, 16.00, 24.00).

It is observed that closer to the pile:

a. the peak stress level is higher

b. the rate of stress increase and decrease is higher

c. the peak stress is obtained *before* the pile tip reaches the transducer level (D/A < Z/A), whereas, farther away from the center axis, the peak stress is obtained *after* the pile has passed the level of the cell.

d. the residual stress level, when the pile tip is much deeper than the transducer, is higher.

As the pile penetrates into the soil a failure zone is generated at the tip of the pile (Figure 6.3.2), and the soil will flow around the pile tip toward the side. In the failure zone at the pile tip, large stresses in the elastic and plastic range and permanent (plastic) volume changes will be generated. Farther away from the pile, the soil rearranges itself to allow for the volume change of the pile penetrating into it, and at large distances presumably only elastic volume changes occur. In these experiments, the pile is closed-ended and there is no formation of a soil plug inside the pile. The soil, being in a medium-dense ($i.e., \gamma = 99pcf$) condition, is expected to densify, with the level of soil compaction decreasing away from the pile. As the pile tip gets closer to the transducer, the disturbance, and therefore the level of stress increase. Once the tip passes the level of the transducer the compression and large disturbance zone moves away from the transducer, relaxation will occur in the soil surrounding the cell, and the stress level decreases.

It can be seen from Figures 6.3.1.1 that for a given position of the pile, after the pile tip has passed the depth of the transducers, the stress level is higher further away from the pile. This is due to the rapid and large decay of stress after its peak value, as monitored by the transducers closest to the pile. This can be explained by the presence of the "tensile" zone (actually decrease in compression) just above the plastic zone (III), and close to the pile. Because of the friction along the pile shaft and the compression at the pile tip, the soil in this area will be "pulled" down, thus allowing for relaxation of the existing compressive stress. Even though the word "tensile" is used, tensile stresses are not observed because of the existing compressive stress level; what is to be understood is that the stress increment is negative, compression is positive. Also the stress will still be increasing farther away from the pile, while closer it is decaying or stabilizing. It can be seen that in this case the frequently-used assumption of radial expansion of a cavity ([24], [40], [42], [106], [157], [163]) as a model for soil response around a pile does not hold: the stress does not increase or decay monotonically with the radial distance from the pile. From previous studies ([8], [86])

it was observed and concluded that the excess radial stress due to driving was negligible compared to the overburden stress beyond a distance equal to about 16 pile radii. It can be seen that for the experiments conducted in dry sand this is not true, because at a distance of 24 pile radii, there is still an excess stress due to driving, of the order of the overburden stress.

Figure 6.3.1.1.a shows that, for the transducer closest to the pile, the stress drops to a minimum after the peak and then goes up again to reach the final value of residual stress. Also the peak value is very high, if compared to the peaks experienced by cells at the same radial distance but at greater depths in the soil (Figures 6.3.1.1 b and c). It is expected that the cell is in fact closer to the pile than the R/A = 2.67 value which is aimed at during experimental set-up (see section 6.3.1.5). Hence, the relaxation will be larger, and as the pile tip moves away, and large disturbances die out, the soil reaches a steady state of stress.

6.3.1.2 Vertical distribution of the radial measured stress

Figures 6.3.1.2.a and b show the output of transducers reading radial stress and located at the same radial distance R/A = 2.67, and at various depths (Z/A= 10.67, 21.33, 26.67, 32.00, 37.33, 42.67). Figure (a) gives stresses in real (linear assumption) terms, and (b) in non-dimensional form where the stress is normalized by the respective overburden stress at each transducer depth.

It is observed that as the transducer depth increases:

a. the overall peak stress level increases

b. there is consistency in the rate of increase and decrease of the stress

c. the peak is reached sooner, the farther up the pile is from the transducer level

d. the final residual stress level increases

In Figure 6.3.1.2.b, it is interesting to note that the non-dimensional peak stress is approximately the same for all the transducers, but the final residual stresses still increase with depth.

6.3.1.3 Comparison of radial and vertical measured stresses

Figures 6.3.1.3.a to 6.3.1.3.e show the variation of radial and vertical stresses at a given location. Figures a to c show the evolution of the stress fields for 3 pairs

of transducers at a given radial distance (R/A=5.33) and at different depths (Z/A= 21.33, 26.67, 37.33), where the vertical stress is shown in a solid line and the radial stress in a dashed line. Figures d and e present the vertical stress change for 2 pairs of cells located at the same depth (Z/A=32.00) but different radial distances (R/A=2.67 and 8.00).

We can observe a consistency in the behavior between the two cells of each pair. The vertical stress peaks before the radial stress and shows a local minimum when the radial stress peaks. The stress history can be decomposed into several stages in terms of the relative location of pile tip and transducer:

1. The pile tip is well above the transducer level. The disturbance due to the insertion of the pile is felt as an essentially uni-axial compression. The axis of compression is close to vertical and the soil is under confined compression. There is reduction of volume, the sand grains are pushed closer together due to the predominance of effective normal stress over shearing stress.

2. The pile tip is closer to the transducer. The vertical stress reaches a peak. The horizontal stress is increasing faster; the axis of compression has rotated to a more horizontal position.

3. The horizontal stress is higher than the vertical stress, and both are higher than the overburden stress. Loading is essentially uni-axial, but the principal axis is close to horizontal. The equilibrium of the soil element under uniaxial loading results in a decrease of the normal stress.

4. The radial stress reaches its peak and the vertical stress its local minimum. This is the point of maximum shear.

5. Unloading of the horizontal stress occurs, the vertical stress increases to a local maximum, and the soil element is back to a state of stress close to the one of stage 2.

6. The pile has passed the level of the transducers, relaxation proceeds, so that both radial and vertical stresses decrease to reach a final residual level.

For small depths the radial stress increase is larger than the vertical stress increase (Fig. a). As the transducer depth increases the excess vertical and radial stresses become the same (Figs. a to c). For small radial distances the radial stress increase is larger. As

the transducer is placed farther away from the pile, the excess stress in both vertical and radial direction becomes the same (Figs. d and e).

Figures 6.3.1.3.f and g give the distributions in radial and vertical directions of the vertical stress. Apart from the difference in shape for the vertical stress curve (camel) compared to the radial stress curve (dromedary), we observe the same trends as described in 6.3.1.1 and 6.3.1.2.

6.3.1.4 Measured soil stress contours

The stress contours presented in Figures 6.3.1.4.a and b compile the results of a variety of different tests into a global picture of the stress field. Because of the inherent symmetries of the experimental set-up only a section of the container is drawn. For a given position of the pile, (D/A= 15.0, 25.0), the stress level measured by each cell is obtained from the previously described static stress histories. These values of stress are placed at the transducers' locations, in the section, to draw contours. The radial stress contours are presented on the right side, and the vertical stress contours on the left side. The walls of the bucket are shown, for some boundary effects are expected.

It was decided to present this graph in non-dimensional form where the depth and radial distance position of the transducer are normalized by the radius of the pile (Z/A, and R/A respectively); and the stresses by the initial overburden stress. However, it has to be said that these contours have an indicative value and should not be understood as presenting exact values. There are many reasons for this but the main ones are:

- some differences in soil and test conditions between different experiments
- different driving histories from test to test
- variations in the soil-cell interactions: uncertainties in the location of the cells, effect of the non-uniform placement of the soil
- movement, especially of the closer cells, during driving
- linear calibration assumption, the contours of stresses for the non-linear soil-cell model assumption are predsented later in Figure 6.3.3.5
- insufficient number of cells

However, from these contours we can observe that as the pile gets deeper:

- the zone of compression below the pile increases in size
- the zone of influence further away from the pile wall increases
- the upper lobe in the contours along the pile stretches: the zone of compression extends further up and away from the pile
- the pile/soil interaction is truly three-dimensional

From the shape of the contours we see that the radial stress does not decay monotonically as a function of the radial distance. We then know that the analytical analysis of expansion of a cylindrical cavity will not fit the data in this case. Also, because the soil is dry, permanent volume changes have occurred.

6.3.1.5 Peak measured radial stress variation

Figure 6.3.1.5 presents the variation of the peak stress as a function of the radial distance in non-dimensional terms (Peak Stress / σ_V, R/A). For each point in the graph, two error bars could be drawn: in the horizontal direction to allow for the error in the transducer location, and in the vertical direction for errors in the stress measurement. The two points showing a very large stress indicate the stress levels close to the pile. For these two transducers the stress history during driving presents the peculiarity of a fast rise to a very high peak stress followed by a sharp decrease to a local minimum and then an increase to a final state of the stress (see Figure 6.3.1.1.b). It is concluded that these two cells were, in fact, closer to the pile than was estimated experimentally.

Errors in position of the cells are to be expected for many reasons, but in particular, in these experiments they are caused by the non-concentricity of the container, the possible motion of the cells as the placement of the soil proceeds, and pile alignment during driving. Also closer to the center axis (small radial distance) the relative error becomes larger. It is observed that all the data can be fitted with a hyperbolic curve. A logarithmic decay curve, as predicted with the model of cylindrical expansion of a cavity, does not fit the data well. Using an upper fit of the hyperbolic curve:

$$\text{Peak Stress}/\sigma_V = 20 * \frac{1}{R/A}$$

a maximum peak non-dimensional stress of 20 at the boundary of the pile (R/A = 1) is obtained. With that curve the new position for the two cells with high peaks is estimated to be R/A= 1.6 and 1.5 respectively.

6.3.2 Soil Dynamics

In Chapter 5 we have shown that the interpretation of the pressure cell output in terms of soil stresses requires an understanding of the stress history during driving and thus an understanding of the soil dynamics. The instrumentation used in these experiments has enabled us to record the soil stress transients during the hammer impacts on the pile. Being able to look at both the pile and the soil transients during driving, and therefore at the pile-soil dynamic interaction, is something new and thus requires a careful analysis. So, to get a first picture of the soil dynamics, we first look at the dynamic stress field using the linear assumption in this section. In the following plots, model time is chosen as the time scale. For each transducer's depth a g-level is calculated giving a model to prototype scaling value. Because of the g-level gradient, prototype time plots would have different record lengths for transducers at different depths. In chosing model time, the time scale is the same for all the transducers. Centrifuge modeling gives a one-to-one relation between model and prototype stresses; therefore the stresses shown in the plots are both model and prototype stresses.

6.3.2.1 Measured transient stress following a blow

Figures 6.3.2.1.a and b show the soil radial dynamic stress history following a blow, for a transducer located at a depth Z/A = 26.67 and a radial distance R/A = 2.67; the pile depth is D/A = 24.1, and 26.80 respectively. Radial excess over static stress is shown. The static stress history of this transducer, presented in Figure 6.3.1.2.a, shows that before the pile tip reaches the level of the transducer the static stress level at the transducer location increases, and once the pile tip passes the level of the transducer, the static stress level decreases.

In Figure 6.3.2.1.a, the pile tip has not yet reached the level of the transducer, which is situated very close to the pile axis. In the area where the transducer is located, the soil is submitted to large deformations and important densification to allow for the penetration of the pile. The transducer is in the failure zone of the pile tip compression area. The excess

stress at the end of the blow, which corresponds to the increment of the static stress field, is positive, which in turn means an increase of the static stress as described above. Large dynamic compressive excess over static stress is observed. Also the final residual stress increase at the end of the blow is small compared to the peak stress experienced during the blow. This demonstrates that the energy of the blow is absorbed by the rearrangement of the soil by elastic and also plastic deformation, including, in particular, volume decrease.

In Figure 6.3.2.1.b, the pile tip has passed the level of the transducer. This time the excess stress at the end of the blow is negative, which corresponds to a decrease of the static stress as described above; also, large dynamic tensile excess stress is observed. The figure shows relaxation of the compression level, which indicates that the transducer is not in the compression part of the failure zone mentioned above but in the "tensile" region as described in section 6.3.1.1. In this case, pile skin friction stresses are predominant and these cause tension at the level at the transducer.

6.3.2.2 Dynamic measured stresses, wave speed and stress decay

Figure 6.3.2.2.a: Shows the time variation of stress for the transducers of Figure 6.3.1.1.b at Z/A = 26.67 and different radial distances (R/A = 2.57, 5.33, 8.00, 16.00, 24.00). The pile tip is at this stage above the transducers' level, at a depth (D/A) of 21.3. This means that the transducers are all seeing compressive stress. We can also observe evidence of the propagation of the P-wave, the velocity of which can be deduced from the delays between the rising edges of the records. The average velocity at this depth: Z/A = 26.67 has been calculated to be 1260 ft/sec, compared to 17,000 ft/sec for the pile. Also a higher velocity is observed closer to the pile where the soil is under higher compressive stresses.

Figures 6.3.2.2.b and c show the output of two transducers located at the center axis below the pile top and reading vertical stresses. They are at depths of Z/A = 48.0 and Z/A = 56.7 respectively. In Figure 6.3.2.2.b, the pile tip is a depth of D/A = 19.4, and at D/A = −39.4 in Figure 6.3.2.2.c. In both figures the transducers see compression but, as could be expected, the deeper the pile tip is, the larger the compression measured. The velocity of the P-wave can also be measured. In Figure 6.3.2.2.b the speed is 1450 ft/sec. This value is already higher than the previous 1260 ft/sec because the soil is at a higher

confining pressure at this depth. The increase of Young's modulus with confining pressure was given in section 3.1.1. The P-wave velocity given by Eqn. (6.3) also increases with confining pressure. In Figure 6.3.2.2.c, the speed is 1735 ft/sec. The difference gives an account of the densification and remolding of the soil caused by the insertion of the pile. The confining stress level at that stage of driving is higher at these locations than the initial confining pressure.

In Figures 6.3.2.2. a, b, and c, the decay of the peak (dynamic) stress value can be observed both radially and vertically. We also see that the higher the stress the greater the decay (cf. figures b and c). In figures a and c, the peak stress for the transducer located close to the container boundary is not very important. This suggests that the reflection of the compression wave does exist but is not a too important phenomenon in these experiments. The duration of the compression for the transducer located close to the pile is larger than the time required by the P-wave to go to the container wall and to come back after having reflected from it. In contrast, the duration of the compression for the transducer located closer to the container wall is much smaller. This can be explained by the large decay of the transient stress.

However, the presence of the container boundaries does have some effect on the pile-soil dynamic interaction and this indicates limitations to the representativeness of these experiments with respect to the simpler case of a single pile driven in a half space.

6.3.2.3 Radial distribution of the dynamic radial measured stresses

The positions of the transducers of Figure 6.3.1.1.b at Z/A = 26.67 and different radial distances (R/A = 2.57, 5.33, 8.00, 16.00, 24.00), are shown in Figure 6.3.2.3.a, as well as the position of the tip of the pile for various blows (blow # 50 (B50), to blow # 100 (B100 or B0A)).

Figure 6.3.2.3.b (3 pages) shows the transient stress history of the different transducers for various blows as the pile is being driven into the soil. Only part of the time history of each blow is shown since the most significant part occurs at the beginning. Also, during this experiment we have evidence of a second smaller impact of the hammer on the pile, which generates a second wave of dynamic soil stress; for clarity the time history has been cut before the second impact.

Similar shapes of transient loading for all transducers are observed, with variation mostly in the amplitudes of stresses. The shape changes indicated by the different transient histories as the pile moves down are seen on all the transducers. There are four typical shapes of transient behavior schematically represented in Figure 6.3.2.3.c. The first one, S1, (see T70PT1 blows 50 to 80) corresponds to the presence of a compression zone in the area of the transducer (as explained in section 6.3.1, the pile tip has not reached the transducer level). The second one, S2, corresponds to the beginning of relaxation after the peak static stress, when the peak transient stress is compressive, but the final level of stress at the end of the blow shows a decrease of stress. The third one, S3, (see T70PT1, blow 90) corresponds to a transition zone (pile tip at level of transducer), while the fourth one, S4, (see T70PT1, blow 100 (0A)) corresponds to the presence of a tensile zone in the area of the transducer (pile tip below transducer). The meaningful history (corresponding to the major increase and decrease of the static stress field) for a transducer output while the pile is driven can be described as a series of S1 with increasing amplitude, followed by a very few S2 (less than 10 blows) with decreasing amplitude, a few S3 (less than 10 blows), and then a series of S4. When the stress reaches its final level, the signal shows low amplitude stress variations that account for the presence of waves propagating in the soil and still reaching the transducer.

On the loading part of the stress curve the transient stress is essentially compression with an increasing amplitude as we get closer to the peak. Once the peak is passed we first have smaller compressions and then essentially relaxation. In analogy with the peak static stress (see section 6.3.1.1), the peak transient stress is reached sooner as we get closer to the pile. Also the duration of the compression-relaxation cycle is shorter as the transducer gets closer to the pile axis.

6.3.2.4 Vertical distribution of dynamic radial measured stresses

The positions of some of the transducers of Figure 6.3.1.2.a reading radial stress and located at the same radial distance R/A = 2.67, and at various depths (Z/A= 21.33 (PT2), 26.67 (PT3), 32.00 (PT4), 37.33 (PT5)) and a transducer reading vertical stress and located at R/A= 5.33 and Z/A=26.67 (PT11), are shown in Figure 6.3.2.4.a, as well as the position of the pile tip for various blows (blow # 20 (B50), to blow # 230 (B230 or B3B)).

Figure 6.3.2.4.b (7 pages) shows the transient records of the transducers of Figure 6.3.2.4.a for various blows throughout the driving history.

For the transducers reading radial stresses, a consistency in the history of shapes and amplitudes of the transients can be observed, as mentioned in the previous section. Because the transducers are located at different depths, the propagation of these shapes, and the evolution of the amplitudes, can easily be observed as the pile progresses downwards.

For the transducer reading vertical stress, the history can be described also in terms of typical blow shapes. This time the transducer output history can be described as a series of S1 with increasing amplitude, followed by a series of S1 of decreasing amplitude. In the case of a vertical stress record history the second series of S1 lasts longer than in the case of a radial stress history. This coincides with the difference in shape of the static stress field described in section 6.3.1.3. The history proceeds with blows S2 and S3 and low amplitude variations. It is observed in the dynamic as well as in the static history (section 6.3.1.3) that the vertical stress shows higher transient peak stresses before the radial stress.

6.3.2.5 Conclusion

By using the linear assumption we have been able to identify the typical stress history seen by a transducer according to its location in the soil. When compared to the model defined in Chapter 5, the linear assumption actually represents an upper bound. In the typical shapes of transient stress S1, S2, S3, S4 (and the stress histories), it can be seen clearly that the peak values are much larger than the final residual stresses. This implies that the soil stress dynamics reflect the energy dissipation in the soil. This in turn entails a number of important non-linear phenomena that happen during driving (*e.g.*, large stresses, large deformations, and plastic deformations), which cast doubt on the validity of the linear assumption for the soil-cell interaction.

There are also limitations in the use of a fixed interaction model, the soil-cell model described in Chapter 5 (SCM), throughout the driving history, but this will give us a better estimation of the stress field because the model takes into account the non-linear behavior of the soil.

6.3.3 Calculated Static Stress Field: Soil-Cell Model Assumption

In Chapter 5 it is shown that the linear assumption for the interpretation of the pressure cells output in terms of soil stresses, as was assumed in the above section, is not correct. Thus to obtain a correct picture of the stress field, we need to investigate closely the soil dynamics and then the stress history during driving. The model described in Chapter 5 is a history-dependent model; that means that, in order to calculate the stress at a given point, at a particular instant in time during the pile driving history, it is necessary to know the full past stress history before that point.

The incremental state of stress in the soil after each impact of the hammer on the pile is the result of the transient stress history. This in turn implies that for a given transducer the final static stress field can be calculated using the model only by going through the full dynamic time history of stress at each blow. This has been done for selected transducers, and permits the same presentation of results to be made, as in the case of the linear assumption.

6.3.3.1 Implications of the soil-cell model assumption

Before presenting the results obtained using the soil-cell interaction model, it is necessary to say how the complete stress history throughout the driving, needed as input to the model, is obtained.

Recreating the missing blow histories

The dynamic data for each transducer are available only for every tenth blow. To record the complete history for each blow of every transducer for every test would have required equipment not available physically or financially. However, the procedure to be described can be justified by the fact that over 10 blows, the increase in depth of the pile is sufficiently small that the sensor sees practically the same waves coming from the pile. In the previous discussion it was pointed out that a stress interpretation by the nonlinear transducer calibration model requires a complete stress history. As the transient stress record for a transducer is available for every tenth blow only, this history is lacking for the previous 9 blows of each recorded blow. In order to get the complete history, it is necessary to recreate the effects of these 9 blows. The following reasoning to recreate the missing dynamic histories of the blows was used.

Figure 6.3.3.1.a shows values of stress directly evaluated from the output voltage values of the transducer from dynamic and static records. For all the measurements obtained from the dynamic records there is only one value every 10 blows; in between we link the points by a straight line (*i.e.*, linear interpolation). The following is presented:

1. the measured stress at the beginning of the dynamic record for each recorded tenth blow (axis shows "calibrated" line);
2. the measured stress at the end of the dynamic record (dashed line);
3. the measured static stress at each blow from the static record of the second ATD (solid line);
4. the peak transient stress during a blow (dotted line);
5. the minimum transient stress during a blow (dotted line);

The correlation between 1, 2, and 3 confirms that the use of the linear interpolation does not bring significant modifications of the measured static stress history. Therefore, to recreate the missing blows we could use a linear interpolation of the recorded ones.

Now, from Figure 6.3.3.1.b which shows the history of incremental (1st order derivative) measured stress, we see that the peak and minimum stress incremental histories are very different. It can be seen that the peak transient value can increase while the minimum value decreases. If a linear interpolation of a record is done, it is not possible to obtain simultaneously an increase of the peak and a decrease of the minimum, but only an increase or a decrease of both the peak and the minimum. Therefore, the use of the linear interpolation to create the missing blow histories would then have unwanted consequences such as the distortion of the expected signal.

The choice was made to repeat each blow 10 times, which replaces the linear interpolation by a step approximation. This, in turn, implies that the same final static output will be found 10 times, which will not correlate well with the static data. Thus, the final output values for each blow will be given by the static data.

To calculate the stress field at a given time the following steps have to be followed:

1. reconstruct the blow history by using the method described above (*i.e.*, repeating the effect of blow 20 for blows 16 through 25);

2. implement the correction given by the static stress field (which corresponds to adding an extra point to each blow);
3. run the complete blow history through the model;
4. write on file for each blow the static stress and output, the peak and minimum transient stresses and output, and the absolute maximum stress and output encountered.

Implication of soil-cell model assumption for one blow

Figure 6.3.3.1.c shows the transient records of a transducer located at Z/A = 26.67, R/A = 2.67 obtained using the linear assumption and the soil-cell model. There are shown on the figure are several characteristic points on the records such as initial, peak, minimum, and final points. The points are also shown in Figure 6.3.3.1.d where the calculated stress is plotted versus the measured stress. In the case of the linear assumption, the calculated stress is equal to the measured stress, so the points lie on the diagonal. For the use of the model, the logarithmic decay and the asymptotic reloading can be followed. The points are not on the diagonal anymore, and lower values of stress compared to the linear values are observed.

Figures 6.3.3.1 e and f present the same sequence as Figures 6.3.3.1.c and d, for the same transducer, with the pile at a depth of D/A = 26.8, instead of 22.6. The transient record then shows tensile stress instead of compression stress. The stress level is far below the past maximum stress, and there is then no contact between the hysteresis behavior of the stress signal and the diagonal line of the linear assumption.

Comparison in the dynamic history between the linear and soil-cell model assumptions

To illustrate the difference between the linear assumption and the model assumption, we first compare the stress history (min, max, and static), measured (linear assumption), and calculated (model assumption), for one particular transducer in a given test.

The results are given in figures 6.3.3.1.g to 6.3.3.1.k. The derived results from the model were obtained by running the model through the complete dynamic data. The following can be said about the resulting static values:

a. It should first be said that globally the behaviors in the linear and model assumptions are the same with differences of amplitude but not of physical representativeness.

b. The smoothed steps that can be seen on the plots are due to repeating each blow 10 times.

c. Figures 6.3.3.1.g and h: globally, it can be said that the transient peak and minimum stresses in the model assumption have a greater value relative to the static value than to the linear assumption.

d. Figures 6.3.3.1.i, j, and k show the comparison of peak stress (i), static stress (j), and minimum stress (k), for the linear and model assumptions. The two peak stress (i) histories are the same as the stress increases, but show small differences as they decrease, since the model peak stress is lower, as expected from the behavior of the model. The minimum stress (k) histories are quite different and show large differences in amplitudes. This is due to the fact that the minimum stress corresponds to the point on the logarithmic decay curve, which gives the biggest difference in stress for a given transducer output. The static stress value (j) according to the model is substantially lower than the value given by the linear assumption. In a certain way it can be said that the model takes into account the existence of an "integration" part in the filtering effect the soil has on the stress dynamics. Another conclusion is that this difference repeated over an entire driving history will result in a substantially different set of final values of the residual stress field after driving.

Figure 6.3.3.1.l shows the entire dynamic history, blow by blow both, both in the linear and model assumptions of the transducer located at Z/A = 26.67, R/A = 2.67 , (PT3, T90), which illustrate completely what is described above in terms of peak, minimum, and static stresses.

6.3.3.2 Calculated stress distribution

Figure 6.3.3.2 presents the values of the radial distribution of the static radial stress field once the model has been applied (T70, PT1 to PT5). The same test and transducers presented in Figure 6.3.1.1.b were chosen so that comparison would be facilitated. Globally, as mentioned in the previous section, the behavior is the same as in figure 6.3.1.1.b., with amplitudes and residual stress, however, sensibly less important.

From the model, we now know that the soil experiences very large transient stresses that will be largely dissipated since the static stresses are comparatively small. We expect therefore a lesser effect from pile driving on the soil than the linear assumption was previously telling us.

Figures 6.3.3.3.a and b present the values of the vertical distribution of the static radial stress field once the model has been applied (T90, PT1 to PT6). The same test and transducers presented in Figures 6.3.1.2.a and b were chosen so that comparison would be facilitated. As stated above, the same global behavior for the driving history is observed, but sustantially lower stress levels are obtained. In Figure 6.3.3.3.b, the normalization of the static radial stress by the overburden stress is not meaningful anymore.

Figure 6.3.3.4 shows the comparison of the linear and model assumptions for a pair of transducers seeing radial and vertical stresses (TA0, PT2 and PT6). For both the vertical stress and the radial stress history, similarity in behavior is observed between the linear assumption and the soil-cell model results, with a reduction in the level of stress for both cases calculated by the use of the model.

Contours of the radial stress field are shown in Figures 6.3.3.5 a and b, for a pile depth of D/A = 15 and D/A = 25 respectively. The distortions observed in the linear case are accentuated in the non-linear case. The lobes on the side extend further up as the pile penetrates into the soil, which would indicate a larger importance of the side friction on the pile shaft. The compression and failure zone under the pile tip can be observed.

6.3.4 Discussion and conclusion

It could be argued that the non-linear soil-cell model may provide a lower bound on the estimation of the soil stress field during and after driving because it gives quite low values. This can be explained by the fact that the model represents the non-linearity in the static soil-cell interaction, which is larger than the dynamic non-linearity of the soil-cell interaction. Also, it has to be kept in mind that the pile driving stress history is mainly dynamic. The linear assumption misleads us in the estimation of the stress level, for it does not take into account the non-linear behavior of the soil and of the soil-cell system. The true soil stresses are believed to be close to the calculated stresses (stresses obtained using the soil-cell model). Current pile driving analysis uses measurements of the pile dynamics

to obtain soil parameters. Those parameters relate to the dynamic properties of the soil, but are directly used to predict pile bearing capacity values. These are dependent on the static parameter values of the soil. The SCM assumption shows even more clearly than the linear assumption that the transient stresses in the soil are very large compared to the final static stresses. Therefore, a large discrepancy in the values obtained from dynamic measurements to predict static values is to be expected.

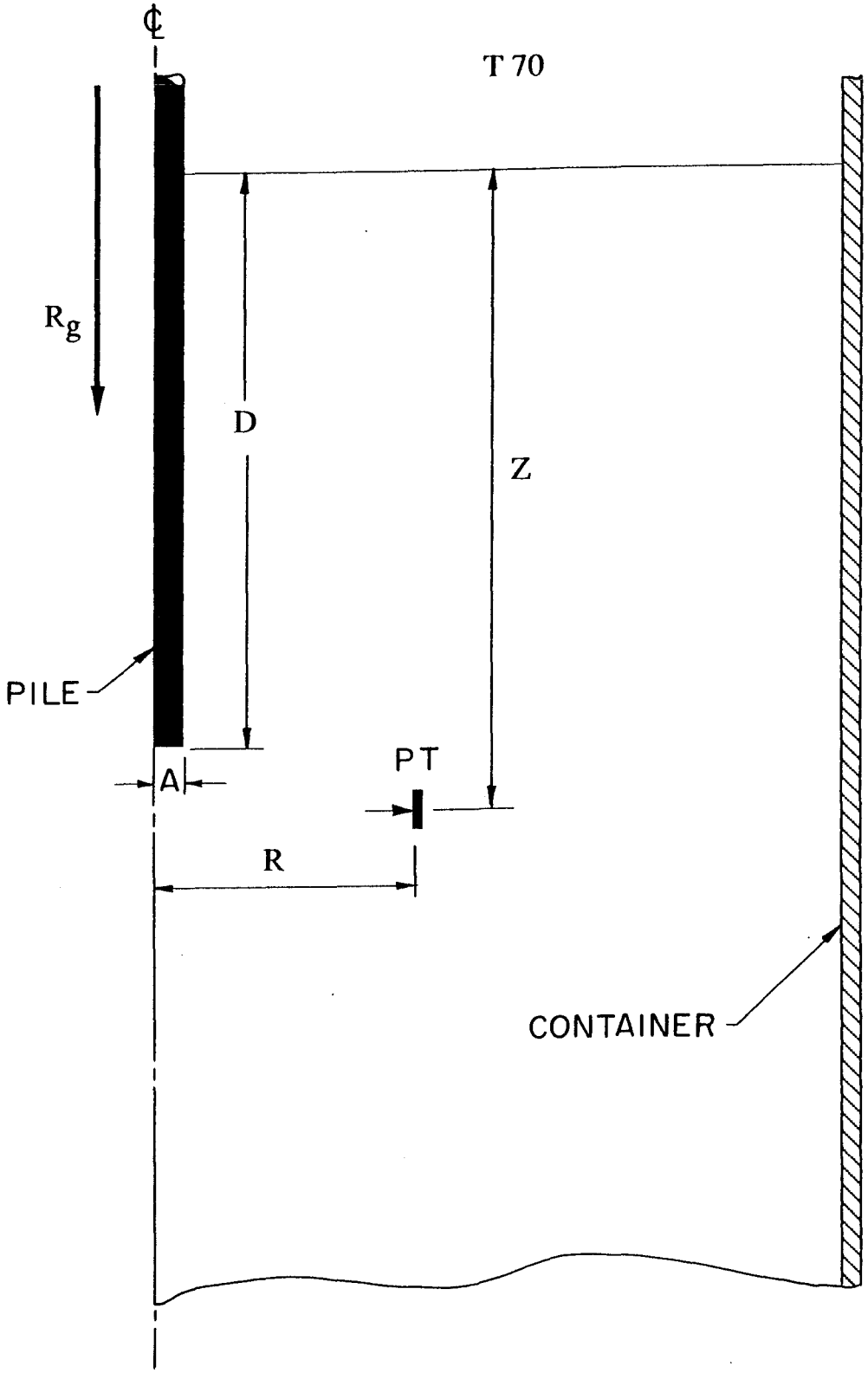

Figure 6.1 Definition of dimensions and positions

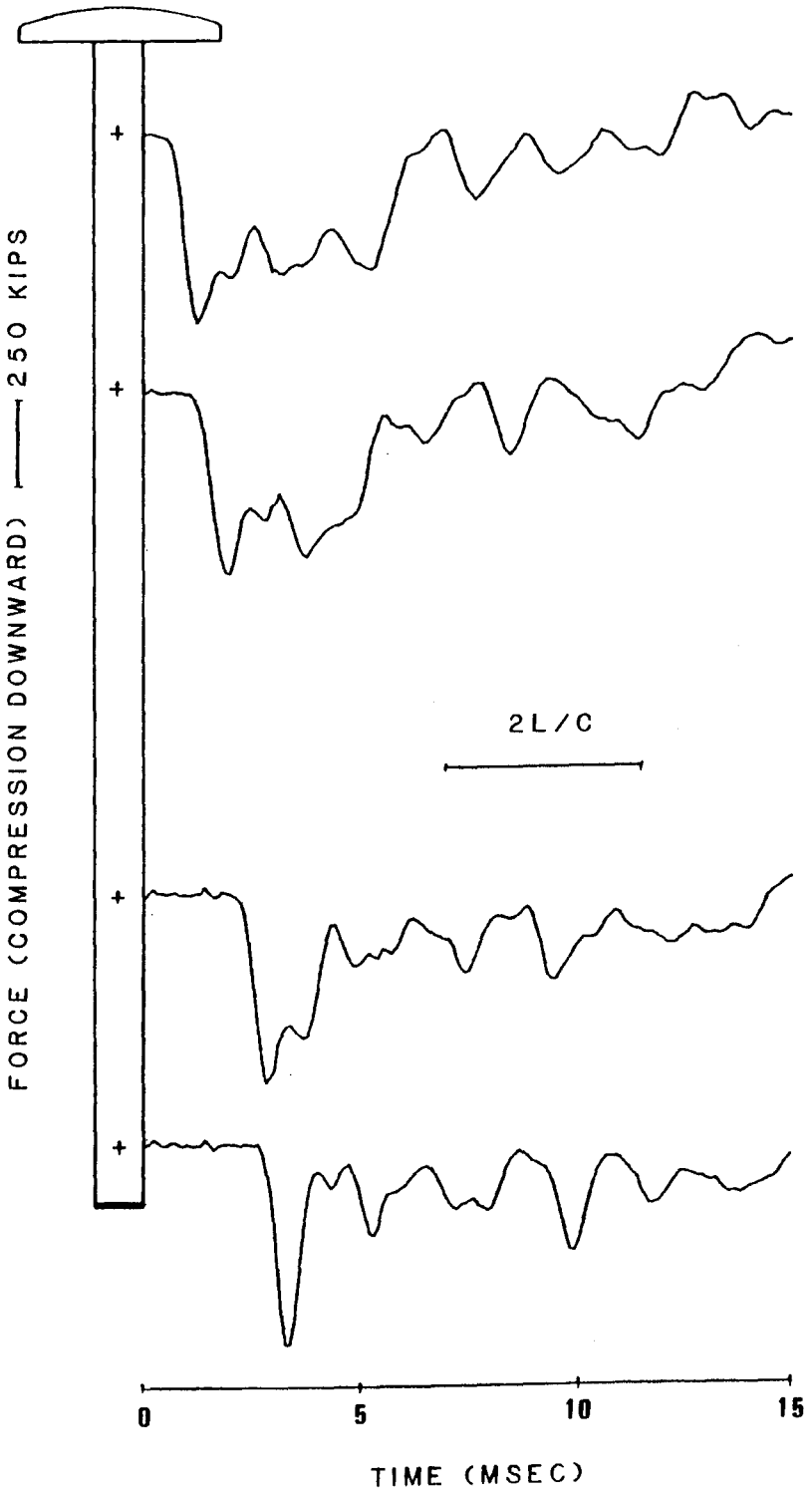

Figure 6.2.1 Response of the pile to the hammer impact
Force records from four strain gages along the pile
D/A = 16.0. Compression down

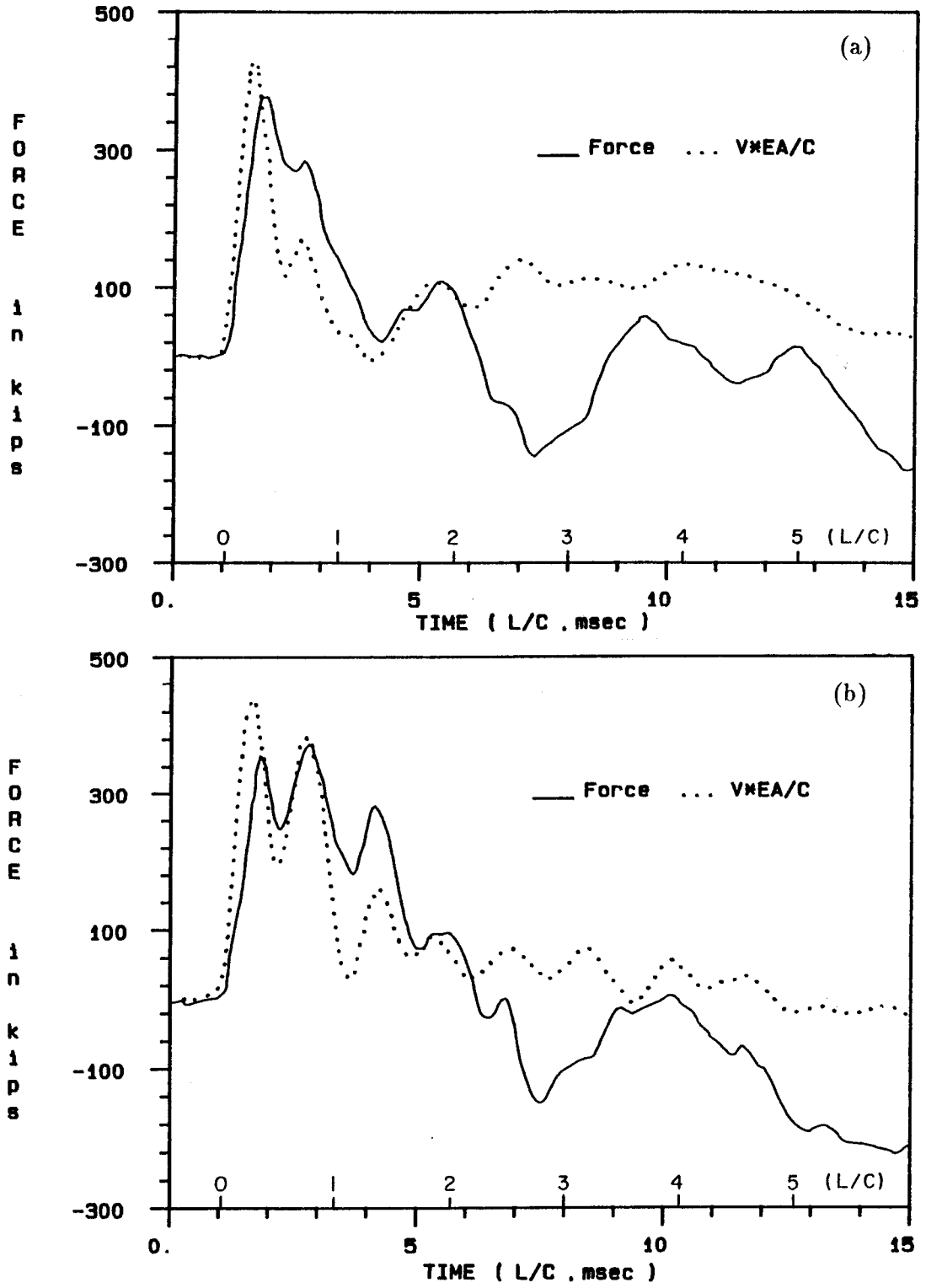

Figure 6.2.2 Comparison of the force at the top of the pile obtained from strain gage record (Measured Force) and acceleration record (V*EA/C:calculated force)
(a) D/A = 14.7
(b) D/A = 25.6

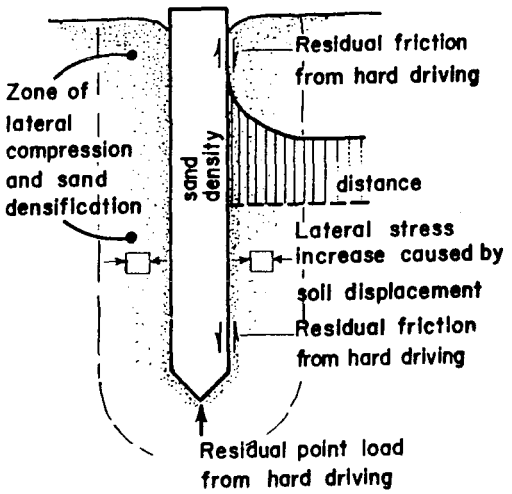

Figure 6.3.0.1 Effect of placement of pile into a soil mass (from Vesic)

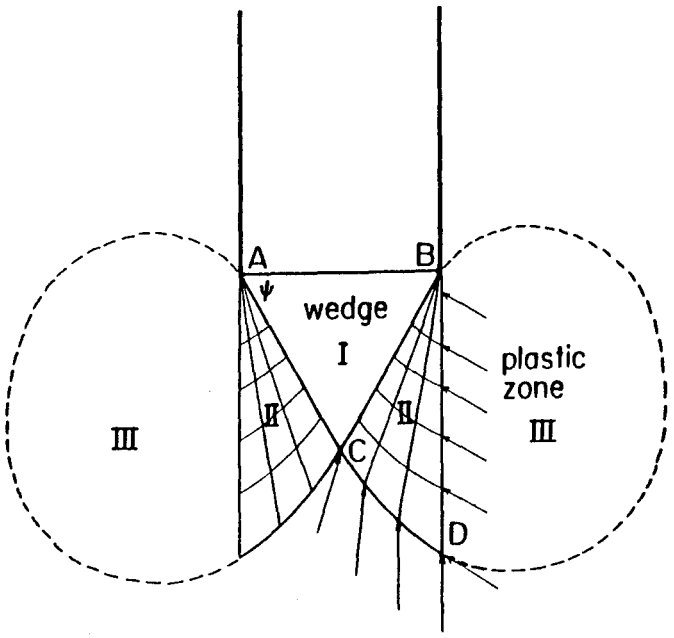

Figure 6.3.0.2 Assumed failure pattern under pile point (from Vesic)

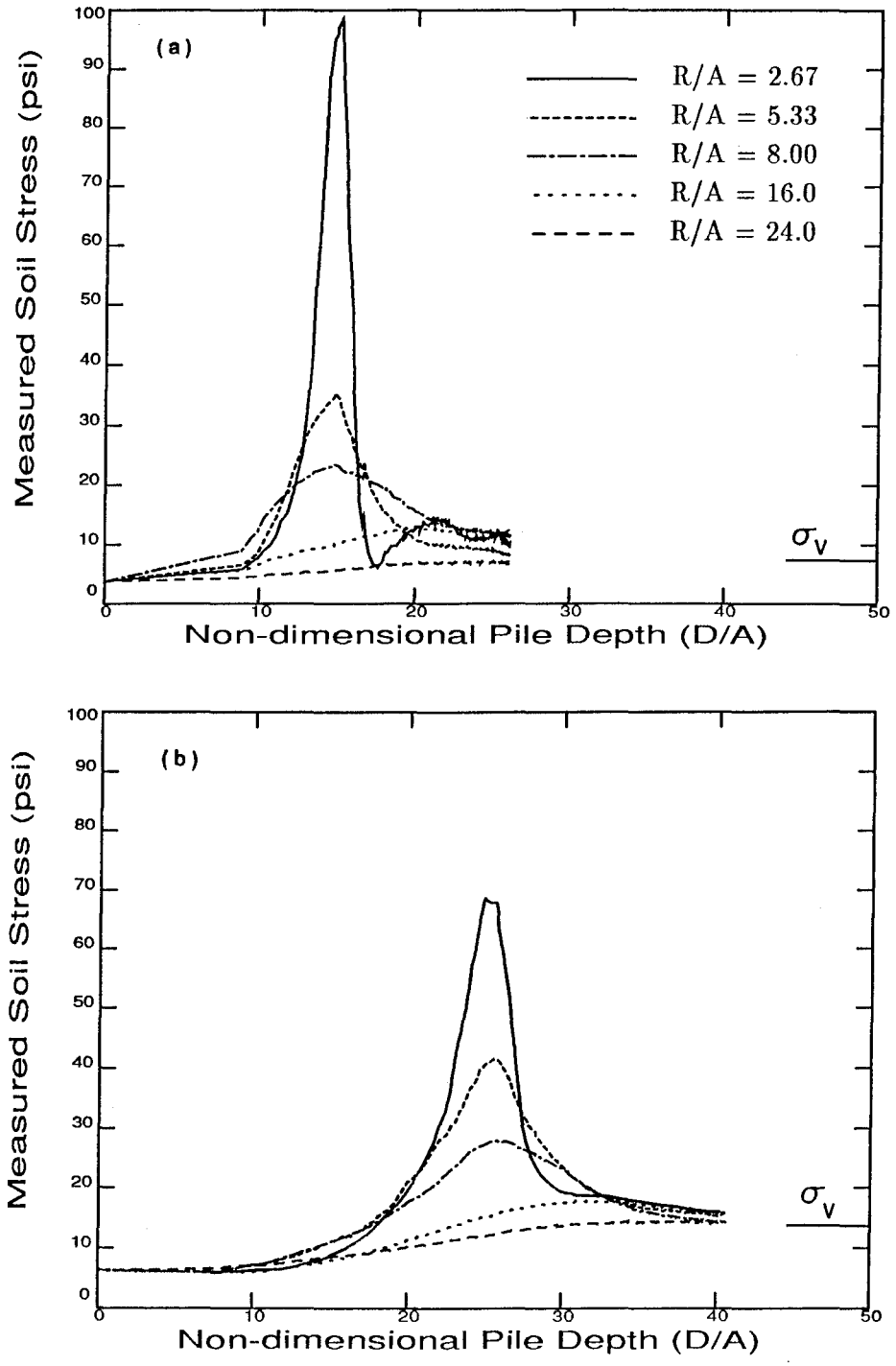

Figure 6.3.1.1 Radial distribution of the radial measured stress
(a) Z/A = 16.00
(b) Z/A = 26.67

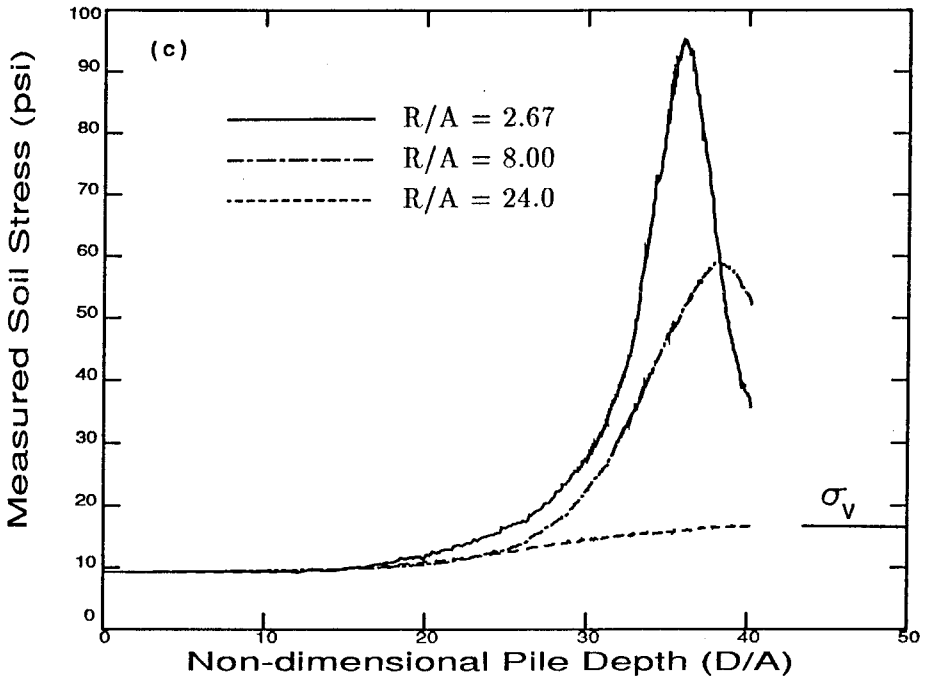

Figure 6.3.1.1 Radial distribution of the radial measured stress
(c) Z/A = 37.33

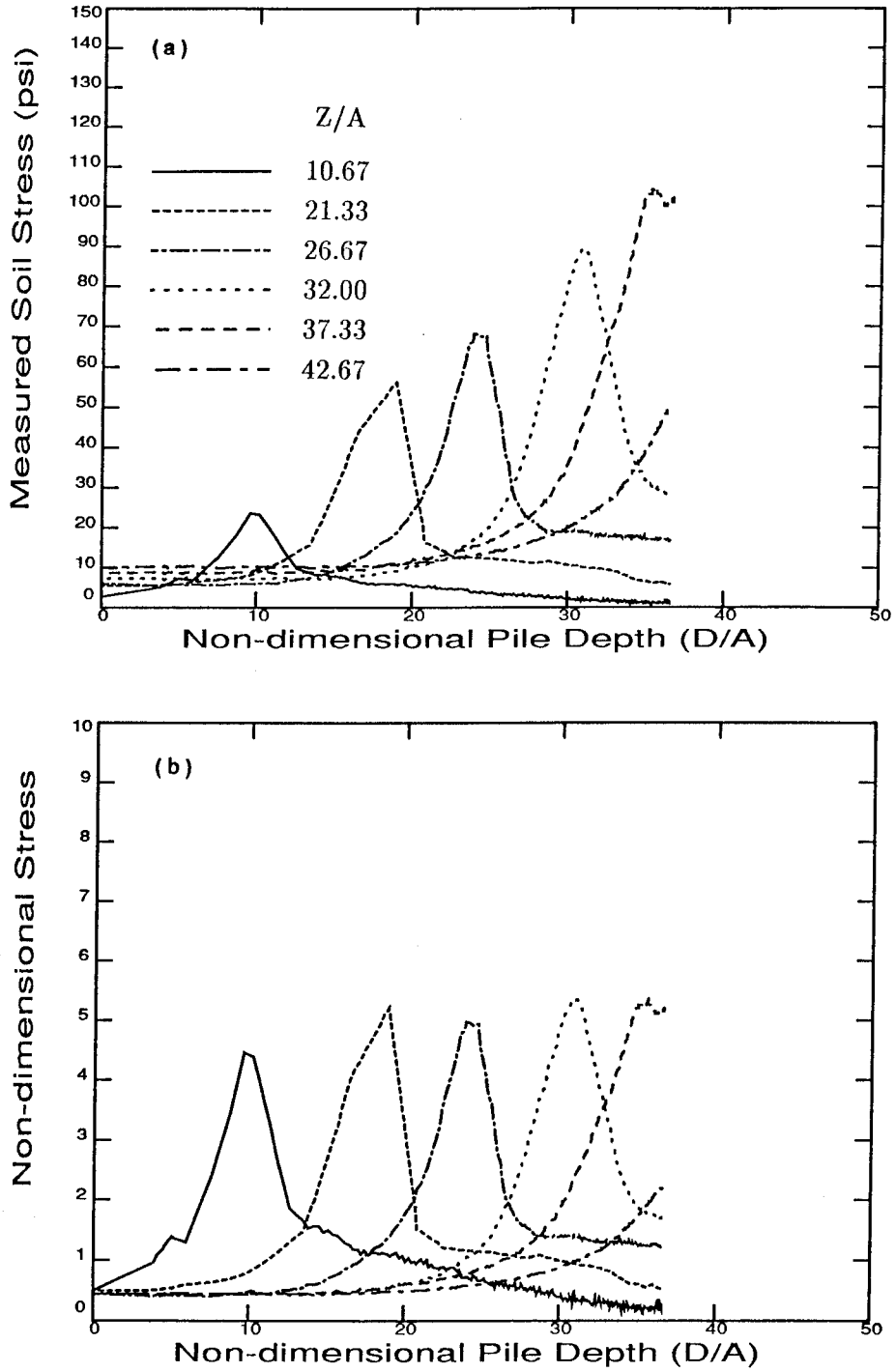

Figure 6.3.1.2 Vertical distribution of the radial measured stress
R/A = 2.67
(a) Measured stress
(b) Non-dimensional stress

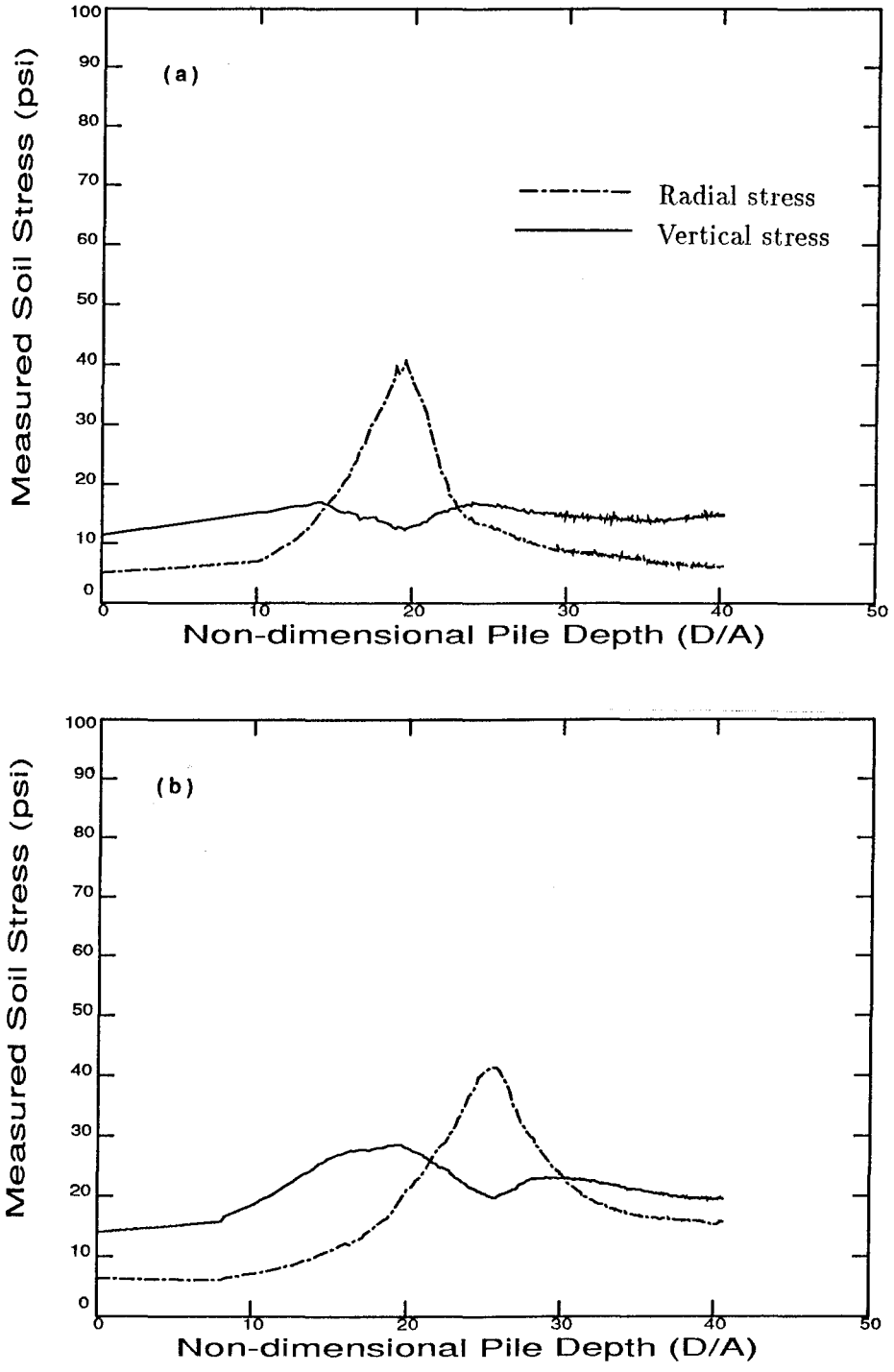

Figure 6.3.1.3 Comparison of radial and vertical measured stresses
R/A = 5.33
(a) Z/A = 21.33
(b) Z/A = 26.67

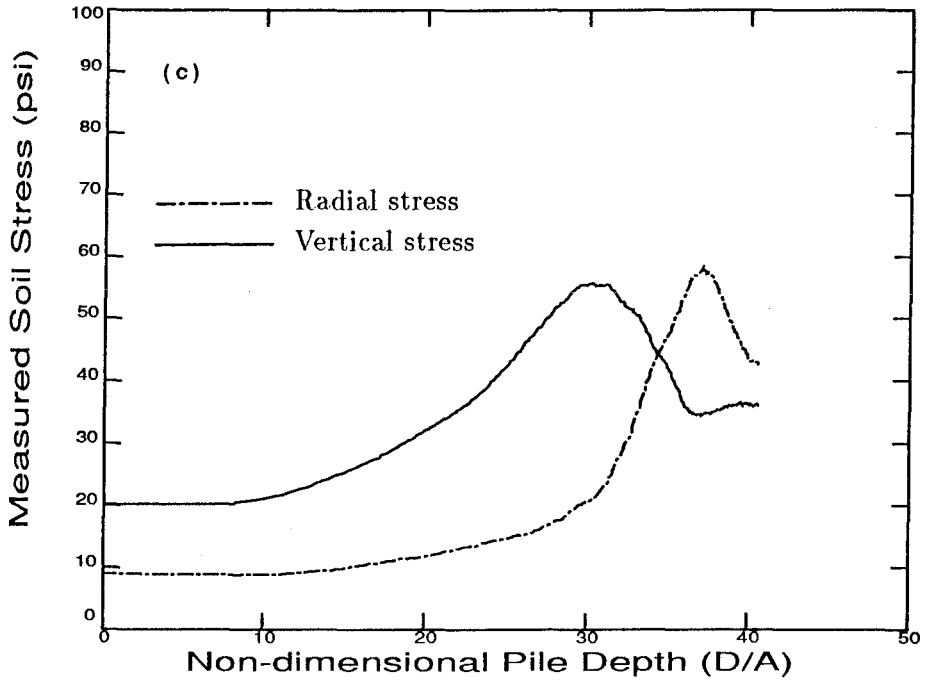

Figure 6.3.1.3 Comparison of radial and vertical measured stresses
R/A = 5.33
(c) Z/A = 37.33

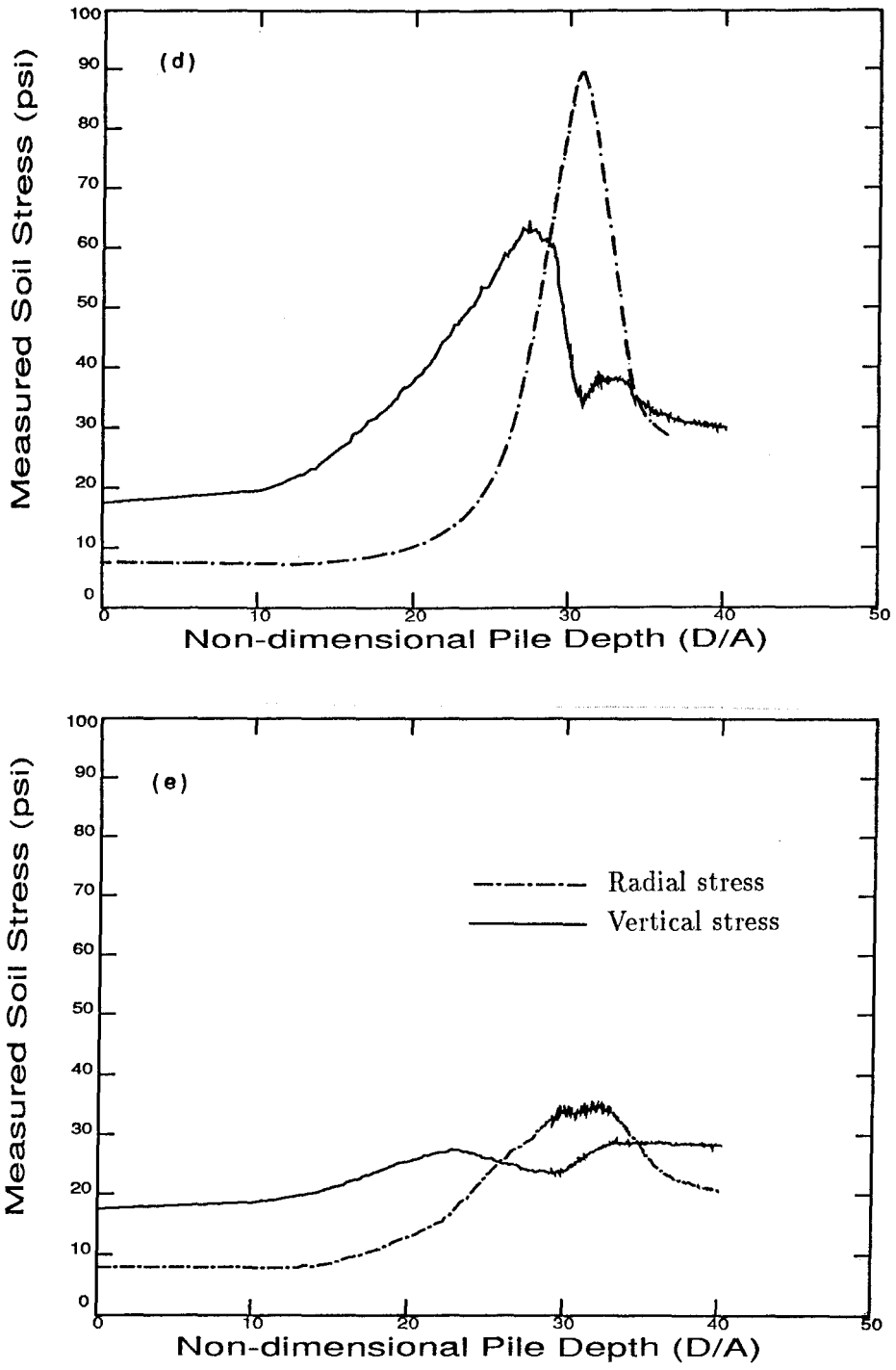

Figure 6.3.1.3 Comparison of radial and vertical measured stresses
Z/A = 32.0
(d) R/A = 2.67
(e) R/A = 8.00

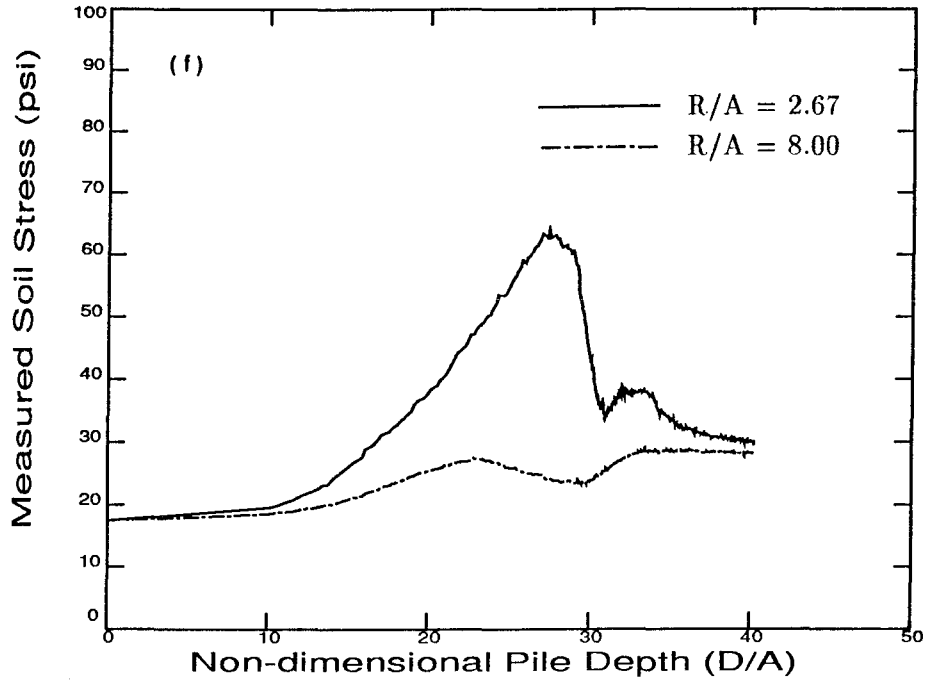

Figure 6.3.1.3 Comparison of radial and vertical measured stresses (f) Z/A = 32.00

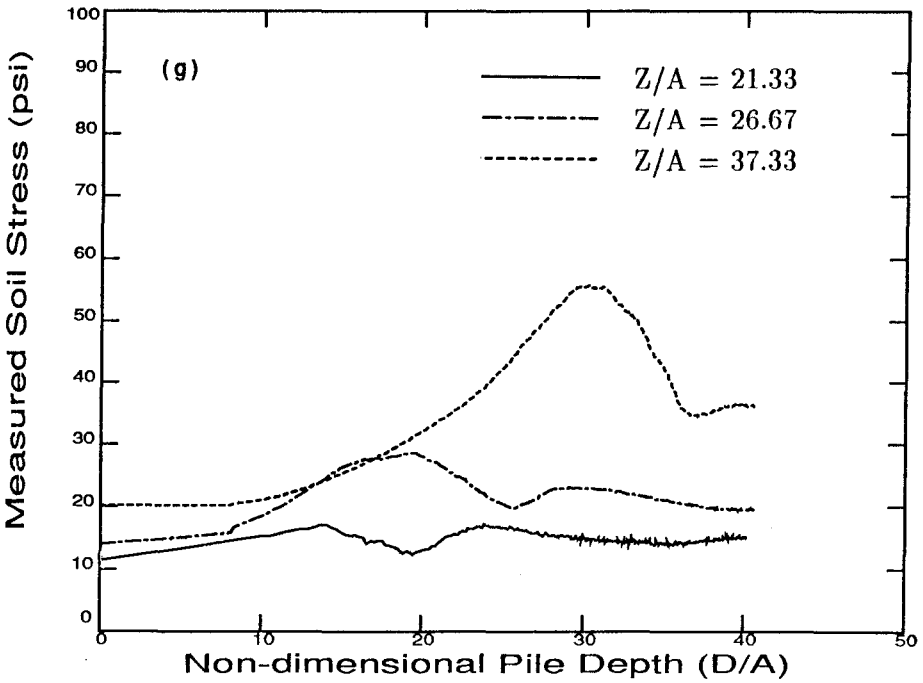

Figure 6.3.1.3 Comparison of radial and vertical measured stresses (g) R/A = 5.33

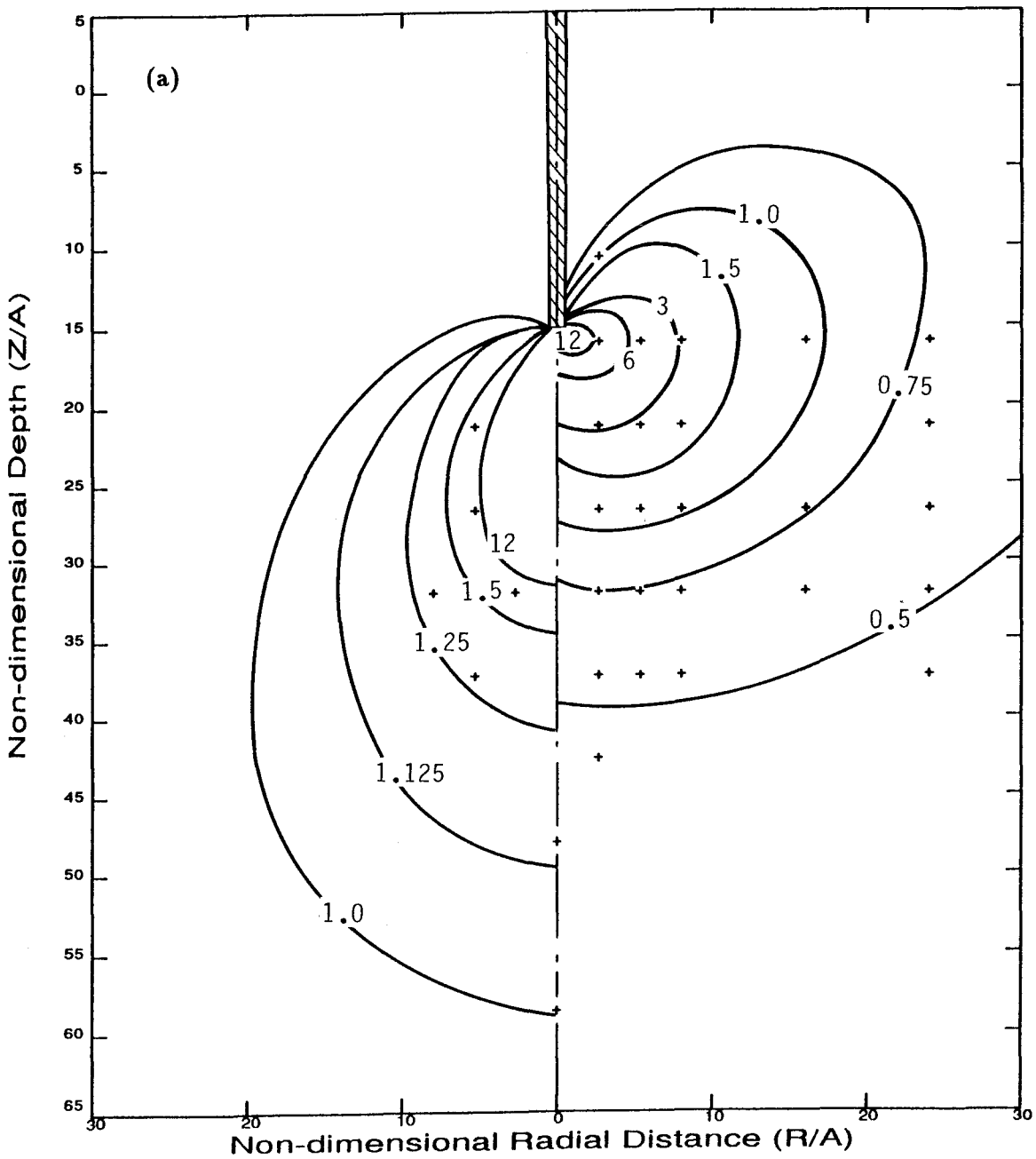

Figure 6.3.1.4 Measured vertical(left) and radial(right) stress contours
(a) D/A = 15

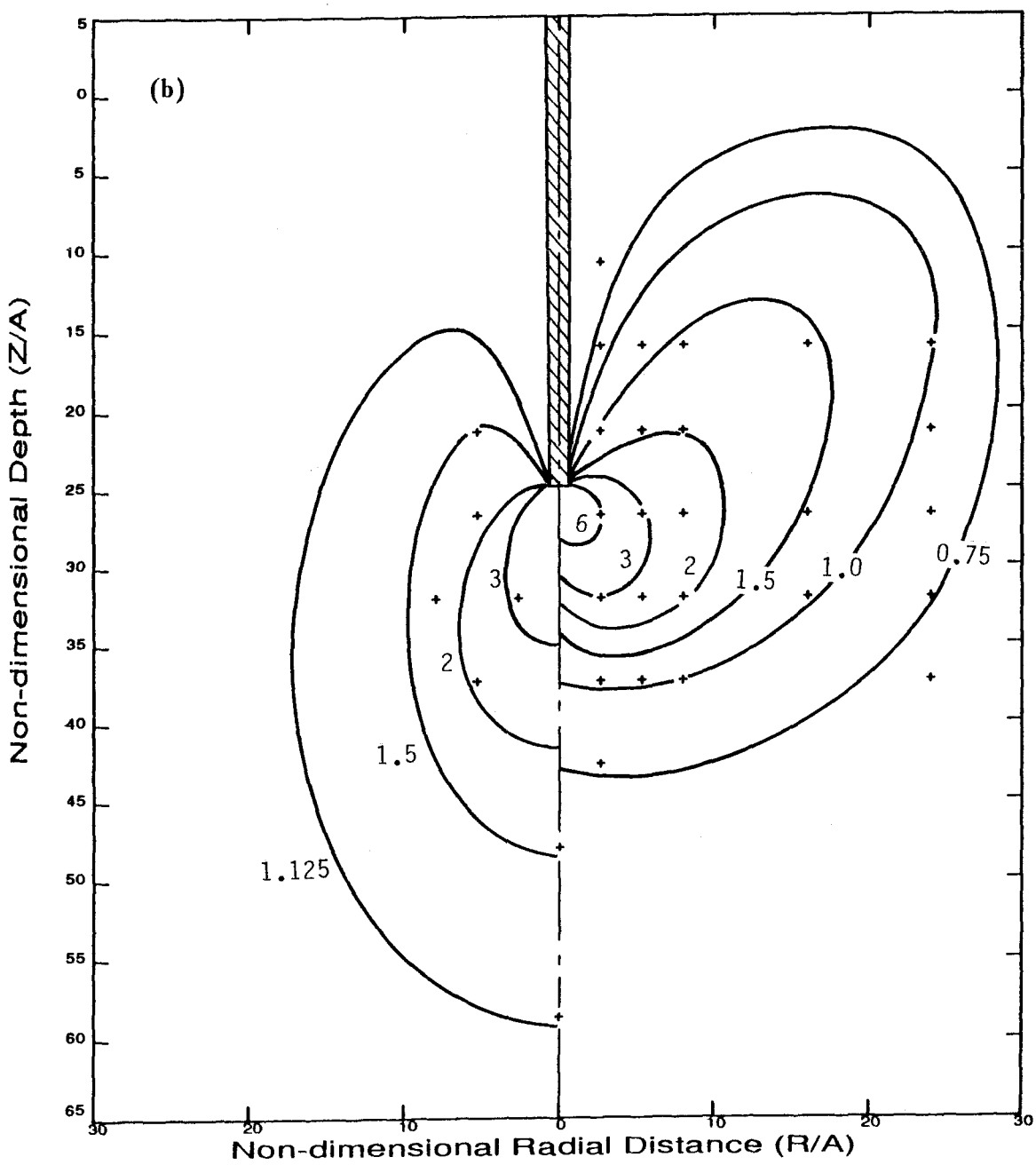

Figure 6.3.1.4 Measured vertical(left) and radial(right) stress contours
(b) D/A = 25

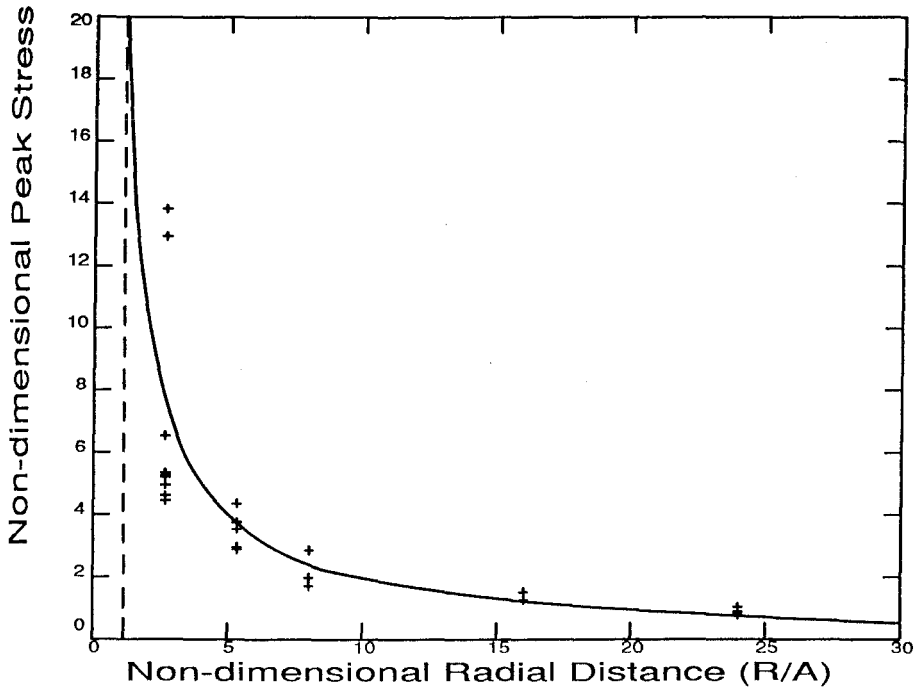

Figure 6.3.1.5 Non-dimensional peak-measured-radial stress variation with distance from the pile axis

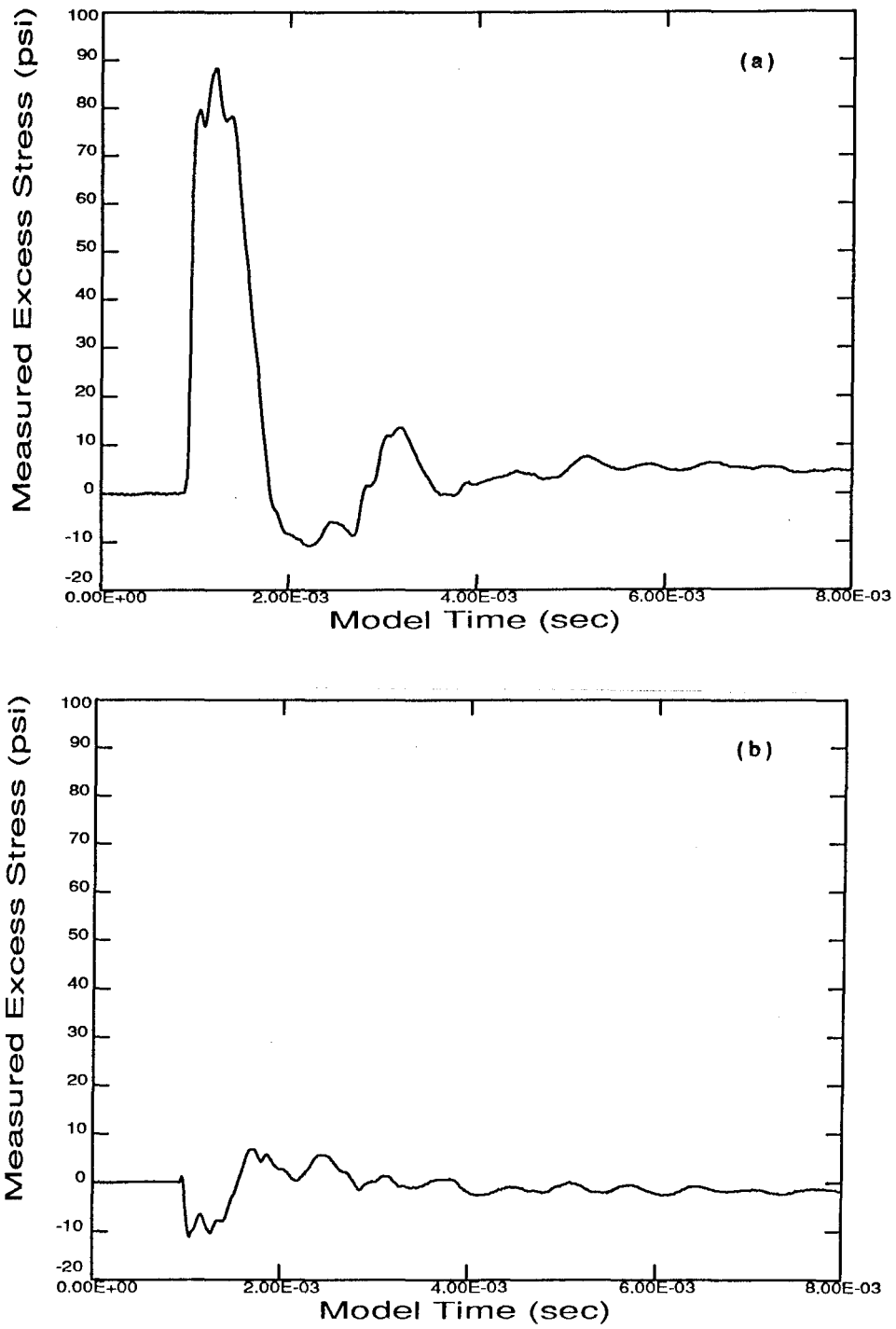

Figure 6.3.2.1 Measured transient stress following a blow
(a) Z/A = 26.67, R/A = 2.67; D/A = 24.1
(b) Z/A = 26.67, R/A = 2.67; D/A = 26.8

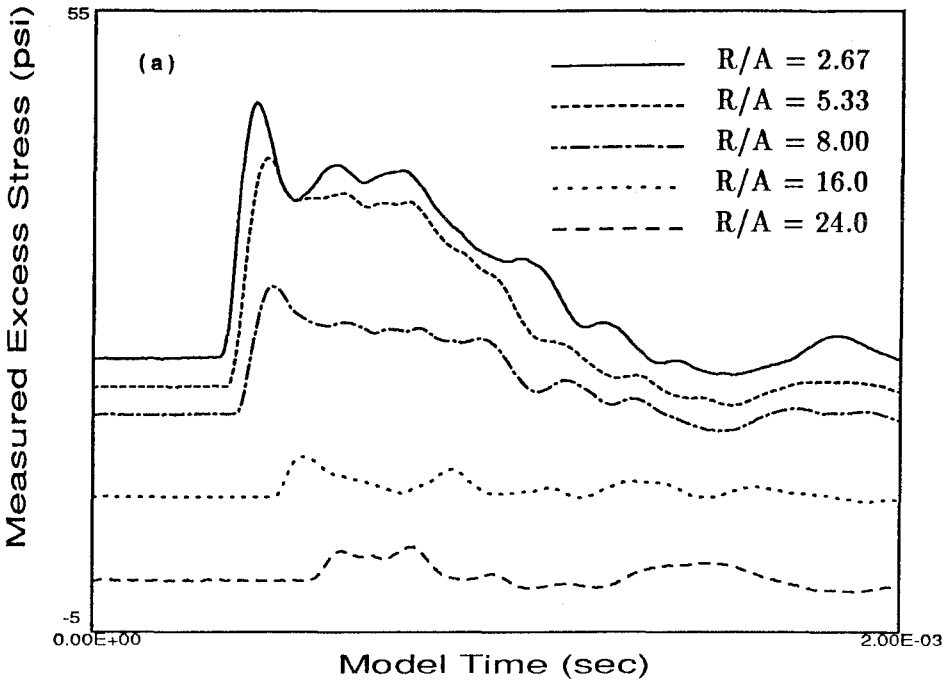

Figure 6.3.2.2 Radial dynamic measured stresses, wave speed and stress decay (a) Z/A = 26.67; D/A =21.3

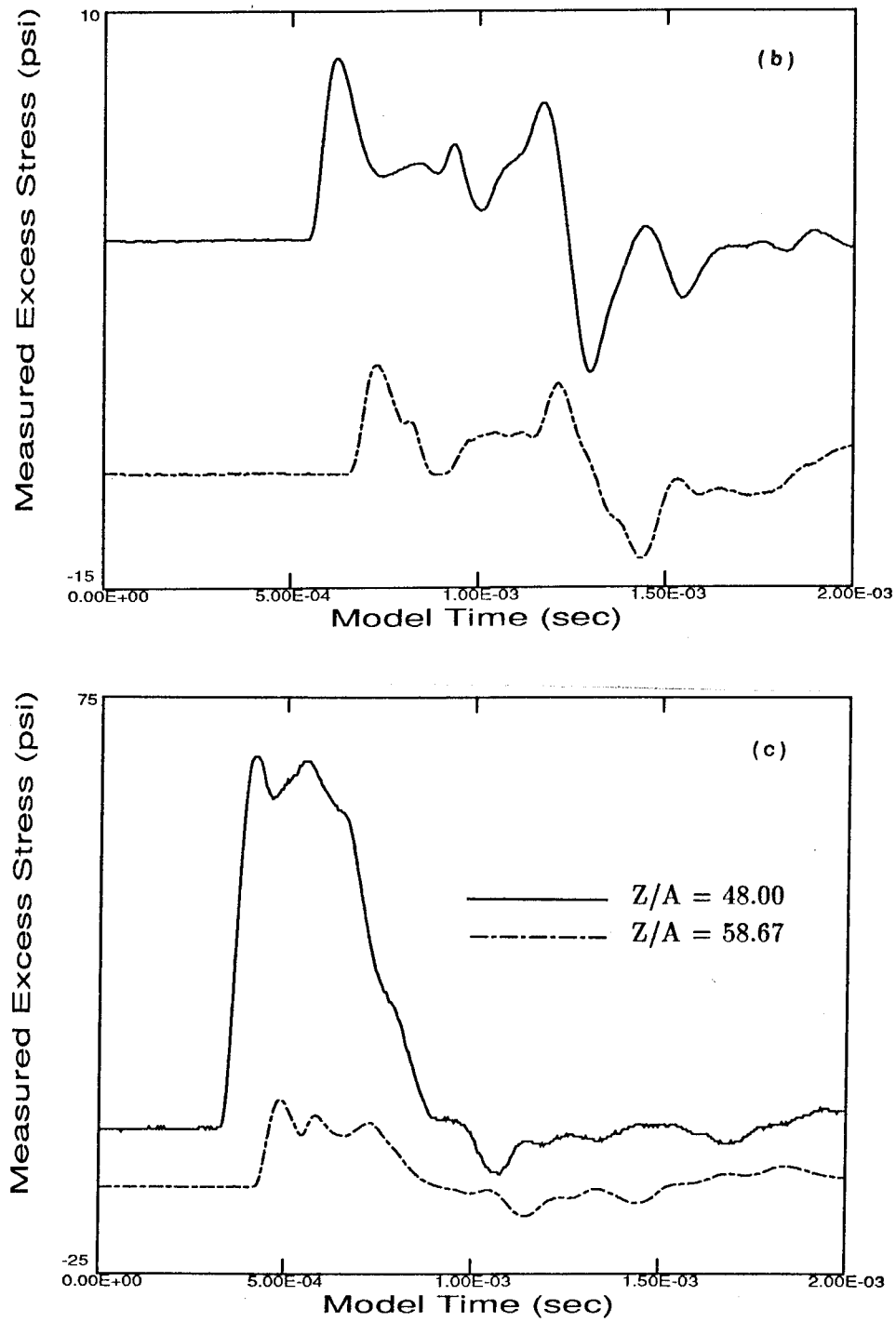

Figure 6.3.2.2 Vertical dynamic measured stresses, wave speed and stress decay
R/A = 0.0
(b) D/A = 19.4
(c) D/A = 39.6

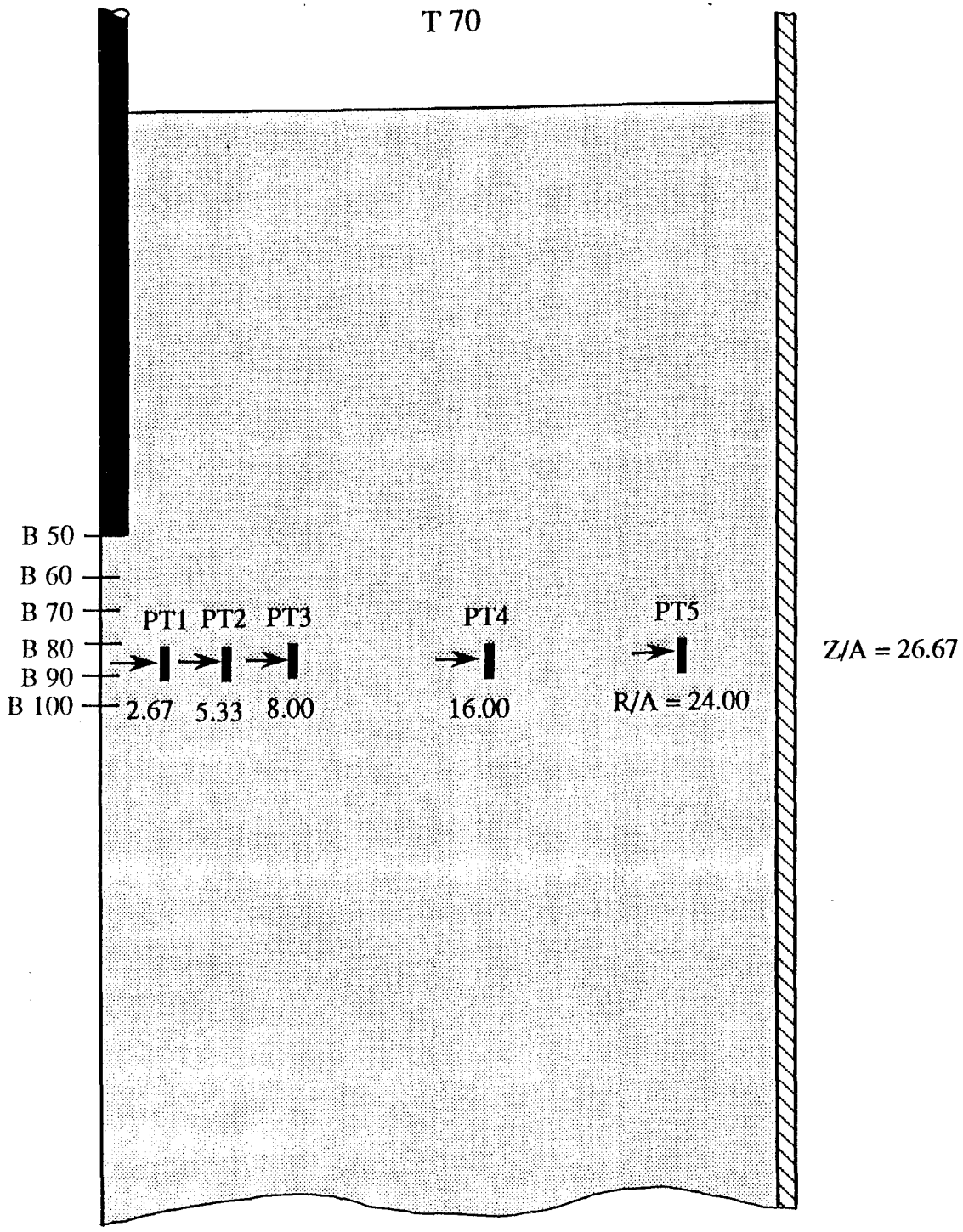

Figure 6.3.2.3 Radial distribution of dynamic radial measured stress
(a) Positions of the transducers,
and depth of the pile for the different blows

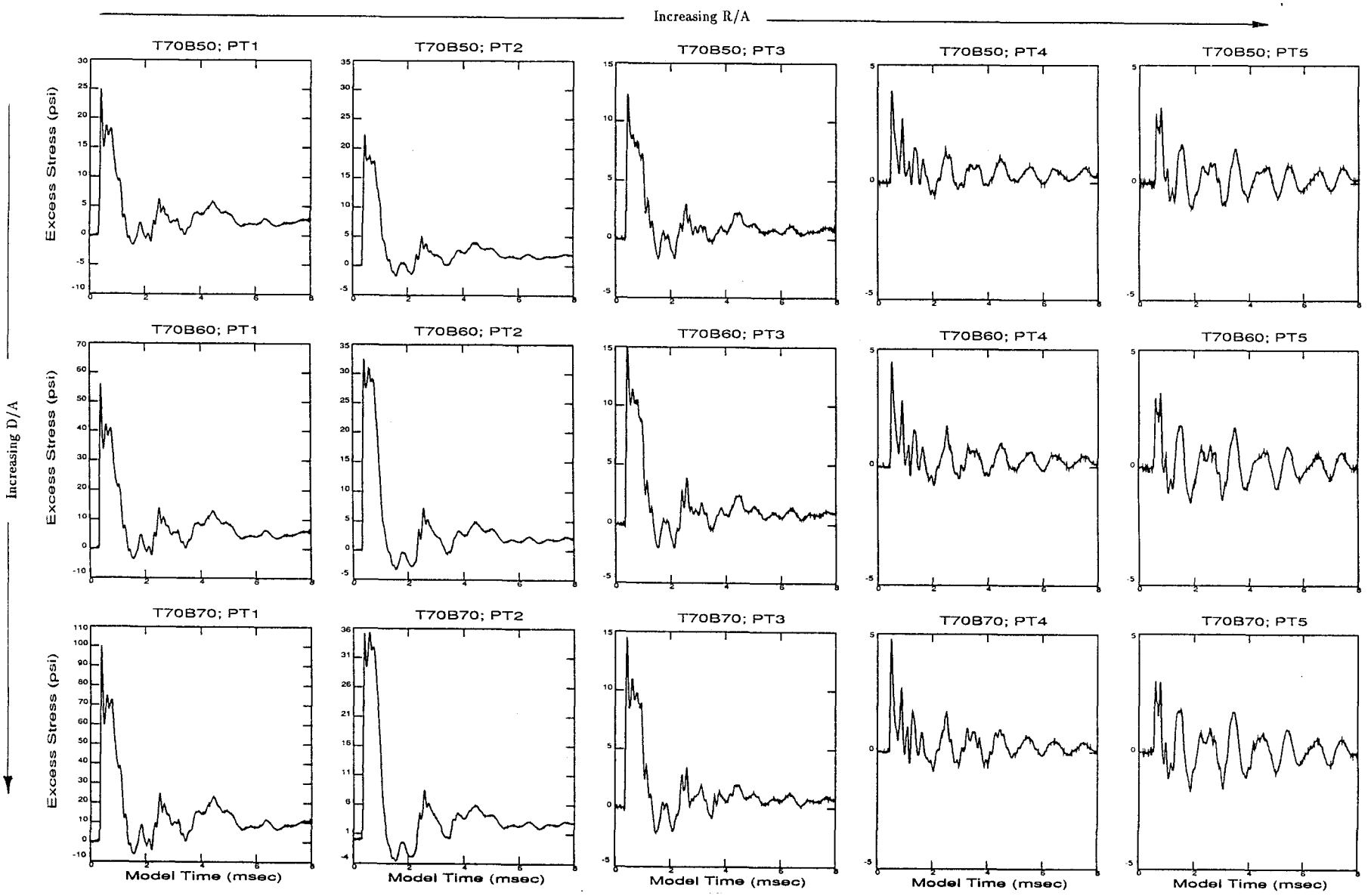

Figure 6.3.2.3 Radial distribution of dynamic radial measured stress
(b) Measured transient excess stress (Page 1 of 3)

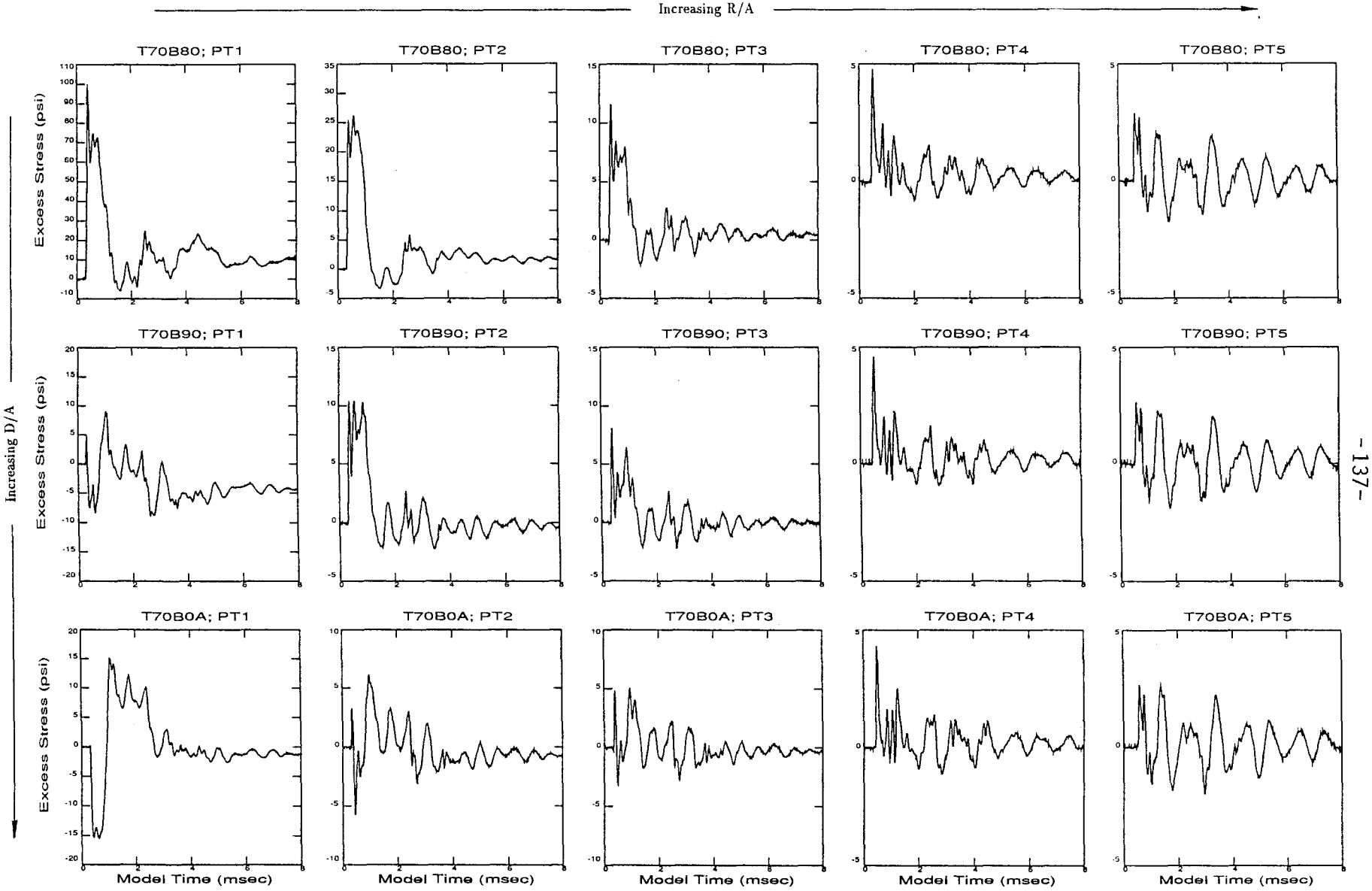

Figure 6.3.2.3 Radial distribution of dynamic radial measured stress
(b) Measured transient excess stress (Page 2 of 3)

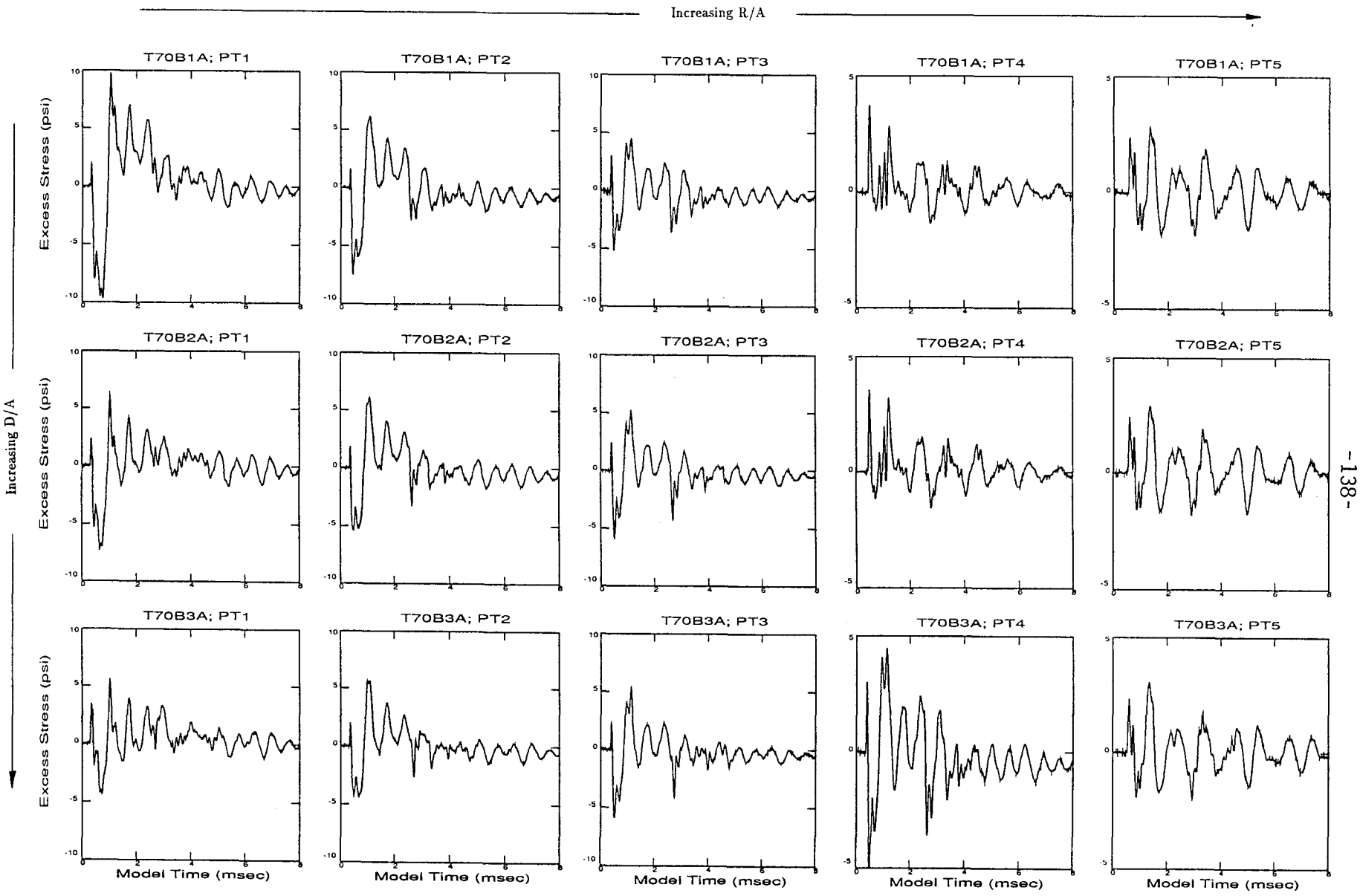

Figure 6.3.2.3 Radial distribution of dynamic radial measured stress
(b) Measured transient excess stress (Page 3 of 3)

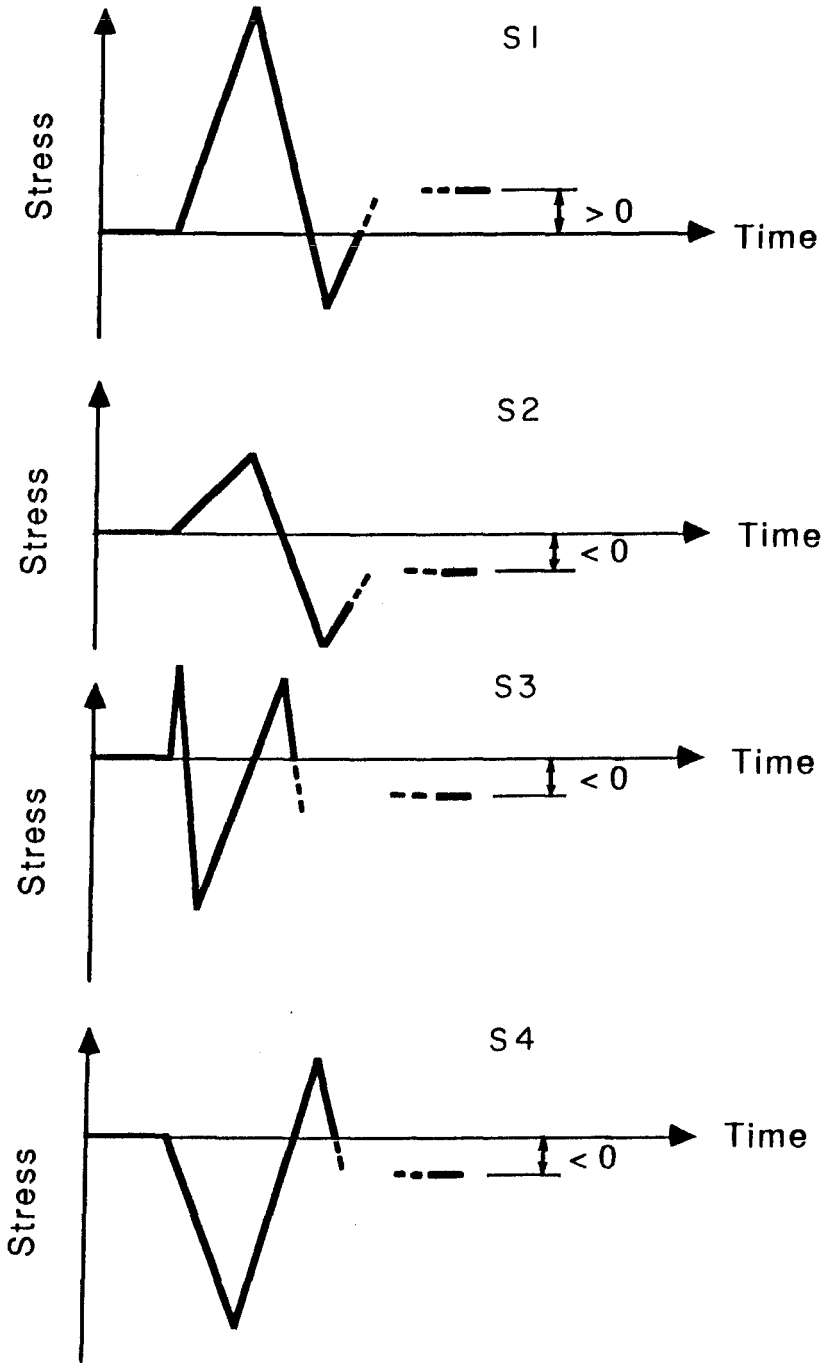

Figure 6.3.2.3 Measured transient excess stress
(c) Typical transient record shapes

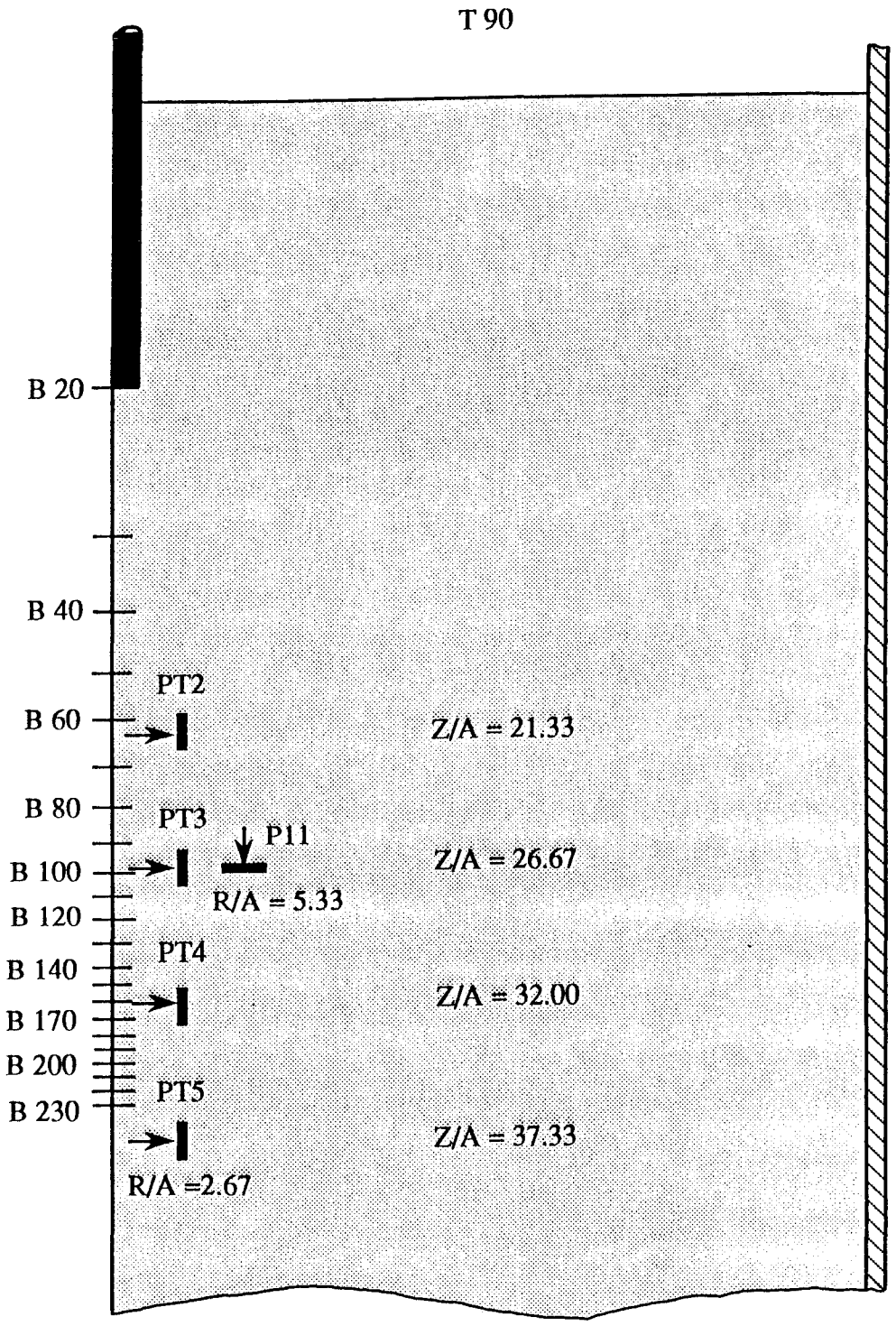

Figure 6.3.2.4 Vertical distribution of dynamic radial measured stress
(a) Positions of the transducers, and depth of the pile for the different blows

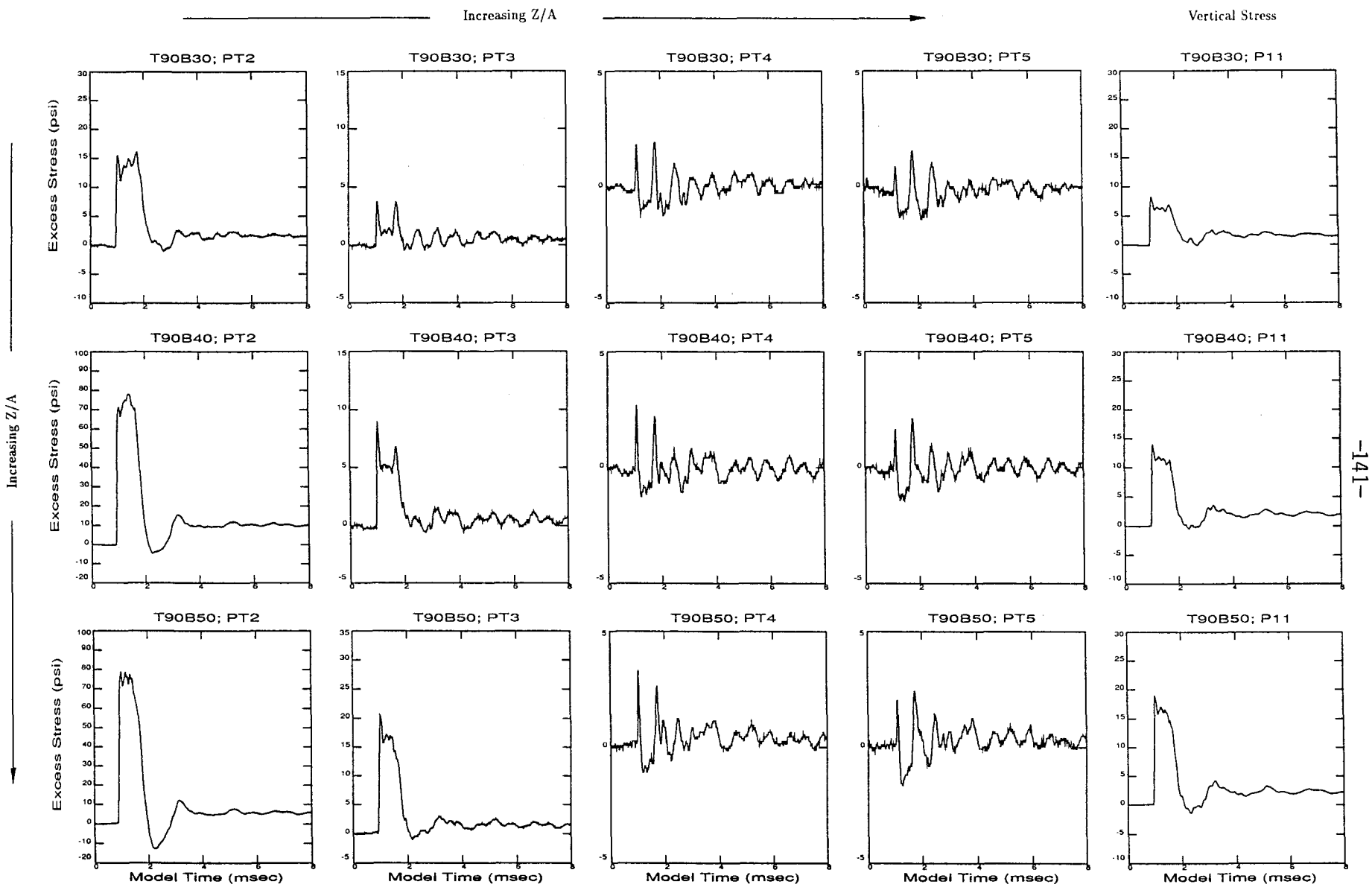

Figure 6.3.2.4 Vertical distribution of dynamic radial and vertical measured stress
(b) Measured transient excess stress (Page 1 of 7)

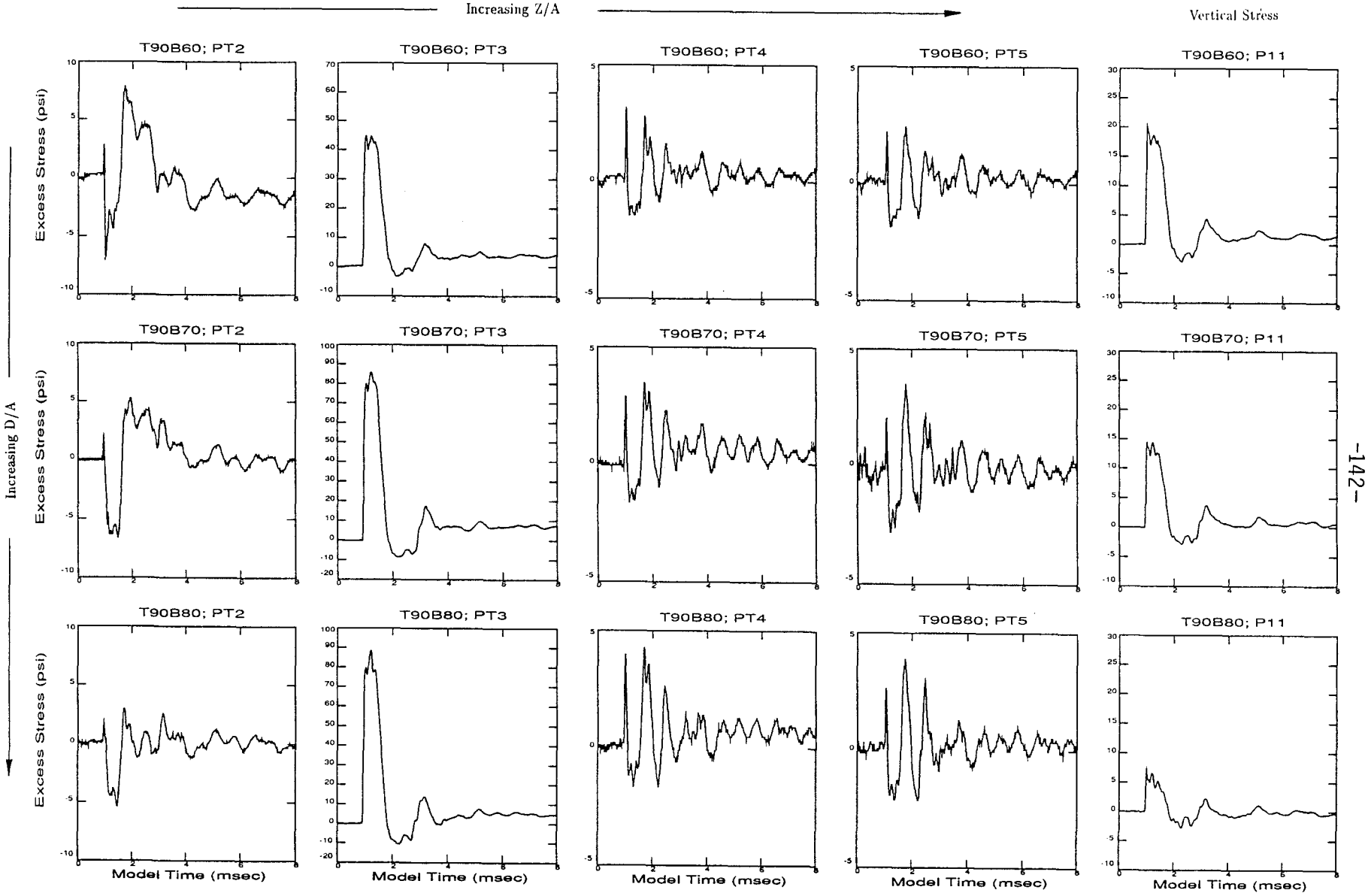

Figure 6.3.2.4 Vertical distribution of dynamic radial and vertical measured stress
(b) Measured transient excess stress (Page 2 of 7)

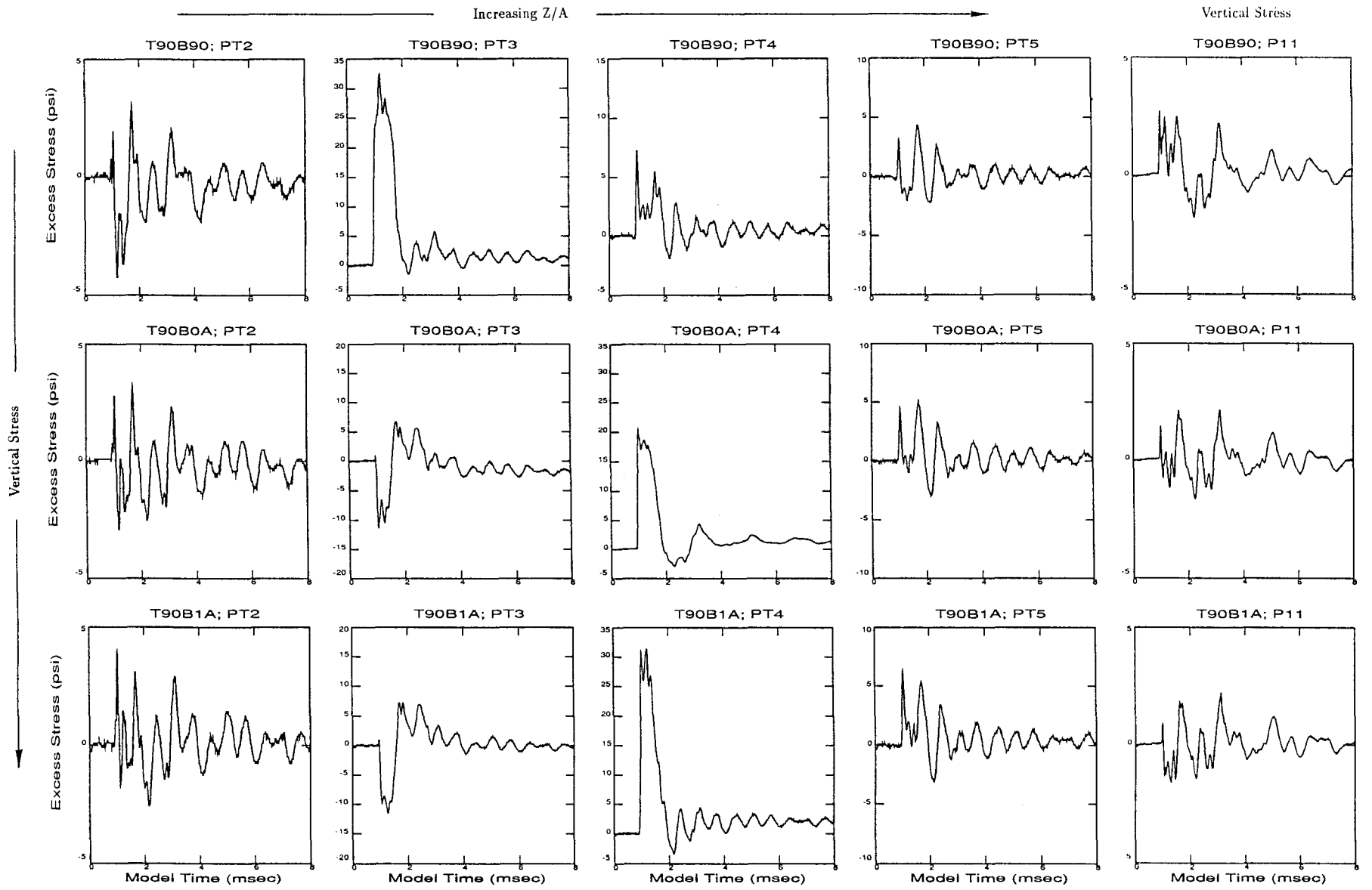

Figure 6.3.2.4 Vertical distribution of dynamic radial and vertical measured stress
(b) Measured transient excess stress (Page 3 of 7)

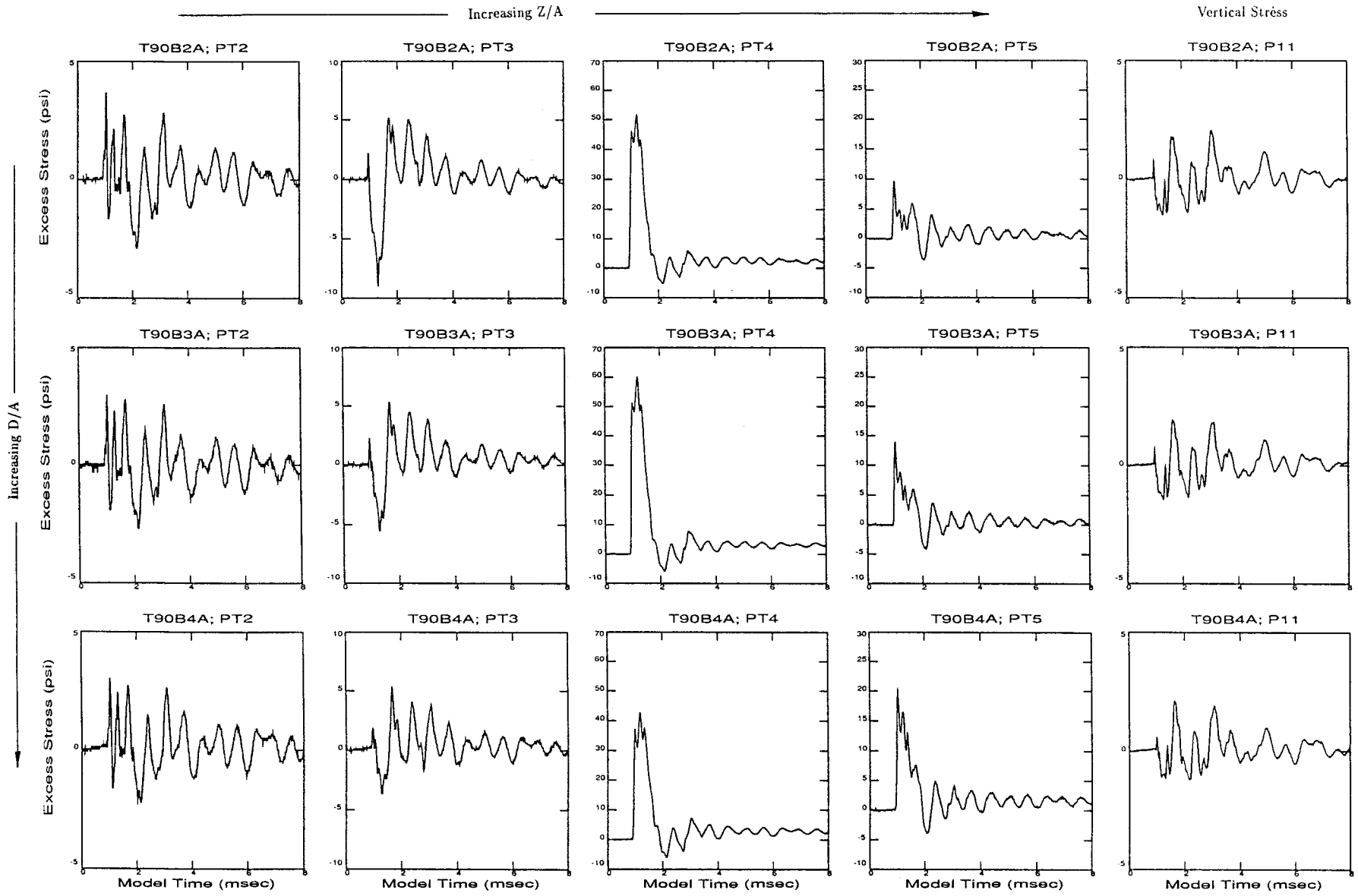

Figure 6.3.2.4 Vertical distribution of dynamic radial and vertical measured stress
(b) Measured transient excess stress (Page 4 of 7)

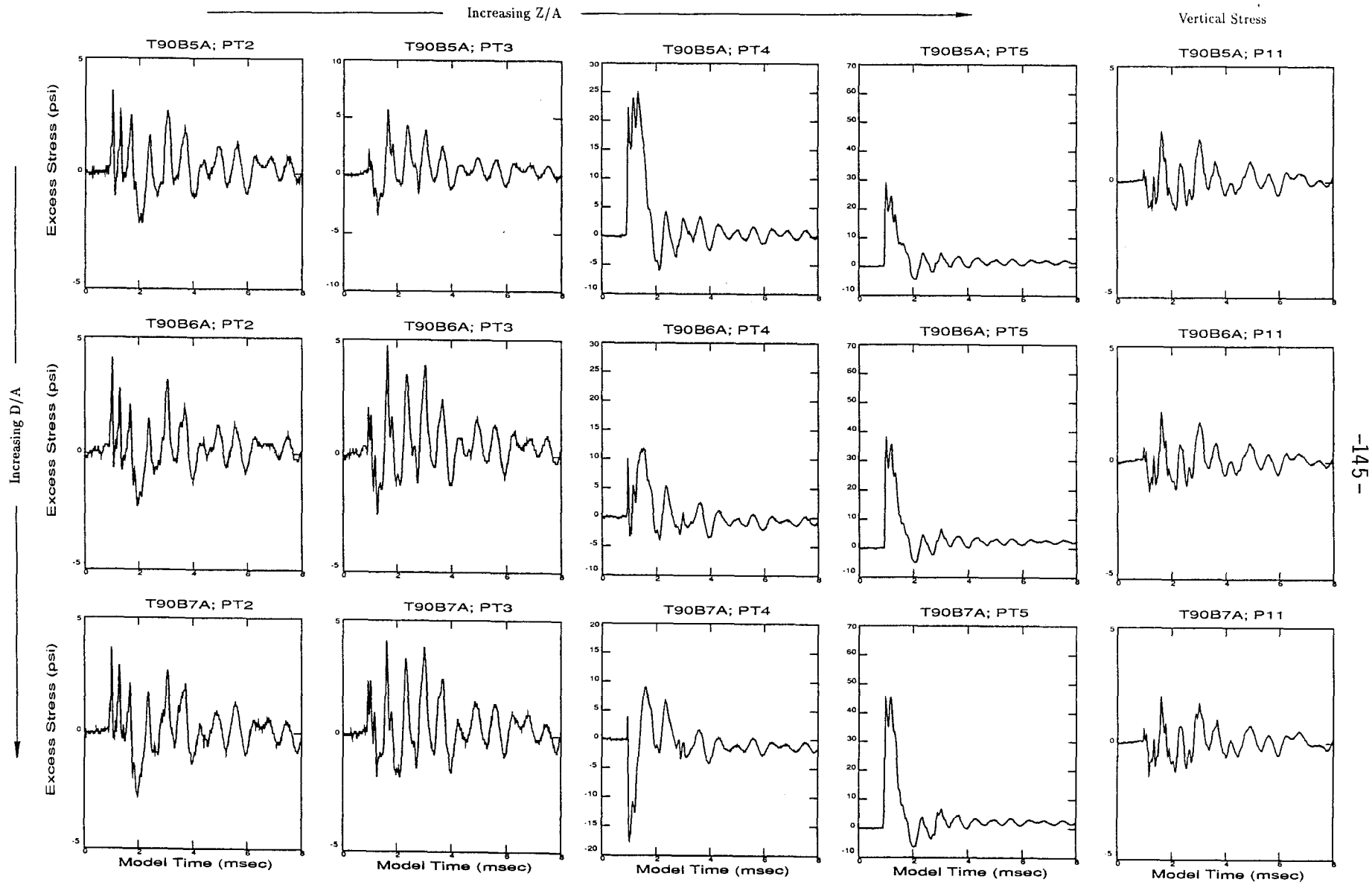

Figure 6.3.2.4 Vertical distribution of dynamic radial and vertical measured stress
(b) Measured transient excess stress (Page 5 of 7)

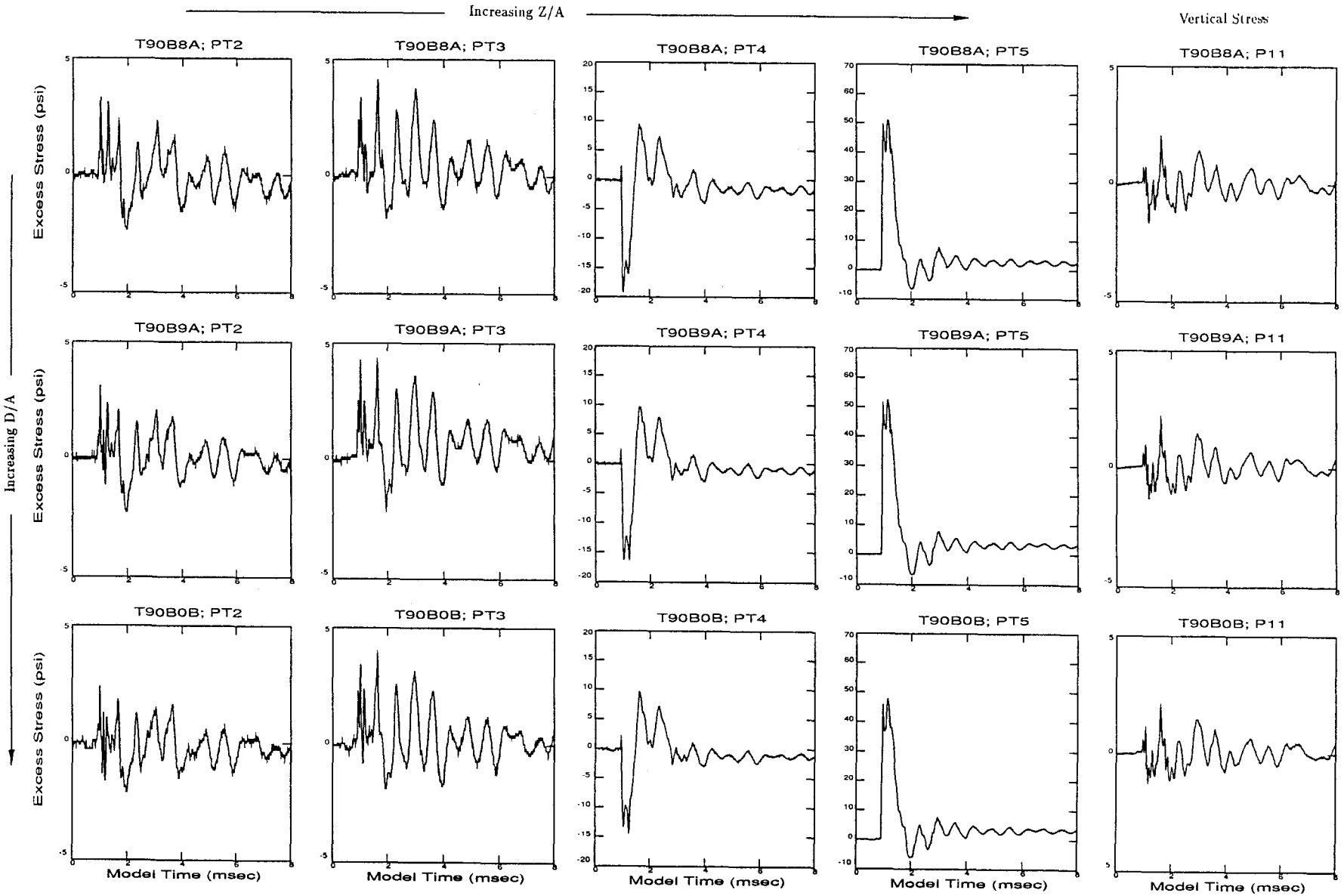

Figure 6.3.2.4 Vertical distribution of dynamic radial and vertical measured stress
(b) Measured transient excess stress (Page 6 of 7)

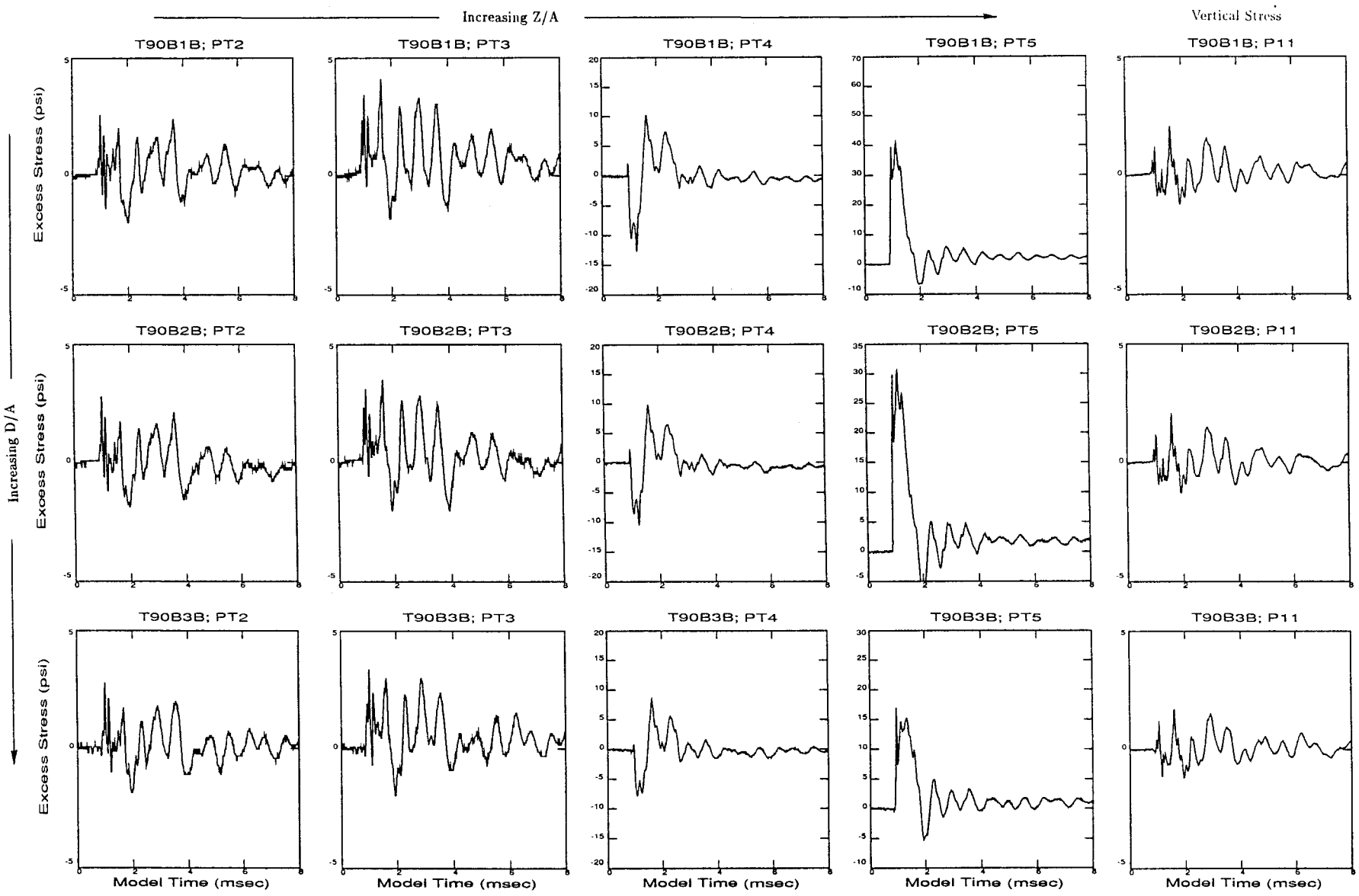

Figure 6.3.2.4 Vertical distribution of dynamic radial and vertical measured stress
(b) Measured transient excess stress (Page 7 of 7)

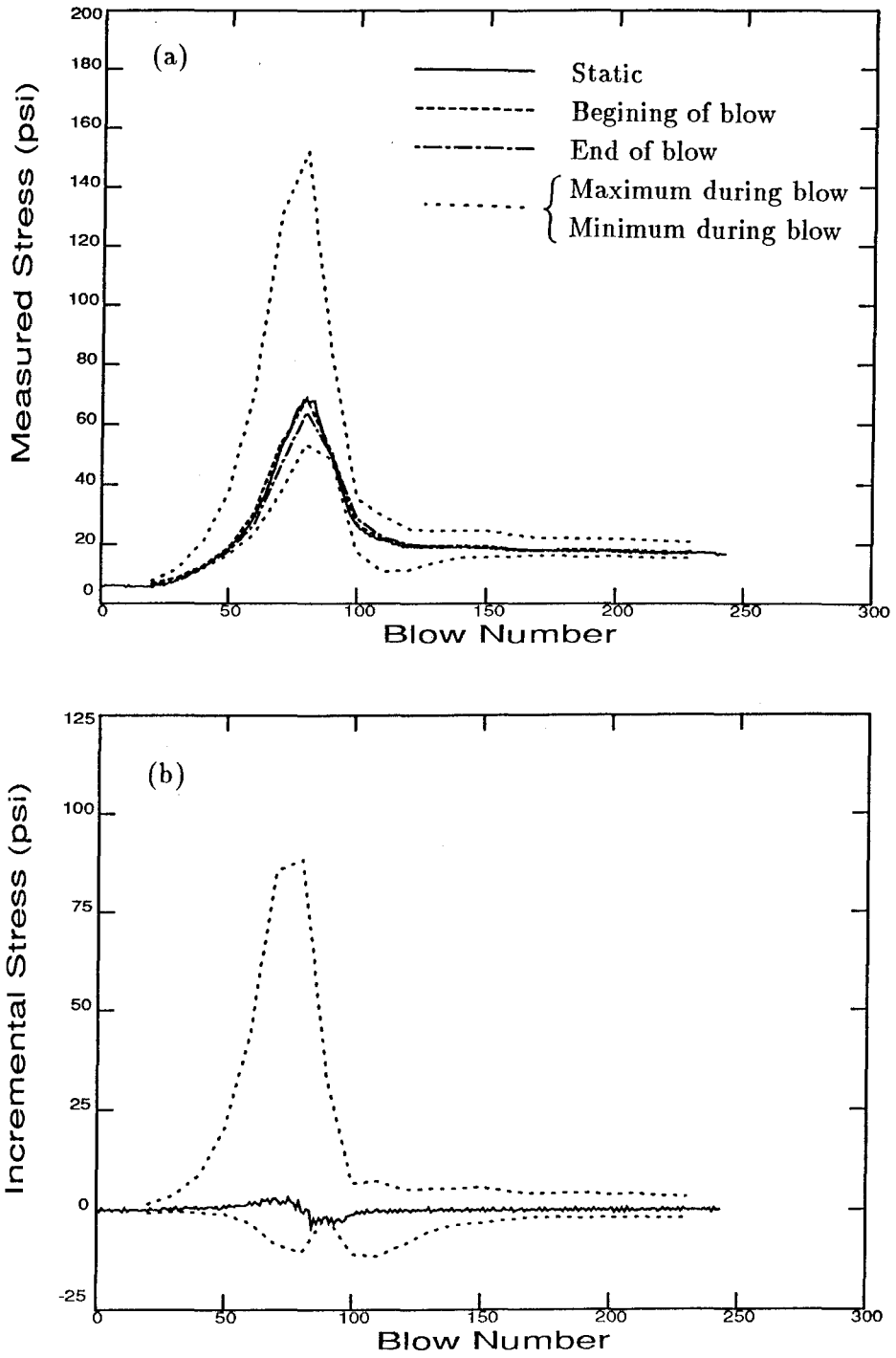

Figure 6.3.3.1 Static and dynamic stress histories of a transducer, Z/A = 26.67, R/A = 2.67; linear assumption Recreating the missing blow history
(a) Stresses, (b) Incremental stresses

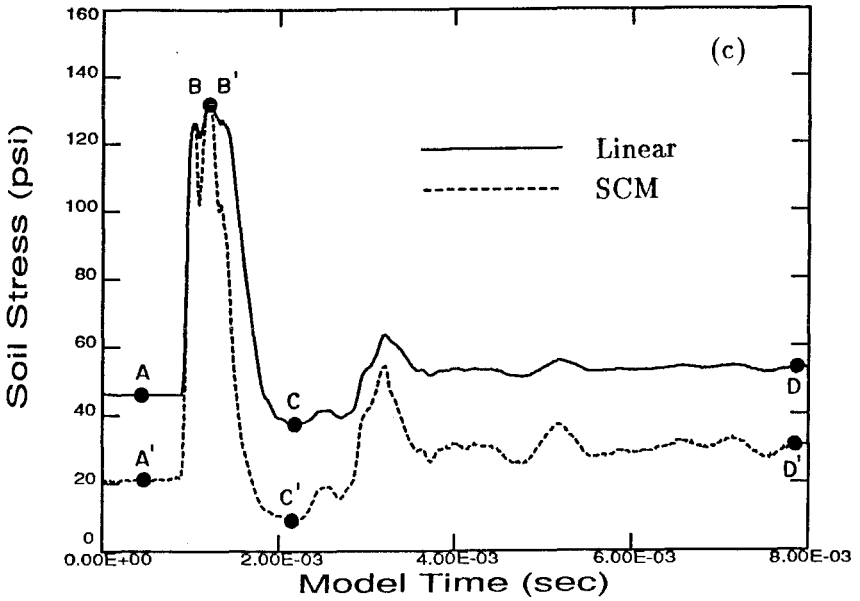

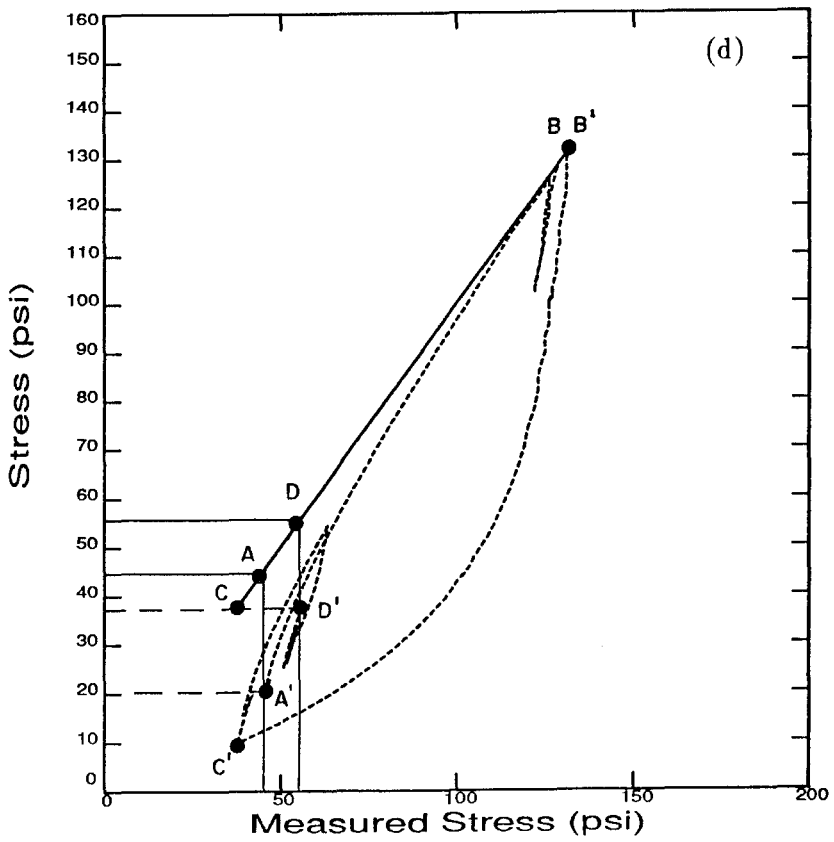

Figure 6.3.3.1 Implications of the SCM assumption for a blow
Z/A = 26.67, R/A = 2.67; D/A = 22.6
(c) Transient stress following a blow
(d) Stress paths for the linear and model assumption

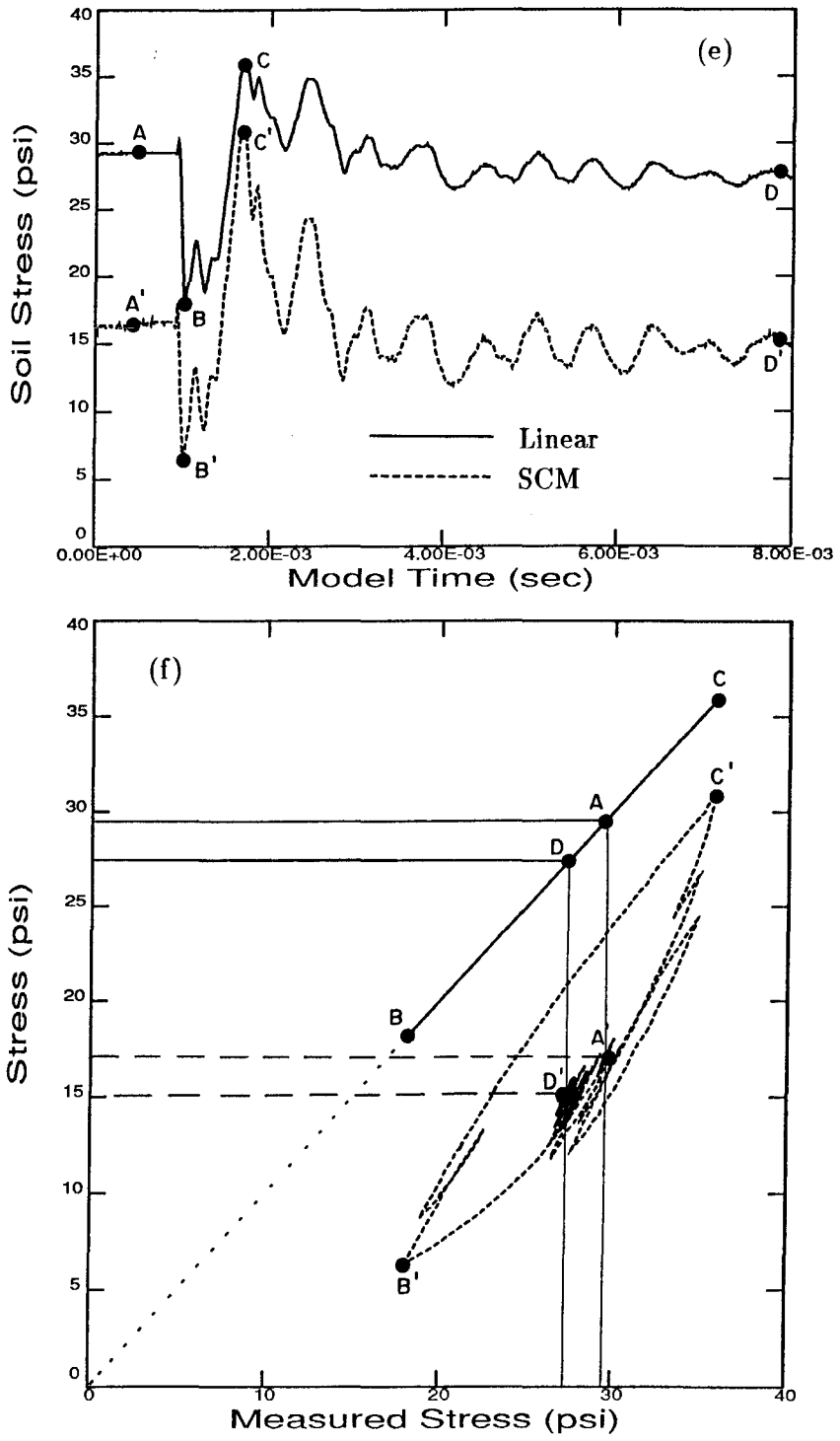

Figure 6.3.3.1 Implications of the SCM assumption for a blow
Z/A = 26.67, R/A = 2.67; D/A = 26.8
(e) Transient stress following a blow
(f) Stress paths for the linear and model assumption

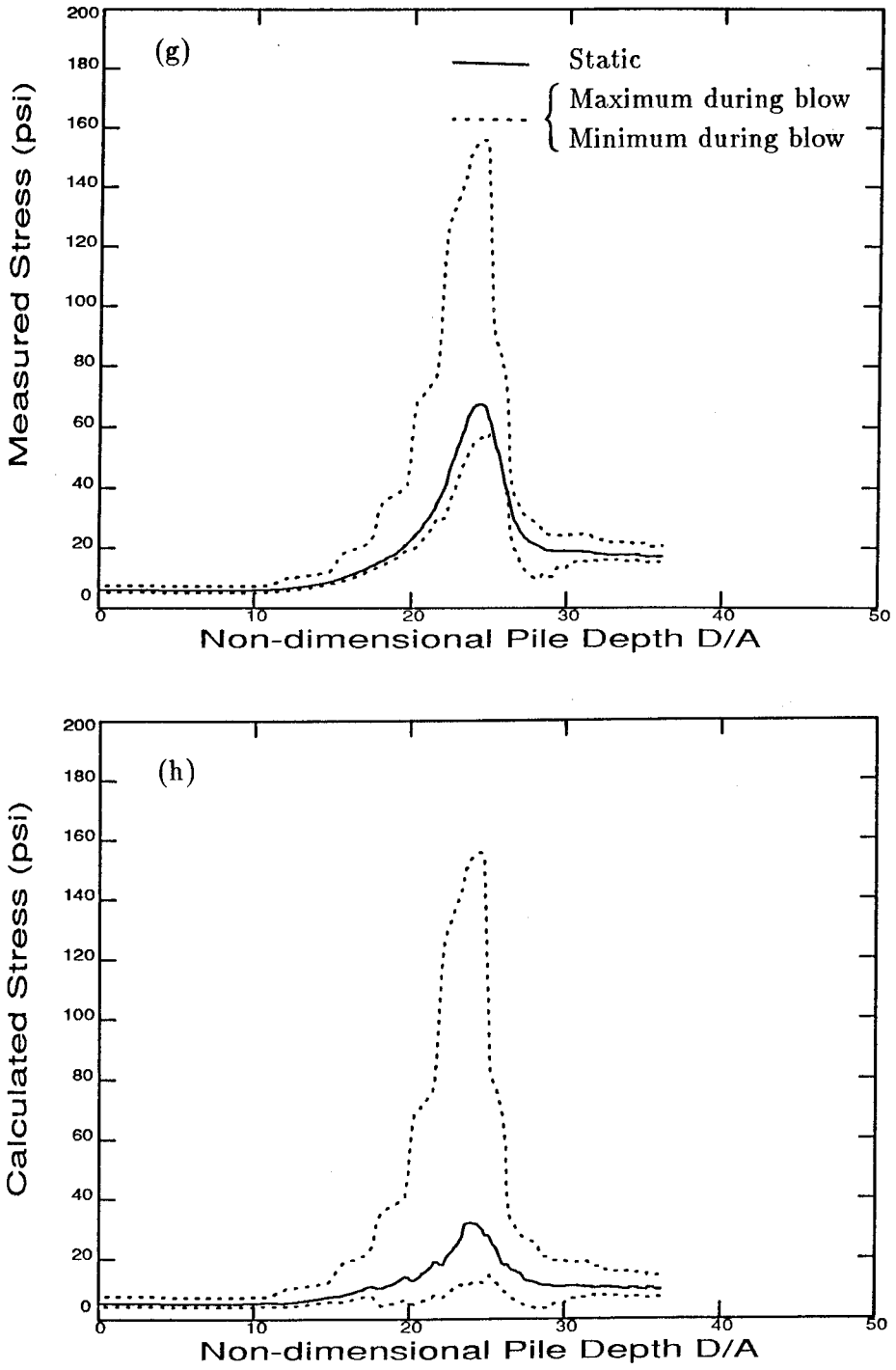

Figure 6.3.3.1 Comparison between the linear (g) and SCM (h) assumptions, of the dynamic stress history of a transducer Z/A = 26.67, R/A = 2.67

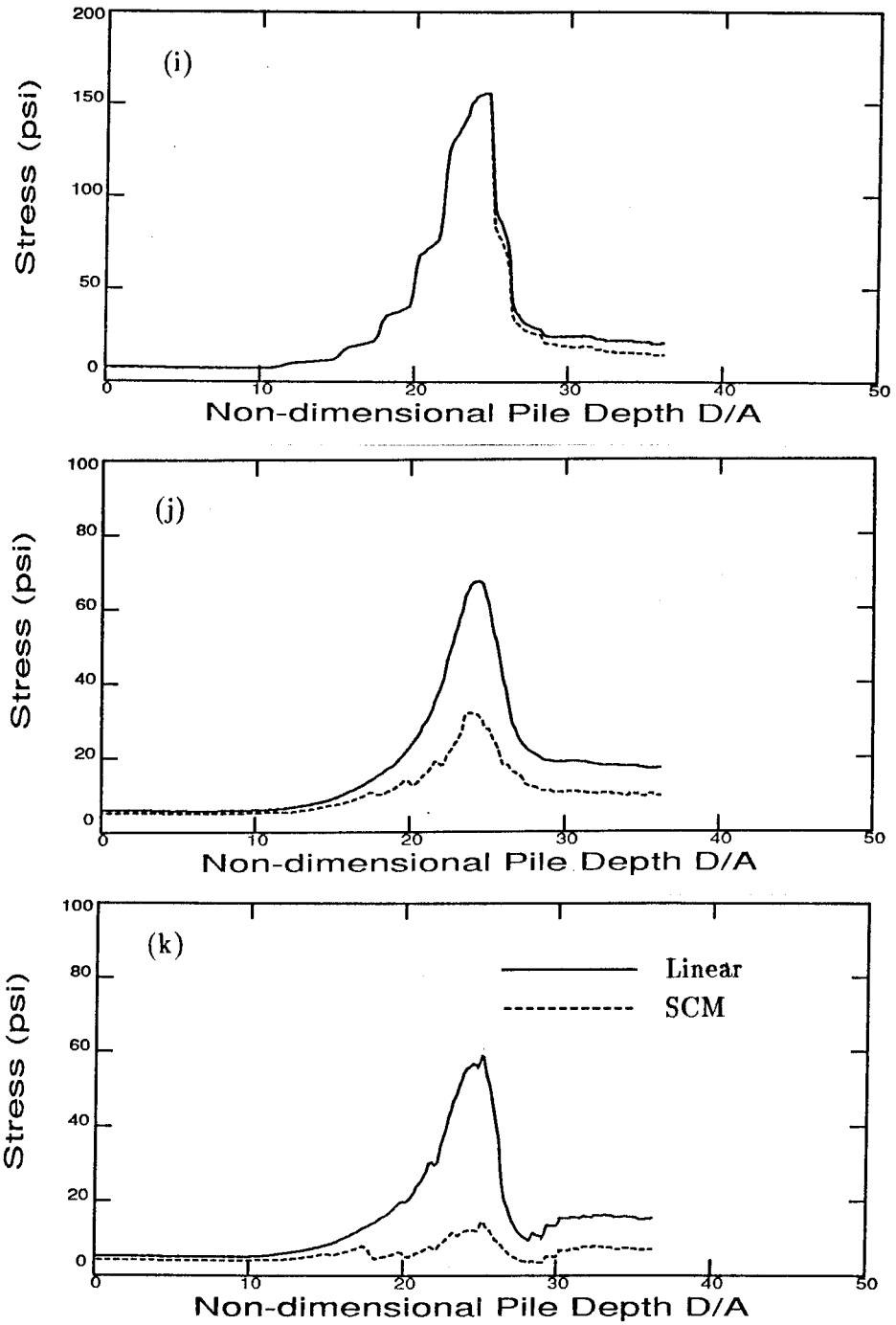

Figure 6.3.3.1 Comparison between the linear and SCM assumptions, of the dynamic stress history of a transducer
Z/A = 26.67, R/A = 2.67
(i) Maximum dynamic stress history
(j) "Static" stress history
(k) Minimum dynamic stress history

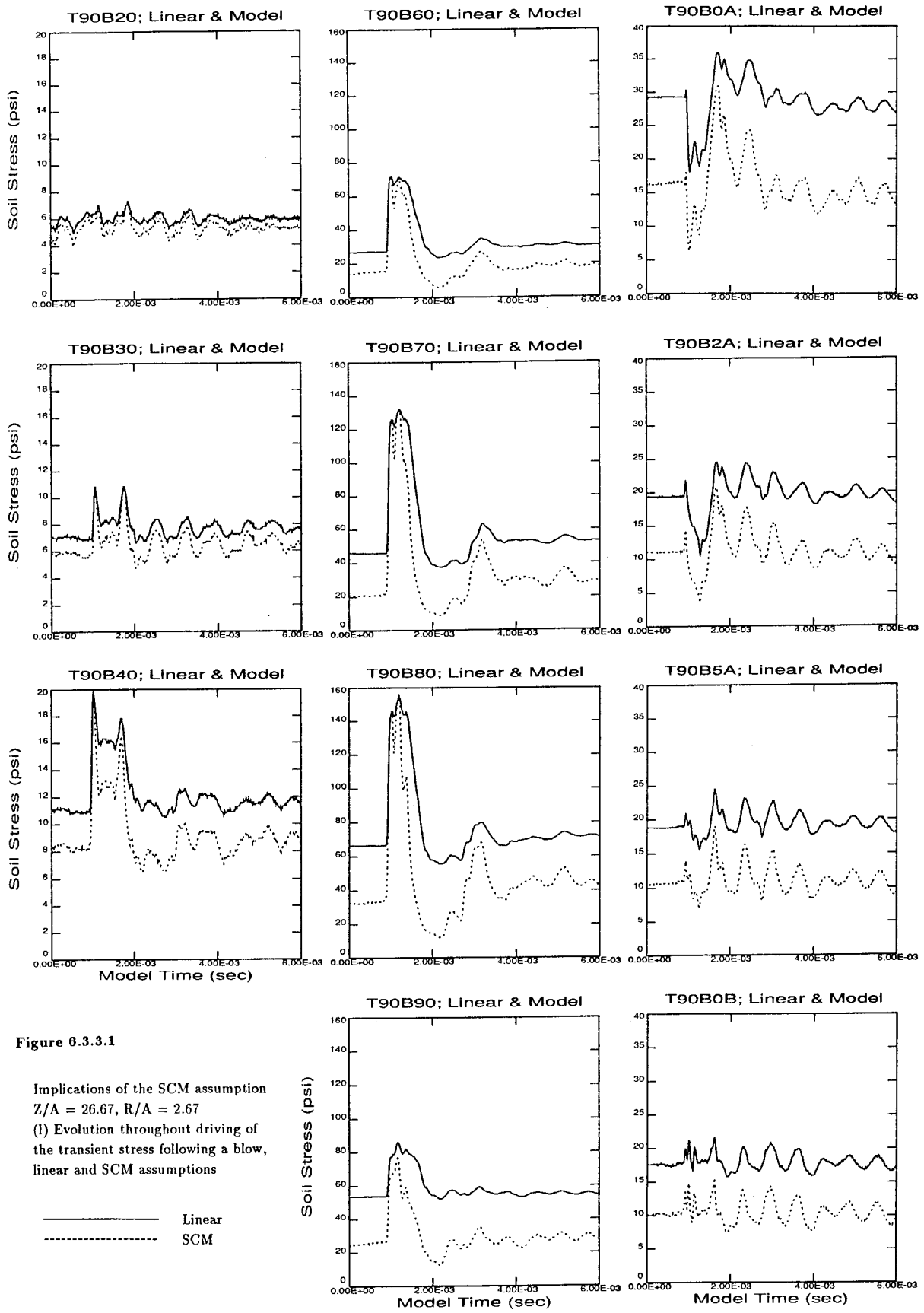

Figure 6.3.3.1

Implications of the SCM assumption
Z/A = 26.67, R/A = 2.67
(l) Evolution throughout driving of the transient stress following a blow, linear and SCM assumptions

——————— Linear
--------------------- SCM

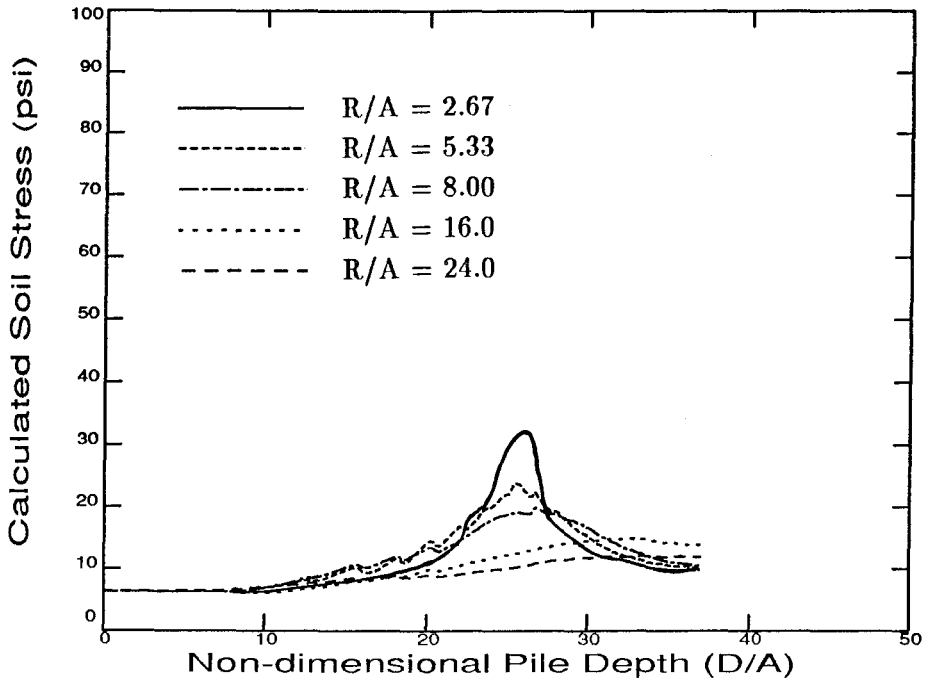

Figure 6.3.3.2 Radial distribution of the radial calculated stress Z/A = 26.67

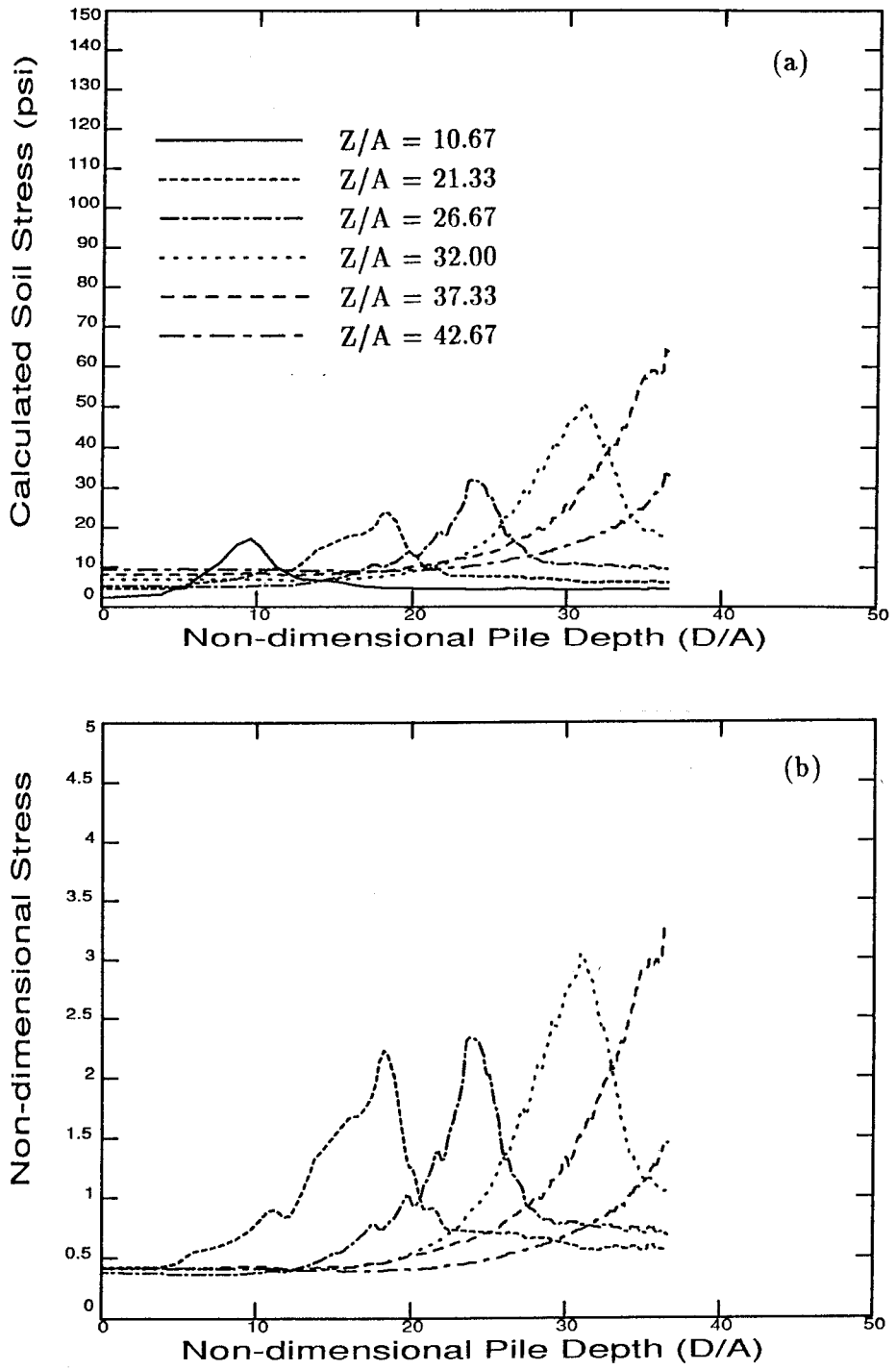

Figure 6.3.3.3 Vertical distribution of the radial calculated stress
R/A = 2.67
(a) Calculated stress
(b) Non-dimensional stress

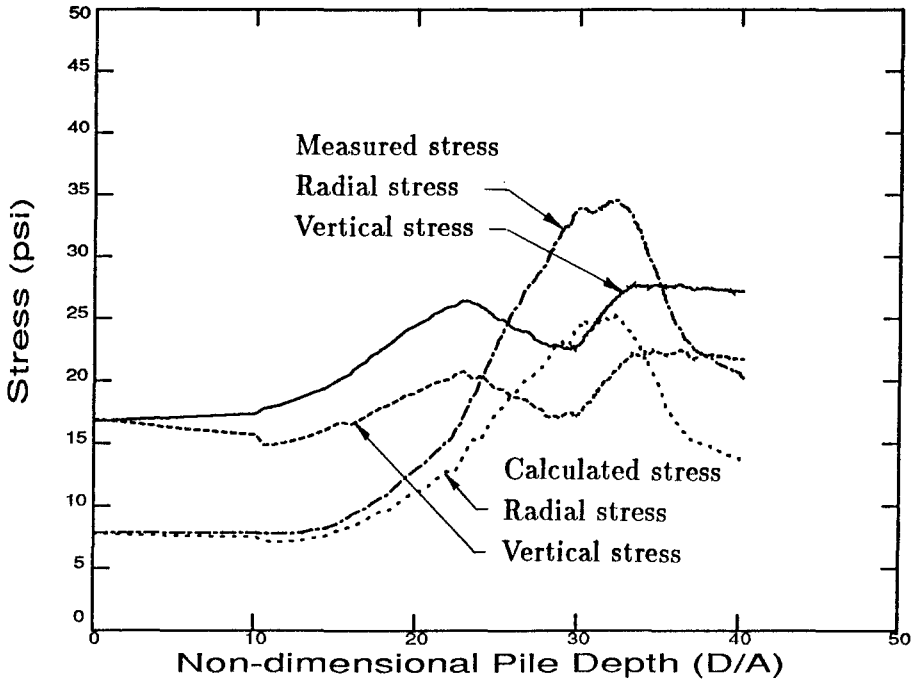

Figure 6.3.3.4 Comparison of radial and vertical, measured and calculated stresses; Z/A = 32.0, R/A = 8.00

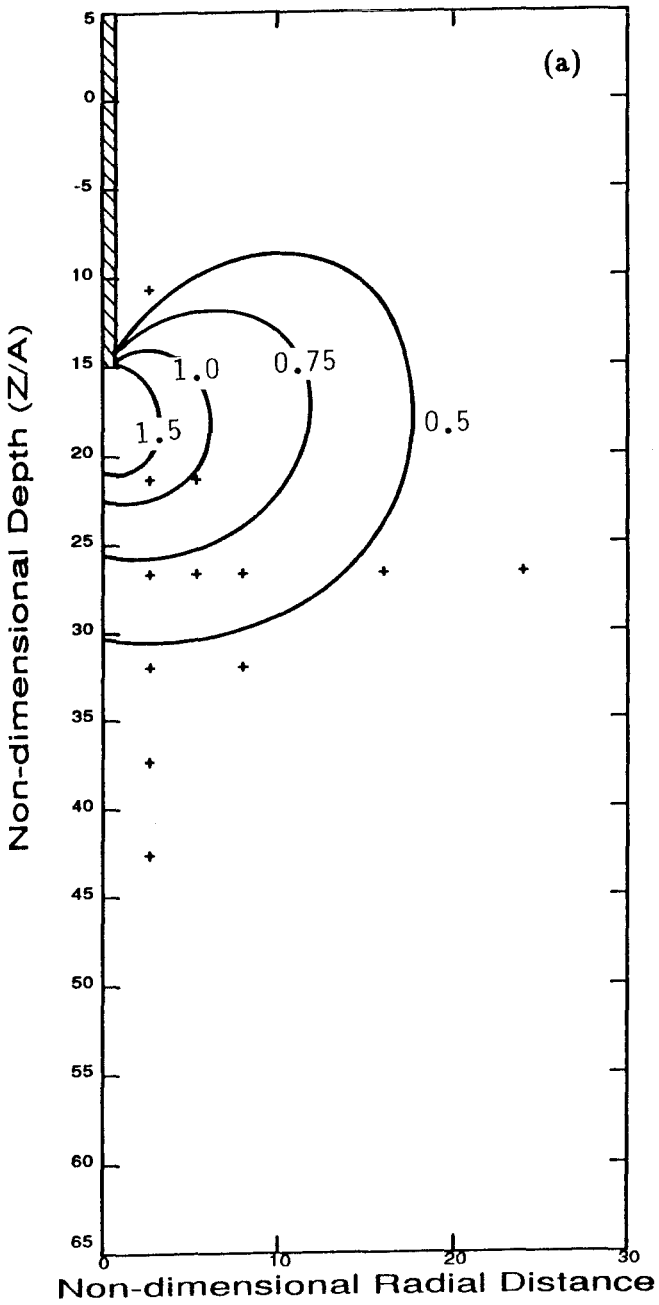

Figure 6.3.3.5 Calculated radial stress contours
(a) D/A = 15

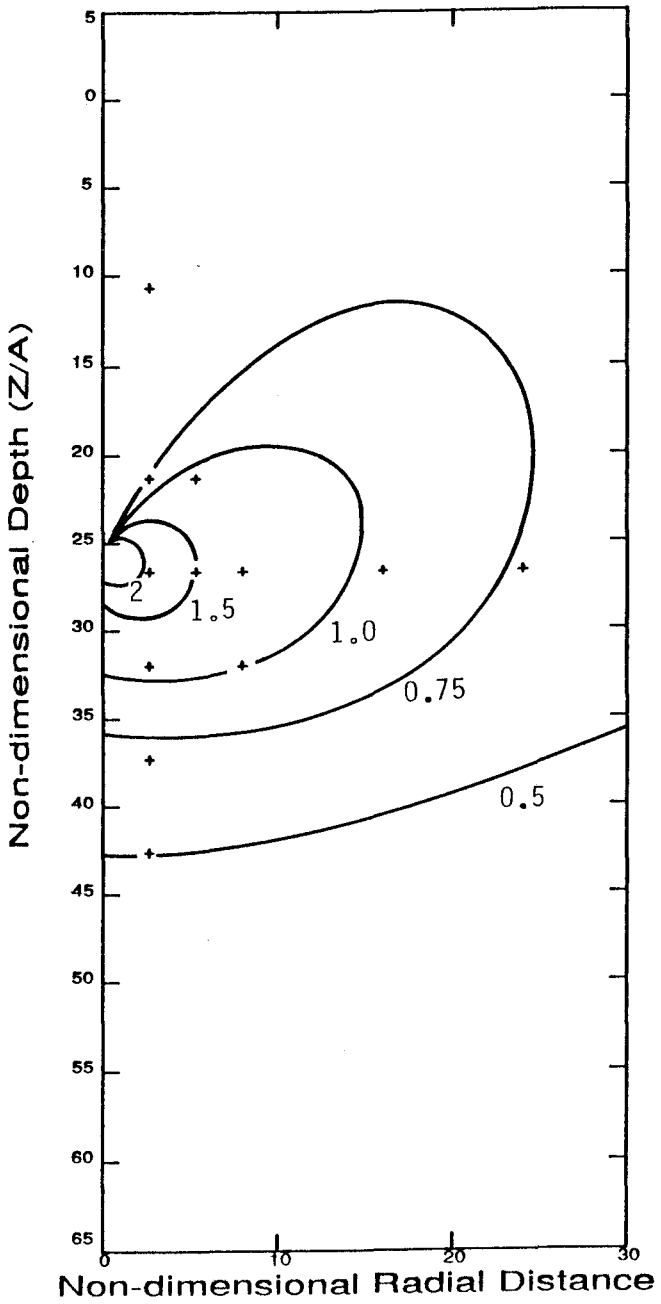

Figure 6.3.3.5 Calculated radial stress contours
(b) D/A = 25

Chapter 7

CONCLUSIONS AND RECOMMENDATIONS

7.1 CONCLUSIONS

A series of pile driving experiments has been conducted in a geotechnical centrifuge to determine the evolution of the soil stress field around the driven pile, both at the dynamic level of the pile-soil interaction following the hammer impact, and at the static level of pile installation in the soil mass.

The development of a soil-cell model, to account for the non-linear behavior of the interaction between the measuring device and the soil medium, has proven the importance of the special consideration needed in the interpretation of soil stress measurement. Also the misleading estimation of stress obtained by the linear approximation of the soil-cell interaction has been confirmed by the calculation of more realistic soil stresses using the model.

These tests provide the first full set of experimental data concerning the soil response during driving for a pile installed in dry sand. These results will enable the development of more accurate pile driving models, and will be useful in the verification of such models. It is essential in the modelling of a system to be able to predict the response of the various parts of the system. Until now only information on the dynamic response of the pile was available, limiting the validity of the modeling of the soil medium. The data obtained here will enable the pile driving model to be checked for the prediction of soil response, and therefore will lead to a better estimation of the soil characteristics consequent to driving, which up to now is the major difficulty of the analysis. This in turn is essential for the prediction of pile capacity, the key factor of pile driving analysis.

7.2 RECOMMENDATIONS

The experimental results of this research contribute to a better understanding of the pile-soil system during driving, and also uncovered a need for further work. The centrifuge technique allowed us to perform model experiments, which are the most suitable for obtaining information on the soil response. Continuation of centrifuge experiments is warranted with different soils, and improved equipment and instrumentation. In particular, a longer arm for the centrifuge would be required to render insignificant the g-level gradient for the experiment. There is also a need to improve driving equipment, allowing for a perfect alignment of the soil container, the pile driving mechanism and the pile, so as to avoid pile bending and buckling, and to offer a large range of driving rate, for the study of the effect of stress relaxation after each blow. An important consideration is the use of a better device for the measurement of soil stress. As pressure cells are the only current technology available for the measurement of soil stress, the design of miniature pressure cells fulfilling the requirements stated in Chapter 5 is essential, as well as systematic calibration in the soil investigated, and under the experimental loading conditions (both static and dynamic). The data acquisition system should allow for the storage of the complete driving history of the pressure cell readings for the use of a soil-cell interaction model. A next step is to conduct experiments on piles driven in saturated sands and clays. This implies important problems related to the scaling of the dynamic response of the soil and the pore pressure dissipation, as well the need for adequate instrumentation for dynamic measurement of pore fluid pressures.

The use of the soil-cell model, and in particular the integration of data over an experiment's history, has proven to be important for the dynamic problem of pile driving, and should be considered for the study of other problems of soil dynamics.

The necessity of recreating the complete dynamic history for the soil stress field around the driven pile, implies the need to drive the piles in flight rather than pushing them at 1 g or even at the test acceleration.

Continuation of pile driving experiments and development of analysis methods for the understanding of the pile-soil system are needed to provide the engineer with a good tool for the design and control of piles.

REFERENCES

1. Abbott, P. A., K. B. Simmons, C. M. Reiff, and S. Mitchell, "Recent Soil Stress Gage Research," *Proceedings of the International Symposium on Wave Propagation and Dynamic Properties of Earth Materials*, Univ. of New Mexico, Albuquerque, 1967, pp. 221–238.

2. Allard, M. A., "Tests on Piles Installed in Flight in the Centrifuge," *Proceedings of the Symposium on Recent Advances in Geotechnical Centrifuge Modeling*, University of California, Davis, July 18-20, 1984.

3. Allard, M. A., "Caltech Centrifuge Manual," Soil Mechanics Laboratory, California Institute of Technology, Pasadena, 1983.

4. Allard, M. A., Scott, R. F., and J. R. Lee, "Driveability of Piles. Experiments on Model Piles Driven in Flight in the Centrifuge," *Proceedings of the Third International Conference on Numerical Methods in Offshore Piling*, Nantes, May 21–22, 1986, pp. 91–104.

5. Appendino, M., "Prediction of Static Ultimate Resistance from Driving Data," *Proceedings of the International Seminar on the Application of Stress-Wave Theory on Piles*, Stockholm, June 4–5, 1980, pp. 273–296.

6. Askegaard, V., "Measurement of Pressure in Solids by Means of Pressure Cells," Bulletin No. 17, Structural Research Laboratory, Technical University of Denmark, Copenhagen, 1963.

7. Atkinson, J. H., and P. L. Bransby, **The Mechanics of Soils: An Introduction to Critical State Soil Mechanics**, McGraw-Hill, Maidenhead, 1978.

8. Bakholdin, B. V., and N. M. Vol'shakov, "Investigation of the State of Stress of Clays during Pile Driving," *Journal of Soil Mechanics and Foundation Engineering*, Vol. 10, 1973, pp. 300–305.

9. Balthaus, H. G., and H. Früchtenicht, "Model Tests for the Evaluation of Static Bearing Capacity of Piles from Dynamic Measurements," *Proceedings of the Second International Conference on the Application of Stress-Wave Theory on Piles*, Stockholm, May 27–30, 1984, pp. 41–49.

10. Balthaus, H., "Numerical Modelling of Pile Driving Based on an Automatic CAPWAP Search Procedure," *Proceedings of the Third International Conference on the Application of Stress-Wave Theory to Piles*, Ottawa, May 25–27, 1988, pp. 219–230.

11. Bea, R. G., "Soil Strain Rate Effects on Axial Pile Capacity," *Proceedings of the Second International Conference on Numerical Methods in Offshore Piling*, Austin, Texas, April 29–30, 1982, pp. 107–132.

12. Beer, G., and J. L. Meek, "Infinite Domain Elements," *International Journal for Numerical Methods in Engineering*, Vol. 17, 1981, pp. 43–52.

13. Beringen, F. L., and H. van Koten, "Skin Friction Data in Sands from Dynamic Load Tests," *Proceedings of the Second International Conference on the Application of Stress-Wave Theory on Piles*, Stockholm, May 27–30, 1984, pp. 170–177.

14. Bieganousky, W. A., and W. F. Marcuson, "Uniform Placement of Sand," *Journal of the Geotechnical Engineering Division, ASCE*, Vol. 102, No. GT3, March 1976, pp. 229–233.

15. Boulon, M., and P. Foray, "Physical and Numerical Simulation of Lateral Shaft Friction along Offshore Piles in Sand," *Proceedings of the Third International Conference on Numerical Methods in Offshore Piling*, Nantes, May 21–22, 1986, pp. 127–148.

16. Bowles, J. E., **Analytical and Computational Methods in Foundation Engineering**, McGraw-Hill, New York, 1974.

17. Bredenberg, H., and G. Holm, "Evaluation of Pile Driving Criterion from CASE-Measurements," *Proceedings of the International Symposium on Penetrability and Drivability of Piles,* San Francisco, 10 August, 1985, pp. 159–162.

18. Bridgman, P. W., "Dimensional Analysis," Yale University Press, Revised Ed., 1931, 113 pp.

19. Bucky, P. B., "Use of Models for the Study of Mining Problems," *American Institute of Mining and Metallurgical Engineers*, Tech. Pub. No. 425, 1931, pp. 3–28.

20. Burgess, I. W., and C. A. Tang, "Effect of Driving Support Conditions on Pile Wandering," **Numerical Methods in Offshore Piling**, Institution of Civil Engineers, London, 1979, pp. 9–17.

21. Burridge, P. B., "Failure of Slopes," Soil Mechanics Laboratory, California Institute of Technology, Pasadena, Report No. SML 87–01, 1987.

22. Bustamante, M., R. Frank, L. Gianeselli, and J. Klos, "Vérification Expérimentale des Formules de Battage," *Proceedings of the International Symposium on Penetrability and Drivability of Piles,* San Francisco, 10 August, 1985, pp. 163–166.

23. Carter, J. P., M. F. Randolph, and C. P. Wroth, "Some Aspects of the Performance of Open- and Closed-Ended Piles," **Numerical Methods in Offshore Piling**, Institution of Civil Engineers, London, 1979, pp. 137–142.

24. Carter, J. P., M. F. Randolph, and C. P. Wroth, "Stress and Pore Pressure Changes in Clay During and After the Expansion of a Cylindrical Cavity," *International Journal for Numerical and Analytical Methods in Geomechanics*, Vol. 3, 1979, pp. 305–322.

25. Cheney, J. A., "American Literature on Geotechnical Centrifuge Modeling 1931–1984," *Proceedings of the Symposium on Recent Advances in Geotechnical Centrifuge Modeling*, University of California, Davis, July 1984, pp. 1–25.

26. Cheng, S. S. M., and S. A. Ahmad, "Comparison of Pile Capacity Evaluated by Dynamic Measurements and Static Loading Tests — Five Case Studies in Ontario, Canada," *Proceedings of the Third International Conference on the Application of Stress-Wave Theory to Piles*, Ottawa, May 25–27, 1988, pp. 477–489.

27. Chow, Y. K., R. Radhakrishnan, K. Y. Wong, G. P. Karunaratne, and S. L. Lee, "Estimation of Pile Capacity from Stress-Wave Measurements," *Proceedings of the Third International Conference on the Application of Stress-Wave Theory to Piles*, Ottawa, May 25–27, 1988, pp. 616–634.

28. Chow, Y. K., and I. M. Smith, "Infinite Elements for Dynamic Foundation Analysis," *4th International Conference on Numerical Methods in Geomechanics*, Edmonton, May 31–June 4, 1982, pp. 15–22.

29. Chow, Y. K., K. Y. Wong, G. P. Karunaratne, and S. L. Lee, "Wave Equation Analysis of Piles — A Rational Theoretical Approach," *Proceedings of the Third International Conference on the Application of Stress-Wave Theory to Piles*, Ottawa, May 25–27, 1988, pp. 208–218.

30. Clark, J. I., and G. G. Meyerhof, "The Behavior of Driven Piles in Clay: (I) An Investigation of Soil Stress and Pore Water Pressures as Related to Soil Properties," *Canadian Geotechnical Journal*, No. 4, 1972, pp. 351–373.

31. Clough, R. W., and J. Penzien, **Dynamics of Structures**, McGraw-Hill, New York, 1975.

32. Collins, R., K. L. Lee, G. P. Lilly,, and R. A. Westmann, "Mechanics of Pressure Cells," *Experimental Mechanics*, Vol. 12, No. 11, Nov. 1972, pp. 514–519.

33. Corté, J. F., and M. Bustamante, "Experimental Evaluation of the Determination of Pile Bearing Capacity from Dynamic Tests," *Proceedings of the Second International Conference on the Application of Stress-Wave Theory on Piles*, Stockholm, May 27–30, 1984, pp. 17–24.

34. Corté, J. F., and P. Lepert, "Lateral Resistance During Driving and Dynamic Pile Testing," *Proceedings of the Third International Conference on Numerical Methods in Offshore Piling*, Nantes, May 21–22, 1986, pp. 19–34.

35. Coutinho, A. L. G., A. M. Costa, J. L. D. Alves, L. Landau and N. F. F. Ebecken, "Pile Driving Simulation and Analysis by the Finite Element Method," *Proceedings of the Third International Conference on the Application of Stress-Wave Theory to Piles*, Ottawa, May 25–27, 1988, pp. 197–207.

36. Coutinho, A. L. G. A., L. Landau, N. F. F. Ebecken, E. C. P. Lima and A. M. Costa, "Pile Driveability of Offshore Piles Using the Finite Element Methods," *Proceedings of the International Conference on Finite Elements in Computational Mechanics*, Bombay, T. Kant, Editor, Pergamon Press, Oxford, 1985.

37. Coyle, H. M., and R. R. Castello, "New Design Correlations for Piles in Sand," *Journal of the Geotechnical Engineering Division, ASCE*, Vol. 107, No. GT7, July 1981, pp. 965–986.

38. Craig, W. H., "Installation Studies for Model Piles," in **The Application of Centrifuge Modelling to Geotechnical Design**, W. H. Craig (ed.), Peter W. Rowe Laboratory, University of Manchester Engineering Department, April 16–18, 1984, pp. 440–455.

39. Dangla, P., and J. F. Corté, "Impedances for Pile Toe Reaction During Driving," *Proceedings of the Third International Conference on the Application of Stress-Wave Theory to Piles*, Ottawa, May 25–27, 1988, pp. 186–196.

40. Davis, R. O., and G. Mullenger, "A Simple Rate-Type Constitutive Model for Soil with a Critical State," *International Journal for Numerical and Analytical Methods in Geomechanics*, Vol. 2, 1978, pp. 255–282.

41. Davis, R. O., and P. J. Phelan, "Numerical Approximations in Pile-Driving Analysis," *International Journal for Numerical and Analytical Methods in Geomechanics*, Vol. 2, 1978, pp. 303–310.

42. Davis, R. O., R. F. Scott, and G. Mullenger, "Rapid Expansion of a Cylindrical Cavity in a Rate-Type Soil," *International Journal for Numerical and Analytical Methods in Geomechanics*, Vol. 8, 1984, pp. 125–140.

43. Day, S. M., "Finite Element Analysis of Seismic Scattering Problems," Ph.D. Thesis, University of California, San Diego, 1977.

44. Denver, H., "Tests with an Instrumented Model Pile," *Proceedings of the Second International Conference on the Application of Stress-Wave Theory on Piles*, Stockholm, May 27–30, 1984, pp. 143–153.

45. Denver, H., and R. Skov, "Investigation of the Stress-Wave Method by Instrumented Piles," *Proceedings of the Third International Conference on the Application of Stress-Wave Theory to Piles*, Ottawa, May 25–27, 1988, pp. 613–625.

46. Durelli, A. J., and W. F. Riley, "Performance of Embedded Pressure Gages under Static and Dynamic Loadings," *Symposium on Soil Dynamics, American Society for Testing and Materials*, Philadelphia, Pa., 1961, pp. 20–34.

47. Ebecken, N., E. Prates de Lima, L. Landau, and A. Coutinho, "Numerical Simulation of Pile Driving by Finite Elements: Some Practical Applications on the Brazilian Coast," *Proceedings of the Second International Conference on the Application of Stress-Wave Theory on Piles*, Stockholm, May 27–30, 1984, pp. 350–359.

48. Fong, C. K., and W. J. Dickson, "Pile/Soil Interaction and Load Versus Deflection," *Proceedings of the Second International Conference on the Application of Stress-Wave Theory on Piles*, Stockholm, May 27–30, 1984, pp. 1–8.

49. Frank, R., A. Guenot, and P. Humbert, "Numerical Analysis of Contacts in Geomechanics," *4th International Conference on Numerical Methods in Geomechanics*, Edmonton, May 31–June 4, 1982, pp. 37–45

50. Frydman, S., "State of the Art Report — Soil Structure Interaction," Report for International Society of Soil Mechanics and Foundation Engineering Subcommittee on Centrifugal Modelling, June 1984.

51. Frydman, S., "Centrifuge Modelling of Soil-Structure Interaction," **Centrifuges in Soil Mechanics**, Craig, James & Schofield (eds.), A. A. Balkema, Rotterdam, 1988, pp. 169–182.

52. Fuglsang, L. D., and N. K. Ovesen, "The Application of the Theory of Modelling to Centrifuge Studies," **Centrifuges in Soil Mechanics**, Craig, James & Schofield (eds.), A. A. Balkema, Rotterdam, 1988, pp. 119–138.

53. Fujita, K., and O. Kusabe, "On the Evaluation of Static Bearing Capacity," *Proceedings of the Third International Conference on the Application of Stress-Wave Theory to Piles*, Ottawa, May 25–27, 1988, pp. 525–534.

54. Geddes, J. D., "Stresses in Foundation Soils Due to Vertical Subsurface Loading," *Géotechnique*, Vol. 16, 1966, pp. 231–155.

55. Geddes, J. D., "Boussinesq Based Approximations to the Vertical Stresses Caused by Pile Type Subsurface Loadings," *Géotechnique*, Vol. 19, 1969, No. 4, pp. 509–514.

56. Goble, G. G., W. D. Kovacs, and F. Rausche, "Field Demonstration: Response of Instrumented Piles to Driving and Load Testing," *Proceedings of the Specialty Conference on Performance of Earth and Earth-Supported Structures*, Purdue University, Lafayette, June 11–14, 1972, pp. 3–38.

57. Goble, G. G., and F. Rausche, "Wave Equation Analysis of Pile Driving — WEAP Program," Prepared for the U.S. D.O.T., Federal Highway Administration, Implementation Division, Office of Research and Development, July 1976.

58. Goble, G. G., F. Rausche, and G. E. Likins, Jr., "The Analysis of Pile Driving — A State of the Art," *Proceedings of the International Seminar on the Application of Stress-Wave Theory on Piles*, Stockholm, June 4–5, 1980, pp. 131–162.

59. Goble, G. G., F. K. Walker, and F. Rausche, "Pile Bearing Capacity — Prediction Vs. Performance," *Proceedings of the Specialty Conference on Performance of Earth and Earth-Supported Structures*, Purdue University, Lafayette, June 11–14, 1972, pp. 1243–1259.

60. Gozdz, A., "Pile Driving Analysis by the Method of Space-Time Elements," *Proceedings of the Third International Conference on the Application of Stress-Wave Theory to Piles*, Ottawa, May 25–27, 1988, pp. 285–293.

61. Grillo, O., "Influence Scale and Influence Chart for the Computation of Stresses Due, Respectively, to Surface Point Load and Pile Loads," *Proceedings of the 2nd*

International Conference on Soil Mechanics and Foundation Engineering, Rotterdam, 1948.

62. Hadala, P. F., "The Effect of Placement Methods on the Response of Soil Stress Gauges," *Proceedings of the International Symposium on Wave Propagation and Dynamic Properties of Earth Materials*, Univ. of New Mexico, Albuquerque, 1967, pp. 255–263.

63. Heritier, B., and J. Paquet, "Détermination de la Capacité Portante des Pieux par les Méthodes Dynamiques, *Proceedings of the International Symposium on Penetrability and Drivability of Piles,* San Francisco, 10 August, 1985, pp. 169–172.

64. Hjeldnes, E. I., "Stress Waves in Model Piles Driven in Sand, " *Proceedings of the International Seminar on the Application of Stress-Wave Theory on Piles*, Stockholm, June 4–5, 1980, pp. 305–310.

65. Holeyman, A., "Contribution à l'Etude du Comportement Dynamique Non-linéaire des Pieux lors de leur Battage," Service de Mécaniques des Soils, Université Libre de Bruxelles, Faculté des Sciences Appliqueés, Bruxelles, 1984.

66. Holeyman, A. E., "Modelling of Dynamic Behaviour at the Pile Base," *Proceedings of the Third International Conference on the Application of Stress-Wave Theory to Piles*, Ottawa, May 25–27, 1988, pp. 174–185.

67. Holloway D. M., J. M. E. Audibert, and A. R. Dover, "Recent Advances in Predicting Pile Driveability," *Proceedings of the Tenth Annual Offshore Technology Conference*, OTC 3273, pp. 1915–1924.

68. Holm, G., M. Jansson, and B. Möller, "Dynamic and Static Load Testing of Friction Piles in Loose Sand," *Proceedings of the Second International Conference on the Application of Stress-Wave Theory on Piles*, Stockholm, May 27–30, 1984, pp. 240–243.

69. Hoorslev, M. J., "The Changeable Interaction Between Soils and Pressure Cells: Tests and Reviews at the Waterways Experiment Station," *Report, U.S. Army Engineering Waterways Experiment Station*, Vicksburg, Miss., June 1976.

70. Hughes, T. J. R., **The Finite Element Method, Linear, Static and Dynamic Finite Element Analysis**, Prentice-Hall, Inc., Englewood Cliffs, New Jersey, 1987.

71. Hushman, B., "Experimental Studies of Dynamic Response of Foundations," Soil Mechanics Laboratory, California Institute of Technology, Pasadena, Report No. SML 83–02, 1983.

72. Iwanowski, T., and A. Bodare, "On Soil Damping Factors Used in Wave Analysis of Pile Driving," *Proceedings of the Third International Conference on the Application of Stress-Wave Theory to Piles*, Ottawa, May 25–27, 1988, pp. 343–352.

73. Kishida, T., T. Fukaya, and H. Hanzawa, "Prediction of Pile-Bearing Capacity by the Wave Equation," *Proceedings of the International Symposium on Penetrability and Drivability of Piles,* San Francisco, 10 August, 1985, pp. 177–180.

74. Ko, H-Y., "Summary of the State-of-the-Art in Centrifuge Model Testing," **Centrifuges in Soil Mechanics**, Craig, James & Schofield (eds.), A. A. Balkema, Rotterdam, 1988, pp. 11–18.

75. Ko, H.-Y., R. H. Atkinson, G. G. Goble, and C. D. Ealy, "Centrifugal Modeling of Pile Foundations," *Proceedings of the Symposium on Analysis and Design of Pile Foundations*, San Francisco, October 1984, ASCE, pp. 21–40.

76. Konagai, K., M. Takahashi, and S. Ogawa, "Experiments Study on Soil-Pile Dynamics Using Electromagnetic Induction Type Shock Wave Source," *Proceedings of Japan Society of Civil Engineers, Structural Engineering/Earthquake Engineering*, Vol. 2, No. 1, April 1985, pp. 175–184.

77. Krizek, R. J., M. H. Farzin, A. E. Z. Wissa, and R. T. Martin, "Evaluation of Stress Cell Performance," *Journal of the Geotechnical Engineering Division, ASCE*, Vol. 100, Dec. 1974, pp. 1275–1295.

78. Lacy, H., and J. Moskowitz, "Pile Capacity in Uniform Medium Dense Sand," *Proceedings of the Third International Conference on the Application of Stress-Wave Theory to Piles*, Ottawa, May 25–27, 1988, pp. 749–671.

79. Lee, S. L., Y. K. Chow, G. P. Karunaratne, and K. Y. Wong, "Rational Wave Equation Model for Pile-Driving Analysis," *Journal of the Geotechnical Engineering Division, ASCE*, Vol. 114, No. 3, March 1988, pp. 306–325.

80. Leifer, S. A., R. C. Kirby, and M. I. Esrig, "Effect of Radial Variation in Modulus on Stresses After Consolidation Around a Driven Pile," **Numerical Methods in Offshore Piling**, Institution of Civil Engineers, London, 1979, pp. 129–135.

81. Lepert, P., J. F. Corté, and A. Goulois, "Experimental Set-Up for Investigation of Shaft Resistance During Driving," *Proceedings of the Third International Conference on the Application of Stress-Wave Theory to Piles*, Ottawa, May 25–27, 1988, pp. 422–430.

82. Lepert, P., J. F. Corté, A. Goulois, and J. Meunier, "Shaft Resistance During Driving, in Sand, from Laboratory Tests," *Proceedings of the Third International Conference on the Application of Stress-Wave Theory to Piles*, Ottawa, May 25–27, 1988, pp. 431–440.

83. Levacher, D. R., "On the Accuracy and the Development of a Pile Driving Computer Program," *Proceedings of the Third International Conference on Numerical Methods in Offshore Piling*, Nantes, May 21–22, 1986, pp. 35–52.

84. Levacher, D. R., and A. Oularbi, "Dynamic Behaviour of a Model Pile Toe in Sand," *Proceedings of the Third International Conference on the Application of Stress-Wave Theory to Piles*, Ottawa, May 25–27, 1988, pp. 294–302.

85. Liang, S-X., K-W. Zhang, X-F. Yang, and Y. Mo, "A Method of Matching Measured Signal for the Wave Equation Analysis of Piles," *Proceedings of the Third International Conference on the Application of Stress-Wave Theory to Piles*, Ottawa, May 25–27, 1988, pp. 231–238.

86. Lo, K. Y., and A. G. Stermac, "Induced Pore Pressures during Pile-Driving Operations," *Proceedings of the 6th International Conference on Soil Mechanics and Foundation Engineering*, Montreal, 2, 1965, pp. 285–289.

87. Love, A. E. H., **A Treatise on the Mathematical Theory of Elasticity**, Dover, New York, 1941.

88. Matsumoto, T., Y. Nishida, H. Ohta, and K. Kawakami, "Analysis of Stress-Waves in a Pile Based on Two-Point Stress Measurements," *Proceedings of the Third International Conference on the Application of Stress-Wave Theory to Piles*, Ottawa, May 25–27, 1988, pp. 318–336.

89. Mattes, N. S., and H. G. Poulos, "Settlement of Single Compressible Pile," *Journal of Soil Mechanics and Foundation Engineering*, Vol. 95 (SM1), January 1969, pp. 181–207.

90. Meunier, J., and A. Goulois, "Practice and Interpretation of Instrumented Tests During Pile Driving," *Proceedings of the Third International Conference on Numerical Methods in Offshore Piling*, Nantes, May 21–22, 1986, pp. 75–90.

91. Middendorp, B., and P. J. van Brederode, "Skin Friction Models for Sand from Static and Dynamic Laboratory Load Tests," *Proceedings of the Second International Conference on the Application of Stress-Wave Theory on Piles*, Stockholm, May 27–30, 1984, pp. 210–220.

92. Mikasa, M., and N. Takada, "Significance of Centrifugal Model Test in Soil Mechanics," *Proceedings of the 8th International Conference on Soil Mechanics and Foundation Engineering*, Vol. 1, Part 2, 1973, pp. 273–278.

93. Miklowitz, J., **The Theory of Elastic Waves and Waveguides**, North-Holland Publishing Company, Amsterdam, New York, Oxford, 1978.

94. Miklowitz, J., **Modern Problems in Wave Propagation**, Wiley, New York, 1978.

95. Mindlin, R. D., "Force at a Point in the Interior of a Semi-Infinite Solid," *Physics*, Vol. 7, No. 5, May 1936, pp. 195–202.

96. Mindlin, R. D., and G. Hermann, "One-Dimensional Theory of Compressional Waves in an Elastic Rod," *Proceedings of the 1st U.S. National Congress of Applied Mechanics*, Chicago, June 11–16, 1951, pp. 187–191.

97. Monfore, G. E. "An Analysis of the Stress Distribution In and Near Stress Gauges Embedded in Elastic Solid," U.S. Department of Interior, Bureau of Reclamation, Denver, Col., Structural Research Laboratory, Report No. Sp-26, 1950.

98. Motherwell, J. T., "Axial Capacity and Driveability of Piles in Sand," *Proceedings of the Second International Conference on Numerical Methods in Offshore Piling*, Austin, Texas, April 29–30, 1982, pp. 183–196.

99. Naylor, D. J., and G. N. Pande, **Finite Elements in Geotechnical Engineering**, Pineridge Press, Swansea, U.K., 1981.

100. Novak, M., "Soil-Pile Interaction under Dynamic Loads," **Numerical Methods in Offshore Piling**, Institution of Civil Engineers, London, 1979, pp. 41–50.

101. Nunez, I. L., P. J. Hoadley, M. F. Randolph, and J. M. Hulett, "Driving and Tension Loading of Piles in Sand on a Centrifuge," **Centrifuge 88**, Corté (ed.), Balkema, Rotterdam, 1988, pp. 353–362.

102. Ohara, S., "On Relation Between Characteristic of Cell and Measurement of Dynamic Pore Water Pressure," *Trans. of JSCE*, No. 108, Civil Engineering in Japan, 1965., pp. 100–101.

103. Omar, R. M., and T. J. Poskitt, "Directional Stability of Piles During Driving," **Numerical Methods in Offshore Piling**, Institution of Civil Engineers, London, 1979, pp. 19–28.

104. Ortiz, L. A., "Dynamic Centrifuge Testing of Cantilever Retaining Walls," Soil Mechanics Laboratory, California Institute of Technology, Pasadena, Report No. SML 82–02, 1982.

105. Ovesen, N. K., "Centrifugal Testing Applied to Bearing Capacity Problems of Footings on Sand," *Géotechnique*, Vol. 25, No. 2, 1975, pp. 394–401.

106. Palmer, A. C., and R. J. Mitchell, "Plane-Strain Expansion of a Cylindrical Cavity in Clay," *Roscoe Memorial Symposium*, Cambridge, March 29–31, 1971.

107. Paquet, J., "Checking Bearing Capacity by Dynamic Loading. Choice of Methodology," *Proceedings of the Third International Conference on the Application of Stress-Wave Theory to Piles*, Ottawa, May 25–27, 1988, pp. 383–398.

108. Pokrovsky, G. I., and I. Fedorov, "An Investigation by Means of Models, of Stress Distribution in the Ground and the Setting of Foundations," in **Validity of Use of Centrifuge to Recreate Stress State in Soil**, 1933.

109. Pokrovsky, G. I., and I. S. Fyodorov, "Centrifugal Model Testing in the Construction Industry" (in Russian), Publishing House of Literature for the Construction Industry, Moscow, 1968.

110. Poulos, H. G., and E. H. Davis, **Elastic Solutions for Soil and Rock Mechanics**, Wiley, New York, 1974.

111. Poulos, H. G., and E. H. Davis, **Pile Foundation Analysis and Design**, Wiley, New York, 1980.

112. Pu, J.-L., and H.-Y. Ko, "Experimental Determination of Bearing Capacity in Sand by Centrifuge Footing," in **Centrifuge 88**, Corté (ed.), Balkema, Rotterdam, 1988, pp. 293–299.

113. Randolph, M. F., and H. A. Simons, "An Improved Soil Model for One-Dimensional Pile Driving Analysis," *Proceedings of the Third International Conference on Numerical Methods in Offshore Piling*, Nantes, May 21–22, 1986, pp. 3–18.

114. Randolph, M. F., "Analysis of the Dynamics of Pile Driving," in **Developments in Soil Mechanics — IV: Advanced Geotechnical Analyses**, P. K. Banerjee and R. Butterfield (eds.), Elsevier Applied Science Publishers Ltd., to be published.

115. Rausche, F., F. Moses, and G. G. Goble, "Soil Resistance Predictions from Pile Dynamics," *Journal of the Soil Mechanics and Foundations Division, ASCE*, Vol. 98, No. SM9, September 1972, pp. 917–937.

116. Rausche, F., G. G. Goble, and G. E. Likins, "Recent WEAP Developments," *Proceedings of the Third International Conference on the Application of Stress-Wave Theory to Piles*, Ottawa, May 25–27, 1988, pp. 164–173.

117. Roark, R. J., **Formulas for Stress and Strain**, McGraw-Hill, New York, 1954.

118. Rocha, M., "The Possibility of Solving Soil Mechanics Problems by the Use of Models," *Proceedings of the Fourth International Conference on Soil Mechanics and Foundation Engineering*, Vol. 1, 1957, pp. 183–188.

119. Roscoe, K. H., "Soils and Model Tests," *Journal of Strain Analysis*, Vol. 3, 1968, pp. 57–64.

120. Roscoe, K. H., and J. B. Burland, "On the Generalized Stress-Strain Behaviour of Wet Clays," in **Engineering Plasticity**, Hayman and Lecke (eds.), Cambridge University Press, 1968, pp. 535–609.

121. Sakai, T., "The Wave Equation for the Pile Driving Analysis," *Proceedings of the Third International Conference on the Application of Stress-Wave Theory to Piles*, Ottawa, May 25–27, 1988, pp. 251–260.

122. Sakai, T., M. Tanikawa, R. Sugimura, T. Takaoka, N. Kawabata, N. Koyama, and M. Honma, "Dynamic Behavior of Shaft Resistance and Bearing Capacity of Pile," *Proceedings of the Third International Conference on the Application of Stress-Wave Theory to Piles*, Ottawa, May 25–27, 1988, pp. 261–270.

123. Samson, C. H., T. J. Hirsch, and L. L. Lowery, "Computer Study for Dynamic Behavior of Piling," *Journal of the Structural Division, ASCE*, Vol. 89, No. ST4, Proc. Paper 3608, August 1963, pp. 413–449.

124. Sankaran, K. S., N. R. Krishnaswamy, and B. K. Sharas Chandra, "Stresses in Soil Around Vertical Compressible Piles," *Journal of the Geotechnical Engineering Division, ASCE*, Vol. 107, No. GT1, January 1981, pp. 107–112.

125. Schofield, A. N., "An Introduction to Centrifuge Modelling," **Centrifuges in Soil Mechanics**, Craig, James & Schofield (eds.), A. A. Balkema, Rotterdam, 1988, pp. 1–10.

126. Schofield, A. N., and C. P. Wroth, **Critical State Soil Mechanics**, McGraw-Hill, London, 1968.

127. Scott, R. F., **Principles of Soil Mechanics**, Addison-Wesley Publishing Co., Reading, Massachusetts, 1963.

128. Scott, R. F., "The Centrifugal Technique in Geotechnology — Selected Papers," Soil Mechanics Laboratory, California Institute of Technology, Pasadena, California, November 1975.

129. Scott, R. F., "Centrifuge Studies of Cyclic Lateral Load-Displacement Behavior of Single Piles," Soil Mechanics Laboratory, Division of Engineering and Applied Science, California Institute of Technology, Pasadena, California, 1977.

130. Scott, R. F., "Cyclic Static Model Pile Tests in a Centrifuge," *Offshore Technology Conference*, Paper No. 3492, 1979.

131. Scott, R. F., **Foundation Analysis**, Prentice-Hall, Inc., Englewood Cliffs, New Jersey, 1981.

132. Scott, R. F., "Centrifuge Model Testing at Caltech," *Soil Dynamics and Earthquake Engineering*, Vol. 2, No. 4, 1983, pp. 188–198.

133. Scott, R. F., "Physical and Numerical Models," **Centrifuges in Soil Mechanics**, Craig, James & Schofield (eds.), A. A. Balkema, Rotterdam, 1988, pp. 103–118.

134. Scott, R. F., H-P. Liu, and J. Ting, "Dynamic Pile Tests by Centrifuge Modeling," *Proceedings of the Sixth World Conference on Earthquake Engineering*, New Delhi, Paper 4–50, January 1977.

135. Scott, R. F., and N. R. Morgan, "Feasibility and Desirability of Constructing a Very Large Centrifuge for Geotechnical Studies," California Institute of Technology and Jet Propulsion Laboratory, Report 760–170, March 1977.

136. Scott, R. F., J. M. Ting, and J. Lee, "Comparison of Centrifuge and Full Scale Dynamic Pile Tests," *International Conference on Soil Dynamics and Earthquake Engineering*, Southampton, U.K., July 1982.

137. Selig, E. T., "A Review of Stress and Strain Measurements in Soils," *Proceedings, Symposium on Soil-Structure Interaction*, Tucson, 1964, pp. 172–186.

138. Selig, E. T., and H. G. Tobin, "Investigation of Piezoresistive Soil Stress Gages," *Proceedings of the International Symposium on Wave Propagation and Dynamic Properties of Earth Materials*, Univ. of New Mexico, Albuquerque, 1967, pp. 239–254.

139. Shastri, S. M., and S. Malumdar, "A Dynamic Finite Element Analysis of Stress-Wave Propagation and Rock Fragmentation in Blasting," *4th International Conference on Numerical Methods in Geomechanics*, Edmonton, May 31–June 4, 1982, pp. 437–447.

140. Shou-Xin, L., C. Ke-Ya, Z. Fu-Liang, and L. Yang-Bin, "Prediction of Pile Bearing Capacity by Stress Wave Theory," *Proceedings of the Second International Conference on the Application of Stress-Wave Theory on Piles*, Stockholm, May 27–30, 1984, pp. 33–40.

141. Smith, E. A. L., "Pile Driving Analysis by the Wave Equation," *Journal of the Soil Mechanics and Foundations Division, ASCE*, Vol. 86, No. SM4, August 1960, pp. 35–163.

142. Smith, I. M., "A Survey of Numerical Methods in Offshore Piling," **Numerical Methods in Offshore Piling**, Institution of Civil Engineers, London, 1979, pp. 1–8.

143. Smith, I. M., and Y. K. Chow "Three-Dimensional Analysis of Pile Drivability," *Proceedings of the Second International Conference on Numerical Methods in Offshore Piling*, Austin, Texas, April 29–30, 1982, pp. 1–19.

144. Smith, W. D., "A Nonreflecting Plane Boundary for Wave Propagation Problems," *Journal of Computational Physics*, Vol. 15, 1974, pp. 482–504.

145. Smith, W. D., "The Application of Finite Element Analysis to Body Wave Propagation Problems," *Geophysics J.*, Vol. 42, 1975, pp. 747–768.

146. Sorensen T., and B. Hansen, "Pile Driving Formulae - An Investigation Based on Dimensional Considerations and Statistical Analysis," *Proceedings of the Fourth International Conference on Soil Mechanics and Foundation Engineering*, London, 1957.

147. Tagaya, K., and M. Korematsu, "Pile Driveability Test on Full-scale Offshore Structure for Yanbu Tanker Terminal," *Proceedings of the VII Pan American Conference on Soil Mechanics and Foundation Engineering*, June 20–24, 1983.

148. Tan, T.-S., "Two Phase Soil Study: A. Finite Strain Consolidation, B. Centrifuge Scaling Considerations," Soil Mechanics Laboratory, California Institute of Technology, Pasadena, Report No. SML 85–01, August 1985.

149. Taylor, D. W., "Review of Pressure Distribution Theories and Earth Pressure Cell Investigation," Report *U.S. Army Engineers, Waterways Experiment Station,* Vicksburg, Nov. 1945.

150. Taylor, D. W., "Pressure Distribution Theories, Earth Pressure Cell Investigations and Pressure Distribution Data," Report *U.S. Army Engineers, Waterways Experiment Station,* Vicksburg, 1947.

151. Terzaghi, K., **Theoretical Soil Mechanics**, Wiley, New York, 1943.

152. Thompson, C. D., and M. Devata, "Evaluation of Ultimate Bearing Capacity of Different Piles by Wave Equation Analysis," *Proceedings of the International Seminar on the Application of Stress-Wave Theory on Piles*, Stockholm, June 4–5, 1980, pp. 163–196.

153. Thompson, C. D., and G. G. Goble, "High Case Shaft Damping Constants in Sands," *Proceedings of the Third International Conference on the Application of Stress-Wave Theory to Piles*, Ottawa, May 25–27, 1988, pp. 555–566.

154. Tory A. C., and R. W. Sparrow, "The influence of diaphragm flexibility on the performance of an earth pressure cell," *Journal of Scientific Instruments*, Vol. 44, No. 9, Sept. 1967, pp. 781–785.

155. Triandafilidis, G. E., "Soil-Stress Gage Design and Evaluation," *Journal of Testing and Evaluation*, American Society for Testing and Materials, Philadelphia, Vol. 2, No. 3, May 1974, pp. 781–785.

156. Trollope, D. H., and I. K. Lee, "The Performance of a Laboratory Earth Pressure Cell," *Australian Journal of Applied Science*, Vol. 8, No. 2, June, 1957, pp. 84–97.

157. Vesic, A. S., "Expansion of Cavities in Infinite Soil Mass," *Journal of Soil Mechanics and Foundation Engineering*, No. 98 (SM3), 1972, pp. 265–290.

158. Vesic, A. S., "Design of Pile Foundations," *Report, National Cooperative Highway Research Program Synthesis of Highway Practice*, No. 42, Transportation Research Board, National Research Council, Washington, D.C., 1977.

159. Vijayvergiya, V. N., "Soil Response During Pile Driving," **Numerical Methods in Offshore Piling**, Institution of Civil Engineers, London, 1979, pp. 35–40.

160. Warrington, D.C., "A New Type of Wave Equation Analysis Program," *Proceedings of the Third International Conference on the Application of Stress-Wave Theory to Piles*, Ottawa, May 25–27, 1988, pp. 142–151.

161. Weiler, W. A., and F. H. Kulhawy, "Factors affecting stress cell measurements in soil," *Journal of the Soil Mechanics and Foundations Division, ASCE*, Vol. 108, 1982, pp. 1529–1548.

162. Wilson, E. L., "Structural Analysis of Axisymmetric Solids," *Journal of American Institute of Aeronautics and Astronautics*, Vol. 3, 1965, pp. 2269–74.

163. Wroth, C. P., J. P. Carter, and M. F. Randolph, "Stress Changes Around a Pile Driven into Cohesive Soil," **Numerical Methods in Offshore Piling**, Institution of Civil Engineers, London, 1979, pp. 255–264.

164. Zienkiewicz, O. C., **The Finite Element Method**, 3rd ed., McGraw-Hill, London, 1977.

165. Zelikson, A., "Hydraulic Gradient Simulation of Sequences of Pile Driving and Loading Tests," *Proceedings of the Third International Conference on the Application of Stress-Wave Theory to Piles*, Ottawa, May 25–27, 1988, pp. 152–163.

166. Zelikson, A., and P. Leguay, "Some Basic Data on Piles under Static and Dynamic Loading from Stress Conserving Models," *Proceedings of the Third International Conference on Numerical Methods in Offshore Piling*, Nantes, May 21–22, 1986, pp. 105–126.

APPENDICES

Appendix A: CENTRIFUGE MODELING

In recent years model experiments in the centrifuge have proven to be useful for the investigation of a wide range of geotechnical problems. The need for a centrifuge in experimental geotechnics arises from the nonlinear behavior of soil, the strong dependence of most soil properties on confining pressure, and the gravity-induced nature of the soil stresses. For a scale model of a prototype to give the same behavior as the prototype when the same soil is used, homologous points in the model and prototype must experience the same stresses. This is best achieved by subjecting the 1/N scale model to a gravitational field of N g, where g is the Earth's gravitational acceleration. The principle of centrifuge modeling, established from the above-described physical considerations, can be extended to time-dependent events, such as dynamic soil-structure interaction and, in particular, pile driving. The scaling relations between prototype and model parameters for the centrifuge environment have been extensively discussed (*e.g.*, [18], [19], [25], [51], [52], [71], [74], [92], [104], [105], [108], [109], [118], [119], [125], [128], [135], [133] and [148]). Here are presented only those scaling ratios used in the pile driving experiments described.

Quantity	Full Scale (prototype)	Centrifugal Model at N$*g$
Length	1	1/N
Acceleration	1	N
Mass	1	$1/N^3$
Density	1	1
Stress	1	1
Strain	1	1
Time (dynamic problems)	1	1/N
Frequency (dynamic problems)	1	1/N
Velocity	1	1
Force	1	$1/N^2$

Table A.1 Scaling Ratios

CONFIGU-RATION	BRIDGE/STRAIN ARRANGEMENT	DESCRIPTION	OUTPUT EQUATION - E_o/E IN mV/V	$\frac{\text{ACTUAL STRAIN}}{\text{INDICATED STRAIN}} = \frac{\varepsilon}{\hat{\varepsilon}}$	COMMENTS
1	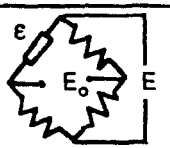	Single active gage in uniaxial tension or compression.	$\frac{E_o}{E} = \frac{F\varepsilon \times 10^{-3}}{4 + 2F\varepsilon \times 10^{-6}}$	$\frac{\varepsilon}{\hat{\varepsilon}} = 1 + \frac{F\hat{\varepsilon} \times 10^{-6}}{2 - F\hat{\varepsilon} \times 10^{-6}}$	Nonlinear.(1)
2	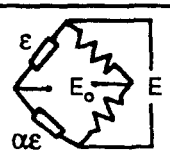	Two active gages in uniaxial stress field.	$\frac{E_o}{E} = \frac{F\varepsilon(1-\alpha) \times 10^{-3}}{4 + 2F\varepsilon(1+\alpha) \times 10^{-6}}$	$\frac{\varepsilon}{\hat{\varepsilon}} = 1 + \frac{F\hat{\varepsilon}(1+\alpha) \times 10^{-6}}{2 - F\hat{\varepsilon}(1+\alpha) \times 10^{-6}}$	Nonlinear.(1)
3	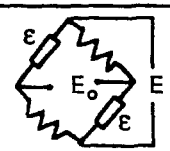	Two active gages with equal strains of same sign (bending cancellation).	$\frac{E_o}{E} = \frac{F\varepsilon \times 10^{-3}}{2 + F\varepsilon \times 10^{-6}}$	$\frac{\varepsilon}{\hat{\varepsilon}} = 1 + \frac{F\hat{\varepsilon} \times 10^{-6}}{2 - F\hat{\varepsilon} \times 10^{-6}}$	Nonlinear.(1)
4	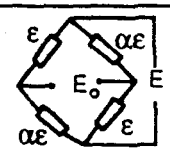	Four active gages in uniaxial stress field.	$\frac{E_o}{E} = \frac{F\varepsilon(1-\alpha) \times 10^{-3}}{2 + F\varepsilon(1+\alpha) \times 10^{-6}}$	$\frac{\varepsilon}{\hat{\varepsilon}} = 1 + \frac{F\hat{\varepsilon}(1+\alpha) \times 10^{-6}}{2 - F\hat{\varepsilon}(1+\alpha) \times 10^{-6}}$	Nonlinear.(1)
5	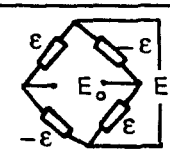	Four active gages with pairs subjected to equal and opposite strains (beam in bending).	$\frac{E_o}{E} = F\varepsilon \times 10^{-3}$	$\frac{\varepsilon}{\hat{\varepsilon}} = 1$	Linear.

Notes : (1) Incremental correction can be read directly from a graph.
F = Gage Factor

Appendix B.1 Wheatstone bridge configurations

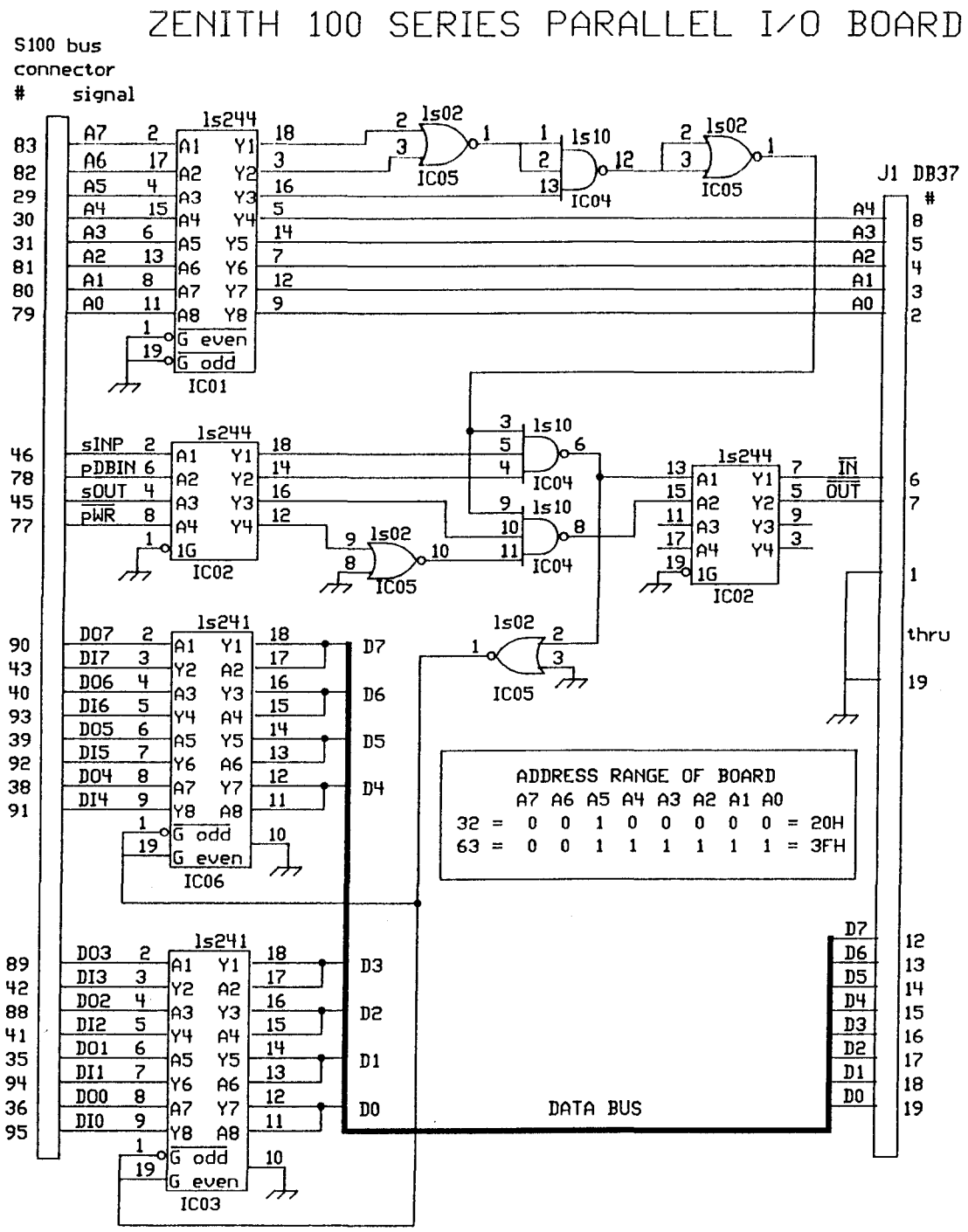

Appendix C.1 Z120 interface card

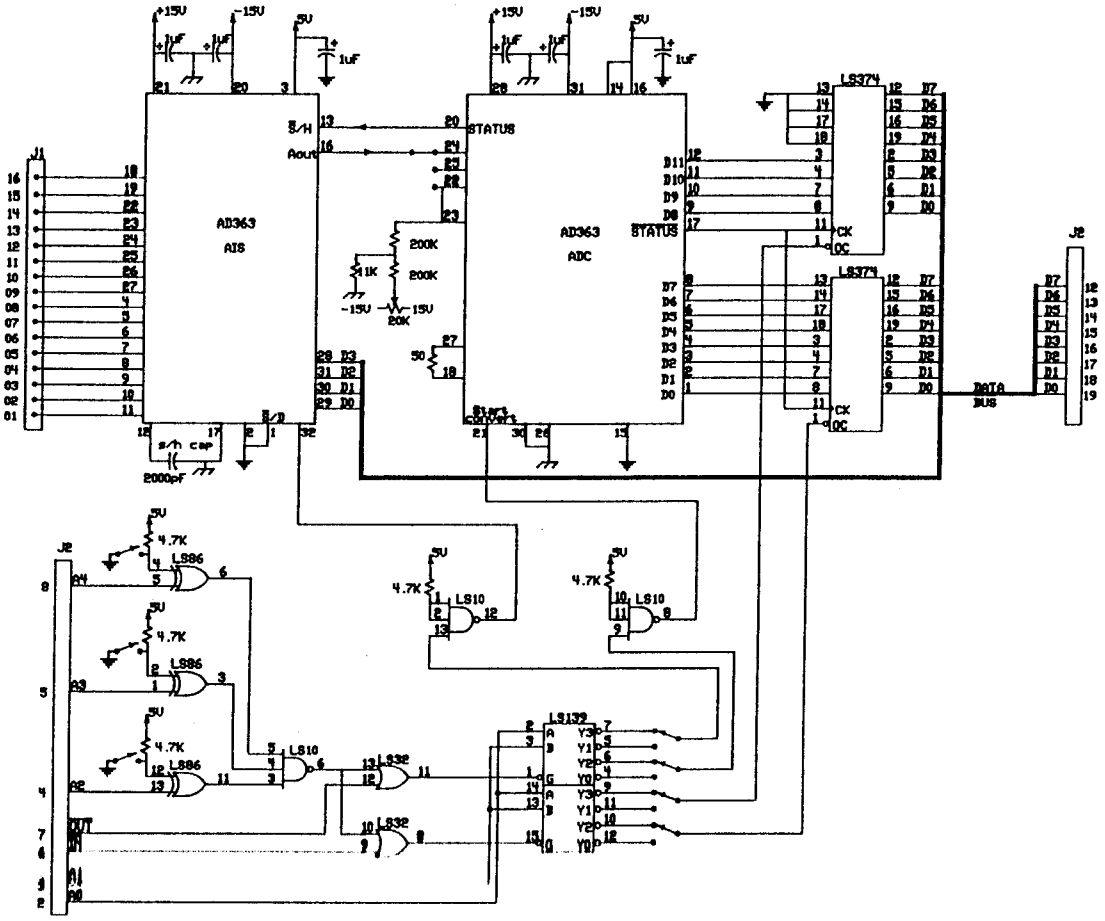

Appendix C.2 Analog to digital converter (John R. Lee)

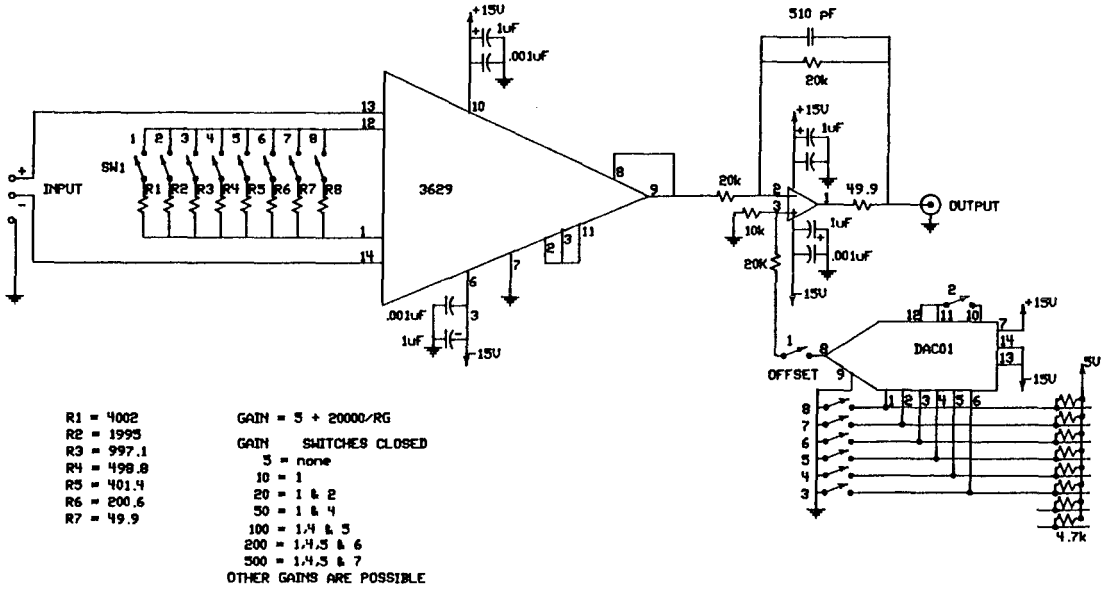

Appendix C.3 Centrifuge 16 channel amplifier (John R. Lee)

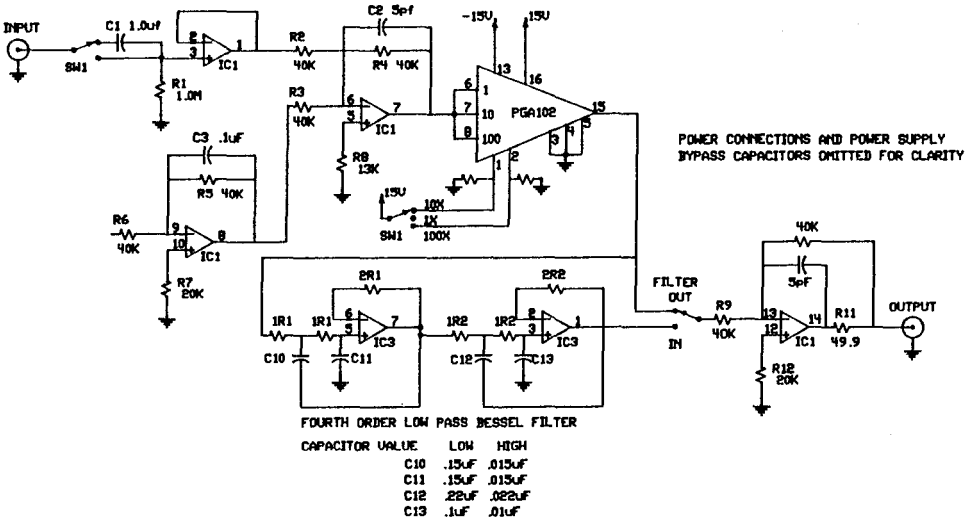

Appendix C.4 Signal conditioner (John R. Lee)

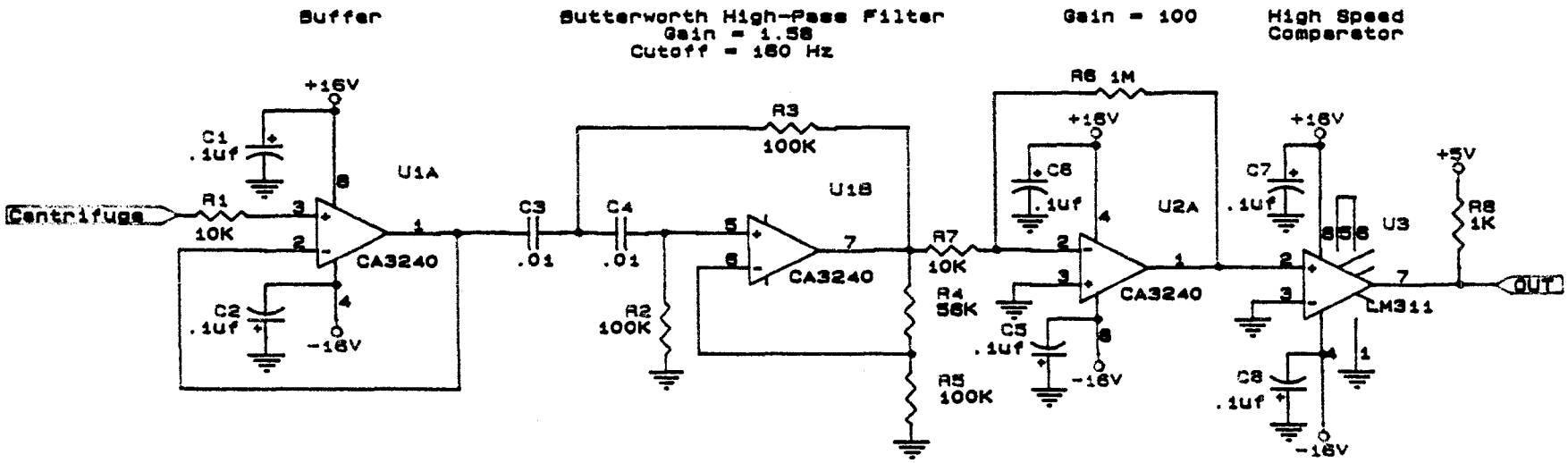

Appendix C.5 RPM counter front end (Brian W. Rague)

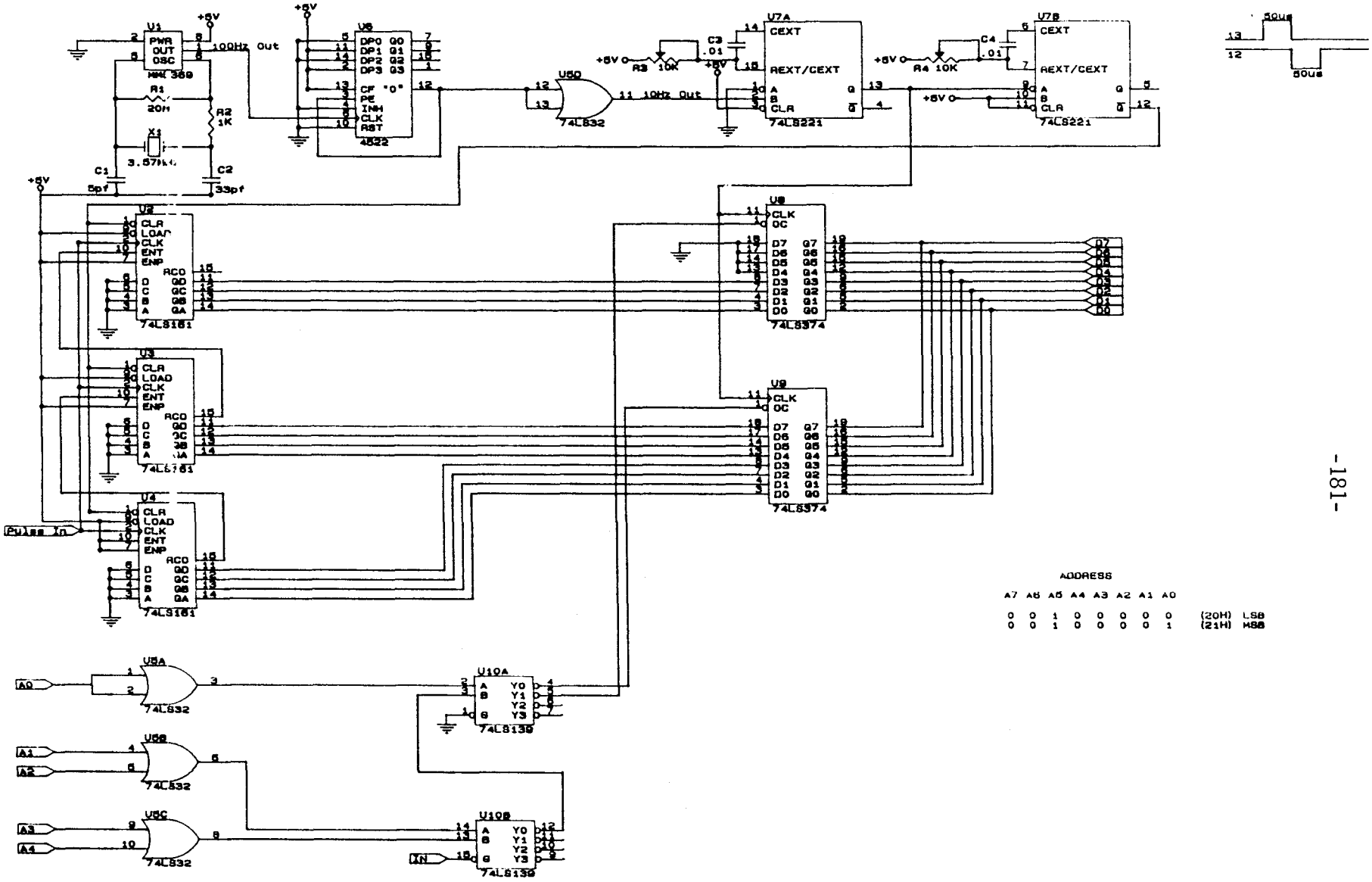

Appendix C.6 RPM detector card (Brian W. Rague)